Target-based discovery of novel inhibitors of enzymatic targets from *Wolbachia* endosymbionts and evaluation as antifilarial drug candidates

Dissertation

zur

Erlangung des Doktorgrades (Dr. rer. nat.)

der

Mathematisch-Naturwissenschaftlichen Fakultät

der

Rheinischen Friedrich-Wilhelms-Universität Bonn

vorgelegt von:

Christian Stephan Lentz

aus

Prüm

Bonn, Februar 2013

Angefertigt mit Genehmigung der Mathematisch-Naturwissenschaftlichen Fakultät
der Rheinischen Friedrich-Wilhelms-Universität Bonn

1. Gutachter: Prof. Dr. med. Achim Hörauf
2. Gutachter: Prof. Dr. rer. nat. Michael Famulok

Tag der Promotion: 29.05.2013
Erscheinungsjahr: 2013

Erratum

On page 25 of this dissertation (Chapter 2. Materials, Methods & Preparative Experiments) the entry for the composition of the PPDK activity assay buffer was erroneous. The correct specification for this buffer is as follows:

PPDK activity assay buffer

1X PPDK-PBS Buffer: 1X PBS, 20 mM NH_4Cl, 1 mM $MgCl_2$, pH 7.1

Contents

List of abbreviations

5-ALA	5-Aminolevulinic acid
ALB	Albendazole
BHQ-1	Black Hole Quencher-1
BSA	Bovine serum albumin
BTP	Bis-tris propane
CD	2-Hydroxypropyl-β-cyclodextrin
cDNA	Complementary DNA
d	Day
DEC	Diethylcarbamazine
DMAB	Para-dimethylaminobenzaldehyde
DMSO	Dimethyl sulfoxide
DNA	Deoxyribonucleic acid
dpi	Days post infection
DTT	Dithiothreitol
EBSS	Earl's Balanced Salt Solution
EDTA	Ethylenediaminetetraacetic acid
FAM	Fluoresceine amidite
FC	Ferrochelatase
Fig.	Figure
h	Hour
HEX	Hexachloro-fluoresceine
HTS	High-Throughput Screening
i.m.	Intramuscular
i.p.	Intraperitoneal
i.t.	Intrathoracic
i.v.	Intravenous
IMMIP	Institute for Medical Microbiology, Immunology and Parasitology, Bonn, Germany
IPTG	Isopropyl β-D-1-thiogalactopyranoside
IVM	Ivermectin
LDH	Lactic acid dehydrogenase
LIMES Institute	Life & Medical Sciences Institute, Laboratory of Chemical Biology, Bonn, Germany
LF	Lymphatic filariasis
MDA	Mass Drug Administration Program
MER	Modified Ehrlich's Reagent
MF	Microfilariae
MTT	3-(4,5-dimethylthiazol-2-yl)-2,5-diphenyltetrazolium bromide
NLR	Non-linear regression analysis
OD	Optical density
Oncho	Onchocerciasis
p.i.	Post infection
PAGE	Polyacrylamide gel electrophoresis
PBG	Porphobilinogen
PCR	Polymerase Chain Reaction
PDB	Protein Data Bank
PDR	Pyruvate Detection Reagent
PEP	Phosphoenol pyruvate
PK	Pyruvate kinase

PPDK	Pyruvate phosphate dikinase
RBC	Red blood cell(s) / erythrocyte(s)
RD	Restriction digested
RNA	Ribonucleic acid
rpm	Rotations per minute
RT	Room temperature
SA	Succinyl Acetone
SAR	Structure-Activity Relationship
SD	Standard deviation
SDS	Sodium dodecyl sulfate
SEM	Standard error of the mean
TAMRA	Tetramethylrhodamine
TSA	Thermal shift assay
Tris	Tris(hydroxymethyl)aminomethane
VS	Virtual screening
WHO	World Health Organisation

Chapter 1

Introduction

1.1 Infections with filarial nematodes: Past and present

"*SiR,-Permit me to call the attention of your readers, and especially that of foreigners, to some recent additions to our knowledge of the prevalence and probable source of various haematozoa infecting mankind and animals.*" [50]: "*Those who take an interest in helminthological studies may remember that in the month of July last I was permitted to announce in THE LANCET the discovery of a new entozoon. In honour of the discoverer I named the worm "Filaria Bancrofti"*" [51]. In these words T. Spencer Cobbold addressed the editors and the public readership of The Lancet in the 1870's and praised the work by Lewis, Wucherer, Bancroft and others who worked on the recent discoveries of human pathogenic filarial nematodes that were assumed as the causative agents of elephantiasis by Manson a few years later [215]. While the presence of this scourge was documented already by ancient craftworks that date back to Pharaonic Egypt, roughly 3000 years before the causative agents were discovered, today, more than 130 years after this discovery this vector-borne disease is known as lymphatic filariasis (LF) and is still considered a major public health problem in endemic tropical and subtropical regions of the old and new world by the WHO [3]. More than 120 million people worldwide suffer from infection, while more than 1.2 billion people are at risk of infection. *Filaria bancrofti* is now called *Wuchereria bancrofti* that, along with *Brugia malayi* and *Brugia timori*, constitutes the causative agents of LF. Another filarial disease that appears on the WHO's list of neglected tropical diseases is Onchocerciasis (Oncho) caused by the filarial nematode *Onchocerca volvulus*. This disease is mainly endemic in Sub-Saharan Afica with foci in Latin America and Yemen with a total of ∼37 million people infected worldwide [1, 2, 4].

1.2 Life cycle of filarial nematodes and pathogenesis

Chronic manifestations of both diseases are dreaded as they are among the leading causes of disability in the developing world. They burden patients with social stigmata and confront their families and societies with considerable economic losses. Pathologies are closely related to the complex life cycle of the parasitic worms (see **Fig. 1.1**): Filarial larval stages infect the human host during the blood meal of an infected arthropod intermediate host, i.e. a variety of mosquito vectors for lymphatic filariae or the black fly, genus *Simulium*, for *O. volvulus*. These L3 larvae migrate within the human body to their destined tissue-sites and develop into

adults after several molts. The causative agents of LF reside in worm nests in the lymphatics while *O. volvulus* is found in subcutaneous nodules. Adult worms are able to persist in the human host for more than a decade and their reproductive activity leads to the production and release of millions of L1 stage larvae (microfilaria, MF) for many years. While in LF microfilariae appear in the blood of the patients (microfilaremia), in Oncho, MF migrate within the dermis (microfilaridermia). Both localizations allow the uptake of MF during another blood meal of their required arthropod vector, in which MF develop into infective L3 larvae. Continuous reinfection and immunomodulation by the worms lead to chronic disease in which a complex interplay of excretory/secretory worm products and the host inflammatory reaction may lead to the tissue-destructive and -remodelling effects characteristic for severe patholgies: Hydrocele and lymphedema that may develop into elephantiasis are characteristic for LF. In Oncho manifestations of skin disease including dermatitis and depigmentation are common. Ocular onchocerciasis may develop as a result of the inflammatory reaction elicited by MF in the eye and may provoke keratitis and blindness (hence the alternative name River Blindness for Onchocerciasis) [249, 119, 206].

1.3 An introduction to *Wolbachia* endobacteria

Filarial nematodes are known to carry endosymbiotic bacteria of the genus *Wolbachia*, obligate intracellular bacteria that belong to the order of *Rickettsiales* and class of α-proteobacteria [76]. *Wolbachia pipientis* was discovered by Hertig and Wolbach in 1924 in gonad cells and eggs of the mosquito *Culex pipiens* [110]. Today it is expected that *Wolbachia* are able to infect $\sim$66% of arthropod species with either very high ($> 90\%$) or very low ($< 10\%$) infection frequencies [113]. *Wolbachia* strains infecting arthropods are endosymbionts [63] or reproductive parasites that induce a sex-ratio distortion by different mechanisms like cytoplasmic incompatibility [29, 218], feminization [218], male killing [128] or parthenogenesis [127, 239] (all reviewed in [21]).

Within filarial nematodes, *Wolbachia* were first described as Rickettsia-like microorganisms in the hypodermal chords of larvae of the dog heart worm *Dirofilaria immitis* and of *Brugia pahangi* [174] almost thirty years ago. Two years later, these microorganisms were also identified in the lateral chords of adult worms and the uteri, oocytes and MF of female *O. volvulus* [152] and *B. malayi* worms [151] and were found to be vertically transmitted [151]. In contrast to their parasitic arthropod-infecting counterparts, *Wolbachia* always have a mutualistic relationship to their nematode hosts. Although *Wolbachia* are named as one species (*Wolbachia pipientis*), phylogenetic analyses have clustered *Wolbachia* strains into currently nine different "supergroups", but this classification is continuously revisited. Supergroups A and B traditionally contain the classic *Wolbachia* that infect arthropods and the members were classified according to their *ftsZ* gene sequence [264]. More recently performed phylogenetic studies also accounted for other phylogenetics, such as of 16S rRNA and *Wolbachia* Surface Protein [76] or other protein protein coding genes [32]. Further *Wolbachia* from collembolan and isopteran species are contained in supergroups E and H [256, 30]. Supergroup G was first described to comprise *Wolbachia* from spiders [219], but was later suggested to be removed as the strain apparently resulted from a recombination event between A and B lineages [19].

Wolbachia supergroups C and D contain the endosymbionts of filarial nematodes: C comprises *Wolbachia* from *Onchocerca spp.* and *Dirofilaria spp.*, while the endosymbionts of *Brugia spp.*, *W. bancrofti*, as well as those of the rodent filarial nematode *Litomosoides sigmodontis* are assigned to the D group [20]. *Wolbachia* of the filaria *Dipetalonema gracile* were assigned to group J, the first endosymbiont

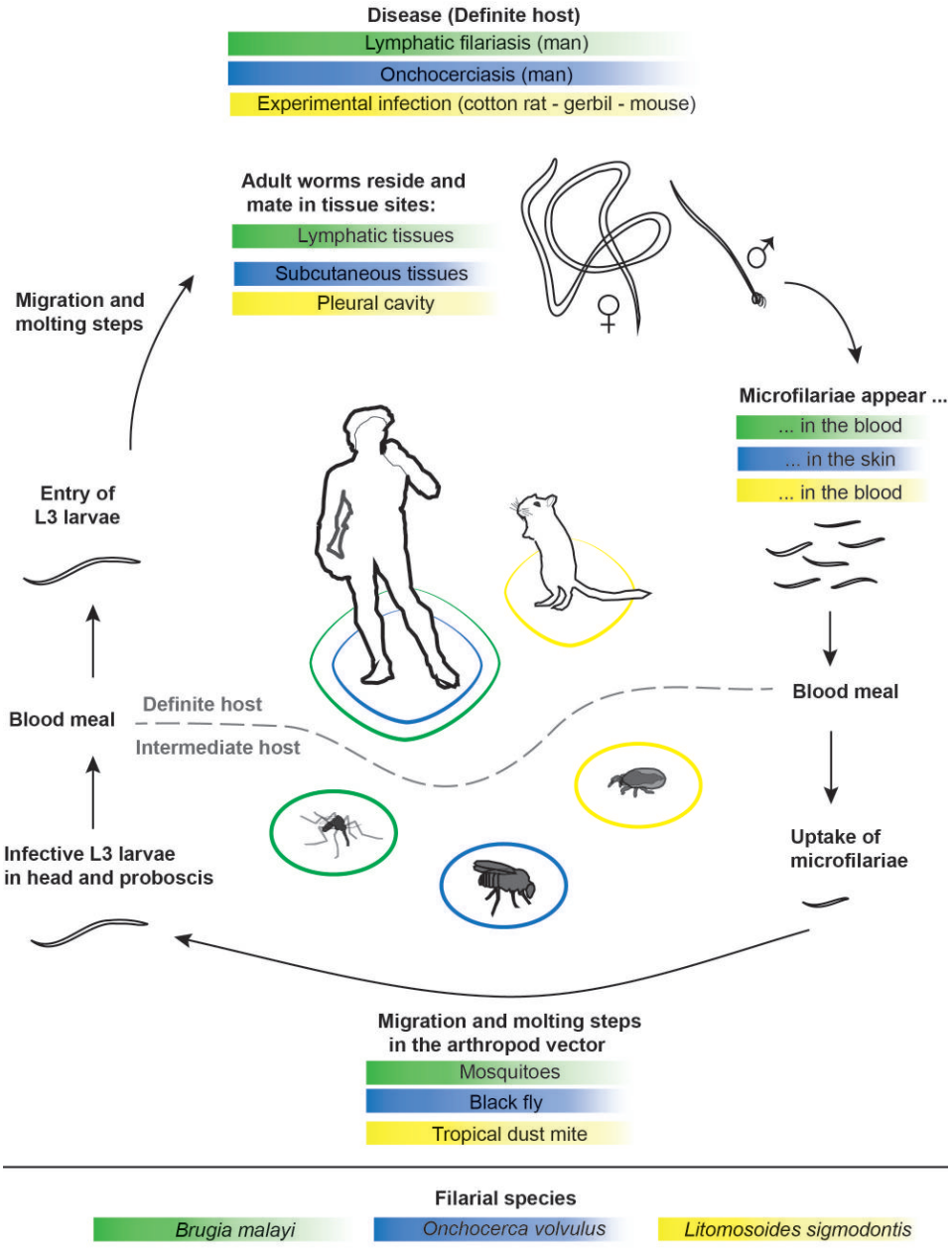

Figure 1.1: Life cycle of filarial nematodes

The figure depicts key stages of the infection cycle of different filarial nematodes in their mammalian definite host (upper part) and the arthropod intermediate host (lower part). For the different filarial species the corresponding details on the infection cycle are highlighted in color: *B. malayi* (green), *O. volvulus* (blue) and the rodent parasite *L.sigmodontis* (yellow).

of a plant-parasitic nematode (*Radopholus similis*) to supergroup I [101]. Of note, F-group *Wolbachia* are a relatively heterogenous group with a broad host range including both filarial nematode (*Mansonella spp.* and others) [41, 162] and arthropod species like lice [55] or scorpions [18].

Interestingly, several filarial nematodes including *Loa loa*, the causative agent of loiasis, *Acanthocheilenoma spp.* or *O. flexuosa* were shown not to harbor *Wolbachia* endobacteria [172, 253, 175]. Furthermore, with the exception of the recently identified group I nematode *R. similis* [101], no *Wolbachia* have been identified in non-filarial nematodes [31]. Within the possible scenarios of endosymbiont acquisition by filarial nematodes, in general, a single infection event of a common filarial ancestor with secondary loss of the endosymbiont from species that are found to be *Wolbachia*-free is favoured over a multiple-infection scenario [31, 43, 248]. This hypothesis has recently been strengthened by the identification of *Wolbachia*-like gene sequences in the genomes of *Wolbachia*-free filarial worms [175]. However the divergent F lineage has possibly been acquired by filariae rather recently in a secondary infection event while certain ancient filarial lineages (e.g. Oswaldofilariinae) seem to have branched off before the acquisition of the endosymbiont by an onchocercid ancestor [77].

Wolbachia generally reside in vacuoles in the cytoplasm of their host cells [152] and endosymbiont numbers are conrolled by autophagy of the filarial host [259]. While *Wolbachia* numbers in the lateral chords of MF and L3 larvae are very low, higher levels are found in L4 larvae with peak multiplication rates for young adults. *Wolbachia* are mainly found in the female reproductive tract, including ovaries and embryos [80]. This asymmetric distribution pattern within the body of the worm is due to asymmetric segregation of *Wolbachia* towards posterior blastomeres during the first division rounds of embryonic cells. Out of these posterior blastomeres germline cells will emerge and the population of lateral chords is enabled by syncytial formation involving cells of the *Wolbachia*-containing lineage [158]. In the same study, single *Wolbachia* were also found in the secretory canal, indicating a possible secretion of the endosymbiont by its hosts.

Wolbachia are also of major importance for the pathogenesis of filarial diseases. Due to their prokaryotic structural components like *Wolbachia* Surface Protein they are able to activate pattern-recognition receptors such as Toll-like receptor 2 and thus drive innate immune responses [221, 114]. *Wolbachia* components are able to recruit neutrophils to the site of infection and thus trigger the detrimental immunological cascade in the cornea that may cause stromal haze and develop into blindness [221, 94]. *Wolbachia* components are also considered to contribute to the chronic inflammation and tissue-remodeling effects leading to lymphedema [62, 206]. Finally, the endosymbiont has been correlated with side effects of antifilarial chemotherapy which leads to a massive release of *Wolbachia* antigen upon death of filarial worms that subsequently induce severe inflammatory reactions [56].

1.4 Mutualism between *Wolbachia* and filarial nematodes

In the past, evidence for the mutualistic role of *Wolbachia* within filarial nematodes was mostly restricted to functional defects of the worms elicited by depletion of *Wolbachia* by antibiotic treatment. A remarkable coincidence between *Wolbachia* from nematodes and arthropods is the preferential localization in the female reproductive tract, that allows the cytoplasmic transmission from mother to progeny. It is therfore not surprising that endosymbiotic *Wolbachia* are required to sustain filarial fertility and embryogenesis [116, 118]. Development of female worms of the

model filarial nematode *L. sigmodontis* requires higher *Wolbachia* levels than the development of males does, such that a reduction of *Wolbachia* levels in adult females by antibiotic treatment led to a sex-ratio distortion of worms in the daughter generation [9]. In addition, *Wolbachia* have been described to be required to sustain the L4-L5 larval molt of *B. pahangi* [42].

Analysis of the *Wolbachia*-filaria symbiosis was brought to the next level by elucidation of the genome of *Wolbachia* endosymbiont of *B. malayi* [81] and the draft nuclear genome of its host *B. malayi* [93]. The endosymbiont possesses a very reduced genome ∼1.1 Mb with a G+C content of 34%, while the nematode genome is predicted to be 90 - 95 Mb with a G+C content of 30.5% containing 14,500 - 17,800 protein-coding genes, which is several thousand genes less than reported for the free-living nematode *Caenorhabditis elegans* (19,507 genes) [265]. Several biochemical pathways for the synthesis of essential molecules of life are only conserved in either the filarial host or the endosymbiont genome indicating these organisms have evolved an elaborate division of labor. In addition to providing a defined and protective habitat for their endosymbionts, the worms seem to provide amino acids to the *Wolbachia* which only have the genes required for *de novo* synthesis of *meso*-diaminopimelinic acid, a prokaryote-specific amino acid incorporated in bacterial peptidoglycan. Furthermore, *Wolbachia* are unable to synthesize several essential vitamins and cofactors *de novo* including biotin, folate, Coenzyme A, lipoic acid, ubiquinone and pyridoxal phosphate and thus likely depend on their supply by the host [81]. In contrast, *Wolbachia* have conserved genes required for *de novo* synthesis of purine, flavins and heme that are mostly absent from the filarial genome. The dependence on heme biosynthesis of *Wolbachia* may explain the previously mentioned defects in reproduction and molting [42] as there is evidence for a functional ecdysone signalling system (activated by ecdysteroid-like hormones) [252, 99] that commonly coordinates these events and mostly involves heme-dependent cytochrome P450 [129].

1.5 Model systems of filarial nematodes

In order to study the biology of parasitic filarial worms under defined experimental conditions, biomedical research relies strongly on the use of common laboratory animals such as mice and rats unless clinical material is used. This fact often precludes the detailed study of human pathogenic filarial species, whose life cycle is mostly not compatible with rodent hosts and requires related model organisms, instead. The only exception is *B. malayi* which can be cultivated in Mongolian gerbils and mosquitoes [10]. For the current study the two following model filarial nematodes of rodents, *Litomosoides sigmodontis* and *Acanthocheilonema viteae*, were used.

1.5.1 *Litomosoides sigmodontis*

Litomosoides sigmodontis (Chandler, 1931) naturally infects the cotton rat (*Sigmodon hispidus* as the definite host and infective larvae are transmitted by the dust mite *Ornithonyssus bacoti* [17]. Adult filarial worms of these species reside in the thoracic cavity (single worms may also be found sporadically in the peritoneal cavity), but do not evoke evident pathology, a feature in common with *Mansonella perstans*, which may cause clinically mild infections in humans [121]. As in the cotton rat, *L. sigmodontis* may reach patent infection in Mongolian gerbils (*Meriones unguiculatus*) with similar worm burden [122, 12]. An overview of the *L. sigmodontis* life cycle is also given in **Fig. 1.1**. *L. sigmodontis* is able to reach patency in the BALB/c mouse strain although lower worm burdens are achieved in the pleural cavity and worms are smaller compared to those developing in the natural host,

the cotton rat [203]. In BALB/c mice, L3 larvae reach the pleural cavity at ∼7 dpi, where they molt to the L4 stage. L4 larvae again molt into adult worms at ∼4 weeks post infection and the mice may become microfilaremic at ∼55 - 60 dpi [122, 7, 16]. Other mouse strains (e.g. C57BL/6 mice) are not permissive for the development of patent infection of *L. sigmodontis* which is likely a consequence of a different bias of the immune system in these mice [15].

Of note, *L. sigmodontis* carries a strain of *Wolbachia* endosymbionts that like *Wolbachia* of *B. malayi* belongs to supergroup D [20]. In consequence, *L. sigmodontis* is not only an excellent model to study the biology and immunology of filarial infections [122, 7], but it is also suitable for testing the effect of drugs that target *Wolbachia* [116].

1.5.2 *Acanthocheilonema viteae*

Another model filarial nematode able to infect Mongolian gerbils is *Acanthocheilonema viteae* (previously named *Dipetalonema viteae*), that is transmitted by tick vectors (*Ornithodoros moubata*). This filaria infects predominantly the subcutaneous and intramuscular tissue of their hosts [243]. In contrast to *L. sigmodontis*, *A. viteae*, like other *Acanthocheilonema* species, do not have *Wolbachia* symbionts [116, 175, 254]. Absence of *Wolbachia* renders this filarial nematode a control organism for the study of *Wolbachia*-targeting drugs.

1.6 Antifilarial drugs

Before the different drugs used for the treatment of filarial diseases are introduced, it should be remarked that the efficacy of antifilarial drugs may be classified as to which life stages of the worms are efficiently killed: Drugs that kill MF are termed "microfilaricidal drugs", while those that induce death of adult worms are termed "macrofilaricidal". It is further differentiated between classical anthelminthics that target worm processes and antibiotics that deplete *Wolbachia* endosymbionts and have secondary effects on their filarial hosts. For classical anthelminthics the mode of action was mostly delineated from studies using non-filarial nematodes like *Ascaris suum* or *Caenorhabditis elegans* and is assumed to apply to filarial nematodes, often without experimental verification.

1.6.1 Classical anthelmintics

In many countries endemic for filariases Mass Drug Administration Programs (MDA) are carried out that aim for the elimination of Onchocerciasis as a public health problem and envisage the final eradication of LF [3, 1, 2, 4]. These programs employ annual treatment rounds of single-dose combination therapies with classical anthelmintics (diethylcarbamazine (DEC) + albendazole (ALB) or ivermectin (IVM) + ALB).

DEC is regarded as the most powerful antifilarial drug with efficient microfilaricidal and weak macrofilaricidal effect [193] and is used exclusively against LF. Its molecular targets and mechanism of action remain unknown [92]. One study revealed DEC-elicited defects of *W. bancrofti* microfilariae *in vitro* and *in vivo*, evident in exsheathment, apoptosis and organelle damage [201]. Other studies using murine models demonstrated that functional host pathways (arachidonic acid pathway and inducible nitric-oxide synthase (iNOS)) were required to achieve a reduction of microfilaremia by DEC-treatment [173].

IVM is the most prominent member of the macrocyclic lactone drugs to which also moxidectin belongs. The main effect of IVM is its agonistic activity on nema-

tode glutamate-gated chloride channels (GluCl) (with lower potency also on other ligand-gated ion channels) depolarizing interneurons and inhibitory motoneurons resulting in a flaccid paralysis of the worms, affecting body wall and pharyngeal musculature [123, 144, 202]. For MF of *B. malayi* an IVM-elicited neuromuscular block of the excretory-secretory apparatus has been demonstrated that putatively disrupts immunomodulation via excretory/secretory products enabling a rapid clearance of MF by the human immune system [186]. Consequently, for IVM only microfilaricidal activity has been reported [125].

In Onchocerciasis patients, DEC provokes serious adverse events (Mazzotti reaction) [82] which prevents the use of this drug for MDA in Oncho-co-endemic areas. As a consequence, Onchocerciasis control programs rely exclusively on IVM. IVM, in turn, may cause severe encephalopathies in highly microfilaremic patients infected with loiasis [88, 46], another comparatively benign filarial disease caused by the eye worm *Loa loa* [195]. Sub-optimal responses against IVM in clinical medicine and clear IVM-resistance in veterinary medicine have been reported in several studies [192, 49, 90] and are raising serious concern about the future efficacy of this drug in disease eradication programs. Macroyclic lactone resistance may involve altered sequences or expression of P-glycoprotein drug-efflux transporters [35] or GluCl-subunits [170, 95]. For DEC similar observations of drug resistance have been made [73, 238].

ALB belongs to the class of broad-spectrum benzimidazole anthelminthics. These drugs specifically target nematode β-tubulin and induce disintegration of microtubules [156]. A recent study revealed that albendazole sulfone, one of the two major metabolites of albendazole *in vivo*, also reduced *Wolbachia* levels [226]. The authors conclude that it must be considered that the antifilarial activity by ALB is a combination of destabilization of microtubules in the nematode and an effect on *Wolbachia*. However, while prolonged treatment with higher doses was observed to have some macrofilaricidal effects, the single doses used in combination to DEC/IVM during MDA are mainly to enhance the microfilaricidal effect of DEC/IVM and the low macrofilaricidal effect of DEC [194].

1.6.2 *Wolbachia*-depleting antibiotics

In the late 1990s pioneering studies first aimed to dissect the role of *Wolbachia* for the biology of their filarial hosts by eliminating the endosymbionts by antibiotic treatment. Hoerauf and coworkers found that tetracycline treatment of *L. sigmodontis*-infected mice efficiently depleted the endobacteria from their host causing infertility of adult female worms [116], while several other antibiotics such as chloramphenicol, macrolides or ciprofloxacin had no effect on *Wolbachia* levels and did not affect worm fertility [118]. In parallel, studies on *B. pahangi* and *D. immitis*-infected dogs reported a block of filarial embryogenesis after tetracycline treatment [22]. A milestone in antifilarial drug discovery subsequently was the successful demonstration that doxycycline treatment leads to depletion of the endobacteria from *O. volvulus in vivo* resulting in sterility and death of adult worms [117, 115, 159, 247]. Thus *Wolbachia* were established as an excellent antifilarial drug target to treat human disease. Doxycyline, and tetracyclines in general, are inhibitors of protein translation preventing the attachment of aminoacyl-tRNAs to the ribosomal acceptor site and have a bacteriostatic effect [47].

The antifilarial effect achieved by *Wolbachia*-depleting antibiotics in the clinic has several major advantages compared to classical anthelmintic therapy. Doxycycline therapy induces a long-term sterililizing effect and has pronounced macrofilaricidal activity [248, 61, 120]. Pathology was also reported to be ameliorated after doxycycline therapy [62, 167]. Due to the slow death of adult worms ($>$ 12 months after treatment) and the lack of abrupt release of highly-inflammatory *Wolbachia*

antigens, doxycycline causes few side effects [62]. Furthermore, the absence of *Wolbachia* endobacteria in *L. loa* [172, 40] allows the safe use of *Wolbachia*-targeting drugs in areas co-endemic for loiasis. However, the long treatment regimen of 3-5 weeks required for efficient depletion of *Wolbachia* is a major disadvantage and contraindications for children and pregnant and breast-feeding women prevent the use of this drug in MDA [119, 91]. Nevertheless, studies undertaken in Cameroon successfully demonstrated the general feasibility of large-scale distribution of doxycycline (100 mg/day for 6 weeks) on a community-directed basis even for such prolonged treatment times [261, 244]. Another registered drug with activity against *Wolbachia* is rifampicin, an antibiotic commonly used for the treatment of tuberculosis targeting the bacterial DNA-dependent RNA polymerase [258, 251, 233]. Combination therapy of doxycycline with rifampicin has been shown to shorten the required treatment regimens [60] and is a first step towards the development of anti-*Wolbachia* therapies and treatment regimens more suitable for MDA.

1.6.3 A call for the development of novel antifilarial drugs

Antifilarial treatment in MDA mainly has microfilaricidal effects and aims at a reduction of transmission. As the long-lived adult worms are only temporarily paralyzed and start production of MF again 6 - 12 months after treatment [14], MDA programs have to be done repeatedly over the entire life-span of the filariae in order to be successful. Adult filariae are able to persist in their human hosts for more than a decade and, in consequence, MDA programs using microfilaricidal drugs are organisationally and economically very challenging, especially in the context of political instabilities in many endemic countries. On this background development of resistance against DEC, and especially IVM, the mainstay of antifilarial therapy is a serious threat to the ambitious goals of WHO's elimination programs [25, 91]. Therefore the discovery of novel, preferentially macrofilaricidal, antifilarial drugs has become a priority in biomedical filarial research. The great efficacy and specificity possible with *Wolbachia*-targeting antibiotics make this endobacterium a prime target for novel strategies in antifilarial drug discovery. Sequencing of the *Wolbachia* genome and identification of essential biochemical pathways in these endobacteria allowed the designation of *Wolbachia* enzymes as putative drug targets [81, 93, 207, 124, 232]. In the current study, two prioritized potential drug targets, the heme biosynthetic enzyme δ-aminolevulinic acid dehydratase (ALAD) and the glycolytic/gluconeogenetic enzyme pyruvate phosphate dikinase (PPDK), were subjected to a target-based drug discovery approach to satisfy current needs for novel antifilarial agents.

1.7 Heme biosynthesis in filarial nematodes

Biosynthesis of tetrapyrroles is a highly conserved biosynthetic pathway that is elementary for the production of biomolecules with paramount importance for living organisms. In porphyrins the four pyrrole rings are linked at the α postion via methine bridges and the most prominent porphyrin, heme, complexes a ferrous (Fe^{2+}) or ferric iron (Fe^{3+}) at the center of the ring. Heme is an essential prosthetic group in enzymes involved in a broad spectrum of vital processes in life. Heme-dependent proteins are, e.g. hemoglobin/myoglobin (oxygen transport) [260], cytochrome b and cytochrome c oxidase (oxidative phosphorylation in bacteria and mitochondria) [150], cytochrome P450 (metabolization and detoxification of xenobiotics) [53], catalases and peroxidases (degradation of harmful H_2O_2 [276, 277]), cyclooxygenases (prostaglandin biosynthesis) [166] and many more.

Chlorins contain three pyrrole and one pyrroline ring. Their most prominent

members, the chlorophylls required for photosynthesis in plant cloroplasts, complex a magnesium ion in the center of the ring [245]. Further tetrapyrrole-derivatives represent the core of cobalamins (vitaminB_{12}) [217].

Heme biosynthesis is a complex metabolic pathway that includes six common precursors and, in eukaryotic cells, is compartmentalized between the cytosol and mitochondria in metazoan and fungal cells and between the mitochondria and the chlorplast in plants (**Fig. 1.2**). The only biosynthetic step which uses variable substrates and enzymes, respectively, in different organisms is the first step: In the C_4 or Shemin pathway of non-photosynthetic eukaryotes and α-proteobacteria δ-aminolevulinic acid synthase uses glycine and succinyl-CoA for the synthesis of 5-aminolevulinic acid (5-ALA), while the alternative C_5 pathway for 5-ALA synthesis in photosynthetic organisms, archaea and most bacteria requires two enzymatic steps starting with glutamyl-tRNA [255]. The next steps are common in all tetrapyrrole synthesizing organisms: δ-aminolevulinic acid dehydratase (ALAD, also known as porphobilinogen synthase, PBGS, E.C. 4.2.1.24) catalyzes the asymmetric condensation of two molecules of 5-ALA to the pyrrole porphobilinogen. Porphobilinogen deaminase then produces the linear tetrapyrrole hydroymethylbilane, which is cyclized by uroporphyrinogen III synthase to uroporphyrinogen III. The three following enzymatic steps catalyzed by uroporphyrinogen III decarboxylase, coproporphyrinogen III oxidase and protoporphyrinogen IX oxidase alterate the side chains of the cyclic tetrapyrroles and produce the precursors coproporphyrinogen III, protoporphyrinogen IX and protoporphyrin IX. The final step is the incorporation of Fe^{2+} into the center of protoporphyrin IX to form heme b, the most common heme form [107]. Chlorophyll synthesis branches off with the incorporation of Mg^{2+} into protoporphyrin IX by Mg^{2+} chelatase [52].

The *Wolbachia* genome contains all genes necessary for *de novo* heme biosynthesis except the *hemG* or *hemY* gene encoding protoporphyrinogen IX oxidase (PPO) in γ-proteobacteria or eukaryotes. As in other bacteria, this function is probably encoded by a yet unidentified gene [81]. Unlike *Wolbachia*, their nematode host *B. malayi* lacks all heme-biosynthetic genes except the gene for ferrochelatase (FC) catalyzing the final step of heme biosynthesis [93]. Interestingly, phylogenetic analysis of the FC gene homolog revealed a putative horizontal gene transfer from an α-proteobacterium that likely belongs to the Rhizobiales [232] and not from *Wolbachia*.

Suitability of endobacterial heme biosynthesis as an antifilarial drug target was validated by Wu and coworkers [270] who showed that inhibitors of ALAD (succinyl acetone) and FC (N-methyl mesoporphyrin) reduced the motility of *B. malayi* adult female worms in an *ex vivo* survival assay. Addition of exogenous heme did not rescue these worms indicating the filariae were unable to use this external heme source for their needs. Further evidence for the biological relevance of *Wolbachia*-derived heme biosynthesis in symbiosis was uncovered by microarray studies analysing differential gene expression of *L. sigmodontis* after depletion of *Wolbachia* by doxycycline treatment [241]. Several mitochondrial heme-dependent genes were up-regulated in response to *Wolbachia*-depletion, while expression patterns of these genes in *Wolbachia*-free *A. viteae* were unaffected by tetracycline treatment. This differential gene expression is regarded as a desperate response of the worm to overcome malfunctioning of its mitochondrial respiratory chain as a consequence of heme-deficiency subsequent to endosymbiont loss.

In order to develop drugs that are efficient against *Wolbachia*, but harmless for humans, potential drug targets must be species-specific. The heme-biosynthetic enzyme with the greatest structural divergence from its human ortholog, and therefore the best suited for the discovery of such inhibitors, is δ-aminolevulinic acid dehydratase of *Wolbachia* of *Brugia malayi* (wALAD). As currently known inhibitors, such as the already mentioned substrate analog succinyl acetone, target structural

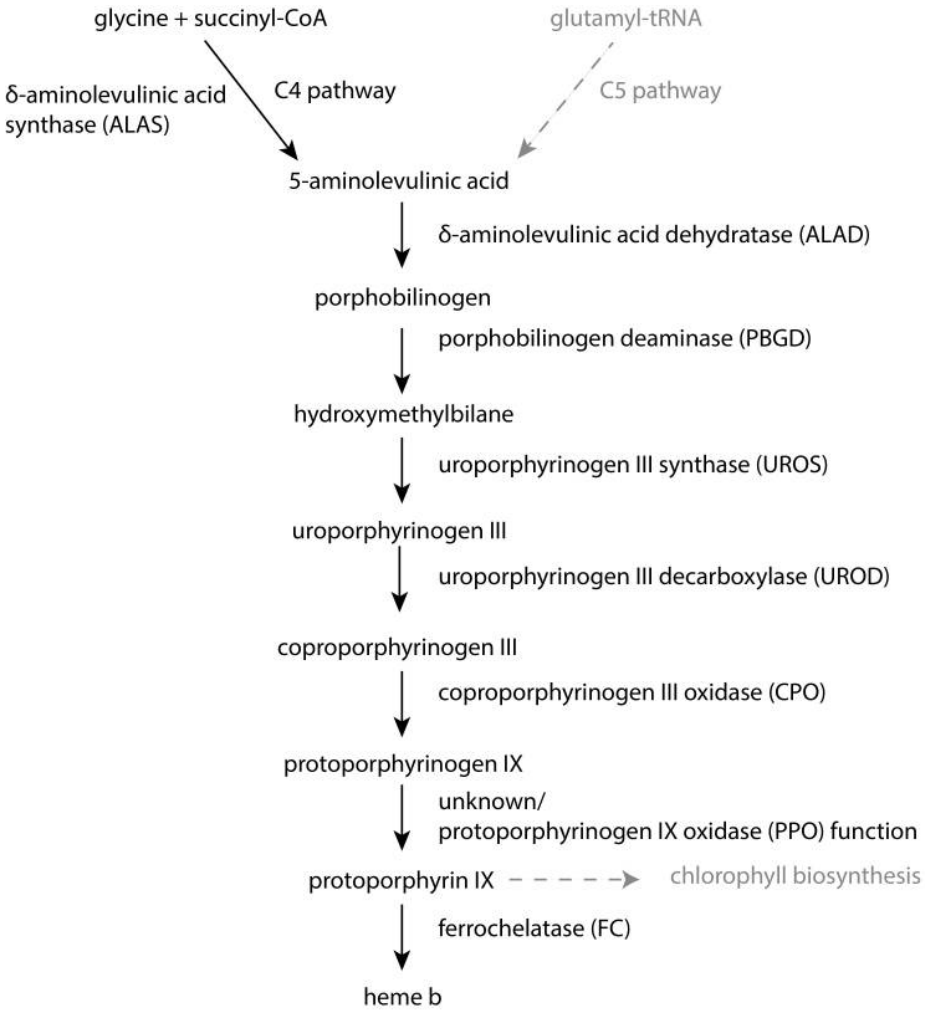

Figure 1.2: Heme biosynthesis pathway

Overview of the heme biosynthesis pathway in *Wolbachia* with the involved substrates and enzymes (with common abbreviations) is depicted in black font. This pathway is shared by non-photosynthetic eukaryotic organisms such as mammals and other α-proteobacteria. The alternate C5 pathway for the production of 5-ALA in plants and other bacteria, as well as the branching point for chlorophyll biosynthesis of photosynthetic organisms are depicted in gray.

features that are highly conserved in ALAD orthologs from different species, discovery of *Wolbachia*-specific inhibitors of ALAD enzymatic function was a major ambition of this study.

1.8 δ-Aminolevulinic Acid Dehydratase (ALAD)

δ-aminolevulinic acid dehydratase (ALAD) is a homo-oligomeric enzyme with each subunit of the protein adopting an $(\alpha/\beta)_8$-barrel (TIM-barrel) fold with an extruded N-terminal arm region important for intersubunit contacts [72, 83]. The active site is located in a cavity in the center of the α/β_8-barrel domain and catalyzes the condensation of 2 molecules of 5-aminolevulinic acid (5-ALA) to porphobilinogen [134]. Distinct binding sites for the 5-ALA molecules exist that are termed A-site and P-site. The corresponding substrate molecules that give rise to the acetyl and propionyl moieties, respectively, in the final porphobilinogen product are called A-side 5-ALA and P-side 5-ALA (**Fig. 1.3, [134]**).

ALAD enzymes are the prototype of so-called morpheeins, i.e. allosteric proteins that form an equilibrium of different quaternary assemblies that show characteristic differences in their functional properties, i.e. catalytic activities in the case of ALAD [135, 137]. The basic building blocks are asymmetric dimers which may adopt different allosterically driven conformations that lead to an orientational rearrangement of the N-terminal arm towards the $(\alpha/\beta)_8$-barrel ("hugging dimer" vs. "detached dimer" and "pro-octamer dimer" vs. "pro-hexamer dimer") [37, 137]. These dimers have an intrinsic propensity to form different higher molecular weight oligomers, most commonly hexameric or octameric assemblies. Hexameric assemblies are usually characterized by low enzymatic activity [37], while the octamer represents the conformation of high enzymatic activity.

Although the catalytic mechanism including the involved catalytic amino acids of the active center are well conserved throughout orthologous enzymes of different organisms, decisive differences are observed in the metal-cofactor requirements of different ALAD orthologs with structural and functional differences both at active and allosteric sites [229, 133]. Mammalian enzymes, including the human ortholog (hALAD), as well as orthologs of yeast and several bacteria, share a Zn^{2+}-binding cysteine-rich consensus sequence (DXCXCX(Y/F)X_3G(H/Q)CG) [133]. While binding and Schiff-base formation of the first P-side 5-ALA molecule with an active site lysine-residue (Lys_{252} of hALAD) occurs independent of any metal ions, formation of a ternary complex between the active site Cys-residues, Zn^{2+} and C_4-carbonyl oxygen and C_5-NH_2 nitrogen atoms of A-side 5-ALA are required for binding of this second molecule, followed by closure of the active-site lid and conductance of the catalytic reaction in a Knorr-type mechanism [133]. In contrast, enzymatic activity of *Wolbachia* ALAD (wALAD) was shown to be Zn^{2+}-independent, but required Mg^{2+} [270]. Dependence on binding of catalytic Mg^{2+} to the active site and/or stimulation of catalytic activity by Mg^{2+} binding to an allosteric site (Mg_c-site) has been demonstrated for a variety of other ALAD orthologs from plants, bacteria and protozoa [26, 205, 83, 148, 227]. The allosteric Mg^{2+}-binding site is located at the subunit interface of two pro-octamer dimers and the induced allosteric effect is a major stabilizer of the active octameric assembly [137]. In the crystal structure of *Pseudomonas aeruginosa* ALAD Mg^{2+} of the allosteric site was coordinated to Glu_{245} and five H_2O molecules and was revealed to induce a conformation that allows closure of the active site lid prior to catalysis [83]. The conserved glutamic acid ligand of allosteric Mg^{2+} is also conserved in wALAD, but is absent in the hALAD sequence. Whether catalytic Mg^{2+} or allosteric Mg^{2+} leads to the observed Mg^{2+}-responsiveness of wALAD has not been dissected. Instead of the Cys-rich Zn^{2+}-binding motif of hALAD, wALAD features

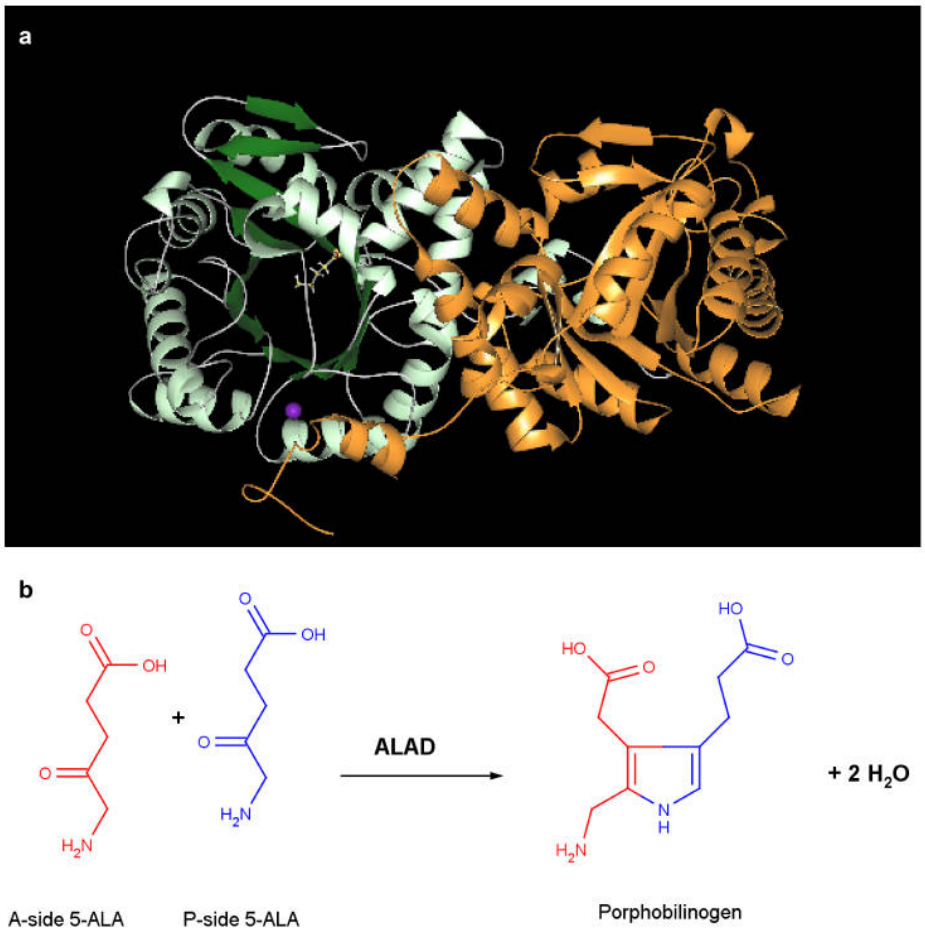

Figure 1.3: The chemical reaction catalyzed by δ-aminolevulinic acid dehydratase
a) Quaternary structure of the assymetric "hugging" dimer of *P. aeruginosa* ALAD (PDB structure 1B4K [83]) as the building block of the active octameric assembly. Secondary structure elements of the active protomer (with open active site) are shown in a ribbon diagram and are highlighted in color: β-sheets (dark green), α-helices (light green) and loops (white). Structural elements of the second inactive protomer are uniformly displayed in orange. The allosteric Mg_c-ion is displayed as a purple ball, the active site - directed inhibitor levulinic acid is displayed in ball and stick representation. The image was created using Marvin Space 5.8.1 (ChemAxon, Budapest, Hungary). **b)** The chemical reaction catalyzed by ALAD.

an aspartic acid rich sequence characteristic of Zn^{2+}-independent orthologs. Although no species-selective inhibitor of wALAD was known prior to this work, the outlined phylogenetic variations in the metal binding sites with their corresponding structural and functional differences provide the molecular basis for the development of selective inhibitors that specifically target ALAD orthologs from certain organisms. It should thus be possible to identify inhibitors of potential therapeutic significance that specifically target wALAD and interrupt heme biosynthesis in the filarial endosymbiont without affecting this essential biochemical pathway in humans.

1.9 Pyruvate Phosphate Dikinase (PPDK)

Another promising anti-*Wolbachia* drug target is the enzyme pyruvate phosphate dikinase (PPDK; E.C.2.7.9.1) [212], which is found exclusively in prokaryotes, protozoa and plants, but not in mammals. PPDK catalyzes the following reversible conversion of phosphoenol pyruvate (PEP) to pyruvate [74, 268]:

$$phosphenolpyruvate + AMP + PP_i \overset{PPDK,Mg^{2+}}{\Longleftrightarrow} pyruvate + ATP + P_i \qquad (1.1)$$

PPDK may, in principle, function both in the glyocolytic and gluconeogenetic direction, whereas mammalian cells use pyruvate kinase (PK) for glycolysis and a two-step mechanism involving the conversion of pyruvate to oxaloacetate by pyruvate carboxylase followed by conversion of oxaloacetate into PEP by PEP carboxykinase for gluconeogenesis. In glycolysis, PK catalyzes one substrate-level phosphorylation, i.e. phosphoryl transfer from PEP onto ADP creating ATP. In contrast, PPDK uses AMP and pyrophosphate as cosubstrates with PEP to catalyze a double phosphoryl transfer to AMP to form ATP with the release of orthophosphate. Consequently the latter mechanism is energetically more favourable with higher ATP-yields per glucose catabolism [177] and the small ΔG generally allows reversibility of the reaction [268]. *Wolbachia* lack 6-phosphfructokinase, an enzyme catalyzing an irreversible glycolytic reaction, but they do possess a gene encoding fructose-1,6-bisphosphatase, the corrsponding gluconeogenetic enzyme [81]. As glucose-6-phosphate utilizing enzymes are not encoded in the endobacterial genome, gluconeogenesis in *Wolbachia* likely ends with the production of fructose-6-phosphate a precursor of bacterial peptidoglycan components [81]. Despite the absence of the initial glycolytic enzymes hexokinase, phosphoglucose isomerase and 6-phosphofructokinase *Wolbachia* may simply import downstream glycolytic metabolites from the filariae in order to produce pyruvate. ^{32}P-NMR studies revealed that *B. malayi* stores high concentrations of PEP as an energy reservoir [230] that, if accessible to the endobacteria, may also be exploited by PPDK functioning in the glycolytic direction. The absence of PPDK from mammalian cells and the lack of sequence homology to PK due to its unique reaction mechanism make PPDK an excellent drug target [212].

1.10 Aim of this work

The discovery of novel chemotherapeutic options to treat lymphatic filariasis and onchocerciasis is a fundamental requirement in order to overcome resistance development against conventional antifilarial drugs and to finally eradicate these filarial diseases. Given the excellence of the *Wolbachia* endosymbiont as a target for antifilarial chemotherapy, the aim of the current study was to subject two essential enzymes of these endobacteria to a target-based drug discovery approach and to validate the potential of identified inhibitors as novel antifilarial drug candidates. The target proteins were pyruvate phosphate dikinase (PPDK), a glycolytic/gluconeogenetic enzyme without mammalian ortholog, and δ-aminolevulinic acid dehydratase (ALAD), an enzyme with substantial sequence variation from the human ortholog that catalyzes the second step of heme biosynthesis in *Wolbachia*. For both target proteins enzymatic assays were established and implemented in High-Throughput Screening against a diversity-based chemical library comprising $\sim$18,000 drug-like small molecules in order to identify novel inhibitors. Candidate inhibitors were characterised with regard to specificity and the underlying inhibitory mechanism. Eventually, using a filarial *ex vivo* culture system and a natural murine infection model employing the rodent filarial nematode *Litomosoides sigmodontis*, validated inhibitors were tested for their potency as novel antifilarial agents. Any successful candidate might open new avenues for the development of potent antifilarial drug leads that may also be applicable to other human pathogens.

Chapter 2

Materials, Methods & Preparative Experiments

The specific origin of reagents or instruments used in the experiments of this work are stated in the corresponding sections. If the source of the reagents is not mentioned, they were purchased from Sigma Aldrich (Munich, Germany) or Merck (Darmstadt, Germany). Glassware was from Schott (Mainz, Germany) or Sklarny Kavalier (Sàzava, Czech Republic).

2.1 Materials

2.1.1 Instruments and Equipment

The following standard instruments and equipment were used throughout the experimental procedures if not stated otherewise.

Centrifuges

Hettich Mikro 200 (Hettich-Zentrifugen, Tuttlingen, Germany)
Used for micro reaction tubes in DNA preparation protocols at RT

Eppendorf Centrifuge 5417R (Eppendorf AG, Hamburg, Germany)
Used for micro reaction tubes at different temperatures

Heraeus Multifuge 4KR (Heraeus Instruments, Osterode, Germany)
Used with LH-4000 rotor (75006475) for 96-well plates and 15 and 50 mL reaction tubes

Sorvall Evolution RC Superspeed Centrifuge (Thermo Scientific, Dreieich, Germany)
Used with SLC 4000 rotor for large volumes of bacterial cell cultures in 1 L centrifugation beakers.

Hettich EBA 20 (Hettich-Zentrifugen, Tuttlingen, Germany)
Used with E1624 rotor for *P. falciparum* culture

Syringes and needles

Syringes and needles used were from B.Braun Melsungen AG (Melsungen, Germany) or Beckton Dickinson S.A. (Fraga, Spain).

Syringes: Omnifix®- F 1 ml (Braun), BD Discardit II (5 mL, 10 mL, 20 mL) (BD)

Needles: Sterican 0,40 mm x 20 mm (Braun); BD Microlance^{TM} 3 0,9 mm x 40 mm

Microscopes

Leitz Diaplan Photomikroskop (Leitz, Wetzlar, Germany)

Zeiss Axioskop 50 (Carl Zeiss AG, Jena, Germany)

Leica DM IL Durchlichtmikroskop (Leica Microsystems, Wetzlar, Germany)

Pipettes and Pipettors

Pipettes were from Eppendorf (Eppendorf AG, Hamburg, Deutschland) or Gilson Inc. (Middleton, USA).

Spectrophotometer

Nanovue Plus spectrophotometer (GE Healthcare Europe, Germany)

SpectraMAX 340 Pc with analysis software SoftMax Pro (Molecular Devices, Sunnyvale, USA)

Infinite^{TM}200 NanoQuant (Tecan, Männedorf, Switzerland)

Shaker

Shaker MS2 (IKA-Werke GmbH, Staufen, Germany)

IKA KS 250B (IKA-Werke GmbH, Staufen, Germany)

Stuart mini orbital shaker SSM1 (Bibby Scientific Limited, Stone, Staffordshire, UK)

Thermo Shaker

Eppendorf Thermomixer compact (Eppendorf AG, Hamburg, Germany)

Vortex-Mixer (VWR International GmbH, Darmstadt, Germany)

2.1.2 Reagents and Solutions

All solutions were prepared with ultrapure H_2O produced with a Direct-Q® 3 UV Ultrapure (Type 1) Water System in combination with a BioPak ultrafilter for ultrapure pyrogen-free, DNAse-free and RNAse-free water (Merck Millipore, Darmstadt, Germany).

ALAD activity assay buffers

wALAD Buffer 1: 100 mM Tris (pH 8.0), 5 mM DTT, 10 mM $MgCl_2$

wALAD Buffer 2: 100 mM Tris (pH 8.0), 5 mM DTT, 1 mM $MgCl_2$

hALAD Buffer: 100 mM Tris (pH 7.5), 5 mM DTT, 10 μM $ZnCl_2$

Bacterial strains

Top 10 *E. coli*: Strain used for primary transformation of cloned genes and plasmid purification. The strain was purchased from Life Technologies (Darmstadt, Germany).

T7 Express competent *E. coli* (NEB 2566 *E. coli*): Strain used for recombinant protein expression. The strain was purchased from New England Biolabs (Ipswich, MA, USA)

BL 21 *E. coli*: Strain used for recombinant protein expression. The strain was purchased from Life Technologies (Darmstadt, Germany).

Pseudomonas aeruginosa (PA01) were kindly provided by Dr. B. Henrichfreise (Institute for Medical Microbiology, Immunology and Parasitology, Pharmaceutical Microbiology Unit, University of Bonn)

E. coli were grown on/in LB agar/bouillon (see below), *P. aeruginosa* on/in Müller-Hinton agar/bouillon (CM0405, Oxoid Limited, Basingstoke, UK). All media were prepared according to standard protocols of the Nährbodenküche in the IMMIP. Permanent cultures of bacterial strains were supplemented with 15% DMSO and kept at -80 °C.

Cell lines, cell culture media and reagents

Cell culture reagents were from PAA Lab. (Pasching, Austria) or Life Technologies (Darmstadt, Germany). Sterile plastic ware like cell culture plates (F-bottom), cell culture flasks and pipettes were from Greiner Bio-One (Frickenhausen, Germany).

LLC-MK2 cells and culture medium:
LLC-MK2 monkey kidney cells from the rhesus monkey *Macaca mulatta*) were kindly provided by S. Townson (London School of Hygiene & Tropical Medicine, UK). LLC-MK2 culture medium was Minimal Essential Medium with 10% fetal bovine serum, 2 mM L-glutamine and 1X Penicillin/Streptomycin.

HEK cells and culture medium:
Human Embryonic Kidney (HEK) cells co-transfected with Toll-Like Receptor 1/6 (HEK cells) were from Life Technologies (Darmstadt, Germany). The culture medium was Dulbecco's modified eagle medium (DMEM High Glucose, L-Glutamine) with 10% fetal bovine serum and 10 μg/mL blasticidin.

***P. falciparum* culture medium**:
P. falciparum medium 500 mL RPMI (with 25 mM HEPES, without glutamine, with phenol red)

500 μL Gentamycin

5 mL L-Glutamine

25 mg Hypoxanthin

2,5 g Albumax II (was dissolved in 50 mL of RPMI medium at 37 °C and filter sterilized before it was added to medium)

Medium was stored at 4 °C for up to 4 weeks

LB medium and agar

10 g Bacto-tryptone

5 g Bacto-yeast extract

10 g NaCl

ad 1 L

1 pellet NaOH, to adjust to pH 7, autoclave

For agar plates, 15 g agar was added to the medium and agar was poured into petri dishes

Modified Ehrlich's Reagent (MER)

1 g para-dimethlyaminobenzaldehyde

42 mL acetic acid

12 mL perchloric acid

7,3 mL 12% trichloroacetic acid

1XPBS:

137 mM NaCl

2.7 mM KCl

1 mM Na_2HPO_4 x $2H_2O$

1.76 mM KH_2PO_4

PCR Primers

T7-FW:
5'-TAA TAC GAC TCA CTA TAG GG -3'

T7-RV:
5'-GCT AGT TAT TGC TCA GCG G-3'

pALAD FW1-NheI:
5'-GCT AGC AGC TTC ACT CCC GCC-3'

pALAD RV1-XhoI:
5'-CTC GAG ACG CCC CCG TCT TAA TTG TTC T-3'

pALAD FW2-NdeI:
5'-GTC ATA TGA GCT TCA CTC CCG CC-3'

pALAD FW3-SacI:
5'-GTG AGC TCC AGC TTC ACT CCC GCC-3'

pALAD RV2-NotI:
5'-CGG CGG CCG CGA TAC GTT CGA TCT CAT-3'

pALAD RV3-XhoI:
5'-GTC TCG AGA CGC CCC CGT CTT AAT TGT TCT-3'

Tg529-Fw:
5'-GAT ATC AGG ACT GTA GAT GAA GG-3'

Tg529-Rv:
5'-GCG TCG TCT CGT CTA GAT C-3'

Tg529-probe:
5'-6-FAM-AAG CGA CGA GAG TCG GAG AGG GAG-3'-BHQ-1

MM-bactin-FW:
5'-GAT GAG ATT GGC TTT A-3'

MM-bactin-RV:
5'-AAC CGA CTG CTG TCA CCT TC-3'

LsFtsZ-FW:
5'-CGA TGA GAT TAT GGA ACA TAT AA-3'

LsFTsZ-RV:
5'-TTG CAA TTA CTG GTG CTG C-3'

LsFTSZ-probe:
5'-6-FAM-CAG GGA TGG GTG GTG GTA CTG GAA-3'-TAMRA

LsActin-FW:
5'-ATC CAA GCT GTC CTG TCT CT-3'

LsActin-Rv:
5'-TGA GAA TTG ATT TGA GCT AAT G-3'

LsActin-probe:
5'-HEX-ACT ACC GGT ATT GTG CTC GAT T-3'-TAMRA

PPDK activity assay buffer

PPDK Buffer: 250 mM imidazole, 100 mM NH_4Cl, 50 mM $MgCl_2$, pH 6.3

PPDK-PBS Buffer: 1x PBS, 100 mM NH_4Cl, 1 mM $MgCl_2$, pH 7.1

Protein purification buffers

Lysis Buffer: 100 mM Tris-HCl (pH 8.0), 300 mM NaCl, 10 mM imidazole

Wash Buffer: 100 mM Tris-HCl (pH 8.0), 300 mM NaCl, 50 mM imidazole

Elution Buffer: 100 mM Tris-HCl (pH 8.0), 300 mM NaCl, 25 mM imidazole

Pyruvate Detection Reagent (PDR)

2 N HCl (5 parts)

0.167% 2,4-dinitrophenylhydrazine in 1 N HCl (1 part)

S.O.C. medium

10 g Bacto-tryptone

5 g Bacto-yeast extract

5 g NaCl

10 mM $MgSO_4$ glycerol

10 mM $MgCl_2$

ad 1 L with H_2O

adjust pH to 7.0 with NaOH, autoclave

filter sterilize and add glucose to 20 mM final concentration

10X TBE-Buffer:

108 g Tris base

55 g boric acid

9.3 g Na_2EDTA x $2H_2O$

ad 1 L with H_2O

TE-Buffer:

10 mM Tris (pH 7.5)

1 mM EDTA

2.2 Methods

2.2.1 Agarose gel electrophoresis

PCR products and plasmids were analyzed by agarose gel electrophoresis. 1% Agarose gels (Biozym LE Agarose (Biozym Scientific GmbH, Hessisch Oldendorf, Germany) were cast in 0.5% TBE buffer and the DNA-stain Safe Red ™ (Applied Biological Materials Inc., Richmond, BC, Canada) was added at a 1:2000 dilution. Samples were mixed with 6x Gel Loading Dye Blue before application on the gel (New England Biolabs, Ipswich, MA, USA) and 5 μL of a 1 kb DNA ladder (New England Biolabs, Ipswich, MA, USA) was added for reference of band sizes. For standard analytical gels 10 - 30 ng of DNA or 5 - 20 μL PCR product was loaded per sample. For preparative gels the entire PCR product was loaded. Standard gels were run at 120 V for 45 min before DNA-bands were visualised using a Biometra UV solo gel documentation chamber (Biometra, Göttingen, Germany). Bands from preparative gels were viewed and excised on a Biometra UV-transilluminator FLX-20M (Biometra) and DNA was purified using the Invisorb® Spin DNA extraction/Fragment CleanUp kit (STRATEC Molecular GmbH, Berlin, Germany).

2.2.2 Polymerase Chain Reactions (PCR)

All reagents used for PCR were from Qiagen (Hilden, Germany), Fermentas (St. Leon-Rot, Germany), Finnzymes (Vantaa, Finland) or New England Biolabs (Ipswich, MA, USA). Primers were ordered from Biolegio (Nijmegen, The Netherlands).

Phusion Taq PCR

Standard PCR reactions for amplification of gene fragments were carried out using the following standard protocol. Primers were kept in TE-Buffer and used from 10 μM stocks.

	Final concentration	Volume [μL]
5x Buffer HF	1x	4
Fw Primer [10 μM]	500 nM	1
Rv Primer [10 μM]	500 nM	1
dNTP mix [10 mM]	200 μM	0.4
Phusion Taq [2U/μL]	0.02 U	0.2
DNA		1 - 2
H_2O		ad 20

In order to determine optimal annealing temperatures a temperature gradient PCR was run on the iCycler (Bio-Rad Laboratories GmbH, München, Germany). Regular PCR reactions were carried out on a MWG Biotech Primus 96 plus thermocycler (MWG Biotech AG, Ebersberg, Germany).

Cycling protocol:

1.	Denaturation	98 °C	5 min
2.	Amplification cycles: 35		
	a Denaturation	98°C	10 s
	b Annealing	50 °C - 72 °C	20 s
	c Amplification	72 °C	1 min
3.	Last amplification step	72 °C	10 min
4.	Cool down to	8°C	

Colony PCR

The success of cloning procedures was verified directly after colony growth by colony PCR. Single colonies were picked with a loop, streaked out on a fresh agar plate and the loop was inserted into 20 μL H_2O. Bacteria in the resulting suspension were lysed by heating for 10 min to 95 °C and the lysate was directly used as a template for PCR. Clones were analysed by both amplification with the specific and the T7 primer set.

	Final concentration	Volume [μL]
5x Buffer HF	1x	4
Fw Primer [10 μM]	500 nM	1
Rv Primer [10 μM]	500 nM	1
dNTP mix [10 mM]	200 μM	0.4
Phusion Taq [2U/μL]	0.02 U	0.2
Colony lysate		5
H_2O		ad 20

Realtime Polymerase Chain Reactions (Realtime-PCR)

Realtime-PCR reactions were run on a Rotorgene RG-3000 or 6000 (Corbett Life Sciences, Germany). Fluorescence was measured on the FAM channel (excitation at 470 nm; detection at 510 nm) for SYBR Green and FAM-labeled Taqman®-probes. Data analysis was done using Rotorgene 6 software (Qiagen, Hilden, Germany).

Quantification of *T. gondii* by Realtime-PCR *T. gondii* were quantified by Realtime-PCR amplification using a primer set and Taqman probe specific for a 529 bp *T. gondii*repeat DNA sequence (GenBank: AF146527.1). SYBR Green based Realtime-PCR of the *Macaca mulatta β-actin* gene was run separately for normalization on sample DNA-content and the number of LLC-MK2 feeder cells: For each sample ΔCt (Mm-β-actin) values were subtracted from ΔCT (*T.gondii*) to give ΔΔCt values indicative of the *T.gondii*/LLC-MK2 cell ratio. For calculation of the amplification efficiency of PCR reactions standard curves (10-fold dilution rows) of DNA from non-infected LLC-MK2 cells (β-actin PCR) or from the 1% DMSO-treated infected LLC-MK2 (*T.gondii* PCR) were measured.

Protocol for (Mm-*β-actin*) PCR:

Mm-β-actinPCR	Final concentration	Volume [μL]
10X PCR Buffer (incl. 15 mM $MgCl_2$)	1X	2
$MgCl_2$ [25 mM]	1.5	1.2
MM-bactin-FW [5 μM]	300 nM	1.2
MM-bactin-RV [5 μM]	300 nM	1.2
dNTP mix [10 mM]	50 μM	0.1
SYBRGreen I dye		0.2
HotStar Taq [5 u/μL]	0.5 u	0.1
DNA		2
H_2O		12

	Mmβ-actin PCR		
1.	Denaturation	95 °C	15 min
2.	Amplification cycles: 45		
	a Denaturation	94 °C	15 s
	b Annealing	58 °C	20 s
	c Amplification	72 °C	20 s
3.	Melting curve	59 °C - 95 °C	

Protocol for (*T. gondii*) PCR:

***T.gondii* PCR**	Final concentration	Volume [μL]
10X PCR Buffer (incl. 15 mM $MgCl_2$)	1X	2
$MgCl_2$ [25 mM]	2.5	2
Tg529-FW [100 μM]	300 nM	0.06
Tg529-RV [100 μM]	300 nM	0.06
Tg529-probe [5 μM]	50 nM	0.2
dNTP mix [10 mM]	50 μM	0.1
HotStar Taq [5 u/μL]	0.5 u	0.1
DNA		2
H_2O		13.48

	***T.gondii* PCR**		
1.	Denaturation	98 °C	15 min
2.	Amplification cycles: 45		
	a Denaturation	95 °C	10 s
	b Amplification	60 °C	30 s

Data was acquired on the FAM (excitation at 470 nm, detection at 510 nm) for both PCR reactions.

Quantification of *Wolbachia ftsZ* copy-numbers in *L. sigmodontis* *L. sigmodontis Wolbachia* were determined by amplifying the *Wolbachia ftsZ* and *L. sigmodontis-actin* gene by Duplex Realtime-PCR using Taqman® probes. These PCR experiments were physically performed by Katharina Gorski-Rzepinski.

PCR protocols were as follows:

***Wolbachia ftsZ/LsActin* Duplex Realtime PCR**	Final concentration	Volume [μL]
Qiagen's Quantitect Multiplex NoROX Mastermix	1X	10
nuclease-free H_2O		4.1
LsFtsZ-FW [10 μM]	500 nM	1.0
LsFtsZ-RV [10 μM]	500 nM	1.0
LsFtsZ-probe [5 μM]	25 nM	0.1
LsActin-FW [10 μM]	400 nM	0.8
LsActin-RV [10 μM]	400 nM	0.8
LsActin-probe [5 μM]	50 nM	0.2
DNA		2

	***Wolbachia ftsZ/LsActin* Duplex Realtime PCR**		
1.	Denaturation	98 °C	15 min
2.	Amplification cycles: 45		
	a Denaturation	95 °C	15 s
	b Amplification	58 °C	45 s

Data was acquired on the FAM (excitation at 470 nm, detection at 510 nm, gain 10) and JOE channels (excitation at 530 nm, detection at 557 nm, gain 10) to measure 6-FAM fluorescence and HEX fluorescence, respectively. For calculation of *Wolbachia ftsZ* and *LsActin* gene copy numbers, data was normalized on adjusted standard curves for plasmids containing *Wolbachia ftsZ* or *LsActin* genes, respectively. As the performance of this Duplex PCR is very reliable, single plasmid concentration samples were included in the PCR run and a previously recorded standard curve was imported and adjusted to the measured sample.

2.2.3 Cloning

The *P.aeruginosa* ALAD (pALAD) gene was cloned into the pET-21b plasmid vector (Novagen, Merck Chemicals, Darmstadt, Germany) after sequential restriction digest, 5'-dephosphorylation and ligation. Reagents used were from New England Biolabs (Ipswich, MA, USA) unless stated otherwise. Both amplified PCR product and plasmid vectors were restriction digested in the following reaction mixture:

DNA (PCR product or plasmid)	∼500 ng
100X BSA	0.2 μL
10X Buffer 4	2 μL
XhoI	1 μL
NdeI	1 μL
H_2O	ad 20 μL

After incubation at 37 °C for 1 h, restriction enzymes were heat-inactivated for 20 min at 65 °C and DNA was purified using the MinElute PCR purification Kit (Qiagen, Hilden, Germany).

In order to minimize religation of the digested plasmid, only the restricton digested (RD) plasmid DNA was subjected to 5'-dephosphorylation using Antarctic Phosphatase and maximal amounts of DNA.

RD-pET-21b	13 μL (∼150 ng)
10X Phosphatase Buffer	2 μL
H_2O	4 μL
Antarctic Phosphatase	1 μL
Total volume	20 μL

Reactions were incubated for 15 min at 37 °C for efficient dephosphorylation before Antarctic Phosphatase was heat-inactivated at 65 °C for 5 min.

Ligation mixtures were prepared using a 3:1 molar ratio of the 1.1 kb RD-PCR-product (∼30 ng) to the 5.4 kb dephosphorylated RD-pET21b vector (50 ng) in a 10 μL reaction volume. 10 μL 2X Ligase Buffer and 1 μL Quick Ligase were added and the reaction incubated for 10 min at RT.

The ligated pALAD-pET-21b plasmid was then transformed into Top 10 $CaCl_2$-competent *E. coli*. 10 μL of ligation mix was added to a 1.5 mL tube containing 200 μL competent cells thawed on ice and the mixture was mixed by gentle tapping of the tube. After 30 min incubation on ice, cells were heat-shocked for 30 s at 42 °C and immediately placed on ice for 5 min. 600 μL S.O.C. medium equilibrated

to room temperature was added and bacteria were allowed to grow for 60 min at 37 °C, shaking at 150 rpm. Different volumes of transformation mix (50 - 200 μL) were then spread out on a LB-selection agar plates containing 50 μg/mL ampicillin and incubated overnight at 37 °C.

A detailed overview on the pALAD cloning strategy and the corresponding results is given below in the **Preparative experiments** (**Section 2.3**).

2.2.4 Plasmid and genomic DNA preparations

For plasmid purification single bacterial colonies were inoculated into 10 mL selection medium and grown overnight at 37 °C and 150 rpm. The next day bacterial cells were pelleted, lysed and the plasmids purified with the Qiagen Miniprep Kit (Qiagen, Hilden, Germany) according to the manufacturer's protocols.

For *P. aeruginosa* DNA preparation a single colony was inoculated into 4 mL Müller-Hinton-Bouillon (CM0405, Oxoid Limited, Basingstoke, UK) in a 14 mL polypropylene snap cap tube (greiner bio-one, Frickenhausen, Germany) and incubated overnight at 37 °C, 150 rpm. The next day bacterial cells were pelleted, lysed and the plasmids purified according to the "*Protocol for cultured cells*" of the Qiagen DNA Mini Kit.

DNA from *T. gondii* parasites and LLC-MK2 feeder cells was purified from trypsinized cells using the QIACube for fully automated sample preparation using the "*DNA Purification from Blood or Body Fluids (Spin Protocol)*" of the Qiagen DNA Mini Kit.

DNA from single *L. sigmodontis* worms was extracted by Katharina Gorski-Rzepinski using reagents of the Qiagen DNA Mini Kit in a modified protocol. In brief, worms were digested in 180 μL Buffer ATL plus 20 μL Proteinase K at 56 °C over night. Samples were supplemented with 200 μL buffer AL and incubated at 70 °C for 10 min. 200 μL 100% ethanol were added, the tube was quickly vortexed and the lysate was transferred to the wells of a 96-well filter plate (Binding plate, Promega, Madison, WI, USA). The plate was placed into a vacuum filter device (Vac-Man® 96 Vacuum manifold, Promega) and the samples subjected to vacuum filtration. Each well was successively washed with 1 mL of buffer AW1 and AW2. When all remaining liquid had been sucked off by the vacuum after 5 min, the plate was centrifuged at 4,400 rpm at RT (Heraeus Multifuge 4KR with LH-4000 rotor) and residual ethanol was allowed to evaporate (5 min at RT). DNA was dissolved by the addition of 50 μL buffer AE. After 5 min DNA was eluted under vacuum for 5 min into a clean 96-well plate (Brand, Wertheim, Germany).

2.2.5 DNA sequencing reactions

Sequences of the cloned inserts within the expression plasmids were verified by sequencing. Samples were prepared containing 0.3 -0.7 ng plasmid and 20 pmol primer in 7 μL volume and sent to Seqlab (SEQLAB Sequence Laboratories Göttingen GmbH, Göttingen, Germany) for Extended Hot Shot sequencing. pET-21a and pET-21b vectors featured a T7 promotor upstream of the multiple cloning site and cloned inserts were flanked by the T7 promoter and T7 terminator binding sites. Each clone was sequenced in two different reactions in both directions in two different reactions with either T7 promoter or T7 terminator primer.

2.2.6 Recombinant protein expression

pET-21a-based expression plasmids containing the *hemB* gene (ALAD) sequence from *Wolbachia* of *Brugia malayi* (wALAD) and a cDNA-derived human sequence

(hALAD) were kindly provided by Dr. Barton Slatko (New England Biolabs, Ipswich, MA, USA).

The expression plasmids for wALAD, hALAD or pALAD were transformed into T7 Express competent *E. coli* (High Efficiency) (C2566; New England Biolabs) or $CaCl_2$-competent BL21 *E. coli* according to the manufacturer's protocol. Bacteria were grown in standard LB-medium and on LB-agar plates and growth of pET-vector-positive cells were selected with 50 μg/mL Ampicillin. pALAD and wALAD plasmids were co-transformed with the pRIL plasmid (Stratagene, now Agilent Technologies, Heilbronn, Germany) encoding additional arginine, leucine and isoleucine tRNAs that are rare in *E. coli*. The corresponding selection media contained additionally 20 μg/mL Chloramphenicol.

For recombinant ALAD protein expression single colonies of successfully transformed bacteria were inoculated into 8 mL of selection medium in 14 mL polypropylene snap cap tubes (Greiner-bio one, Frickenhausen, Germany) and incubated overnight at 36 °C, 150 rpm. The next morning cultures were diluted 1:100 to 1:1000 in 500 mL selection media in 2 mL culture flasks and grown until OD_{600nm} of 0.1 - 0.2 at 36 °C and further until OD_{600nm} 0.5-0.6 at RT. Optical density of 1 mL aliquots from the bacterial cultures were measuerd with a Fisher Scientific Cell density meter (Thermo Scientific, Dreieich, Germany). wALAD expression protocol was adapted from Wu et al. [270] and optimized: Starting with an 8h culture at 37 °C, the culture was diluted 1:250 into 500 mL medium in 2L flasks. Cultures were grown at RT and 150 rpm until OD_{600nm} 0.5-1.0 was reached.

Protein expression was induced by the addition isopropyl Isopropyl-β-D-thiogalactoside (IPTG; Fermentas, Thermo Scientific, St. Leon-Rot, Germany) for 24 h at 23 °C. IPTG concentrations were 6.25 μM for wALAD and 100 μM for hALAD and pALAD. Bacterial cells were harvested by centrifugation at 6000 rpm, at 4 °C for 10 min on a Sorvall Evolution RC Superspeed Centrifuge with SLC 4000 rotor (Thermo Scientific, Dreieich, Germany). Resulting cell pellets were frozen at -80 °C before they were thawed and resuspended in 10 mL Lysis Buffer per 500 mL of initial cell culture. 30 min incubation on ice in the presence of 0.36 mg/mL Chicken Egg White Lysozyme and 1u/mL Benzonase® nuclease ensured breaking-up of the bacterial cell-wall and digestion of genomic DNA before cells were lysed by repetitive sonification, 6x 10 s followed by 1 min on ice with a Bandelin sonopuls HD 3100 (Bandelin, Berlin, Germany). Lysates were centrifuged for 30 min at 4400 rpm (Heraeus Multifuge 4KR with LH-4000 rotor) at 4°C and supernatants were incubated with 1 mL Ni^{2+}-NTA-Agarose (Qiagen, Hilden, Germany) per 10 mL supernatant for at least 2 h at 4° on a rotating wheel (Dynal® sample mixer, Life technologies, Darmstadt, Germany) before the sample was applied onto a polypropylene column (Qiagen, Hilden, Germany). The Ni^{2+}-NTA-Agarose was washed with excess Wash buffer containing intermediate imidazole concentration (50 mM) before the protein was eluted in six 1 mL fractions with Tris-based Elution buffer containing high imidazole concentration (250 mM). wALAD pellets obtained after centrifugation of lysates were resuspended in Lysis buffer, centrifuged and the supernatant subjected to protein purification with Ni^{2+}-NTA-Agarose.

At each purification step aliquots were taken and protein concentrations determined by Bradford assay. All samples were analyzed on a 12% SDS-gel with subsequent Coomassie blue staining in order to verify the success of recombinant protein expression and the purification procedure. Glycerol was added to the purified protein samples to a final concentration of 10% and protein concentrations were determined as described below. While hALAD protein was stable at 4 °C for several months, pALAD and wALAD were kept at -80 °C for long-term storage.

A detailed overview on the protein purification and corresponding results is given below in the **Preparative experiments** (**Section 2.3**).

Protein concentration measurements

Bradford assay For samples with unknown protein composition the overall protein concentration was measured using the BIO-RAD Protein Assay with BIO-RAD Protein Assay Standard II Bovine Serum Albumin (Bio-Rad Laboratories GmbH, München, Germany). 3 μL per protein sample or BSA standard were transferred to the wells of a 96-well assay plate and 150 μL of a 1:5 dilution of Assay Reagent. Protein concentrations were calculated on the basis of photometrically determined OD_{595nm} measurements with Softmax Pro software (see "Spectrophotometers" in **Section 2.1.1**).

OD_{280nm} measurements $OD_{280\ nm}$ measurements were done with the NanoVue spectrophotometer listed above. Protein concentrations were calculated from primary absorption measurements with the use of specific extinction coefficients of the proteins. Specific extinction coefficients were calculated on the basis of protein sequences fed into the protparam tool of the ExPASy Bioinformatics Resource Portal (http://web.expasy.org/protparam/).

2.2.7 SDS-PAGE

Protein samples for denaturing polyacrylamide gel electrophoresis (SDS-PAGE) were mixed with 5X SDS-Loading Buffer. The protein was denatured by 10 min incubation at 95 °C. 5 μL Roti®Mark Protein standard was used for band reference. Polymerization of the gels were started by addition of 0.1% APS + 0.1% TEMED or 0.06% APS + 0.4% TEMED for resolving and stacking gels, respectively. Protein gels were cast using a Mini Protean® Tetra system (Bio-Rad Laboratories GmbH, München, Germany).

5X SDS-Loading Buffer:

2.5 mL Upper SDS-gel buffer
1 g sodium dodecyl sulfate (SDS)
100 mg DTT
5 mL glycerol
8 μg bromophenol blue
ad 1 L with H_2O, heat to 95 °C to dissolve

Upper SDS-gel Buffer(4X; pH 6.8):

0.5 M Tris base
0.4% SDS
ad 1 L with H_2O, adjust to pH 6.8

Lower SDS-gel Buffer(4X; pH 8.8):

1.5 M Tris base
0.4% SDS
ad 1 L with H_2O, adjust to pH 8.8

10X SDS Running Buffer:

121 g Tris base
179 g Tricine
10 g SDS
ad 1 L with H_2O

Running conditions: 110 V for 10 min, then at 180 V for 35 min.

2.2.8 Coomassie blue protein staining

Gels were stained with Coomassie blue (0.05% Coomassie Brilliant Blue R, 50% methanol, 10% acetic acid) under gentle shaking for 20 min. Gels were destained in 30% methanol for 2 h to overnight and the gel was scanned with a ScanMaker i900 Scanner (Microtek, Germany).

2.2.9 Native PAGE

Non-denaturing polyacrylamide gel electrophoresis (Native PAGE) was used to analyze oligomeric assemblies of ALAD proteins. Gels were cast using a Mini Protean® Tetra system (Bio-Rad Laboratories GmbH, München, Germany). Samples were prepared using 5 - 8 μg protein and different concentrations of $ZnCl_2$, $MgCl_2$, DTT, 5-ALA and wALADin1 in 1X Loading buffer. After preincubation at RT for 30 min (if not indicated otherwise) samples were loaded onto a 7.5% polyacrylamide gel (Rotiphorese-Gel 30 T:C 37,5:1). Polymerization of the gels were started by addition of 0.1% APS + 0.1% TEMED or 0.06% APS + 0.4% TEMED for separating and collecting gels, respectively.

1X Native Page Running Buffer:

25 mM tris (pH 8.8)

80 mM glycine

4X Gel Buffer:

112 mM tris

112 mM sodium acetate

adjust to pH 6.5

2X Native Page Sample Buffer:

0.2 M Tris-HCl (pH 8.8)

40% glycerol,

0.005% bromophenol blue

Running conditions: 50 V, 25 mA at 4 °C for 3-7 h.

2.2.10 In-gel ALAD activity assay

After non-denaturing gel electrophoresis, gels were soaked in Activity Buffer (100 mM Tris (pH 8.0), 10 mM $MgCl_2$, 5 mM DTT and 0.5 mM 5-ALA) and incubated at 37 °C for 30 min - 2 h. The gel was then transferred into Modified Ehrlich's Reagent (MER), quickly rinsed in H_2O and the gel was scanned with a ScanMaker i900 Scanner (Microtek, Germany). Image contrast was adjusted using Adobe Photoshop Elements 3.0 (Adobe Systems, Munich, Germany).

2.2.11 Dialysis of proteins

Proteins were dialyzed for buffer exchange using Slide-A-Lyzer Dialysis 3,5K MWCO cassettes of different volumes (Pierce, Thermo Scientific, München, Germany). Standard dialysis procedures were done overnight at 4 °C. The samples were dialyzed against excess buffer (at least 500X). When a very efficient dilution of sample buffer components was required the dialysis buffer was exchanged after 2 h of dialysis.

2.2.12 High-Throughput screening

Compounds of the chemical library containing of ∼18,000 drug-like small molecules (courtesy of Prof. Famulok, Chemical Biology and Medicinal Chemistry Unit, LIMES-Institute, Bonn, Germany), were used as working solutions at a concentration of 1 mM in DMSO. These screening compound plates had originally been filled by diluting the compounds from a 10 mM stock solution. A liquid-handling workstation (Freedom EVO, Tecan, Männedorf, Germany) was employed to pipet the reaction mixture of both screening assays. Clear flat-bottom 96-well plates (Brand GmbH, Wertheim, Germany) were used as assay plates in the screening procedure.

While the first eleven columns per plate were filled with test compounds, the 12^{th} column was used for positive (DMSO, protein, substrate) and negative control (DMSO, protein, water) of the reaction which were used to calculate Z'-factors [274] (see **Equation 2.1**) for each plate with σ_{c+} and σ_{c-} being the standard deviation of the positive control or negative control, respectively, and μ_{c+} and μ_{c-} being the corresponging mean.

$$Z' = \frac{3\sigma_{c+} + 3\sigma_{c-}}{|\mu_{c+} - \mu_{c-}|} \tag{2.1}$$

2.2.13 Chemical compounds and compound handling

wALADin1 and derivatives were synthesized by V. Halls and Dr. J. Hannam at the LIMES Institute. wALADin derivative **4** and wALADin2 were custom synthesized by Hit2Lead.com (ChemBridge Corporation, San Diego, CA, USA). Other compounds were purchased from ChemBridge or Enamine (Kiev, Ukraine). The final compounds were aliquotted and stored at -20 °C. Aliquots were then dissolved in 100% DMSO to give the desired concentrations (standard: 10 mM).

2.2.14 PPDK functional assays

PPDK-DNPH assay/ HT-Screening

This PPDK activity assay is based on the detection of the reaction product pyruvate by reaction with 2,4-dinitrophenylhydrazine (DNPH) to a coloured hydrazone and was employed for HT-Screening of inhibitors. The final reaction volume was 80 μL and the mixture was pipetted in the following steps:

Reaction scheme	Volume	Final concentration
1. DMSO/ compound	3 μL	37.5 μM
2. Protein in 2X PPDK-PBS buffer	40 μL	100 nM
3. Substrate mix	37 μL	

	Positive control	Negative control
AMP	200 μM	200 μM
PEP	200 μM	
PP_i	500 μM	500 μM

The reaction mixture was incubated for 50 min at RT, until the assay was stopped by the addition of 120 μL Pyruvate Detection Reagent (PDR). After another 10 min incubation at RT OD_{395nm} of the plate was measured. The initial hit-threshold during HT-Screening was chosen to be ± 3SD (60% inhibition). The 20 top hits were obtained from stock solutions and were rescreened in duplicates. Confirmed hits that were further validated in dose-response curves and control experiments.

Coupled PPDK-LDK assay

The reaction of PEP to pyruvate as catalysed by PPDK is coupled to lactic acid dehydrogenase (LDH) from rabbit muscle (L1254, Sigma). The conversion of pyruvate to lactate goes along with the oxidation of $NADH/H^+$ to NAD^+, and thus a decrease of $NADH/H^+$ at absorption at 340 nm can be measured spectrometrically in real time during the course of the reaction.

Reactions were set up in clear flat-bottom 96-well plates (Brand, Wertheim, Germany) as follows:

Reaction scheme	Volume	Final concentration
1. DMSO/ compound	3 μL	37.5 μM
2. Protein mix	40 μL	
PPDK		100 nM
LDH (1 u/μL)		0.006 u/μL
3. Substrate mix	37 μL	

The composition of the substrate solutions were as follows:

	Positive control	Negative control
AMP	500 μM	500 μM
PEP	500 μM	
PP_i	2000 μM	2000 μM
$NADH/H^+$	200 μM	200 μM

Immediately after addition of substrate, the plate was inserted into the spectrophotometer and the OD_{340nm} was read for up to 60 min. Slopes of the substrate turnover were calculated by linear regression over the linear phase of the reaction (including a lag time of 1-4 min).

2.2.15 Pyruvate Kinase assay

Pyruvate Kinase from rabbit muscle (P1506, Sigma) was used as a control assay for the specificity of PPDK inhibitory compounds. The general experimental protocol was as described for the PPDK-DNPH Assay. Instead of PPDK, 0.156 mu/μL Pyruvate Kinase was used and substrate solution contained 200 μM ADP instead of AMP/PP_i. The reaction was stopped by the addition of 120 μL PDR solution in the linear phase after 10 min.

2.2.16 wALAD Assay and High-Throughput Screening

The wALAD reaction mixture was pipetted in three steps (2 μL compound, 23 μL protein-buffer mix, 30 min pre-incubation, 5 μL substrate) with a final reaction volume of 30 μL. The final concentration of the reagents were 67 μM compound, 6.7% DMSO, wALAD, 200 μM 5-Ala in 100 mM Tris (pH 8.0) with 5 mM DTT and 10 mM $MgCl_2$. Assay plates were sealed, shortly spun down and incubated at 36 °C for 20 min. The reaction was stopped by the addition of 200 μL Modified Ehrlich's Reagent (MER) per well. After 10 min incubation at room temperature, absorption was read at 555 nm.
The primary hit threshold was an inhibition exceeding 3 standard deviations (35% inhibition) of the DMSO-control. All primary hits were rescreened in duplicate. In order to focus on high potency hits, the hit threshold for confirmed hits in the rescreen was set to 50% inhibition. Hit validation was completed by dose-response curve and specificity tests and were done with fresh compound from stock solutions.

Purity and identitiy of validated hit compounds were kindly verified by HPLC and MS-analysis done by K. Rothscheidt at the LIMES-Institute.

2.2.17 ALAD IC_{50} assays of different orthologs

The general ALAD assay setup was as described for wALAD High-Throughput Screening assay. IC_{50} determinations were performed manually using different concentrations of the respective proteins under optimal buffer conditions. Besides the already mentioned orthologs from *Wolbachia* (wALAD), *H. sapiens* (hALAD) and *P. aeruginosa* (pALAD), other orthologs were from *Escherichia coli* (EcALAD), *Pisum sativum* (PsALAD), *Vibrio cholerae* (VcALAD) and *Yersinia enterocolitica* (YeALAD). $MgCl_2$ concentration was kept constant at 1 mM for all Mg-stimulated orthologs, $ZnCl_2$ was kept at 10 μM, 5-aminolevulinic acid was 200 μM. Protein concentration and assay time were chosen such that the enzymatic reaction was stopped in its linear phase and that subtrate turnover did not exceed 30%.

Ortholog	Protein concentration	Buffer	Incubation time
wALAD	500 nM	100 mM Tris (pH 8.0), 1 mM $MgCl_2$, 5 mM DTT	20 min
hALAD	250 nM	100 mM Tris (pH 7.5), 10 μM $ZnCl_2$, 5 mM DTT	20 min
pALAD	60 nM	100 mM Tris (pH 8.0), 1 mM $MgCl_2$, 100 mM KCl	10 min
EcALAD	200 nM	100 mM BTP (pH 8.1), 1 mM $MgCl_2$, 10 μM $ZnCl_2$, 5 mM DTT	10 min
PsALAD	300 nM	100 mM BTP (pH 8.5), 1 mM $MgCl_2$, 5 mM DTT	15 min
VcALAD	125 nM	100 mM BTP (pH 8.0), 1 mM $MgCl_2$, 5 mM DTT, 100 mM KCl	10 min
YeALAD	150 nM	100 mM BTP (pH 8.0), 1 mM $MgCl_2$, 5 mM DTT, 100 mM KCl	10 min

Substrate concentration rows (65 μM - 16.7 mM 5-ALA) in the presence of different concentrations of wALADin1 (0 - 100 μM) were recorded for type-of-enzymatic-inhibition studies. Graph Pad Prism 5.0 (GraphPad Software, SanDiego, USA) was used for non-linear regression of the primary data using the "Allosteric sigmoidal" algorithm and for the generation of linear Eadie-Hofstee representations.

Mg^{2+}-response curves (0 - 5 mM) were recorded in the presence of wALADin1 (0 - 100 μM) applying 500 nM wALAD, 200 μM 5-ALA in order to assess Mg^{2+}-dependency of wALADin1 inhibition.

2.2.18 Solubility measurements

wALADin1

The UV-VIS absorbance spectrum of wALADin1 from 200 to 700 nm was measured using the NanoVue spectrophotometer in assay buffer with 1% DMSO. As a reference the absorption spectrum of a 1%DMSO solution in assay buffer was measured and subtracted from the wALADin1 absorption curve. For solubility measurements, different concentrations of wALADin1 were added to assay buffer and incubated at

RT for > 30 min. Samples were then centrifuged for 5 min at 16,000 rpm (Eppendorf 5417R centrifuge, maximum speed) in order to pellet all crystallized compound, if any. The supernatant was transferred to another tube and the absorption at the wALADin1 peak absorption wavelengths was measured. For high wALADin1 concentrations the absorption was measured in the slope region of the absorption curve in order to prevent saturated OD values > 1.

PPDKin1

Samples were prepared as described for wALADin1 with the difference that compounds were dissolved in H_2O or PPDK-PBS buffer with a final DMSO concentration of 3.75%. Solutions were incubated at RT for 24 h before precipitated compound was pelleted by centrifugation at maximum speed in a table-top centrifuge for 5 min.

2.2.19 Thermal Shift Assay

Protein thermal melting curves were measured as a function of fluorescence intensity of the environmentally-sensitive dye Sypro®Orange on a Rotorgene RG-3000 (Corbett Life Sciences, Germany). Protein samples were gradually denatured by increasing the temperature from 27 °C up to 99 °C at a heating rate of 0.5 °C/ 30 s. Fluorescence of Sypro®Orange was excited at 470 nm and detected at 510 nm. Raw data were subjected to 1^{st} derivative analysis of Rotorgene 6 software (Qiagen, Germany). Visualizations were done with Graph Pad Prism 5.0.

ALAD and wALADin1

Samples were prepared for 5 μM (0.2 mg/mL) wALAD in 1 M Tris pH 8.0, 5 mM DTT, 1mM $MgCl_2$, different concentrations of wALADin1, derivatives or 1% DMSO as control and 8-16X Sypro®Orange in a final volume of 20 μL. Control protein concentrations of hALAD, Chicken Egg White Lysozyme and BSA were 0.2 mg/mL, 3 mg/mL and 0.5 mg/mL, respectively. All samples were prepared in triplicates.

2.2.20 Cell culture

General cell culture protocols

LLC-MK2 cells or HEK cells were grown in 75 cm^2 culture flasks with 12 mL of the respective culture media. Cells were split 1:4 every 7 days at 90-100% confluency and the medium was exchanged after 3-4 days of culture. To harvest the cells the old medium was aspirated, the cell lawn washed in an equivalent volume of prewarmed PBS, and cells were incubated in 2 mL 1X Trypsin/EDTA for 3-5 min at 37 °C. Cells were completely detached by the addition of 10 mL culture medium and vigorous pipetting up and down along the bottom of the flask.
All cell culture work was performed under a class II safety cabinet BIOWIZARD (Kojair Tech Oy, Vilppula, Finland). Non-sterile reagents used in cell culture experiments were filtered through a 0.2 μM Cellulose Acetate Filter (VWR International GmbH, Darmstadt, Germany) or autoclaved.

Freezing and thawing

LLC-MK2 cells were grown to confluency in a 75 cm^2 flask that was distributed into 4 cryotubes of frozen cells. Cells were detached by standard Trypsin/EDTA

treatment, centrifuged (5 min, 1200 rpm, 4 °C, Heraeus Multifuge 4KR with LH-4000 rotor) and resuspended in 3 mL standard culture medium. Another 3 mL of ice-cold culture medium containing 20% DMSO was then added dropwise to the cells. Cryotubes were placed in a freezing container (Mr. Frosty ®, Thermo Scientific, Dreieich, Germany) filled with isopropanol and frozen at -80 °C.

For new cultures, the cells were quickly thawed from -80 °C and pelleted (5 min, 1200 rpm, 4 °C, Heraeus Multifuge 4KR with LH-4000 rotor). The DMSO-containing freezing medium was discarded and cells were resuspended in pre-warmed culture medium. Cells were cultivated in 25 cm^2 culture flasks. HEK cells were treated in an equivalent manner but were frozen in liquid nitrogen and were thawed according to the same protocol.

2.2.21 Cytotoxicity assays

50,000 HEK cells or 25,000 LLC-MK2 cells, respectively, were seeded out in 100 μL medium on a flat-bottom 96-well plate and incubated at 37 °C, 5% CO_2 overnight. The next day the medium was replaced by 200 μL filter-sterilized culture medium containing 15.6 μM - 1 mM compound or 1% DMSO as a 100% viability control. As a 0% viability control cells from dried out wells were used. After 48 h incubation (37 °C, 5% CO_2) 20 μL of sterilized 5 mg/mL Thiazolyl Blue in PBS was added for 1 h at 37 °C. MTT-formazan produced by mitochondrial succinate dehydrogenase was dissolved in 200 μL DMSO at 37 °C for 1 h under gentle shaking at 150 rpm. Absorption was measured at 550 nm and primary data were normalized to the median OD_{550nm} of 1% DMSO-treated cells (set to 100% viability) to give percent viability data.

2.2.22 Animal handling

All animals were handled according to European Union and German animal welfare laws. BALB/c mice and Mongolian gerbils for *L. sigmodontis* infection were purchased from Elevage Janvier (Le Genest Saint Isle, France) and were were kept in the home breeding facilities of the IMMIP. Cotton rats were bred in-house at the IMMIP. *A. viteae* infected Mongolian gerbils were kindly provided by Prof. Dr. R. Lucius (Humboldt-Universität Berlin, Germany). Long-term anaesthesia of mice was obtained by i.m. injection of 0.4% Rompun® (Bayer Health Care, Leverkusen, Germany) + 10 mg/mL Ketanest®(Pfizer Pharma AG, Berlin,Germany) in 50 μL PBS. For short-term anaesthesia required for i.t. injections mice were exposed to Isoflurane for 30 - 60 s. Animals were euthanized by exposure to excess Isofluran until breathing and heart function had stopped.

2.2.23 Infection experiments with filarial nematodes

For natural infection with *L. sigmodontis* Mongolian gerbils or anaesthetized mice were exposed overnight to infected tropical dust mites (*Ornithonyssus bacoti*). *L. sigmodontis* infected mites were obtained as part of standard infection cycle in cotton rats (*Sigmodon hispidus*) maintained at the IMMIP by B. Dubben and Dr. S. Specht. For *ex vivo* experiments with *L. sigmdontis* Mongolian gerbils and cotton rats were infected for more than 3 months to ensure patency of infection before the animals were euthanized and adult *L. sigmodontis* worms were isolated from the thoracic cavity. *A. viteae* were isolated from the subcutaneous tissue of Mongolian gerbils 6 - 12 months post infection.

2.2.24 *Ex vivo* co-culture assay with filarial nematodes

Isolated adult female worms of *L. sigmodontis* or *A. viteae* were washed in PBS and LLC-MK2 medium and were placed on a confluent lawn of LLC-MK2 cells in 6-well plates and incubated at 37 °C, 5% CO_2. The next day the medium was taken off for analysis of expelled microfilariae and fresh medium containing drugs at the indicated concentrations were added. Worms were exposed to the drugs for 14 days, with medium exchange every 2 days combined with determination of the number of released microfilariae.

Assessment of worm motility for *L. sigmodontis*

For a rating of the motility of the worms plates were videotaped daily for 1 min and attributed a motility score from 0-5 (**Supplementary videos 1 - 3**). Motility scores for *L. sigmodontis* were defined as follows:

Motility score	*L. sigmodontis* phenotype
5	Maximum motility, rapid, continuous movements
4	Movements are slower and not continuous
3	Longer times of inactivity or worm is partially stretched, worm can still perform changes of its position
2	Worm is mostly stretched and is able to make longer movements not changing its general position
1	Worm is entirely stretched, single movements are visible
0	No movement observed

Healthy *A. viteae* generally move less vigorously than *L. sigmodontis* and movements may be interrupted by periods of inactivity (**Supplementary videos 1, 4, 5**. Motility scores for *A. viteae* were defined as follows:

Motility score	*A. viteae* phenotype
5	Vigorous movements over the entire worm length
4	Movements become less frequent and vigorous
3	Worm is immobile most of the time but is still able to perform characteristic movements with increasing radius
2	Worm is mostly stretched and movements are rather wave-like
1	Worm is entirely stretched, single shivering movements are visible
0	No movement observed

Assessment of worm viability (MTT-assay)

After 14 days viability of the worms was examined by an MTT-Assay protocol modified from Townson et al [251]. Worms were incubated in 2 mL PBS with 0.5 mg/mL Thiazolyl Blue (MTT) at 37 °C for 30 min to allow production of MTT-formazan by mitochondrial succinate dehydrogenase activity. Worms were transferred into 200 μL DMSO and incubated for 1 h at 37 °C at 150 rpm. The concentration of solubilized MTT-formazan was measured as OD_{490nm}. If the measured OD was outside the linear range (OD > 1), smaller volumes, i.e. usually 100 μL were re-measured. Percent viability data were obtained by normalizing MTT assay data to the median OD_{490nm} of 1% DMSO-treated worms (set to 100% viability).

2.2.25 wALADin1 *in vivo* experiments on *L. sigmogontis* infected mice

8-week-old female BALB/c mice were naturally infected with *L. sigmogontis* and treated with different drug formulations.

Intraperitoneal drug delivery: In a first study mice were given 1 mg wALADin1 or 1 mg Doxycycline in 300 μL Minimal Essential Medium (PAA, Pasching, Austria) containing 3.3% DMSO for 14 - 28 days starting at day 1. In a subsequent study, 500 μL wALADin1 (2 mg or 2 x 2 mg with the 2nd dose given after 6 - 10 h) or wALADin1 methyl ester (compound **5**) (2 mg) or vehicle control were administered i.p. for 28 days starting at 1 dpi. Vehicle was 25 mM 2-Hydroxypropyl-β-cyclodextrin in Earl's balanced salt solution (Life Technologies, Darmstadt, Germany) containing 4% DMSO.
Intrathoracic drug delivery: Mice were treated with 100 μL wALADin1 (0.4 mg) i.t. for up to 28 days or vehicle control starting at 1 dpi. Vehicle was 30 mM 2-Hydroxypropyl-β-cyclodextrin in Earl's balanced salt solution (Life Technologies, Darmstadt, Germany) containing 4% DMSO for 14, 21 or 28 days. A control group of untreated infected mice was included.
If not stated otherwise, at 35 dpi mice were euthanized and worms were isolated from the thoracic cavity, counted, staged and their sex and length were determined. For quantification of endosymbiont *Wolbachia* levels, DNA was isolated from 10 single worms per mouse and *Wolbachia ftsZ* copy numbers were determined and normalized to the number of *L. sigmodontis* β*-actin* copy numbers by duplex Realtime-PCR as described previously [9, 241]. In some experiments isolated worms were further subjected to MTT assay as described in **Section 2.2.24**.

2.2.26 *Toxoplasma gondii* culture

Parasites

Toxoplasma gondii RH strain tachyzoites were received in peritoneal lavage fluid of infected NRMI mice which are used as part of the diagnostic laboratory routine of the IMMIP (Dr. I. Reiter-Owona).

Infection of LLC-MK2 cells with *T. gondii* tachyzoites

Two days before infection with *T. gondii* ~20,000 - 25,000 LLC-MK2 cells were seeded into the wells of a 96-well cell culture plate (see also **Section 2.2.20**) and cell concentrations were determined by counting in a Neubauer counting chamber (VWR International GmbH, Darmstadt, Germany). Before infection *T. gondii* tachyzoites were centrifuged for 7 min at 371 g at RT. The supernatant (lavage fluid) was discarded and cells were resuspended in LLC-MK2 medium without antibiotics. The concentration of parasites was determined using a Neubauer counting chamber. The old antibiotics-supplemented medium of the LLC-MK2 cells was removed, cells were washed once with PBS and *T. gondii* tachyzoites in LLC-MK2 medium (free of antibiotics) were added at a multiplicity of infection of 5 in a final volume of 100 μL. After 2 h of culture (37 °C, 5% CO2) the medium was removed and cells were washed twice with PBS in order to remove non-adherent parasites and synchronize parasite replication. 125 μL of fresh LLC-MK2 culture medium free of antibiotics but supplemented with the test compounds at the desired concentrations were transferred to the wells. After 40 - 48 h of infection, supernatants containing free parasites from ruptured cells were taken off and cells were detached by addition of 25 μL 1X Trypsin/EDTA and incubation at 37 °C for 5 min. Additional 100 μL of PBS were added, cells were detached and the sample was combined with the corresponding supernatant. 200 μL of the resulting LLC-MK2/*T. gondii*

tachyzoite suspension was then subjected to DNA extraction (see **Section 2.2.4**). Finally tachyzoite and LLC-MK2 numbers were determined by Real-time PCR with extracted DNA.

2.2.27 *Plasmodium falciparum* culture

The *P. falciparum* culture experiments were physically performed by Martina Fendler.

Parasites

P. falciparum 3D7 strain

P. falciparum culture

A+ citrate blood was obtained from the blood bank of the University Hospital of Bonn. Blood samples were centrifuged at 2000 rpm for 5 min (EBA 20 centrifuge with E1624 rotor). Serum and buffy coat were removed. Tubes were filled with RPMI medium (with 25 mM HEPES, without L-Glutamine, PAA Lab., Pasching, Austria) and centrifuged again for 5 min, 2000 rpm and the upper phase was discarded. This washing procedure was repeated once. Erythrocytes (RBC) were mixed with an equal volume of RPMI and stored at 4 °C for up to 3 weeks. *P. falciparum* 3D7 parasites were cultured in A+ RBC in *P. falciparum* medium at 37 °C under a defined gaseaous atmosphere (3% O_2, 5% CO_2, 92% N_2). Erythrocytes (1200 μL RBC in 13 mL medium) were kept in petri dishes (ϕ=10 cm) and when parasitemia exceeded 5% a dish of fresh RBC was infected by addition of ∼50 μL of infected RBC. Medium was exchanged every 24 h. Old medium was removed without disturbing the sedimented erythrocytes on the bottom of the dish and replaced with an equal volume of fresh medium. Parasitemia of culture samples was determined by Giemsa-staining of blood smears. Blood smears were prepared by rapid smearing of a drop of the sedimented erythrocyte culture over the surface of a microscope slide using the edge of another slide.

Giemsa staining

Blood smears were fixed for at least 1 min in methanol and air dried. Smears were stained in fresh Giemsa Working solution for 15 to 20 min before they were rinsed with buffer solution, quickly immersed in H_2O and dried at air. 1000 erythrocytes per sample were counted under microscope at 100X magnification and the number of infected cells (trophozoites plus schizonts) was determined.

> **Giemsa working solution**: 1 mL Giemsas Azur Eosin-Methylenblau Lösung + 19 mL buffer solution
>
> **Buffer solution**: Na_2HPO_4x 2 H_2O / KH_2PO_4 Puffertabletten pH 7.2 : One tablet was dissolved in 1 L destilled water.

Compound testing in *P. falciparum* culture assay

Compounds were tested for anitplasmodial activity in the *P. falciparum* 3D7 culture and the effect on the development of parasitemia was followed for 4 days. 1.8 mL *P. falciparum* culture medium supplemented with compounds at varying concentrations or 0.5% DMSO as a negative control were transferred into the wells of a 24-well plate with four replicates per condition. 200 μL of infected RBC at a parasitemia adjusted to 0.2% - 0.5% were added. Medium exchange and the collection of blood smears were done on a daily basis.

2.2.28 Sequence alignments

Multiple sequence alignments of orthologous ALAD sequences were performed with GENtle V.1.9.4 (Magnus Manske, Cologne, 2003) using the implemented Clustal W (Scores: Match: 2; Gap external penalty: -1, Gap penalty: -2; BLOSUM matrix). For *Wolbachia*, *H. sapiens* and *P. aeruginosa* ALAD sequences of the recombinant proteins were used according to the sequenced expression plasmids. Sequences of other orthologous proteins were retrieved from the UniProtKB database: *E. coli* (P0ACB2), *V. cholerae* (C3LPU7), *Y. enterocolitica* (F4MUJ9), *P. sativum* (P30124).

2.2.29 Basic Local Alignment Search Tool (BLAST) searches

All BLAST searches were performed on the "BLAST search and download server for Filaria-EU" (http://xyala.cap.ed.ac.uk/downloads/959nematodegenomes/blast/filareu.php) hosted by "959 Nematode Genomes" (www.nematodes.org by Mark L. Blaxter, University of Edinburgh, 2012) using default settings. *HemB* gene homologues within the genome of *A. viteae* were searched for by blastn 2.2.25 [237] search with query input sequences of *Wolbachia* of *B. malayi*, human and yeast sequences (Accession No. AE017321, gene locus Wbm0373; X64467; J03493).
The "All Filarial Genomes 2012-08-24" assemby including *Wolbachia* genomes was searched for homologous *slr1790* gene sequences by tblastn 2.2.25 [237] with the *slr1790* gene product of *Synechocystis sp.* (strain PCC 6803, Accession No. P72793) as query input.

2.2.30 Data and statistical analyses & Software

Microsoft Office Excel 2007 (Microsoft, Redmond, WA, USA) was used for processing and normalization of primary data. All further transformations, statistical analyses and graphical representations were done with Graph Pad Prism 5.0 (GraphPad Software, SanDiego, CA, USA). Enzymatic assay data is shown as mean ± SEM, if not stated otherwise. Worm co-culture and *in vivo* data are presented as median, cell culture data as median with interquartile range. Non-parametric two-tailed Mann-Whitney-U test was employed for significance testing (significance level α=0.05) for statistical analyses.

The following non-linear regression algorithms and transoformation functions of Prism 5.0 were used in this work:

"*$log_{inhibitor}$ vs. normalized response - variable slope*": IC_{50} determinations in the enzymatic assay experiments. Hill-slopes were not restricted due to possible cooperative effects using the ALAD oligomers.

"*$log_{agonist}$ vs. response - variable slope*": EC_{50} determinations of the stimulatory effects of wALADin1/derivatives on several ALAD orthologs

Allosteric sigmoidal algorithm: Standard algorithm used in type-of-inhibition experiments for various proteins accounting for coopertive effects (X as the substrate concentration, Y as enzymatic velocity, V_{MAX} as maximum enzymatic velocity, h as hill slope and Kprime being related to the Michaelis-Menten constant K_M (identical only for h=1)) as indicated in **Equation 2.2**

$$Y = \frac{V_{MAX} \times X^h}{Kprime + X^h} \tag{2.2}$$

Mixed Model Inhibition algorithm: Type-of-inhibition experiments for various proteins

Non-competitive inhibition algorithm: Type-of-inhibition experiments for various proteins

Uncompetitive inhibition algorithm: Type-of-inhibition experiments for various proteins

Competitive inhibition algorithm: Type-of-inhibition experiments for various proteins

Michaelis-Menten algorithm: Determination of K_M values

Eadie-Hofstee Transformation, followed by linear regression analysis: Linearized representation of type-of-inhibition experiments

Hanes-Woolf Transformation, followed by linear regression analysis: Linearized representation of type-of-inhibition experiments

Chemical structures were drawn using MarvinSketch (ChemAxon, Budapest, Hungary). Figures were created with Prism 5.0 (GraphPad Software, San Diego, CA, USA) or Adobe Illustrator CS6 (Adobe Systems, Munich, Germany). Image contrast adjustments and conversion to grayscale were done with Adobe Photoshop CS6 (Adobe Systems, Munich, Germany) or GIMP 2 (http://www.gimp.org). Videos were recorded with a Sony Handycam® DCR-46E Mini DV camcorder (Sony Deutschland, Berlin, Germany) and movies were analyzed and cut with Final Cut Pro (Apple, Cupertino, CA, USA).

2.3 Preparative experiments

Experiments described in this section have a merely preparative character. These experiments include the cloning and recombinant protein expression procedures which are of no higher scientific significance to the current study but are required for production of materials that are the basis for experiments described subsequently in the **Results** (**Chapter 3**).

2.3.1 Cloning of *P. aeruginosa* hemB gene into pET-21b expression vector

For the cloning of the *P. aeruginosa* ALAD (pALAD) gene and subsequent overexpression of the recombinant protein a cloning strategy was set up that included the parallel processing of three different ALAD constructs. For PCR amplification (**Section 2.2.2**) primers were used that included different restriction site sequences that would flank the gene sequence. By choosing restriction sites in the forward primer that have their matching part in the pET-21b sequence either downstream (NdeI) or upstream (SacI) the T7-tag and a reverse primer restriction sites located downstream the His_6-tag sequence (NotI, XhoI) in combination with primer sequence with or without stop codon it was intended to obtain plasmid constructs that would allow the expression of either untagged (UT), His_6-tagged or T7-tagged ALAD protein. The single step results of the cloning procedure in the following are shown for the His6-tagged version, the final protein of which was purified and used for the enzymatic assay experiments. After isolation of genomic *P. aeruginosa* DNA from an overnight culture, the DNA was used as a template for PCR amplification of the *hemB* gene with the different primer sets (**Fig. 2.1**, **Section 2.2.2**). Standard *P.aeruginosa* ALAD PCR contained ∼7.5 ng DNA. The optimal annealing temperature was determined in a temperature gradient PCR and was found to be 72 °C. At this temperature a clear band of the expected size of 1kb and the lowest

non-specific amplification of secondary bands or smears were achieved (**Fig. 2.2 a**). At this optimal temperature multiple 50 μL PCR reactions were run and the products were separated on a preparative 1% Agarose gel (**Fig. 2.2 b**) from which the bands were excised and the PCR product was cleaned up.

The cloning procedure, which is described in detail in **Section 2.2.3**, then involved restriction digestion of the plasmid vector and the purified PCR product. After successful digestion with NdeI and XhoI only the linearized plasmid with a size of 5.4 kb and no supercoiled structures as for the uncut plasmid DNA were visible in (**Fig. 2.3 a**). For the Not I and Sac I-digested plasmid DNA still some faint secondary bands remained. Therefore further experiments requiring NotI/SacI digestion were done with High-Fidelity forms of these restriction enzymes.

After 5'-dephosphorylation of the RD-plasmid in order to prevent religation of the plasmid, the plasmid and RD-PCR product were ligated in a 1:5 molar ratio using Quick Ligase. The ligation mixture was transformed into chemically competent Top 10 E. coli and 3 different plates were streaked out with 100, 150 or 200 μL of the respective constructs and an overall number of 165 colonies for T7-pALAD, 6 colonies of His_6-pALAD and only two colonies of UT-pALAD-tranformed bacteria had grown. The colonies were then subjected to colony PCR using T7 promoter/terminator primers in which most clones for His_6-pALAD (5/6) and T7-pALAD (8/10) revealed insertion of a DNA fragment of $\sim$1 kb when the resulting $\sim$1.2 kb prodcuct band was compared to the $\sim$250 bp amplicon of the empty pET-21b vector (**Fig. 2.4 a**). In contrast, both clones of the untagged construct were negative. PCR-positive colonies were then selected for overnight cultures and plasmid preparation. The purified plasmids were used as a template in both T7-primer-based PCR and in a PCR reaction using specific ALAD primers. A number of positive clones for both T7-pALAD and His_6-pALAD featured both the $\sim$1.2 kb product in the T7-PCR as well as the $\sim$1.0 kb product in the specific PCR (**Fig. 2.4 b, c**). Finally, plasmid DNA was submitted to sequencing and the obtained sequences unequivocally revealed the insertion of the *hemB* gene into the pET-21b vector at the correct position and proved the cloning to be successful.

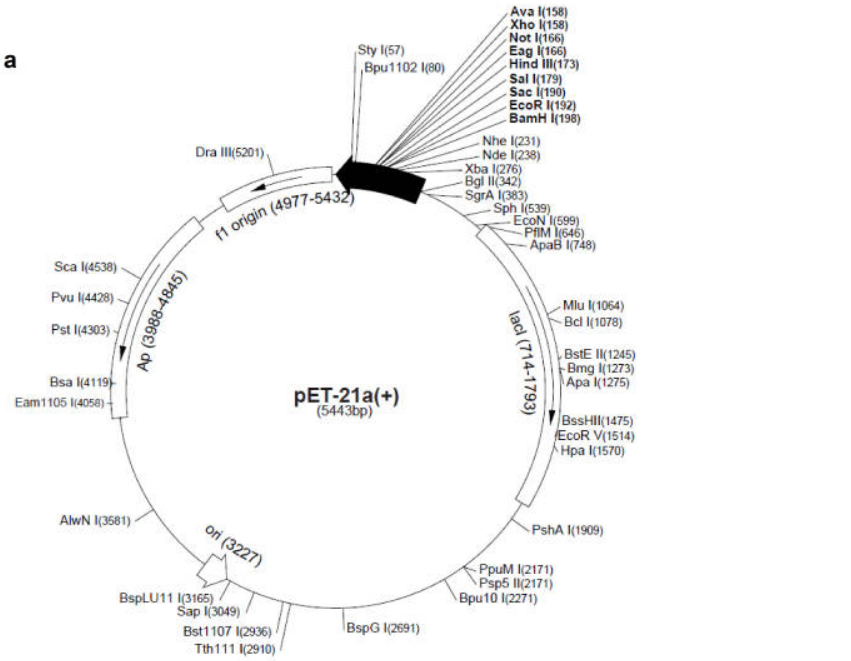

b

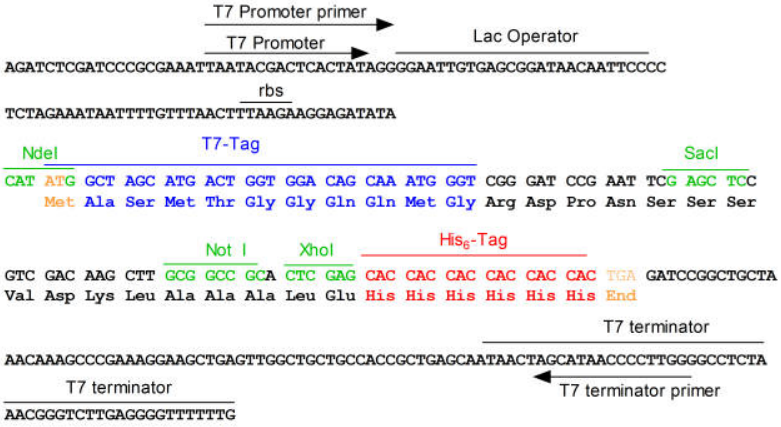

c

	Restriction sites FW-primer	RV-primer	Stop-codon in RV primer	Protein tags	Sizeof PCR product [bp]	#AA	MW protein [kDa]
T7-pALAD	SacI	NotI	yes	T7-Tag	1027	354	38.7
His_6-pALAD	NdeI	XhoI	no	His_6-Tag	1024	345	38.1
UT-pALAD	NdeI	NotI	yes	no	1026	337	37.0

Figure 2.1: Strategy for the cloning of the pALAD gene into the pET-21b vector

a) Vector map of pET-21a/b vector as supplied by the manufacturer. **b)** Gene sequence of the pET-21b multiple cloning site. Start and stop codons are highlighted in orange, restriction sites in green, T7-Tag residues in blue and His_6-Tag residues in red. The sequence was taken from the manufacurer's information sheet and is displayed in a modified version. **c)** Overview of the different pALAD constructs envisionsed including tags and size information.

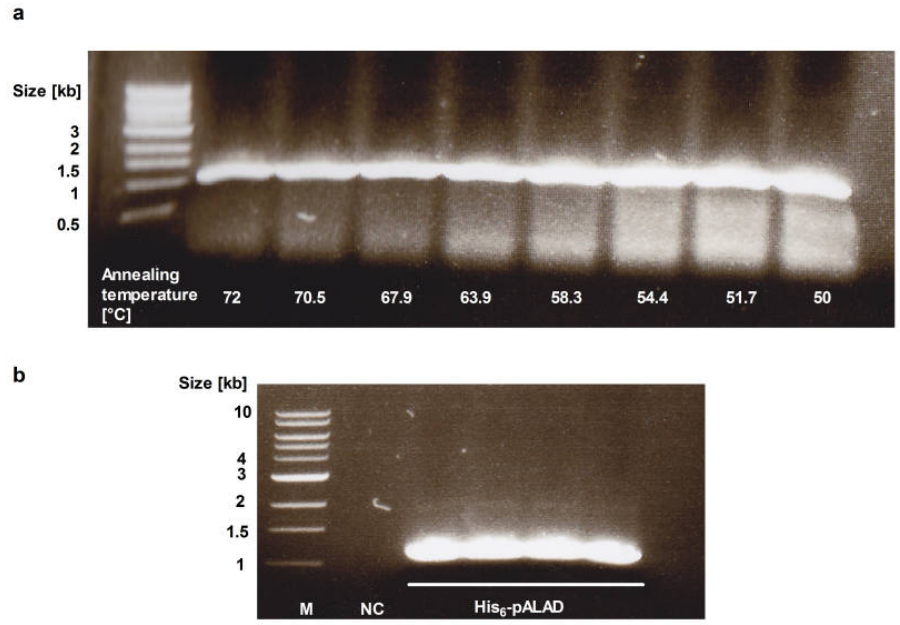

Figure 2.2: PCR amplification of the *P. aeruginosa* ALAD gene
1% Agarose gels stained with SafeRed are shown. **a)** PCR optimization in a gradient PCR where the annealing temperature was varied from 50 °C to 72 °C, as indicated. The specific PCR product (His_6-pALAD) runs at a size of ∼1 kb. **b)** Preparative gel where the products of 4 PCR reactions (at optimal annealing temperature of 72 °C) were applied before excision and clean-up. M = marker; NC = negative control.

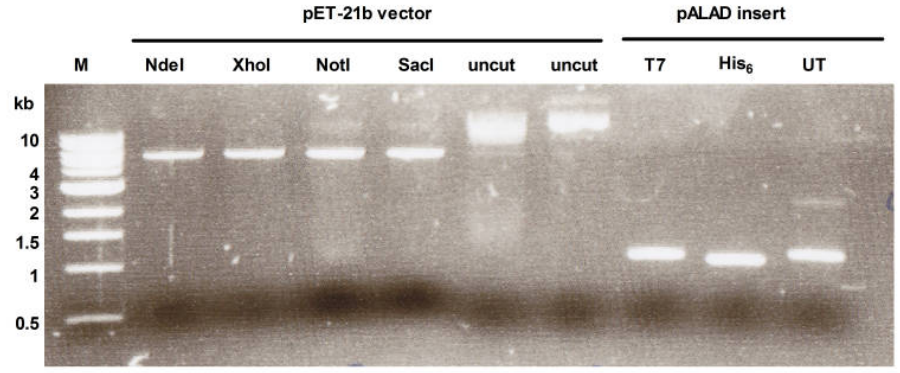

Figure 2.3: Restriction digestion of pET-21b vector
1% Agarose gel stained with SafeRed. After cutting pET-21b with NdeI and XhoI restriction enzymes for 1 h clean single bands were obtained revealing successful linearization of the 5.4 kDa vector DNA compared to uncut plasmids that run in supercoiled forms. M = marker.

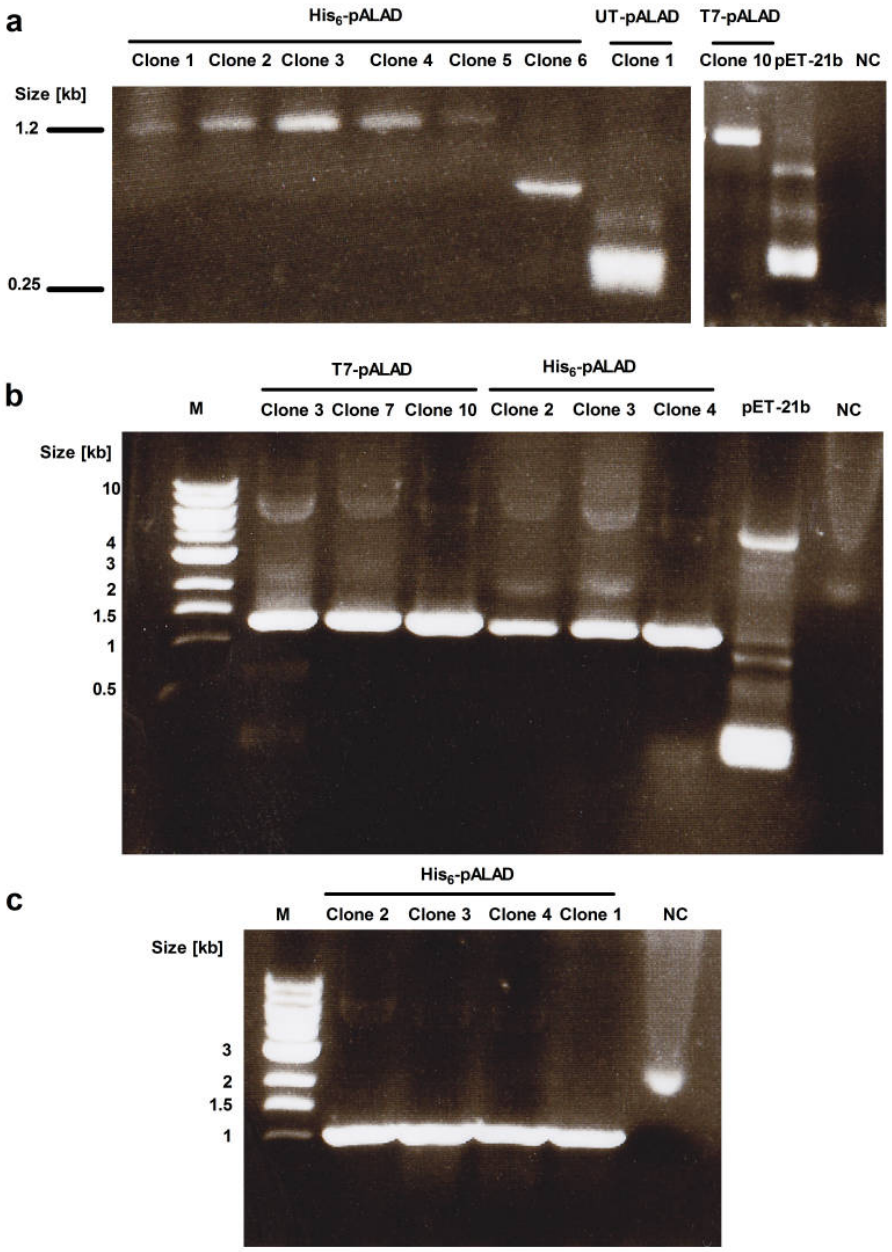

Figure 2.4: PCR analysis of cloned gene sequences

1% Agarose gels stained with SafeRed are shown. **a)** Results from Colony-PCR using the T7 primer set. For His_6-pALAD 5 positive clones (1-6) and one positive clone (10) for T7-pALAD are shown that display an increased PCR product size compared to empty pET-21b vector indicating successful insertion of a 1 kB fragment. Clone 1 of UT-pALAD is negative. **b)** The 1.2 kb PCR product was obtained by T7-primer PCR reaction using purified plasmid DNA template. **c)** Correct insertion of the pALAD gene sequence was further proven by the resulting pET-21b-His_6-pALAD expression vector which yielded the expected product of ∼1 kb after PCR amplification. Primary sequence analysis of the encoded pALAD protein predicted a size of ∼38 kDa and a pI of 5.41. M = marker; NC = negative control.

2.3.2 Recombinant expression of pALAD protein

For recombinant expression of pALAD protein the plasmid DNA was transformed into BL 21 *E. coli* as a T7 expression strain. Bacterial cultures were grown until OD_{600nm} 0.5 - 0.6 before protein expression was induced by the addition of the non-cleavable lactose analog isopropyl β-D-1-thiogalactopyranoside (IPTG) which binds to the lac repressor, thus inducing the lac operon encoded in the pET-21b vector allowing transcription of the inserted *hemB* gene under the control of the T7 promoter. In order to determine optimal induction conditions various concentrations of IPTG (25 μM, 100 μM and 400 μM) were tested for different induction times (2 h vs. o/n) before cells were harvested and lysed. SDS-PAGE with lysate supernatants and pellets revealed that specifically upon induction with IPTG a protein, which runs at the expected size of ∼38 kDa, was expressed in a time- and concentration-dependent manner (**Fig. 2.5**). It appeared both in the supernatant and in the pellet and was most prominent after o/n incubation. While the concentration of soluble putative pALAD protein in the supernatant drastically increased when IPTG concentration was increased from 25 to 100 μM, another 4-fold increase did not further increase the yield of soluble target protein but rather led to a slight reduction. The amount of insoluble pALAD in the pellet was similar between all IPTG concentrations tested.

Based on these results a large batch induction (500 mL culture) with 100 μM IPTG and subsequent purification of His_6-pALAD over Ni^{2+}-NTA-Agarose was performed. Protein samples taken from the different steps of the purification procedure were analyzed by SDS-PAGE (**Fig. 2.6**). Eluates 1-6 contained His_6-pALAD at high purity (> 90%) and the overall yield was ∼46 mg pALAD per 500 mL culture.

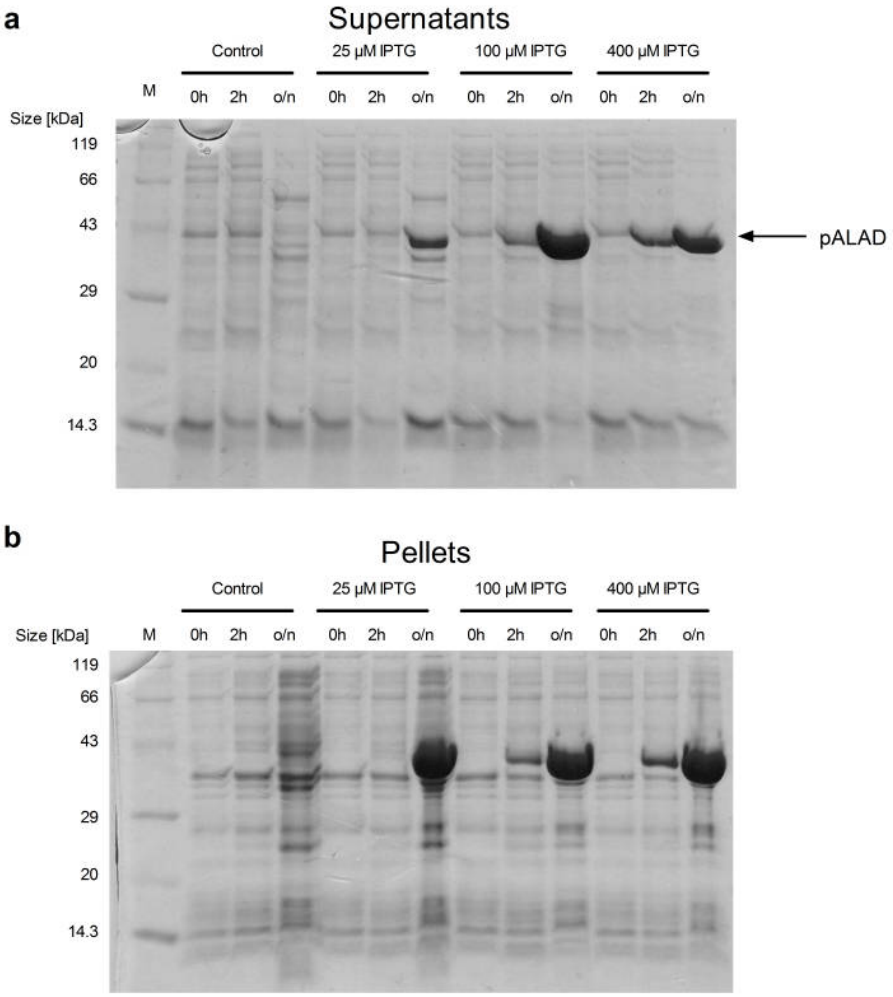

Figure 2.5: Test expression of His_6-tagged pALAD protein
The graph shows Coomassie blue stained 12.5% SDS-page gels loaded with 5 μg protein samples from different steps of a pALAD test expression. **a)** Supernatants of lysates after centrifugation. **b)** Resuspended pellets. A protein of the size of ∼40 kDa was induced by IPTG and is expected to be the target protein.

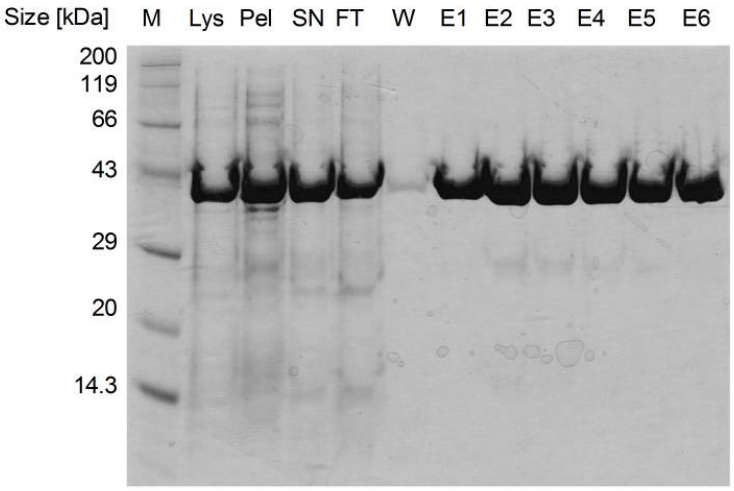

Figure 2.6: Purification of His_6-tagged pALAD protein over Ni^{2+}-NTA-Agarose
Samples were analysed on a 12.5% SDS-PAGE gel and visualized by Coomassie blue staining. High concentrations of the 38 kDa protein are present in the crude lysate as well as in the pellet and supernatant. Eluates contain the target protein at high purity. M = marker, Lys = lysate, Pel = pellet, SN = supernatant, FT = flowthrough, W = wash fraction, E1 - E6 = eluates 1 to 6.

2.3.3 Recombinant expression of wALAD and hALAD protein

Starting from the expression plasmids, His_6-tagged wALAD and hALAD proteins were recombinantly expressed as described previously [270]. The expression protocols were adapted and optimized for the given laboratory conditions and the optimized protocol is described in detail in **Section 2.2.6**. Primary sequence analysis predicted a size of 37.5 kDa (pI = 5.74) for wALAD and a size of 37.4 kDa (pI = 6.43) for hALAD. While, following the standard protocol, hALAD was easily expressed at high purity and with sufficient yield (∼2.5 mg hALAD per 500 mL culture) (**Fig. 2.7 c**), yield for wALAD was very low under standard conditions (< 0.5 mg per 500 mL culture). Even following the described modified protocol, the vast majority of overexpressed protein was not soluble and found in the pellet (**Fig. 2.7 b**). However, purification over Ni^{2+}-NTA-Agarose yielded significant amounts of pure wALAD protein. Interestingly, more (active) protein could be extracted from the pellet that formed after centrifugation of the crude lysate by simple resuspension and further purification. Due to the activity of the protein and the ease of preparation this protein portion does likely not represent inclusion bodies but may result from incomplete bacterial lysis or an intrinsic affinity to cell debris components. Taken together, the modified protocol allowed final yields of 1-2 mg purified wALAD protein per 500 mL culture.

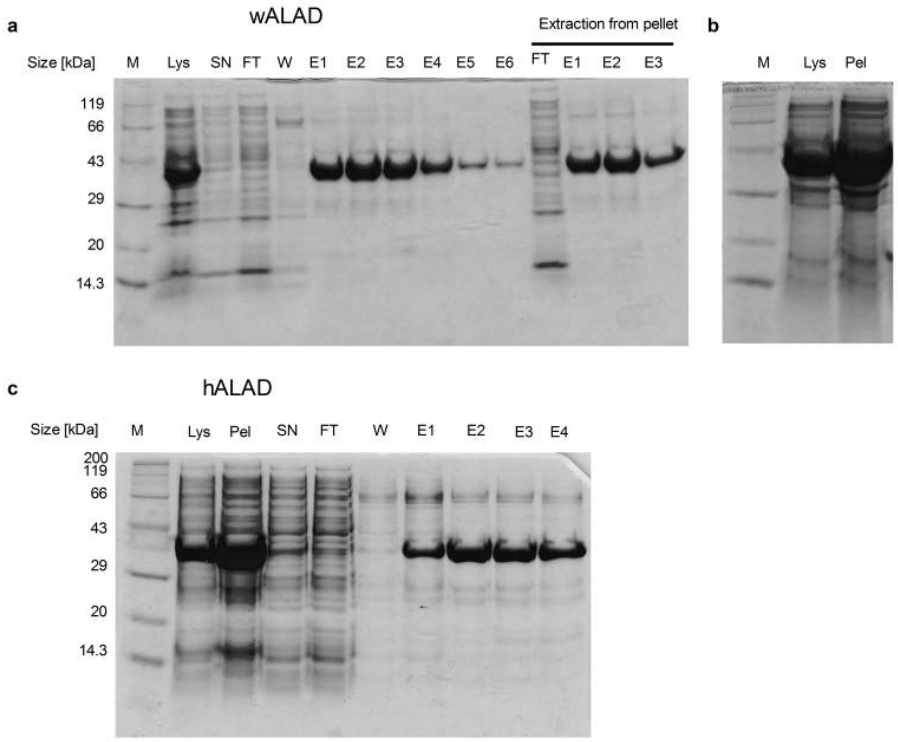

Figure 2.7: Purification of recombinant wALAD and hALAD protein
6 μg or the maximal possible amount of protein samples were analysed on a 12.5% SDS-PAGE gel and visualized by Coomassie blue staining. **a)** The different fractions occurring during purification of wALAD. 37.5 kDa wALAD protein of $>$ 90% purity is present in considerable amounts in eluates 1-4 after primary lysis and after extraction from the pellet. **b)** The majority of the expressed wALAD protein is found insoluble in the pellet. **c**) The different fractions occurring during purification of hALAD. The 38 kDa protein hALAD was successfully expressed and is present at high purity in eluates. M = marker, Lys = lysate, SN = supernatant, E1 - E6 = eluates 1 to 6, FT = flowthrough, Pel = pellet.

Chapter 3

Results

3.1 wALAD HT-Screening

A standard ALAD enzymatic assay was simplified and downscaled to microplate-format. Standard assay conditions [270] were adjusted for 1 μM wALAD to give a robust, yet sensitive HTS-compatible protocol: A modified Ehlich's Reagent (MER) as a combined stopping and color reagent was developped that was based on DMAB, acetic acid and perchloric acid but in which toxic $HgCl_2$ and tedious transfer steps were omitted (the assay principle of the detection of the pyrrole porphobilinogen by Ehrlich's Reagent is depicted in **Fig. 3.1**). Thus the assay was performed in a 30 μL volume in 96-well microplates. For the substrate, 5-ALA, a concentration of 200 μM was chosen, which was below the determined Michaelis-Menten constant K_M of $\sim$311 $\pm$ 52 μM (**Fig. 3.2 a**), but which rendered the assay sensitive for the detection of inhibitors of all kinds. A time-curve experiment revealed that after 20 min the reaction was still in the linear phase and that this timepoint was a suitable assay endpoint (**Fig. 3.2 b**).

This assay was used to screen a diversity-based chemical library of $\sim$18,000 small drug-like molecules for novel inhibitors of wALAD. A general overview of the screening and validation workflow and the results is given in **Fig. 3.3**. The mean Z'-factor of the assay during screening was 0.66 $\pm$ 0.20 indicating excellent assay quality and reliable screening data [274]. The hit-threshold was set to the mean of the DMSO control minus 3 standard deviations which was equivalent to 35% inhibition and yielded 71 primary hits (0.4%). Exemplary primary screening data is shown in (**Fig. 3.2 c**). All hits were rescreened in duplicate. In order to remove low potency hits, the hit threshold during the rescreen was increased to 50% inhibition and was exceeded by 18 confirmed hit compounds (0.1 %). For these compounds IC_{50} concentrations were determined for wALAD and hALAD as a control and compounds were tested for non-specific interference with the porphobilinogen detection assay and hALAD, as shown in **Table 3.1**.

3.1.1 Discovery of wALADin-benzimidazole: species-selective inhibitors of wALAD

The screening revealed a cluster of substituted benzimidazole structures (CG3 5G9, CG3 24H7, CG3 7H5) that inhibited wALAD activity in a dose-dependent manner while activity of the human ortholog hALAD was only marginally affected. The most potent of these compounds inhibited wALAD with an IC_{50}-value of $\sim$11 μM and was termed wALADin1 (***Wolbachia* ALAD in**hibitor 1) (**Fig. 3.2 d**). Inhibition of wALAD by wALADin1 was highly species-selective, as hALAD was inhibited

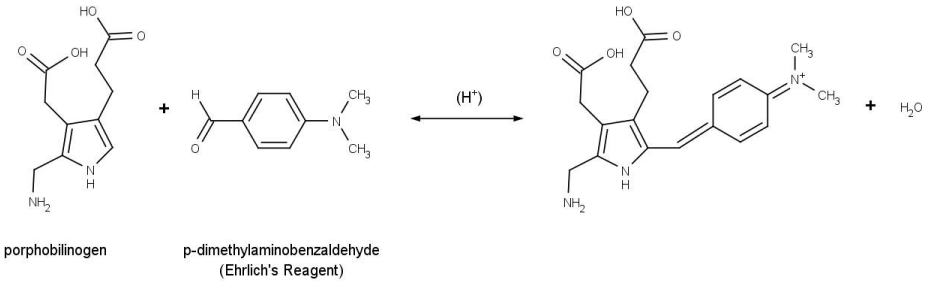

Figure 3.1: Reaction scheme of porphobilinogen detection with Ehrlich's Reagent
Under acidic conditions protonated p-dimethylaminobenzaldehyde reacts in an electrophlilic substitution reaction with the pyrrole at the C_α atom and produces a chromophore with high extinction at 555 nm [6].

only marginally with an extrapolated IC_{50}-value of ∼740 μM at pH 7.5 (within the optimal buffer range of this ortholog), which is a more than 60-fold discrimination in inhibitory potency of the two orthologs (**Fig. 3.2 e)**. At pH 8.0 (the pH optimum of wALAD), hALAD was even less-sensitive to inhibition by wALADin1. Thus, wALADin1 is a novel species-selective inhibitor of wALAD.

Table 3.1: Confirmed wALAD Screening hits

Compound	% Inhibition Primary Screen	% Inhibition Rescreen	% Inhibition PBG Detection	IC_{50} wALAD [μM]	IC_{50} hALAD [μM]	Remark
KR1 4G3	81.0	82.0	none	8.1	19.7	Trivial name: Cacotheline
KR1 3F10	75.2	77.6	none	9.1	15.5	
CG3 5G9	39.5	79.5	none	112	> 500	Substituted benzimidazole
CG3 24H7	57.0	63.0	none	22	> 500	**wALADin1**/ Substituted benzimidazole
CG2 27D2	36.9	63.5	none	∼230	∼781	
CG2 17G2	46.5	73.1	none	158	121	
CG1 23H9	34.3	61.6	none	61	127	
CG6 23G7	52.6	54.2	none	95	∼453	
KR1 7D9	56.4	50.1	17	54	91	
CG5 12B7	38.5	50.0	none	66	70	
CG3 7H5	41.9	48.1	none	52	> 500	Substituted benzimidazole

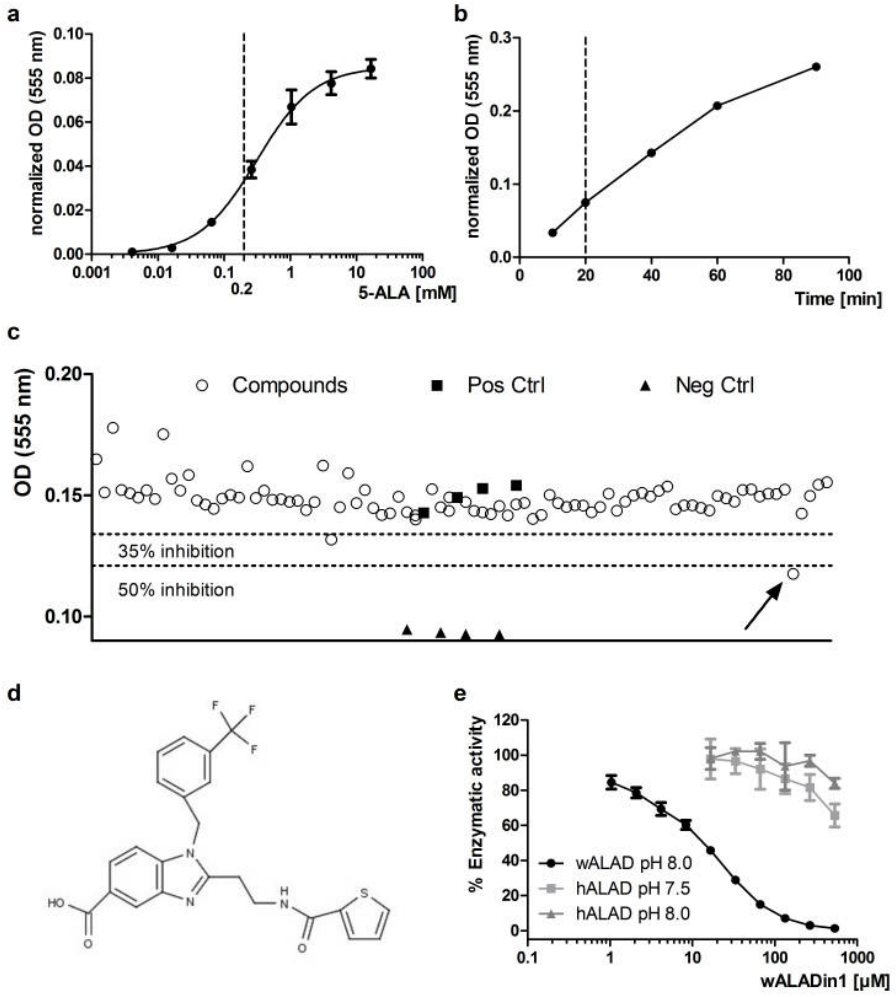

Figure 3.2: wALAD enzymatic assay screening

a) 5-ALA concentration row under screening assay conditions. The dashed vertical lines indicates the concentration of 200 μM subsequently used for HTS. The graph shows means of three independent experiments. **b)** Time curve of the wALAD reaction. After 20 min the reaction is in its steady state phase. Under the described conditions the enzymatic assay was implemented in a HT-screen of a library comprising ∼18,000 small molecules. The cut-off for primary hits was 35% inhibition and was increased to 50% for confirmed hits to be brought forth for further validation. **c)** Primary data from one exemplary screening plate on which the most potent species-selective inhibitor, called wALADin1 (arrow) was detected. **d)** Chemical structure of wALADin1. **e)** wALADin1 specifically inhibited enzymatic activity of the *Wolbachia* ortholog (IC_{50} = ∼11 μM at pH 8.0) while it had only minor effects on the human protein (IC_{50} > 500 μM for pH 7.5; triangles: IC_{50} > 1 mM for pH 8.0). The graph is representative of 3 experiments showing means ± SD of triplicates. Pos Ctrl = positive control with 5-ALA and DMSO; Neg Ctrl = negative control with DMSO and without 5-ALA.

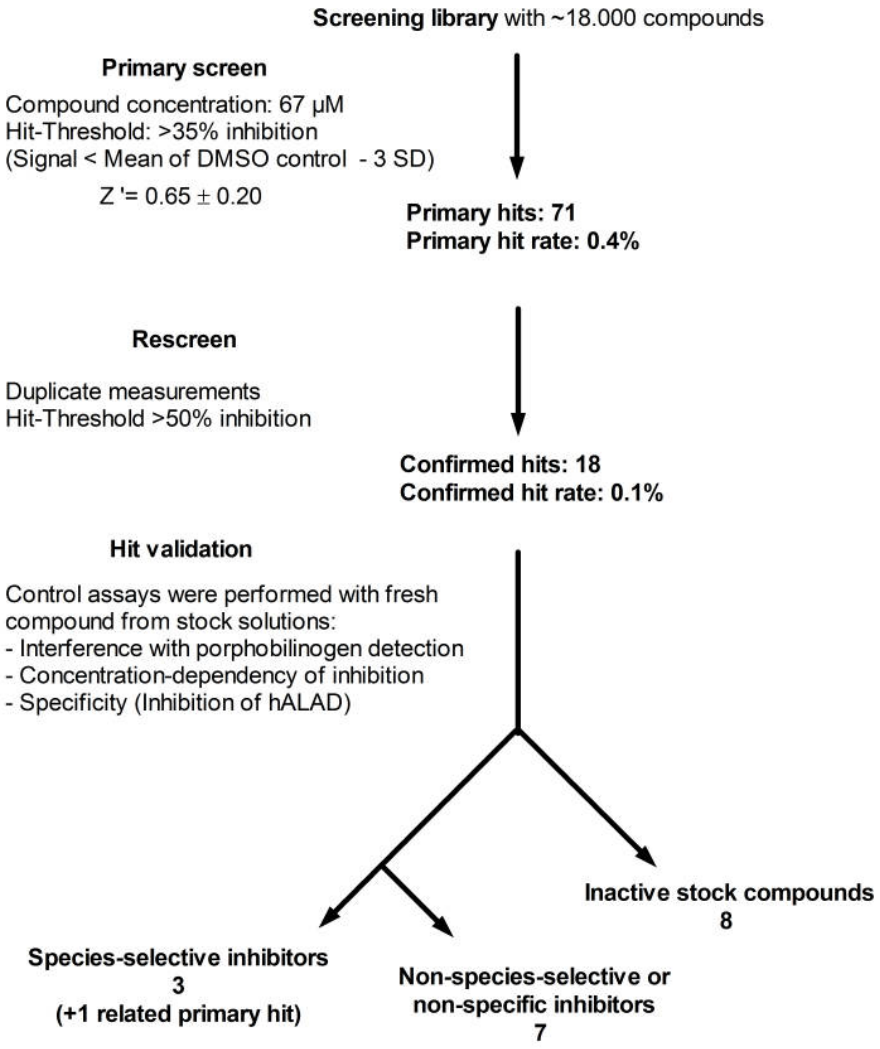

Figure 3.3: Workflow of wALAD HT-Screening and hit validation

3.1.2 Further hit structures

A species-selective inhibitor which was based on a different chemical scaffold than wALADin1 was CG6 23G7. Due to its low potency, this inhibitor was not pursued further (**Table 3.1**).

Another apparently potent inhibitor with differential potency for wALAD and hALAD was cacotheline, a semi-synthetic derivative plant alkaloid brucine. Detailed analysis of cacotheline in enzymatic inhibition experiments revealed that this compound had a non-specific effect: An extinction spectrum of cacotheline in the ragne of visible light revealed that it reacted with DTT, leading to a shift in the peak extinction wavelength from 390 nm to 525 nm (**Fig. 3.4 a**). This shift was, however, only temporary and its lifetime was dependent on the DTT concentration present in the solution (**Fig. 3.4 b**): The higher the DTT concentration, the longer the lifetime. When after 30 min DTT was again added exogenously, the same transition occured again indicating a previous consumption of DTT by cacotheline. As the concentration of cacotheline in solution was only 100 μM and was thus much lower than mM concentrations of DTT, it appears that cacotheline assumes a catalytic function in the consumption (i.e. possibly oxidation) of DTT during which it forms a red-colored intermediate (absorption at 525 nm). As the presence of DTT is required for activity of both wALAD and hALAD, its consumption by cacotheline may explain reduced protein activities as a non-specific artifact.

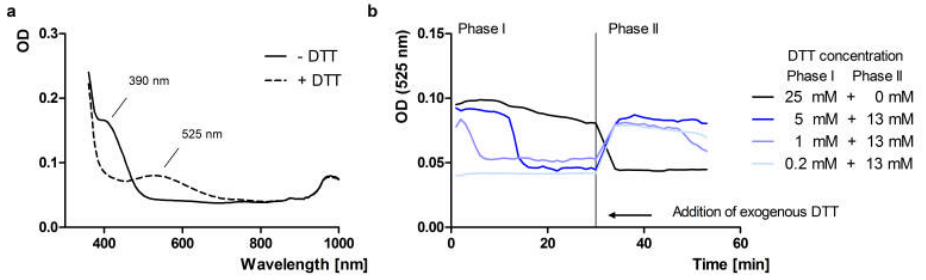

Figure 3.4: Elucidation of the DTT-consuming effect of cacotheline
a) 5 mM DTT leads to a shift in the extinction peak of cacotheline from 390 nm to 525 nm. **b)** The DTT-induced shift in the absorption maximum is temporary and is correlated to DTT concentration (Phase I). Secondary addition of DTT as depicted by the vertical line after 30 min (Phase II) leads again to increased OD_{525nm} indicating a previous depletion of DTT. Cacotheline concentration was 100 μM.

3.2 Functional characterization of wALADin1

3.2.1 Binding experiments

Before a detailed functional characterization of wALADin1 in terms of inhibition was carried out, binding of wALADin1 to wALAD should be demonstrated. For this purpose thermal shift assays (TSA) were employed. This technique uses the fluorescent dye Sypro®Orange that exhibits higher quantum yields when bound to hydrophobic parts of a protein than in aqueous solution [275, 225]. As hydrophobic side chains become exposed upon thermal denaturation, the melting curve of a protein can be measured as an increase in fluorescence intensity. Upon binding of a ligand to the protein the protein tertiary structure is stabilized and requires higher temperatures for denaturation. Already low μM concentrations wALADin1 induced a concentration-dependent increase of the wALAD melting temperature indicating binding of wALADin1 to the protein (**Fig. 3.5 a**). At 25 μM wALADin1, the wALAD protein tolerated $>$ 20 °C higher temperatures compared to the free protein. In contrast, for hALAD $\geq$ 250 μM wALADin1 concentrations were required for a minimal shift of the melting temperature with a maximal ΔTm of 1.5 °C at 1 mM (**Fig. 3.5 b**). Similarly, wALADin1 did not stabilize other control proteins such as BSA or lysozyme (**Fig. 3.5 c, d**) indicating its binding specificity for wALAD.

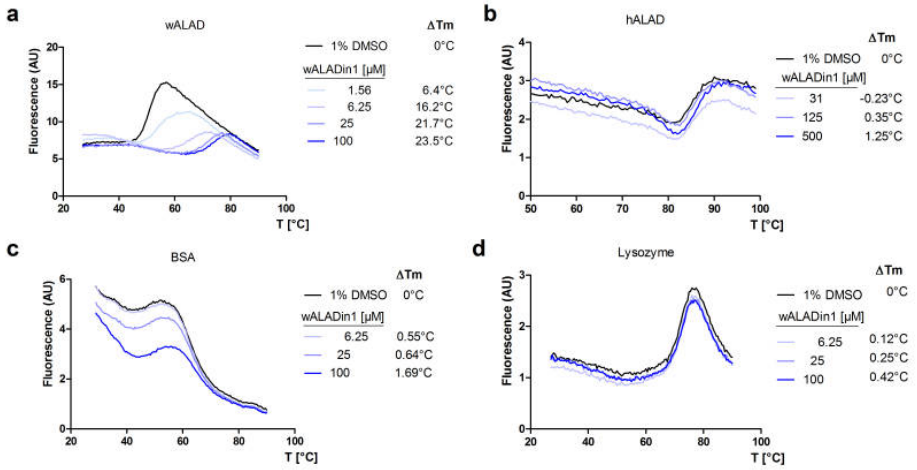

Figure 3.5: Thermal Shift Assay with wALADin1
Protein melting curves as a function of the fluorescence intensity of the environmentally sensitive dye Sypro®Orange: **a)** wALAD protein (5 μM) is thermally stabilized by increasing concentrations of wALADin1 as evident in pronounced shifts of the melting curve at low μM concentrations. Marginal shifts of the melting curves ($<$ 2 °C) observed for **b)** hALAD (0.2 mg/mL or 5 μM), **c)** Chicken Egg White Lysozyme (3 mg/mL) or **d)** BSA (0.5 mg/mL) demonstrate specificity of wALADin1 for wALAD.

3.2.2 wALADin1 and the oligomeric equilibrium of wALAD

As a morpheein wALAD forms a complex equilibrium of multiple homomeric assemblies characterized by different catalytic activities. To determine whether wALADin1 interferes with the oligomeric equilibrium of wALAD, we studied oligomerization properties of wALAD and used hALAD as a control for the localization of hexameric and octameric bands in the native polyacrylamide gels. For hALAD, preincubation with the substrate 5-ALA led to the expected shift towards the active octameric conformation (**Fig. 3.6 a**). In the case of wALAD, a complete transition from hexameric to the octameric state was achieved by the addition of DTT (**Fig. 3.6 a**). The higher molecular weight bands occasionally observed for wALAD may represent aggregated states. (**Fig. 3.6 b**, upper panel). The in-gel activity assay (**Fig. 3.6 b**, lower panel) revealed that, like other orthologs, wALAD is active in the octameric and inactive in the presumably hexameric smaller molecular weight conformation. I also showed that preincubation of wALAD with wALADin1 led to a reduction in porphobilinogen formation detected by MER while octameric band strength remained unaffected as evident from subsequent Coomassie blue staining (**Fig. 3.6 b**). These data show that wALADin1 binds to and inhibits octameric wALAD without disturbing the oligomeric equilibrium.

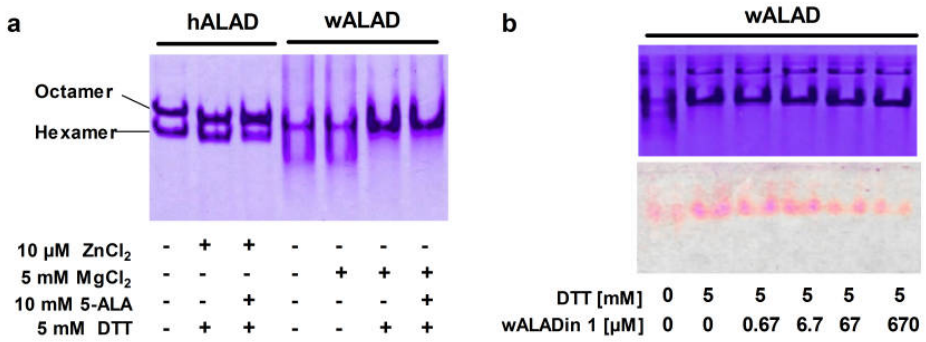

Figure 3.6: wALADin1 and the oligomeric equilibrium of wALAD
a) Non-denaturing 7.5% polyacrylamide gels stained with Coomassie blue loaded with 8 μg hALAD or wALAD. Proteins were pre-incubated for 30 min at RT in the presence or absence of 10 μM $ZnCl_2$, 5 mM $MgCl_2$, 10 mM 5-ALA and/or 5 mM DTT as indicated. Preincubation of hALAD with 5-ALA shifts the equilibrium from the hexameric towards the octameric assembly. 5 mM DTT shifts the wALAD equilibrium completely towards octamer formation. **b)** Native page of 5 μg wALAD protein preincubated with 5 mM DTT and 0 to 670 μM wALADin1 for 30 min at RT. For monitoring of in-gel enzymatic activity, gels were soaked in activity assay buffer containing 5-ALA and incubated for 1h at 36 °C before staining with MER (lower panel) and Coomassie blue (upper panel). Image contrast was adjusted with Adobe Photoshop Elements 3.0.

3.2.3 The molecular mode-of-action of wALADin1

Having confirmed the binding of wALADin1 to the active ALAD oligomer, the inhibitory mechanism of this novel inhibitor was studied. wALAD being a Mg^{2+}-dependent enzyme (EC_{50} ~11 μM, **Fig. 3.7 a**) the influence of Mg^{2+}-concentration on the inhibitory potency of wALADin1 was analyzed. wALADin1 caused a rightward-shift of the Mg^{2+}-response curve indicating a functional competition between inhibition by wALADin1 and the activation induced by Mg^{2+} (**Fig. 3.7 b**). However, non-linear regression ("*log(agonist) vs. response - variable slope*") under the constraint of a shared Hill slope for all data sets predicted decreased maximum enzymatic velocity (V_{max}) for increasing concentrations of wALADin1, indicating that the inhibition by wALADin1 may only be partially overcome by the activation by Mg^{2+}.

The type of inhibition exerted by wALADin1 was studied by cross-titrating different wALADin1 concentrations against varying concentrations of the 5-ALA substrate in the wALAD enzymatic assay. Both non-linear regression analysis and linearized Eadie-Hofstee representation indicate that the wALADin1 inhibitory mechanism is best described as a mixed model inhibition (**Fig. 3.7 c, d**). Best NLR curve fit was obtained employing an "*Allosteric sigmoidal*" model accounting for cooperative effects. Increasing wALADin1 concentrations led to a decrease in V_{max} (non-competitive inhibition) and increase in K_M values (competitive inhibition) as characteristic for mixed model inhibition. Prediction of the inhibition constant K_I required a non-linear regression analysis assuming a global model such as the "*Mixed Model Inhibition*" NLR. Predicted K_I was 5.95 ± 0.95 μM with a corresponding α-value of 31.44 ± 9.59 μM (R^2 = 0.9794) using 1.0 mM $MgCl_2$. The K_I predictions and the α-value varied at different $MgCl_2$ concentrations (0.5 mM $MgCl_2$: K_I = 3.2 μM; α = 43.10, R^2= 0.9759; 5 mM $MgCl_2$: K_I = 25.1 μM; α = 14.74, R^2 = 0.9732). In general, an increase in $MgCl_2$ led to lower predicted affinities (higher K_I) and a more pronounced substrate-competitive character of the inhibition as indicated by increased α as in accordance with a mixed competitive/ non-competitive inhibitory mechanism.[1]

[1] For a morpheein sampling different oligomeric states, it is accepted that two-phasic substrate-concentration rows are observed reflecting the different catalytic activities for the reactive centers in the different conformations [135]. It might therefore be appropriate to assume a double hyperbolic progression accounting for the different binding sites. However, subjecting the data to non-linear regression assuming a double hyperbolic fit gave the following data (R^2 = 0.9902 - 0.9961): 6.7 % DMSO : $V_{max,1}$ = 0.071, μM; $V_{max,2}$ = 0.014, $K_{M,1}$ = 163 μM, $K_{M,2}$ = 3.4 mM); 6.25 μM wALADin1: $V_{max,1}$ = 0.053, μM; $V_{max,2}$ = 0.013, $K_{M,1}$ = 254 μM, $K_{M,2}$ = 4.2 mM, 25 μM wALADin1: $V_{max,1}$ = 0.046, μM; $V_{max,2}$ = 0.023, $K_{M,1}$ = 456 μM, $K_{M,2}$ = 6.4 mM; 100μM wALADin1: $V_{max,1}$ ~0.027, μM; $V_{max,2}$ ~0.023, $K_{M,1}$ ~1.623 mM, $K_{M,2}$ ~1.624 mM. These data are consistent with an increase in both K_M-values and the overall V_{max} upon increasing concentrations of wALADin1. Thus, while marginally improved fits were obtained for three conditions, for 100 μM wALADin1, the fit is clearly not superior to a simple hyperbolic fit. Furthermore, analyses of different data sets based on single experiments (**Fig. 3.22, 3.24**) revealed no evidence for a double-hyperbolic progression. This finding is in accordance with native PAGE data revealing a uniform protein population under assay buffer conditions (**Fig. 3.6**). Thus, suitability of double hyperbolic fits for different data sets of the wALAD protein is ambiguous and even in the mentioned cases where a double hyperbolic fit was slightly superior, the mechanistic conclusions are qualitatively equivalent to those drawn from a simple hyperbolic or "*Allosteric sigmoidal*" fit. Therefore, throughout this work non-linear regression analysis was performed applying the "*Allosteric sigmoidal*" model.

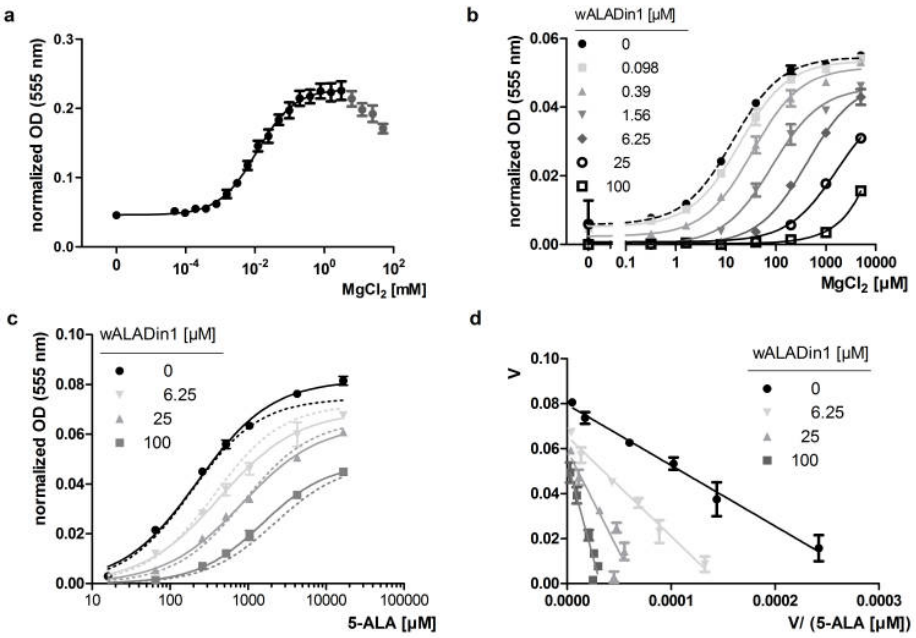

Figure 3.7: The inhibitory mechanism of wALADin1

a) Dose-response curve for $MgCl_2$ on wALAD activity (EC_{50} = 11 μM) depicted as means ± SEM of three independent experiments applying a near-saturating 5-ALA concentration (1 mM). **b)** wALADin1 functionally competes with the activation induced by $Mg2^+$ as evident in a rightward shift of the $Mg2^+$-response curve of wALAD (non-saturating 5-ALA concentration of 0.2 mM). Curves were fit using the "*log(agonist) vs. response - variable slope*" non-linear regression algorithm assuming (constraints: shared hill slope vor all data sets and bottom ≥ 0). **c)** Substrate-concentration rows in the presence of different concentrations of wALADin1. Continuous lines show fit with "*Allosteric sigmoidal*" (R^2 between 0.9893 and 0.9939), dashed lines show fit with "*Mixed Model Inhibition*" non-linear regression algorithm (R^2 = 0.9794). **d)** Linearized Eadie-Hofstee representation of wALAD activity in the presence of wALADin1. The decrease in the y-axis intercept corresponds to a decrease in V_{max}, the increased slope corresponds to an increase in the apparent Michaelis-Menten constant. This classifies wALADin1 as a mixed competitive and non-competitive inhibitor. **b - d** depict means ± SD of two independent experiments.

3.2.4 Solubility of wALADin1

In order to determine the solubility of wALADin1, an absorption spectrum (UV-VIS) of the compound was recorded in wALAD assay buffer with 1% DMSO. The spectrum showed an extinction peak at 228 nm and a shoulder area between 250 nm and 280 nm (**Fig. 3.8 a**). Solubility of the compound was verified as an increase in specific extinction along a two-fold concentration row of wALADin1 in assay buffer/1%DMSO. Centrifugation would remove any precipitated compound from the solution and the linear increase in absorption would be stopped as soon as solubility is exceeded. As the absorption at 228 nm was very strong and exceeded the linear detection range (with OD = 1.0 as the upper limit) already at relatively low concentrations, OD was measured in the shoulder area at 253 nm. Throughout the concentration range tested (up to 1 mM) solutions showed a linear increase in OD_{253nm} (**Fig. 3.8 b**) which revealed solubility of wALADin1 under these conditions.

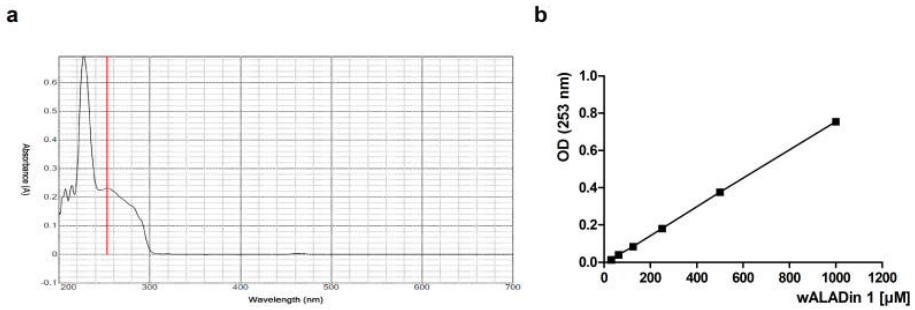

Figure 3.8: UV-VIS absorption spectrum of wALADin1 and solubility measurements
a) UV-VIS absorption spectrum of wALADin1 determined in wALAD assay buffer with 1% DMSO. The vertical line indicates $\lambda = 253$ nm. **b)** A concentration row of wALADin1 in wALAD assay buffer/1% DMSO was prepared, incubated at RT for > 30 min and centrifuged at maximum speed to pellet precipitated compound, if any. The concentration row shows a linear increase increase in OD_{525nm} throughout the concentration range tested. wALADin1 is therefore easily soluble in wALAD assay buffer at concentrations up to 1 mM.

3.3 Antifilarial activity of wALADin1

Having demonstrated and characterized the inhibitory effects of wALADin1 on wALAD at the molecular level, the antifilarial activity of this species-selective inhibitor was addressed. wALADin1 was tested for its activity against the rodent filarial nematode *Litomosoides sigmodontis*, which also harbors *Wolbachia* endobacteria, and is a model for human pathogenic filarial nematodes causing LF/Oncho [203, 258, 7]. These studies were complemented with cytotoxicity experiments applying wALADin1 on both LLC-MK2 (monkey kidney) cells and HEK (human embryonic kidney) cells.

3.3.1 Cytotoxicity tests

Cells were exposed to different concentrations of wALADin 1 for 48 h and cellular viability was measured by MTT assay. For both cell lines 500 μM and 1 mM wALADin1 led to reduced viability values (**Fig. 3.9**). In the co-culture experiments described below the LLC-MK2 cell lawn was intact at 500 μM wALADin1 throughout the 14 days of the experiment and cells did not show signs of apoptosis. Thus, rather than exerting a genuine cytotoxic effect, wALADin1 may have antiproliferative activity on eukaryotic cells at these high concentrations that may account for the reduced viability rates.

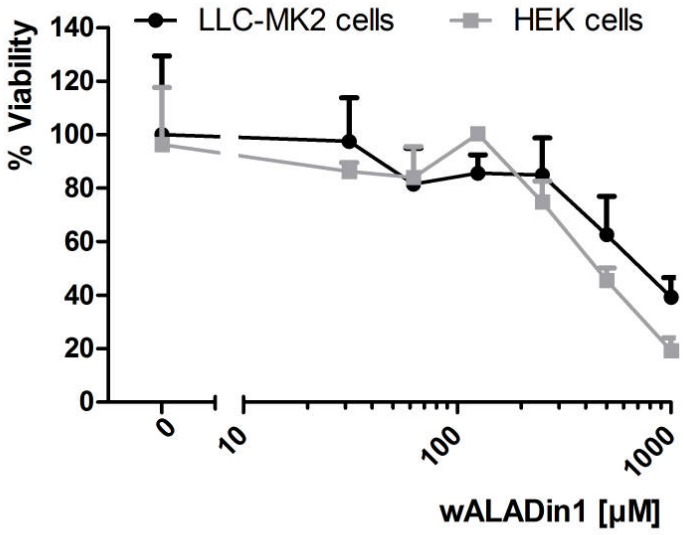

Figure 3.9: Cytotoxicity of wALADin1 on eukaryotic cell lines
Cellular viability measured by MTT assay in Human Embryonic Kidney (HEK) and Monkey Kidney (LLC-MK2) cell lines treated for 48 h with different concentrations of wALADin1. The graph shows median values (n=6) and interquartile range of data normalized to the median OD_{550nm} of 1% DMSO-treated cells as a 100% viability control.

3.3.2 Efficacy of wALADin1 in *L. sigmodontis* co-culture assay

The antifilarial activity of wALADin1 was addressed in an assay system using the model rodent filarial nematode *L. sigmodontis* in co-culture with LLC-MK2 monkey kidney feeder cells. Adult female *L. sigmodontis* worms were exposed to wALADin1 at 125, 250 and 500 μM, concentrations that were $\sim$10 - 50 fold higher than the enzymatic assay IC_{50} concentration. This excess was considered necessary to reach effective concentrations in the biophase of the living worm given that the compound must traverse the worm cuticle and several membranes to reach its enzymatic target and that accumulating substrate would (partially) compete with the inhibitor thus lowering its potency.
Worms were cultured as long as 1% DMSO-treated controls revealed no major impairment of motility (14 - 17 days). During the course of the experiment worm motility was rated daily while worm viability was addressed by MTT-assay at the end of the treatment period. All concentrations tested impaired the motility of *L. sigmodontis* throughout the experiment (**Fig. 3.10 a, b**.) While healthy worms (worms from before treatment and control-treated worms) had rapid, fidgeting and mostly continuous movements, affected worms had a more stretched phenotype and their movements became slower and less continuous. wALADin1-treated worms, however, had a very specific phenotype: Worms wound up in knot-like forms with greatly reduced motility (motility scores 4, 3) culminating in the stretched low-motility phenotype of dying/dead worms (**Fig. 3.10 a, Supplementary Videos 1 - 3**). Quantification of the filaricidal effect of wALADin1 was achieved by measuring the biochemical viabiliy of the worms by MTT assay. Worms treated with either concentration of wALADin1 produced significantly smaller amounts of MTT-formazan compared to the DMSO-treated controls (Mann-Whitney-U test, $p < 0.05$, **Fig. 3.10 a**). Median residual viabilities for the different treatment groups were 44%, 27% or 7.5% viability for 125 μM, 250 μM and 500 μM of wALADin1, respectively. These values allowed a rough estimation of the EC_{50} concentration of $\sim$100 μM which was one order of magnitude higher than the IC_{50} of the *in vitro* enzymatic assay.

In order to prove that the observed antifilarial effect is due to the inhibition of the heme-biosynthesis enzyme ALAD inside the *Wolbachia* endosymbionts, wALADin1 was also tested for activity in the *Wolbachia*-free filarial model nematode *Acanthocheilonema viteae* [176]. As the genome of this filaria has recently been elucidated, a nucleotide blast query against the *A. viteae* genome database (Blaxter, M.L. The genome of the filarial nematode *Acanthocheilonema viteae*, Edinburgh, UK, 2012) was conducted employing the *hemB* gene sequences of *Wolbachia* of *B. malayi*, *H. sapiens* and yeast as input sequences. As no orthologous sequences were found in the genome of *A. viteae* it was concluded that these worms lack ALAD as the molecular target of wALADin1. Thus, *A. viteae* should only be sensitive to non-specific effects exerted by wALADin1 allowing the dissection of specific and non-specific effects of this compound. The only effect seen for *A. viteae* required a wALADin1 concentration of 500 μM and became manifest as a rapid decrease in motility, evident already $\sim$2 h after treatment (**Fig. 3.10 d**). However, after this initial one step decline, motility did not deteriorate until day 12. Any comparison between *L. sigmodontis* and *A. viteae* motility should be done with caution, as the motility phenotypes are generally dissimilar and each refers to its own scoring system. Notwithstanding, wALADin1 did not induce the knot-like phenotype characteristic for wALADin1-treated *L. sigmodontis* on *A. viteae*. The more reliable parameter tested was worm viability. Viability of wALADin1-treated *A. viteae* was not significantly affected (**Fig. 3.10 e**) and lower concentrations had no effect on either worm viability or motility (**Fig. 3.10 d, e; Supplementary Videos 1,**

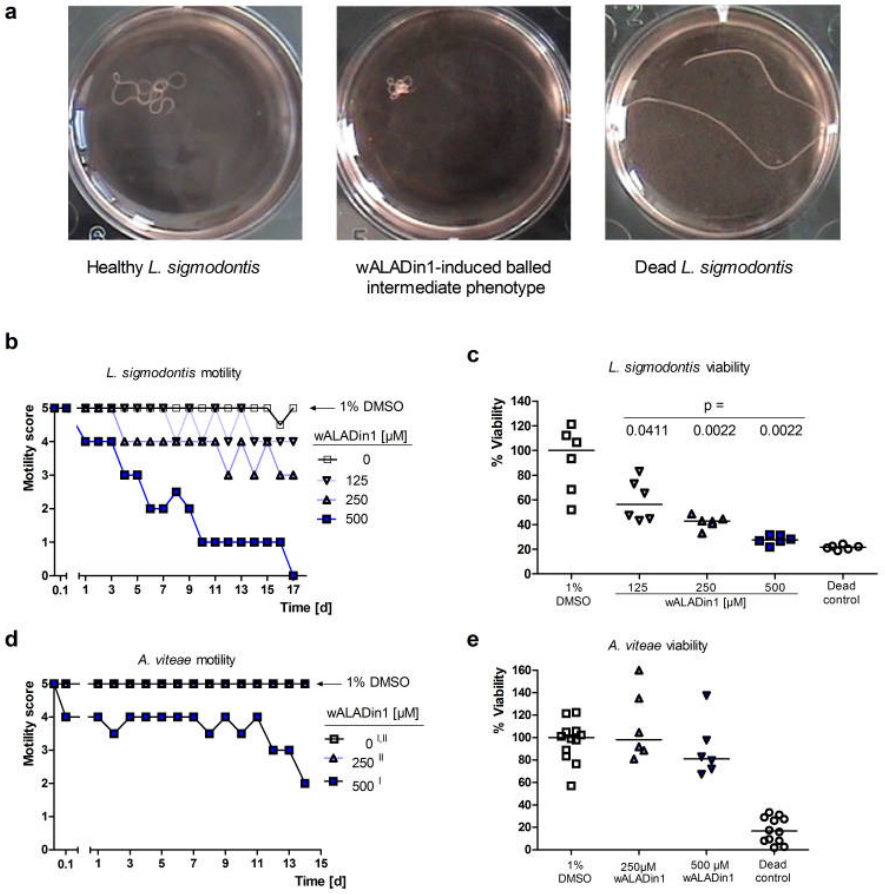

Figure 3.10: wALADin1 has a *Wolbachia*-dependent macrofilaricidal effect

a) - c) Adult females of the *Wolbachia*-harboring *L. sigmodontis* and **d), e)** *Wolbachia*-free *A. viteae* model filarial nematodes were exposed to different concentrations of wALADin1 or 1% DMSO for 14 - 17 days. **a)** Exemplary pictures of *L sigmodontis* worms revealing wALADin1-elicited phenotypes. **b)** All concentrations of wALADin1 showed an antifilarial effect on *L. sigmodontis* evident in a continuous reduction of motility and **c)** significantly impaired viability at the end of treatment (non-parametric, two-tailed Mann-Whitney-U test, $p < 0.05$), **d)** while only 500 μM wALADin1 had a minor non-specific effect on motility of *A. viteae*. **e)** wALADin1 did not affect viability of *A. viteae*. Data are representative of 2 experiments. Motility graphs show median values (n=6). Percent viability data were obtained by normalizing MTT assay data to the median OD_{490nm} of 1% DMSO-treated worms (set to 100% viability). For *A. viteae* data of two independent experiments are shown in **d** that are marked with I and II, respectively. In **e**, normalized viability data of the control groups were pooled and all groups are shown in a single graph. d = days.

4, 5). In comparison, for *L. sigmodontis* there was still a ∼56% impairment at 125 μM. While the non-specific effect on *A. viteae* motility at 500 μM wALADin1 may correspond to the weak cytotoxicity observed at this and higher concentrations (**Fig. 3.9 a**) the specific impairment of *L. sigmodontis* viability throughout all concentrations tested demonstrates the *Wolbachia*-dependency of the filaricidal effects of wALADin1.

3.3.3 Effects of 5-ALA in the *L. sigmodontis* co-culture

I considered that the macrofilaricidal effects induced by wALADin1 may, at least to some extent, be due to increased levels of 5-aminolaevulinic acid (5-ALA) that build up as a consequence of ALAD inhibition. To test this hypothesis, motility and viability of *L. sigmodontis* were measured under exposure to exogenous 5-ALA. Indeed, both motility and viability were reduced under treatment with 1 mM or 5 mM 5-ALA, respectively, while a concentration of 200 μM had little effect (**Fig. 3.11**). Thus, high concentrations of 5-ALA do have a filaricidal effect and this "directed" toxicity may act in combination with a reduction in heme-levels to drive the antifilarial effect of wALADin1.

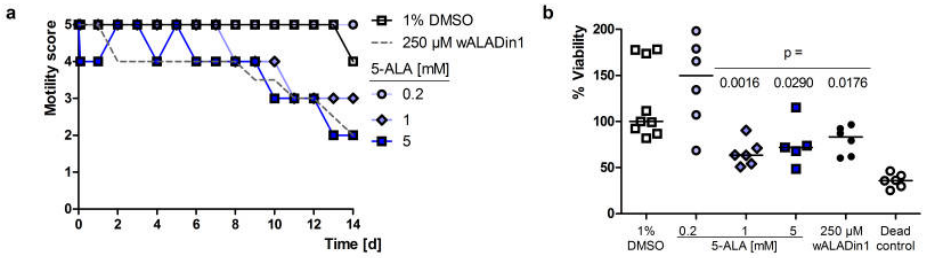

Figure 3.11: 5-ALA has a macrofilaricidal effect on *L. sigmodontis*
Adult *L. sigmodontis* females were exposed to different concentrations of 5-ALA (the substrate of the ALAD enzyme), 1% DMSO or 250 μM wALADin1 as controls. **a)** 1 mM and 5mM 5-ALA induced reduced worm motility and **b)** viability (non-parametric, two-tailed Mann-Whitney-U test, $p < 0.05$, as measured by MTT-assay at the end ot the treatment period. **a** depicts median values (n=6; for 1% DMSO: n=9; for 500 μM wALADin1: n=5), bars in **b** indicate median values. Percent viability data were obtained by normalizing MTT assay data to the median OD_{490nm} of 1% DMSO-treated worms (set to 100% viability). d = days.

3.3.4 BLAST search for a gene with protoporphyrinogen IX oxidase function in *Wolbachia*

The only heme biosynthetic genes for which no homolog has been identified are the *hemY/hemG* genes encoding protoporyphyrinogen IX oxidase catalysing the penultimate step of heme biosynthesis. A candidate gene encoding protoporphyrinogen IX oxidase function recently identified in *Synechocystis spp.* and *Rhodobacter sphaeroides* is the *slr1790* gene [146]. In order to test whether a homolog exists also in the *Wolbachia* genome a tblastn search was undertaken querying all currently available filarial genome databases with the *Synechocystis spp. slr1790* gene (also termed *hemJ*) product. Significant alignments were found in all *Wolbachia* genomes (*D. immitis* - Score = 83, E value = 2e-15; *L. sigmodontis* - Score = 83, E value = 2e-15; *B. malayi* - Score = 77; E value = 1e-13; *O. ochengi* - Score = 77; E = 1e-13), but not in nuclear or mitochondrial genome assemblies of *A. viteae*, *B. malayi*, *D. immitits*, *L. sigmodontis*, *L. loa*, *O. ochengi* or *W. bancrofti* (**Fig.**

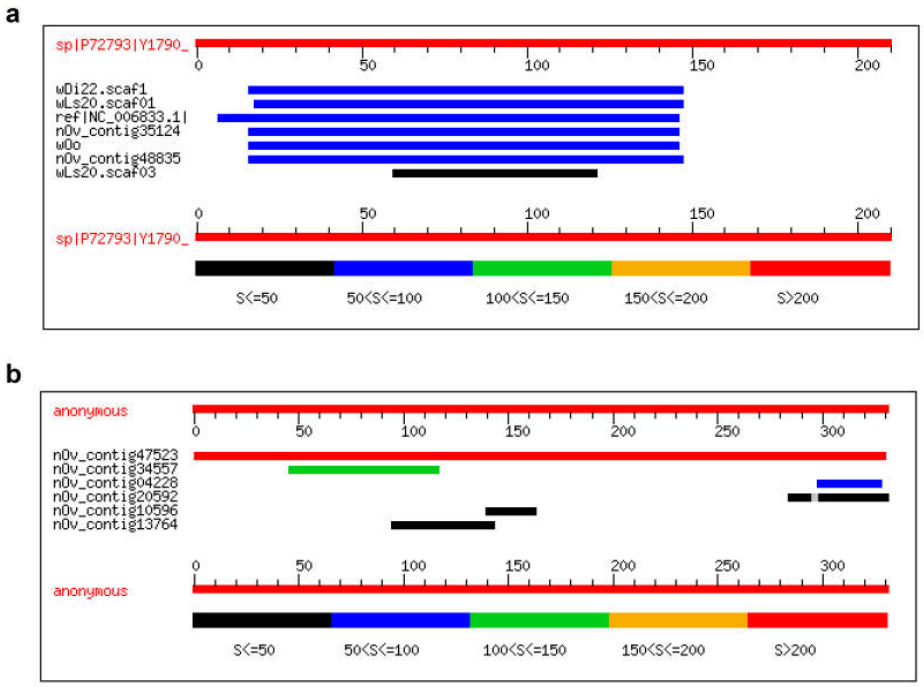

Figure 3.12: Results of a tblastn search for homologs of the *slr1790* gene **a)** Significant alignments produced by tblastn search against the "All Filarial Genomes 2012-08-24" assembly (Mark Blaxter, University of Edinburgh, 2012) with the *slr1790* gene product of *Synechocystis spp.* as input sequence (Uniprot ID: P72793, sp|P72793|Y1790)). Homologous sequences were identified in the *Wolbachia* genomes of *D. immitis* (wDi22.scaf1), *B. malayi*(ref|NC_006833.1|), *L. sigmodontis* (wLs20.scaf01, wLs20.scaf03), *O. ochengi* (wOo) and the genome assembly of *O. volvulus* (nOV_contig35124, nOV_contig48835). **b)** tblastn search against the *O. volvulus* nuclear genome assembly 1.0 (Jeremy Cotton, Wellcome Trust Sanger Institute, 2012) using the wALAD gene sequence (Uniprot ID: Q5GSR3, "anonymous") as input. A gene encoding the *Wolbachia* protein (nOv_contig47523) was identified indicating the presence of *Wolbachia* genes within this assembly. All queries were run over the "BLAST search and download server for Filaria-EU" server (http://xyala.cap.ed.ac.uk/downloads/959nematodegenomes/blast/filareu.php) under default alignment settings.

3.12 a). The significant alignments found for the *O. volvulus* nuclear genome assembly (Score=77, E value = 1e-13) are likely derived from contained *Wolbachia* sequences, as tblastn search using the wALAD gene sequence produced a perfect alignment (Score=680; E value = 0.0) (**Fig. 3.12 b**). Identification of this putative translated protein sequence encoded in the *Wolbachia* genome with significant homology to the *slr1970/hemJ* product suggests it may fulfil the missing protoporphyrin IX oxidase function in the heme biosynthesis pathway of the endosymbiont.

3.4 Tests for antifilarial activity of wALADin1 *in vivo* during *L. sigmodontis* infection

Validation of the antifilarial activity of wALADin1 *in vivo* was done using the model of BALB/c mice naturally infected with *L. sigmodontis*. Treatment was started at 1 day post infection and continued for up to 28 days. The gold standard of anti-*Wolbachia* therapy 1 mg (50 mg/kg) doxycycline for 14 d showed the expected potent antifilarial effect manifest in reduced female worm length and a reduction of intracellular *Wolbachia* by more than 99.9% as measured by quantitative Realtime-PCR. No such effect was evident for worms recovered from mice treated with 1 mg wALADin1 for 14 or 28 d (**Fig. 3.13 a, b**). As the limit of solubility was reached for wALADin1 in the given formulation (Minimal Essential Medium, like in the *ex vivo* culture system, but without supplements) a vehicle with increased solubility of wALADin1 was selected for the delivery of higher doses. As MEM already featured significant improvements in solubility compared to PBS or water, Earl's Balanced Salt Solution (EBSS), the buffer content of MEM, was selected and supplemented with 2-Hydroxypropyl-β-cyclodextrins (CD). Cyclodextrins are cyclic oligosaccharides derived from α-1-4-linked glucose oligomers composed of 6 - 8 subunits that present a hydrophobic core allowing formation of inclusion complexes with biomolecular ligands, thus promoting solubility of the complexed molecules in the aqueous vehicle [235, 98, 153]. Cyclodextrin containing vehicles are successfully employed to deliver poorly soluble drugs in the clinic and have a mostly benign toxicological profile [98]. However, higher doses of wALADin1 in CD-containing vehicles (2 mg or 2 x 2 mg per day) still had no effect on filarial development and *Wolbachia* numbers (**Fig. 3.13 c, d**).

Given the high concentrations required to achieve macrofilaricidal effects in the *ex vivo* setup ($\geq$ 125 μM) and insecurities about bioavailability of the compounds in the mouse, wALADin1 was finally delivered locally to the site of *L. sigmodontis* infection, i.e. the pleural cavity. The experimental layout was slightly changed, as larvae appear first in the pleural cavity $\sim$7 days post infection [122] which was chosen as the starting point for intrathoracic administration of 0.4 mg wALADin1 or CD-containing vehicle in a volume of 100 μL. In order to monitor any antifilarial effect evident in the course of infection, mice were euthanized at different timepoints (21 dpi, 28 dpi, 25 dpi) and length and viability of isolated worms were determined (**Fig. 3.14**). Throughout these time points there was no significant difference between length and viability of worms from wALADin1- and vehicle-treated mice. Both treatment groups seemed to affect worm development in comparison to the non-treated control groups. However, this effect requires further studies including higher mouse numbers and a higher infection rate for a statistically sound analysis (The worm burden of mice in the given experiment was very low with high variations (0 - 9 females per mouse) preventing the use of a data set of "pooled worms" per treatment group for statistical analysis). Whether the apparent antifilarial effect of the vehicle is due to the mere presence of liquid in the pleural cavity, diluting nutrients or growth factors, or is elicited by CD, that may non-specifically complex these biomolecules, remains to be determined.

In summary, at the doses and formulations tested, no beneficial effects of wALADin1 on the outcome of *L. sigmodontis* infection in mice were observed. As this outcome may be the result of insufficient bioavailability of the compound due to rapid metabolization and excretion or non-specific binding *in vivo*, the discovery of wALAD inhibitors with similar or improved biological activity based on the benzimidazole and other scaffolds is of paramount importance. Such compounds may feature improved potency, specificity and pharmokinetic profiles and may achieve the desired *in vivo* efficacy. In the following section a variety of benzimidazole-

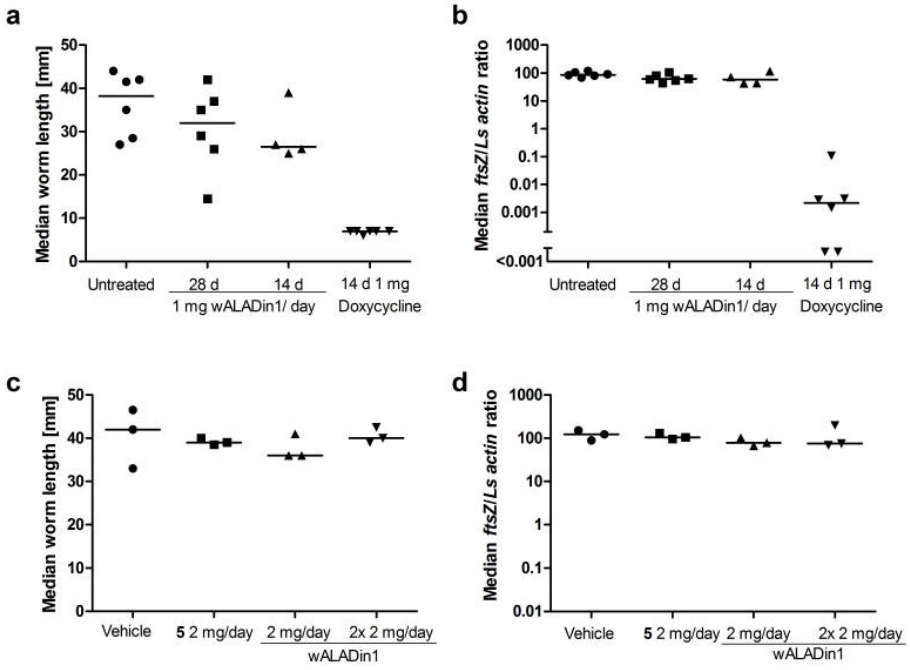

Figure 3.13: Effects of intraperitoneally-delivered wALADin1 on murine *L. sigmodontis* infection

a), b) BALB/c mice were treated i.p. for 14 - 28 days with 1 mg wALADin1 or doxycycline or were left untreated. **c), d)** BALB/c mice were treated for 14 - 28 days with 2 mg wALADin1, 2 x 2 mg wALADin1, 2 mg or vehicle (25 mM 2-Hydroxypropyl-β-cyclodextrin in EBSS) or were left untreated. **a)** Female worm length and **b)** *Wolbachia ftsZ/L.sigmodontis* β*-actin* gene copy ratios showed no effect of wALADin1 treatment on filarial development. Graphs depict the median female worm length or median *ftsZ/Lsactin* gene copy ratio, respectively, of all worms per mouse. No statistically significant difference was observed compared to non-treated and vehicle-treated groups, respectively (non-parametric, two-tailed Mann-Whitney-U-Test, $p > 0.05$).

based wALADin1 derivatives and chemically similar non-benzimidazole based small molecules were tested for their wALAD-inhibitory properties in order to identify such improved inhibitors.

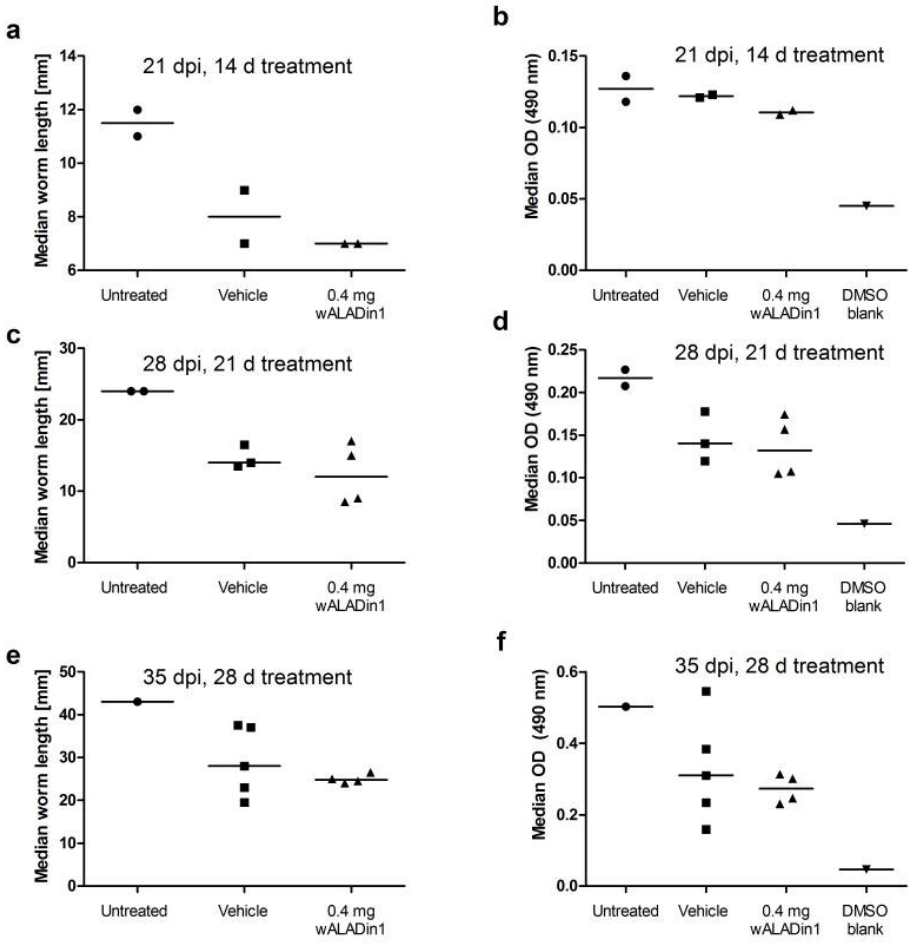

Figure 3.14: Effects of intrathoracically-delivered wALADin1 on murine *L. sigmodontis* infection

BALB/c mice were naturally infected with *L. sigmodontis* and from 7 dpi on treated for 14, 21 or 28 days with 0.4 mg wALADin1, vehicle (30 mM 2-Hydroxypropyl-β-cyclodextrin in EBSS) or were left untreated. Worms were isolated from the thoracic cavity of euthanized mice at **a), b)** 21, **c), d)** 28 or **e), f)** 35 dpi. **a), c), e)** There was no difference in the female worm length or **b), d), f)** biochemical viability as measured by MTT-assay throughout all time points. Graphs depict median female worm length or median OD values (MTT-Assay), respectively, of all worms per mouse. Differences between treatment groups were tested for significance using the non-parametric, two-tailed Mann-Whitney-U-Test. d = days.

3.5 wALADin1 Structure-Activity Relationship studies (SAR)

3.5.1 Inhibitory potency of wALADin1 derivatives in the enzymatic assay

In collaboration with the LIMES-Institute, a set of wALADin1 derivatives were synthesized by Victoria Halls and Dr. Jeffrey Hannam that I tested for activity in the enzymatic assay with the aim to identify more potent inhibitors and to understand the context of chemical structure and biological activity. An overview of the different structures and their inhibitory activities is given in **Table 3.2**. In a first set of derivatives the single substitutent groups attached to the benzimidazole core of wALADin1 at R_1, R_2 and R_3 (**Fig. 3.15**), were replaced by hydrogen atoms in order to determine the general imporance of each substituent for inhibitory activity (Compounds **2**, **3** and **4**). While **3**, with a hydrogen atom as the R_2 substituent, still retained the inhibitory potency of wALADin1 (IC_{50} -values: wALADin1: 11 μM, **3**: 13 μM), loss of the R_1 3-trifluoromethyl benzyl group (**2**) or R_3-carboxylic acid were not tolerated and led to an abrogation of inhibitory activity. The R_2-2-[(2-thienylcarbonyl)amino]ethyl substituent of wALADin1 (473.5 Da) resulted in a smaller molecule **3** (320 Da) with nearly equivalent inhibitory potency and represents an improved drug lead candidate.

Next, the influence of the R_1 carboxylic acid (absent in inactive **4**) on inhibitory function was addressed in more detail. Inactivity of a methyl ester variant of wALADin1 (**5**) further demonstrated a pivotal role of this group for inhibitory activity. The carboxyl moiety may be important in two ways: One explanation is that it simply enhances solubility of the compounds thus enabling concentrations sufficient for an inhibitory effect to occur. Alternatively the carboxylic acid has a functional role during binding/inhibition. We found that a series of consitutional isomers with the carboxylic acid attached to the C_6, C_4 or C_7 (instead of C_5 in wALADin1) of the benzimidazole scaffold (**6**, **7**, **8**) showed a very diverse activity spectrum. **7** was completely inactive, while **6** showed a 29-fold and **8** a 15-fold reduced inhibitory activity with respect to wALADin1. As solubility of these compounds should be very similar, the differential inhibitory potency indicates a functional role of the COOH-group. TSA experiments demonstrated that both **6** and **8** were able to bind to and stabilize the structure of wALAD although with smaller shifts in the melting temperature (ΔTm) than wALADin1 (**Fig. 3.16**). **7**, which was inactive in the enzymatic assay, did not indcuce a melt shift for wALAD, indicating that it was unable to bind to the protein. Elicited ΔTm are generally observed to to be proportional to the binding affinities of protein-stabilizing ligands [198] and reflect nicely the inhibitory potencies of these compounds in the enzymatic assay. However, while **8** was shown to be the slighly more potent inhibitor than **6**, **6** induced a higher ΔTm. This outcome may be explained by different enthalpic and entropic contributions to the free energy of binding of these compounds. It is also important to note that these binding experiments were performed in the absence of substrate. Given the partial substrate-competitive character of wALADin1, it is conceivable that the binding potency of these derivatives is differentially influenced by the absence of 5-ALA in thermal shift assay experiments compared to enzymatic assay experiments resulting in a different ranking of potency. Taken together, both enzymatic inhibition and TSA studies indicate a pivotal role for the R_3-COOH in inhibition and at the level of binding suggesting a direct interaction of this group with the wALAD protein, e.g. by salt bridge formation.

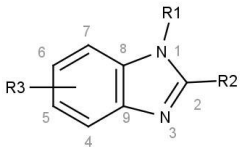

Figure 3.15: Benzimidazole scaffold of wALADin1 derivatives in Table 3.2

Table 3.2: Inhibitory activity of wALADin1 derivatives

					Wolbachia ALAD		human ALAD	
Compound	**R_1 residue**	**R_2 residue**	**R_3 residue**	**R_3 position at benzimidazole**	**IC_{50} [μM]**	**R^2**	**IC_{50} [μM]**	**R^2**
1	3-CF_3-benzyl	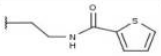	-COOH	C_5	11.1 ± 1.0	0.9517	*~ 739 ± 103*	*0.8582*
2	-H	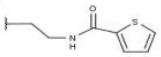	-COOH	C_5	*	-	*	-
3	3-CF_3-benzyl	-H	-COOH	C_5	13.0 ± 1.2	0.9638	197 ± 20	0.9457
4	3-CF_3-benzyl	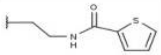	-H	C_5	*	-	*	-
5	3-CF_3-benzyl	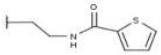	-$COOCH_3$	C_5	*	-	*	-
6	3-CF_3-benzyl	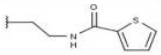	-COOH	C_6	317 ± 53	0.9022	*	-
7	3-CF_3-benzyl	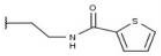	-COOH	C_4	*	-	*	-
8	3-CF_3-benzyl	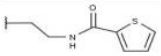	-COOH	C_7	164 ± 14	0.9551	*	-
9	4-CF_3-benzyl	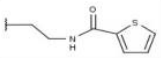	-COOH	C_5	38.6 ± 6.2	0.9670	*~ 618 ± 105*	*0.9186*
10	4-CF_3-benzyl	-H	-COOH	C_5	87.7 ± 10.5	0.9487	173 ± 12	0.9730
11	2-CF_3-benzyl	-H	-COOH	C_5	293 ± 67	0.8503	145 ± 7.2	0.9854
12	benzyl	-H	-COOH	C_5	197 ± 33	0.9042	213 ± 6.3	0.9934
13	3-CH_3-benzyl	-H	-COOH	C_5	134 ± 17	0.9394	222 ± 11	0.9864
14	3-methoxybenzyl	-H	-COOH	C_5	205 ± 12	0.9922	156 ± 7.8	0.9881
15	methyl	-H	-COOH	C_5	*	-	*	-
16	-H	-H	-COOH	C_5	*	-	511 ± 36	0.9780

* Absence of inhibitory activity
Italic font: IC_{50} values were extrapolated because < 50% inhibition was achieved at the highest concentration tested

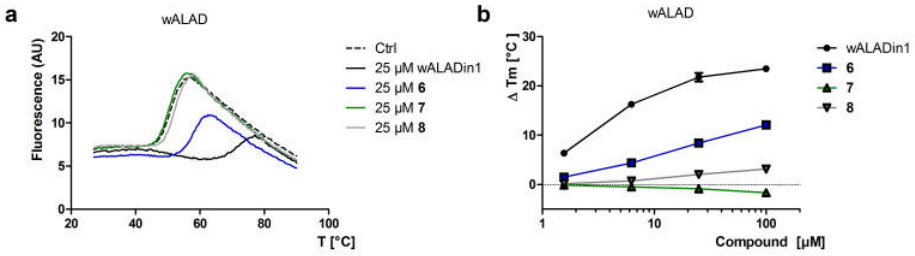

Figure 3.16: Thermal Shift Assay with wALADin1 derivatives
wALAD melting curves measured by an increase in fluorescence of the environmentally-sensitive dye Sypro®Orange (Final concentration: 8 - 16X) upon protein denaturation: **a**) wALAD (5 μM) melting curves in the presence of 25 μM of wALADin1 and isomers **6**, **7**, **8**. **b**) While **6** and **8** induced melt shifts less pronounced than for wALADin1, **7** did have no effect on the melting temperature of wALAD.

Finally, derivatives with modifications at the R_1-substituent were studied. It was noted above that compound **3** was an improved lead candidate and therefore all R_1 derivatives (except **9**) were synthesized containing a hydrogen substituent at R_2 (R_2-H compounds). Thus, two derivatives with the CF_3 residue in R_1 moved from position 3 (wALADin1) to position 4 were available: Compound **9** with an R_2-2-[(2-thienylcarbonyl)amino]ethyl and **10** with an R_2-H substituent. While **9** showed a ∼4-fold (IC_{50} = 38.6 μM), **10** had a ∼8-fold reduced activity (IC_{50} = 87.7 μM) compared to wALADin1 (and **3**). The difference in inhibitory potency of **9** and **10** revealed, that the R_2 substituent may indeed contribute to inhibitory potency. Notwithstanding, presence of the R_1-4-CF_3-benzyl substituent led to a reduction in inhibitory potency for both pairs of molecules with respect to the parent molecule. All further R_1 substituents that comprised 2-trifluoromethyl benzyl (**11**), benzyl (**12**), 3-methyl benzyl (**13**) or 3-methoxybenzyl (**14**) groups showed further reduced inhibitory activities with IC_{50} concentrations between 134 and 297 μM. Of special structural importance are the fluorine residues in the CF_3-benzyl of wALADin1 as their replacement by hydrogen atoms to CH_3-benzyl led to a 10-fold loss of inhibitory activity. The absence of the aromatic ring subsitutent in R_1 in compounds **15** and **16** that featured a CH_3-group or H-atom at this position, instead, abolished any inhibitory activity against wALAD. Having tested the set of R_2-H compounds on the human ALAD ortholog an intriguing finding was made with respect to specificity of the wALADin-inhibitors: All derivatives featuring the R_2–2-[(2-thienylcarbonyl)amino]ethyl had shown no or only marginal inhibitory activity against the human ortholog with **9** being the most potent (IC_{50} = ∼618 μM). In contrast, all compounds featuring the R_2-H substituent except **15** showed substantially higher inhbitory potency for hALAD with IC_{50} values between 145 and 222 μM (**3, 9 - 14**; for **16** IC_{50}= ∼555 $_{\mu}$M). For **14** the specificity profile was reversed: This compound had a lower IC_{50} value for hALAD (156 μM) than for wALAD (205 μM). Thus the R_2–2-[(2-thienylcarbonyl)amino]ethyl substituent appears to be an important mediator of specificity for the *Wolbachia* ortholog that prevents inhibitory activity against other orthologs such as the human protein. Taken together, these comparative studies revealed several important structural properties that contribute to both inhibitory potency and specificity.

3.5.2 Antifilarial activity of wALADin1 derivatives

Two compounds from the set of wALADin1 derivatives were tested for antifilarial activity: **3**, the R_2-H fragment of wALADin1 which showed nearly equipotent inhibitory properties compared to wALADin1 and **6**, an R_1 carboxylic acid constitutional isomer otherwise identical to wALADin1 that showed a nearly 30-fold reduced inhibitory potency in the enzymatic assay. Neither of these compounds had any cytotoxic effect on LLC-MK2 cells at 500 μM (**Fig 3.17 a**).

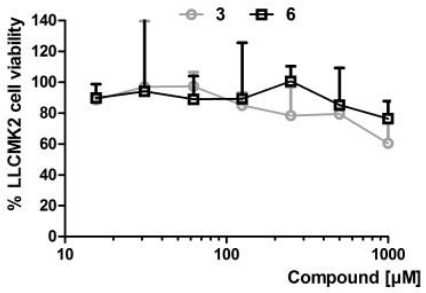

Figure 3.17: Cytotoxicity of selected wALADin1 derivatives
Cellular viability of LLC-MK2 cells treated with compound **6** or **3**. There is no cytotoxicity observed below 1 mM. The graph show median values (n=4) and interquartile range of normalized data.

3 showed generally weaker and delayed antifilarial effects on *L. sigmodontis* compared to wALADin1. However, towards the end of treatment, lower concentrations (125 and 250 μM) induced a reduction in motility similar to those achieved by equal concentrations of wALADin1 (motility scores 3 - 4). Yet, only at 500 μM, there was also a significant reduction in viability quantified by MTT-assay (38% median residual viability), while the trend to lower viabilities continued in a concentration-dependent manner also for the lower concentrations (**Fig. 3.18 b**). Compound **6** also revealed antifilarial activity at 500 μM that was weaker than for wALADin1, but stronger than for **3** and was evident in both motility scores and viability measurements (24% median residual viability, **Fig. 3.18 a, b**). However, while worms treated with **6** had a non-specific appearance, **3** induced a similar balled phenotype as reported above for wALADin1 (**Supplementary Videos 1 - 3**).

It was shown in **Fig. 3.10 d** that, at 500 μM, wALADin1 also had a non-ALAD-dependent antifilarial property evident in the rapid effect on the motility of *Wolbachia*-devoid *A. viteae*. Thus, the antifilarial effects of compounds of the wALADin family may be classified as specific ALAD-dependent with an off-target (or secondary target) effect. The differential antifilarial activity of wALADin1 and **3** in the living worm may be a result of different non-specific contributions of these compounds in addition to the specific effects achieved by inhibition of heme biosynthesis in the endosymbiont. These non-specific effects appear to be less pronounced for **3** as indicated by the delayed antifilarial activity. In contrast, due to the great chemical similarity of **6** to wALADin1 a retention of the non-ALAD-dependent effects is likely, which may be the major cause of the filaricidal effect of this compound. A more detailed elucidation of the biological profile of these and other derivatives will be required to unequivocally determine the differential effects induced by these compounds. Notably, the remarkable antifilarial activity of wALADin1 was qualitatively confirmed also for the 2^{nd} most potent inhibitor and provides a sound basis for the design of more potent antifilarials targeting ALAD of the *Wolbachia*

endosymbionts in the future. It is therefore of great importance to identify chemical structures that share the novel and unique Mg^{2+}-dependent mode of action of the inhibitors of the wALADin family but have a chemotype different to the wALADin1-benzimidazoles. First steps into this direction were undertaken and are presented in the following paragraphs.

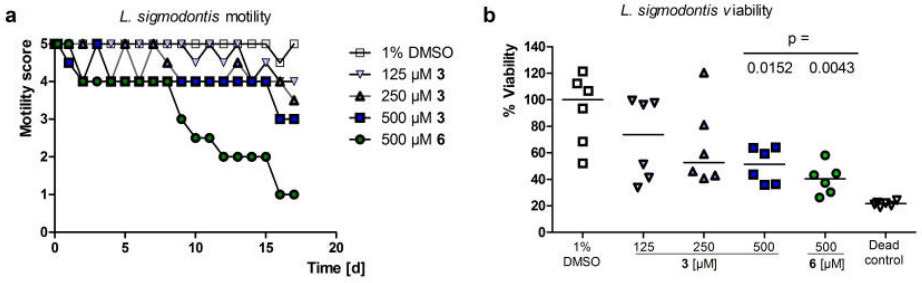

Figure 3.18: Antifilarial activity of selected wALADin1 derivatives
Adult *L. sigmodontis* females were exposed to different concentrations of wALADin1 derivatives **3** and **6** or 1% DMSO for 17 days. The data presented in this graph (incl. the 1% DMSO control) were collected in the same experiment shown in **Fig. 3.10** to allow a better comparison of compound activities. **a)** Both compounds lead to an impairment of *L. sigmodontis* motility and **b)** viability as quantified by MTT-assay at the end of the treatment period. **a** shows median values (n=6), bars in **b)** represent median values. For worm viability data, significance was tested by non-parametric two-tailed Mann-Whitney-U test; significant p-values ($p < 0.05$) are depicted in the graph. d = days.

3.6 wALAD inhibitors with a different chemical scaffold

The chemotype of the inhibitors of the wALADin1 family is a tri-substituted benzimidazole. However, molecules based on a single scaffold generally may be restricted with respect to several characteristic drug-activity related properties like potency, specificity, toxicity or bioavailability. This study therefore aimed at the discovery of other similar inhibitors with different molecular scaffolds. One non-benzimidazole inhibitor of wALAD already identified as a wALAD inhibitor during HTS was the non-aromatic benzothiazole derivative CG6 23G7. A number of compounds that showed molecular similarity to wALADin1 was selected and obtained through different sources and subsequently tested for inhibitory activity. A selection of these compounds with notable biological activity is presented in the following sections.

3.6.1 Inhibitory properties of virtual screening hits

A virtual screening of ∼3.7 million commercially available small molecules was carried out by Dr. D. Stumpfe at the Life Science Informatics (Bonn - Aachen International Center for Bioinformation Technology, LIMES-Institute Bonn, Germany). wALADin1 was used as a single template or in combination with CG3 24C7 (see **Appendix A**) for compounds with different scaffolds that were rated similar in a fingerprint-based similarity screening approach involving atom environment, fragment-based and pharmacophore information (Dr. D. Stumpfe, personal communication). From the top 100 scoring chemical scaffolds molecules were manually selected that featured a carboxyl or other group involving a negative (partial)

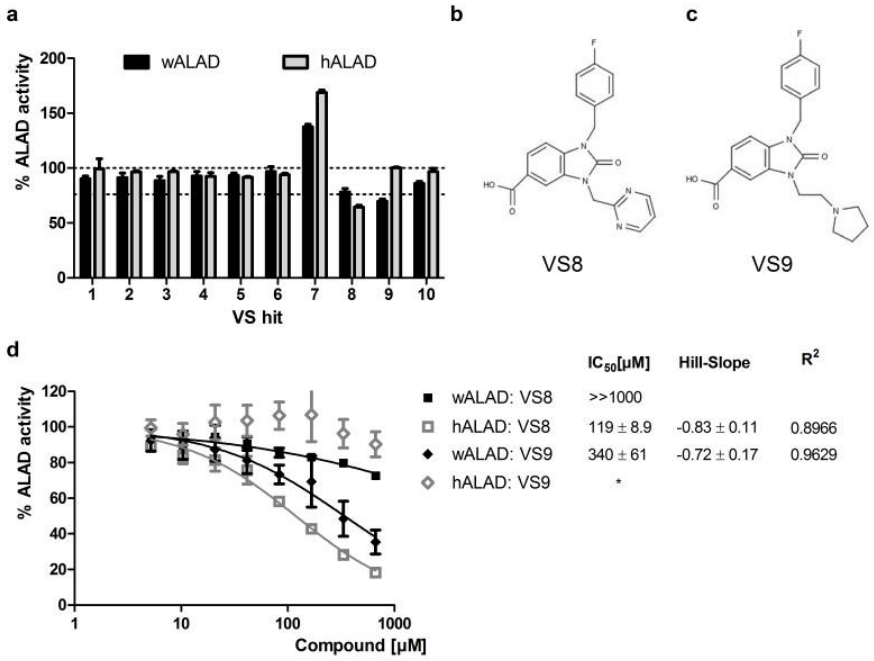

Figure 3.19: wALAD inhibitors VS8 and VS9
a) Percent enzymatic activity values of wALAD and hALAD, respectively, in the presence of virtual screening hits 1 - 9. Compounds were tested at 67 μM in triplicate measurements. Graph shows means ± SD. **b)** Chemical structure of VS8 and **c)** VS9. **d)** Dose-response curves for VS8 and VS9 in the wALAD and hALAD enzymatic assay under standard conditions. Graphs shows means ± SD of two independent experiments. Lines were fit using the "*log(inhibitor) vs. normalized response - Variable slope*" non-linear regression algorithm of GraphPad Prism 5.0. The asterisk marks absence of inhibitory activity

charge because of the dependence on a carboxyl moiety in the wALADin1 structure for inhibitory activity. 9 of these virtual screening hits were purchased and tested for inhibitory activity against wALAD and hALAD at 67 μM (**Fig. 3.19 a**). The chemical structures are shown in **Appendix A**. Only the non-aromatic 1,3-dihydro-2H-benzimidazol-2-one derivatives VS8 and VS9 showed significant inhibition (> 25%) of either ortholog. In contrast to the wALADin1-scaffold these molecules (VS8 and VS9) carry substituents at the N_3 instead of the C_2 atom of the benzimidazole ring (**Fig. 3.19 b, c**). VS8 inhibited hALAD with an IC_{50} concentration of 119 ± 8.9 μM. However, upon exchange of the (2-pyrimidinyl)methyl (VS8) to a 2-(1-pyrrolidinyl)propyl (VS9) activity against hALAD was lost, while inhibitory potency for wALAD increased dramatically to an IC_{50} of 340 ± 61 μM (**Fig. 3.19 d**). The identity of the substituent at the N_3 atom therefore decides specificity of inhibition.

3.6.2 Inhibitory properties of the Peakdale compound set

750 compounds with molecular similarity to wALADin1 had been identified in the in-house library of Peakdale Molecular Limited (Chapel-en-le-Frith, UK) and were purchased for testing of biological activity. Compounds were screened in unicate measurements at a concentration of 67 μM analogous to the initial wALAD screening.

Two highly similar compounds with inhibitory properties were the phenylthio-

phene carboxylic acid structures PD 481 and PD 593 (**Fig. 3.20 a, b**). These structures only differed in the substitution at postition 4 of the phenyl ring, which was either a bromo- (PD 481) or a chloro-substituent (PD 593). These compounds showed very weak IC_{50} values in the wALAD assay of ∼299 ± 57 μM (PD 481) and 521 ± 120 μM (PD 593), respectively (**Fig. 3.20 c**). When tested against hALAD, however, the compounds showed a remarkable 3 - 5 fold increase in inhibitory potency with IC_{50} values of 100 ± 11 μM and 85 ± 5.6 μM, respectively.

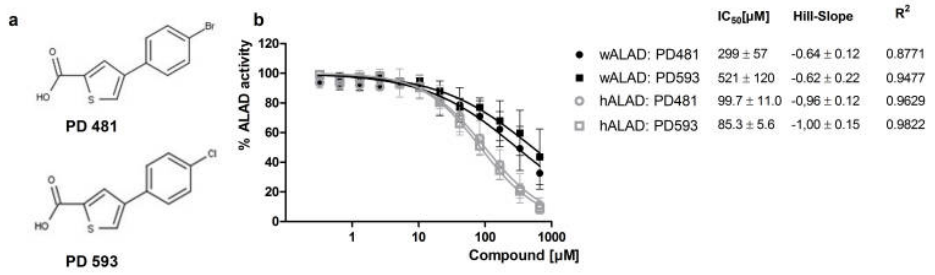

Figure 3.20: wALAD inhibitors PD 481 and PD 593
a) Chemical structures of PD 481 and PD 593 **b)** Dose-response curves for PD 481 and PD 593 in the wALAD and hALAD enzymatic assay under standard conditions. Graphs show means ± SD of two independent experiments. Lines were fit using the "*log(inhibitor) vs. normalized response - Variable slope*" non-linear regression algorithm of GraphPad Prism 5.0.

A much more potent inhibitor was compound PD 640, which inhibited wALAD activity with an IC_{50} concentration of 8.1 ± 0.1 μM while there was no effect on hALAD throughout the concentrations tested (up to 667 μM) (**Table 3.3**). It was thus not only a more specific inhibitor of wALAD than wALADin1, but it also displayed slightly increased inhibitory potency. This compound was therefore termed wALADin2 and represents the 2^{nd} generation of specific wALAD inhibitors. Chemically, the wALADin2 scaffold is a tricyclic quinoline derivative with a carboxyl group attached at the 4-position and a [3-(trifluoromethyl)phenyl]carbonyl attached to the nitrogen atom of the non-aromatic piperdinyl-like third ring (R_2 position, **Fig. 3.21**). Several wALADin2 derivatives were contained in the 750 compound set that are listed in **Table 3.3**, none of which showed inhibitory activity against wALAD. One requirement for inhibitory potency clearly was the trifluoromethlyphenyl group as its replacement by an isobutyl moiety (PD 639) abrogated inhibitory activity completely. Changing the [3-(trifluoromethyl)phenyl]carbonyl substituent to a benzyl moiety (PD 638) equally abrogated activity, as well as smaller substituents like -CH_3 (PD 637) or -H (PD 636). Further, none of the compounds with sulfonyl-, 2-OH-ethyl or propyloxy-linked aromatic rings at the R_2 position were inhibitory. Taken together, identity and length of the R_2 substituent are crucial determinants of inhibitory potency and produce a steep structure-activity profile at this site. Another derivative PD 2O features two alterations in the chemical structure compared to wALADin2: The carboxyl group at R_1 was replaced by a hydrogen atom and carbon atom at position 8 of the quinoline ring was changed to a nitrogen atom, giving rise to a 1,8-naphthyridine core. This compound was also found inactive. Although a role for the change in the heteroaromatic ring structure may not be ruled out, it is likely that the absence of the carboxyl moiety has a stronger influence on the biological properties of this compound. It is therefore assumed that, analogous to wALADin1, the carboxyl group of wALADin2 is another requirement for inhibitory activity.

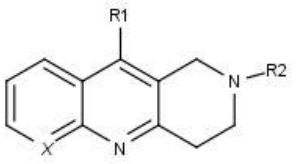

Scaffold

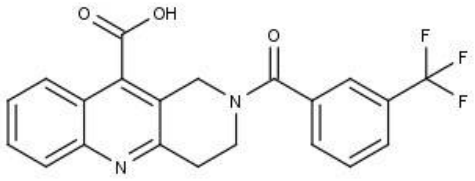

wALADin2 (PD 640)

Figure 3.21: Scaffold of the tricyclic quinoline derivatives in Table 3.3 and chemical structure of wALADin2

Table 3.3: Inhibitory activity of wALADin2 (PD 640) and derivatives

				Wolbachia ALAD		human ALAD	
Compound	**R_1 residue**	**R_2 residue**	**X**	**IC_{50} [µM]**	**R^2**	**IC_{50} [µM]**	**R^2**
PD 636	-COOH	-H	C	*	-	n.d.	-
PD 637	-COOH		C	*	-	n.d.	-
PD 638	-COOH	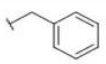	C	*	-	n.d.	-
PD 639	-COOH		C	*	-	n.d.	-
PD 640	-COOH	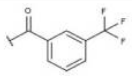	C	8.1 ± 0.8	0.9537	*	-
PD 641	-COOH		C	*	-	n.d.	-
PD 642	-COOH	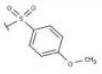	C	*	-	n.d.	-
PD 643	-COOH	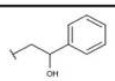	C	*	-	n.d.	-
PD 644	-COOH	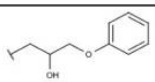	C	*	-	n.d.	-
PD 2O	-H	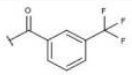	N	*	-	n.d.	-

* Absence of inhibitory activity
n.d.: not determined

wALADin2 was identified based on its molecular similarity to wALADin1. To see whether it also acts by the same mechanism of action substrate-concentration curves were measured for wALAD incubated with different concentrations of wALADin2. In the presence of wALADin2 V_{max} was reduced as evident in the decreased plateaus in the normalized data (**Fig. 3.22 a**) and decreased y-axis intercepts in the linear Eadie-Hofstee representation (**Fig. 3.22 b**). Furthermore, lines in the Eadie-Hofstee diagram ran nearly parallel, with slightly decreased slope for the highest concentration of wALADin2 (100 μM). This indicated a non-competitive mode of action. Although non-linear regression analysis assuming non-competitive inhibition gave superior fits (global $R^2 = 0.9215$) over competitive or uncompetitive inhibiton and was equivalent to mixed model inhibition (α=0.6214, which is very close to 1 indicating mostly non-competitive inhibition; $R^2 = 0.9215$), fit curves did not represent the experimental data very well. Perfectly fit curves could be obtained only by individual fits for each condition assuming an "*Allosteric sigmoidal*" model (R^2 between 0.9818 and 0.9971), which however did not allow unambiguous conclusions with respect to the underlying inhibiton. The given data strongly suggested a non-competitive inhibition, although classical models may underestimate cooperative phenomena that result in non-canonical progression of substrate-concentration curves. This finding was in stark contrast to wALADin1, where, besides non-competitive inhibition, the type-of-inhibition also had a strong substrate-competitive character.

Moreover, the effect of wALADin2 on the Mg^{2+}-response curve was determined. In analogy to wALADin1, wALADin2 induced a rightward shift of the Mg^{2+}-response curve and thus functionally competes with (allosteric) activation by Mg^{2+} (**Fig. 3.22 c**). In contrast, for wALADin2 concentrations ≤ 6.25 μM the maximum enzymatic velocity could clearly be reached. For higher concentrations lower maximum velocities were predicted, however, these predictions may be inadequate as only the lower parts of the curves were covered by data points and plateau activity was not achieved. Setting a constraint to the top value ("shared by all data sets") only led to a marginal deterioration of the R^2 value from 0.9915 to 0.9909, while the same constraint applied to non-linear regression of Mg^{2+}-response curves in the presence of wALADin1 led to a significant impairment of R^2 value from 0.9925 to 0.9452. In addition to being a non-competitive inhibitor, wALADin2 apparently acts entirely competitive to activation by Mg^{2+}, while wALADin1 is only a partial competitor. It is intriguing to speculate that the non-substrate competitive component of inhibition exerted by wALADin inhibitors is due to functional competition with Mg^{2+}. While this is apparently the exclusive mechanism for wALADin2, wALADin1 additionally involves competition with 5-ALA resulting in a mixed model inhibition and only a partial Mg^{2+}-competitive character. Binding of wALADin2 to wALAD was also demonstrated by TSA, although the induced melt shifts were significantly smaller than for wALADin1 (**Fig. 3.23**).

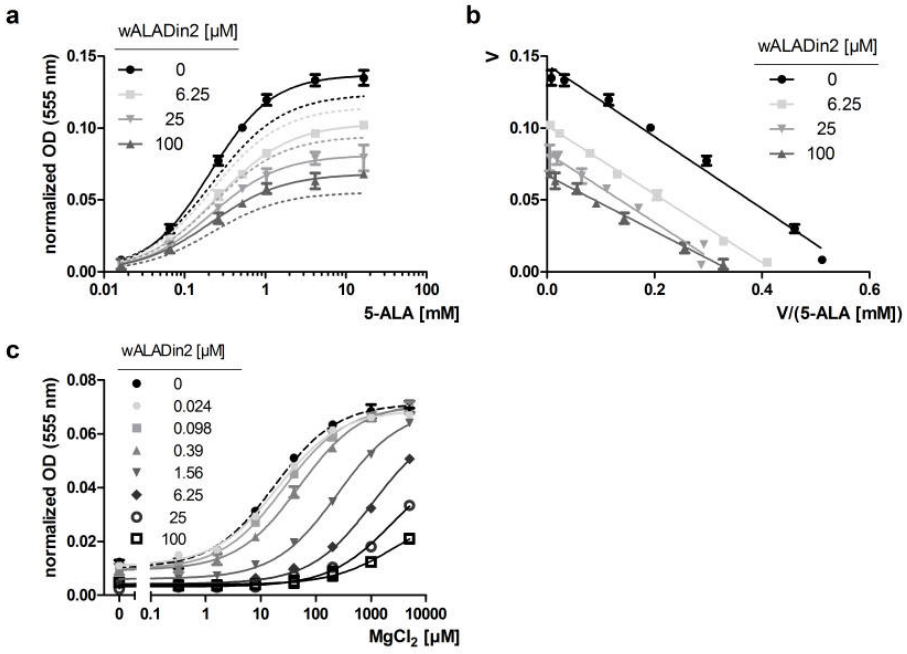

Figure 3.22: Molecular mode of action of wALADin2

a) Substrate-concentration row in the presence of different concentrations of wALADin2. Graph shows means ± SD of triplicates and is representative of three experiments. Continuous lines represent non-linear regression using the "*Allosteric sigmoidal*" inhibition algorithm, dashed lines show curves obtained by non-linear regression using the "*Non-competitive inhibition*" algorithm. **b)** Linear Eadie-Hofstee representation of the experiment shown in **a**. Lines run nearly parallel indicating a non-competitive mechanism of inhibition. **c)** Mg^{2+}-response curve of wALAD was shifted to the right upon increasing concentrations of wALADin2. Graph was fit using "*log(agonist) vs. response - variable slope*" NLR algorithm (constraints: shared slope by all data sets, bottom ≥ 0).

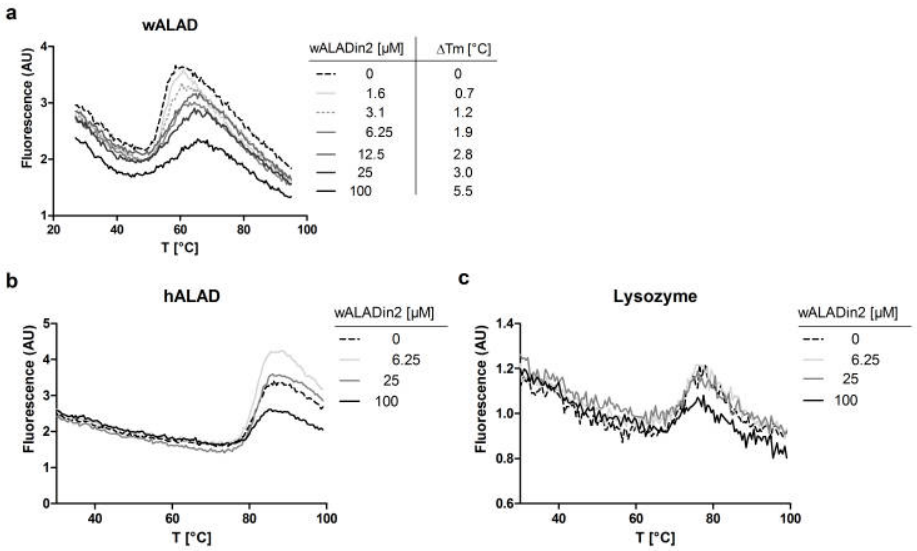

Figure 3.23: Thermal shift assay with wALADin2
a) wALADin2 induced a stabilization of wALAD tertiary structure in a concentration-dependent manner. The binding event is documented as the rightward shift of the wALAD melting curve measured by increased fluorescence of the environmentally-sensitive fluorescent dye Sypro®Orange. In contrast, wALADin2 did not bind to either **b)** hALAD or **c)** Chicken Egg White Lysozyme.

Given these exciting differences in the inhibitory mechanism of wALADin1 and wALADin2, the mode of inhibition of derivative **3** was also studied. This compound behaved qualitatively like wALADin1 and had a mixed competitive/non-competitive mechanism of action and acted as a partial competitor with the activation induced by Mg^{2+} (**Fig. 3.24**).

In conclusion, several wALAD inhibitors with distinct non-benzimidazole chemotypes were discovered, some of which, however, had a preference for the human ortholog. With wALADin2, a wALAD inhibitor was discovered that was even slightly better than wALADin1 in terms of potency and specificity. Intriguingly, wALADin2 also featured differences in the inhibitory mechanism being an entirely non-competitive inhibitor (with respect to substrate 5-ALA) that functionally competes with the activation by Mg^{2+}.

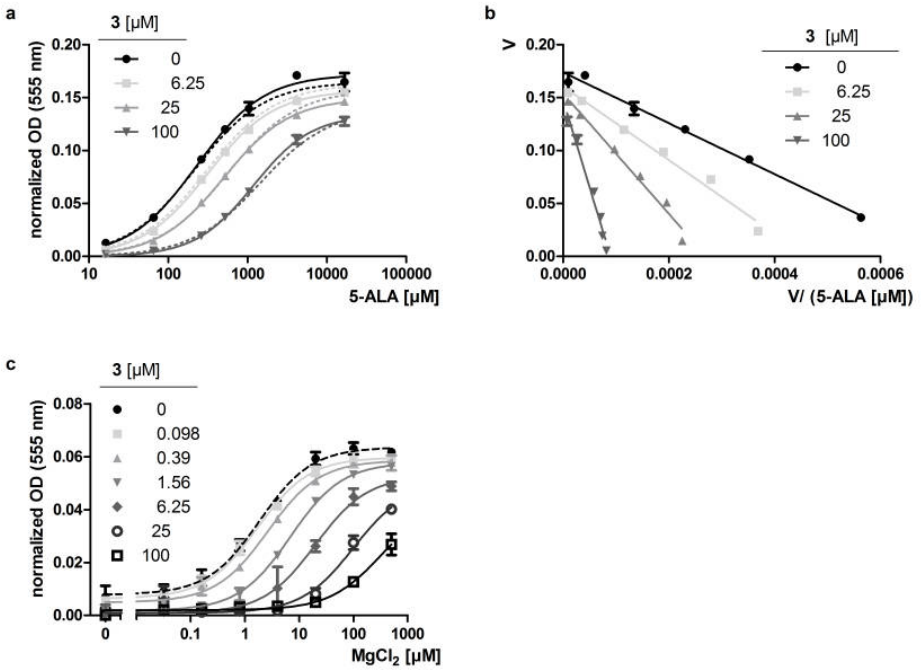

Figure 3.24: Molecular mode of action of wALADin1 derivative 3
a) Substrate-concentration row in the presence of different concentrations of compound **3**. Graph shows means ± SD of triplicates and is representative of two experiments. Continuous lines represent non-linear regression using the "*Allosteric sigmoidal*" inhibition algorithm, dashed lines show curves obtained by non-linear regression using the "*Mixed model inhibition*" algorithm. **b)** The linear Eadie-Hofstee representation confirmed a mixed competitive/non-competitive mechanism of inhibition. **c)** Mg^{2+}-response curve of wALAD is shifted towards the right upon increasing concentrations of compound **3**. Maximum enzymatic velocity is reduced in the presence of **3**. Graph was fit using the "*log(agonist) vs. response - variable slope*" algorithm (constraints: shared slope by all data sets, bottom ≥ 0, $R^2 = 0.9919$).

3.7 ALAD Cross-species SAR

3.7.1 Inhibitory activity of wALADins on different orthologs

Species-selectivity of ALAD inhibition is an exciting characteristic of wALADin1. The molecular mechanism of action involving functional competition with activation by Mg^{2+} implied that it might, in principle, be applicable to other ALAD orthologs activated by Mg^{2+} while Zn^{2+}-dependent proteins might be resistant to inhibition. Therefore wALADin1, its derivatives and wALADin2 were tested for inhibitory activity of a variety of other Mg^{2+}-stimulated ALAD orthologs from plants (the gardener's pea *Pisum sativum*) and bacteria (*Pseudomonas aeruginosa*, *Vibrio cholerae*, *Yersinia enterocolitica* and *Escherichia coli*). The latter ortholog is Zn^{2+}-dependent, but further allosterically activated by Mg^{2+}; all other orthologs are allosterically activated by Mg^{2+}, but are independent of Zn^{2+}. A multiple sequence alignment including protein sequences of all used ALAD orthologs is shown in **Fig. 3.25** where key structural features are highlighted. A more detailed description of metal cofactor requirements of these ALAD orthologs is given in the **Discussion** (**Section 4.4.2, 4.4.3**). The recombinant pea protein used was a truncated version lacking the N-terminal chloroplast transit peptide [148].

All orthologs were tested using respective optimal assay conditions as described in the **Methods** chapter (**Section 2.2.17**). Based on the biological activities of wALADin1 three different classes of ALAD orthologs were defined: One group (referred to as group Y) comprised wALAD and the chloroplast PsALAD for which wALADin inhibitors showed a generally similar inhibitory profile (**Table 3.4 a**). wALADin1 was the most potent compound within the wALADin1-derivatives with similar IC_{50} values of ∼11 μM and 12 μM followed by **3** with 13 μM and 19 μM for wALAD and PsALAD, respectively. Notable differences were evident in the potency of wALADin2, which was ∼10-fold less active against PsALAD (IC_{50} = 88 μM) compared to wALAD (IC_{50} = 8 μM). While **2**, featuring an R_1-H substituent, did not inhibit wALAD, it inhibited PsALAD with an IC_{50} of 114 μM. **15** only inhibited PsALAD (IC_{50} = 260 μM) and for **11** a 5-fold increase in inhibtory potency of PsALAD was observed (IC_{50} = 63 μM vs. 293 μM). Conversely, **8** inhibited wALAD (IC_{50} = 164 μM) but not PsALAD. Other orthologs showed similar inhibitory potencies within ∼2-fold variations in IC_{50} values for both species.

The second group (referred to as group X) represents hALAD and putatively other Mg^{2+}-independent orthologs that depend solely on catalytic Zn^{2+}. As outlined above (**Table 3.2 b**) hALAD was insensitive to inhibition by wALADin1 ($IC_{50} \geq 500$ μM) but was inhibited with moderate potency by other (preferentially smaller) derivatives. These results are shown in **Table 3.4 b** again to allow a better comparison with other orthologs.

The third group (referred to as group Z) comprised orthologs of different metal cofactor-dependence (pALAD, VcALAD, YeALAD, EcALAD, **Table 3.4 c**), but all are allosterically stimulated by Mg^{2+}. Surprisingly, wALADin1 did not inhibit, but rather stimulated enzymatic activity of these proteins to an extent of 20 - 60%. EC_{50} values were in between 60 μM and 70 μM for pALAD, YeALAD and EcALAD but ∼182 μM for VcALAD. For pALAD at the highest concentration activity decreased again. Generally EC_{50} determinations were relatively inexact with R^2 values between 0.5 and 0.92 which may be due to the small increases of activity (maximum + 60% stimulation) and the absence of a defined top activity. Similar to wALADin1, compounds **7** and **9** exerted similar stimulation of enzymatic activity. **7**, a constitutional isomer of wALADin1 differing in the position of the carboxyl group that was inactive on wALAD, was the most potent agonist with EC_{50} values between 15 and 38 μM. Derivative **6** induced weak stimulation of VcALAD and YeALAD (EC_{50} between 200 μM and 300 μM), but not of pALAD and EcALAD. All of these

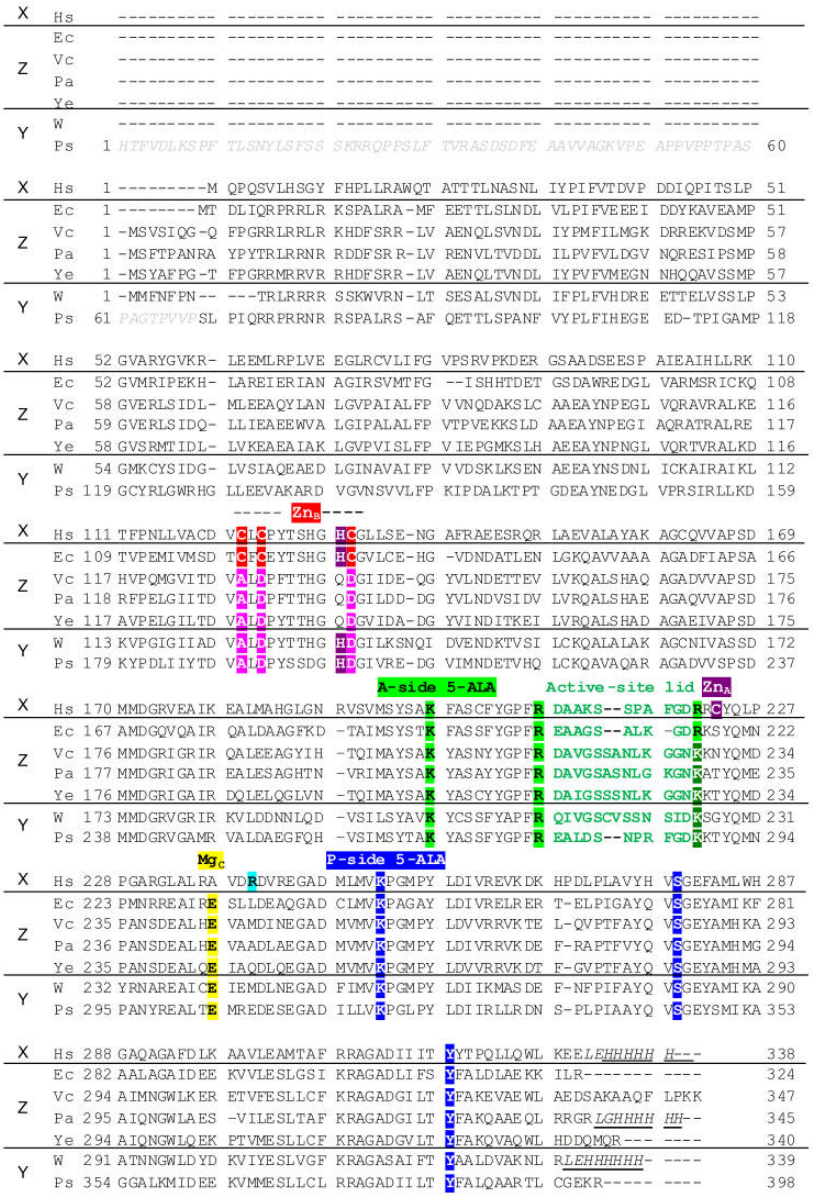

Figure 3.25: Multiple sequence alignment of ALAD orthologs
Multiples sequence alignment of *H. sapiens* (Hs), *E. coli* (Ec), *V. cholerae* (Vc), *P. aeruginosa* (Pa), *Y. enterocolitica* (Ye), *Wolbachia* of *B. malayi* (W) and *P. sativum*(Ps) ALAD orthologs was done using Clustal W. For Hs, Pa and W sequences of the recombinantly expressed proteins are shown including C-terminal tags (italicized, underlined). Other sequences are displayed according to UniProtKB entries (Ec: P0ACB2; Vc: C3LPU7; Ye: F4MUJ9 ; Ps: P30124). The recombinant Ps protein did not contain the N-terminal chloroplast targeting sequence (italicized, gray). X, Y, Z specifies functional assignment according to modulation by wALADin1. Highlighted structural features: P-side 5-ALA (blue), A-side 5-ALA binding (green), active side lid (green font), Zn_A-site (dark purple), Zn_B-binding sited correlated to A-site (red), alternative aspartate-rich motif of Zn^{2+}-independent orthologs (magenta), allosteric Mg_C-site (yellow) and the alternative arginine of non Mg^{2+}-stimulated orthologs(cyan).

Table 3.4: Biological activity of wALADin1 and derivatives on different ALAD orthologs

a

	wALADin1 inhibitory			
	P. sativum		*Wolbachia*	
Compound	IC_{50} [µM]	R^2	IC_{50} [µM]	R^2
wALADin1	11.9 ± 1.2	0.9706	11.1 ± 1.0	0.9517
2	114 ± 13	0.9282	*	-
3	19.1 ± 2.3	0.9475	13.0 ± 1.2	0.9638
4	n.d.	-	*	-
6	91.2 ± 19.2	0.8944	317 ± 53	0.9022
7	*	-	*	-
8	*	-	164 ± 14	0.9551
9	43.5 ± 6.1	0.9472	38.6 ± 6.2	0.9670
10	40.7 ± 3.7	0.9639	87.7 ± 10.5	0.9487
11	63.1 ± 5.7	0.9581	293 ± 67	0.8503
12	193 ± 29	0.9170	197 ± 33	0.9042
13	95.6 ± 10.5	0.9503	134 ± 17	0.9394
14	161 ± 21	0.9343	205 ± 12	0.9922
15	260 ± 42	0.8553	*	-
16	*	-	*	-
wALADin2	88.2 ± 14.2	0.8944	8.1 ± 0.8	0.9537

b

	wALADin1 insensitive	
	H. sapiens	
Compound	IC_{50} [µM]	R^2
wALADin1	*~ 739 ± 103*	*0.8582*
2	*	-
3	197 ± 20	0.9457
4	*	-
6	*	-
7	*	-
8	*	-
9	*	-
10	*~ 618 ± 105*	*0.9186*
11	173 ± 12	0.9730
12	145 ± 7.2	0.9854
13	213 ± 6.3	0.9934
14	222 ± 11	0.9864
15	156 ± 7.8	0.9881
16	*	-
wALADin2	511 ± 36	0.9780

c

	wALADin1 stimulatory							
	P. aeruginosa		*E. coli*		*Y. enterocolitica*		*V. cholerae*	
Compound	EC_{50} [µM] (Max. activity)	R^2	EC_{50} [µM] (Max. activity)	R^2	EC_{50} [µM] (Max. activity)	R^2	EC_{50} [µM] (Max. activity)	R^2
wALADin1	69.0 (122.8%)§	0.6404§	60 ± 21 (120.5 %)	0.8488	66.4 ± 12 (151.7%)	0.8853	182 ± 154 (~160%)	0.6501
2	*	-	*	-	*	-	*	-
3	*	-	*	-	*	-	*	-
4	n.d	-	n.d	-	n.d	-	n.d	-
6	*	-	*	-	269 ± 70 (131.9%)	0.5187	233 ± 163 (115.4%)	0.1123
7	15 ± 21 (135.6%)	0.8227	19 ± 8.7 (116 %)§	0.8227§	23 ± 2.0 (123.2%)	0.9230	38 ± 26 (128.4%)	0.6598
8	*	-	*	-	*	-	*	-
9	68 (139.5%)	0.6921	39 ± 16 (114.2 %)	0.7482	52 ± 13 (142.2%)	0.8387	53 ± 29 (117.1%)	0.5915
10	*	-	*	-	*	-	*	-
11	*	-	*	-	*	-	*	-
12	*	-	*	-	*	-	*	-
13	*	-	*	-	*	-	*	-
14	*	-	*	-	*	-	*IC_{50}: 1379 ± 624*	*0.6392*
15	*	-	*	-	*	-	*IC_{50}: 843 ± 236*	*0.8639*
16	*	-	*	-	*	-	*	-
wALADin2	*	-	*	-	*	-	*	-

* Absence of inhibitory or stimulatory activity

§ Data from the highest concentration (533 µM) was excluded from NLR because biological activity started to decrease

n.d.: not determined

Italic font: IC_{50} values were extrapolated because < 50% inhibition was achieved at the highest concentration tested

IC_{50} in **c** indicates the presence of an inhibitory effect

compounds with stimulatory activity featured the 2-[(2-thienylcarbonyl)amino]ethyl moiety at the R_2 position. None of the other derivatives, including **3** and wALADin2, showed biological activity, except **14** and **15** which very weakly inhibited VcALAD ($IC_{50} \geq 800$ μM).

These different groups X,Y and Z are highlighted in the multiple sequence alignment shown in **Fig. 3.25**, however, no evident structural features directing the outcome of wALADin1 modulation were identified. It was concluded that the outcome of modulation by wALADin1 is variable among different ALAD orthologs and may be both inhibitory and stimulatory. However, the inhibitory effects on the *Wolbachia* and pea ortholog occurred with a more than 6-fold higher potency compared to stimulatory effects on several bacterial orthologs.

3.7.2 The inhibitory mechanism of wALADin1 on *P. sativum* ALAD

The inhibitory effect that wALADin1 has on PsALAD and the influence of 5-ALA and Mg^{2+} concentration was studied in analogy to the experiments described above for wALAD. A dose-response curve for Mg^{2+} revealed a monophasic curve with an EC_{50} concentration of ~257 μM (**Fig. 3.26 a**). wALADin1 induced a marginal rightward shift of the Mg^{2+}-response curve (~2-fold drop in the Mg^{2+} EC_{50} from 231 to 506 μM from 0 to 100 μM wALADin1) while for wALAD (at now equal 5-ALA concentration of 10 mM) 100 μM wALADin1 reduced affinity for Mg^{2+} by nearly 19-fold (24 μM to 453 μM) (**Fig. 3.26 b, c**). Although V_{max} was also clearly reduced for wALAD, this effect seemed more pronounced for the pea protein, especially in relation to the Mg^{2+}-competitive component. A 5-ALA concentration series revealed a mixed competitive/non-competitive inhibition of PsALAD by wALADin1 with reduced V_{max} and increased K_M. This is similar to wALAD, although the Eadie-Hofstee representation for the plant protein was non-linear and could not be clearly interpreted (**Fig. 3.26 d, e**). In conclusion, the mechanism by which wALADin1 exerts its inhibitory function on the pea protein may be described as qualitatively similar to its effect on the *Wolbachia* enzyme, but differs in the potency of the Mg^{2+}-antagonizing activity.

3.7.3 Stimulatory vs. inhibitory activity on the *P. aeruginosa* ALAD

The stimulatory effect of wALADin1 which was evident for several bacterial ALAD orthologs was addressed in more detail using *P. aeruginosa* ALAD (pALAD) as a model. As stimulation was a surprising outcome, buffer conditions were systematically varied to verify whether such an effect was evident under all conditions tested: A transverse scan of the effect of 50 - 200 μM wALADin1 was performed against buffer pH, KCl concentration and 5-ALA concentration. Under the standard pH of 8.0 (as well as at pH 8.5) wALADin1 was found to stimulate pALAD activity (**Fig. 3.27**) as observed (**Table 3.4**). This effect was more pronounced at 100 mM KCl than in the absence of KCl. Conditions were determined under which wALADin1 induced inhibition and not stimulation. Inhibition was most pronounced at pH 7.5 in the absence of KCl and at non-saturating 5-ALA conditions (0.2 mM). At near-saturating 5-ALA concentration (1 mM) the inhibitory effect was nearly abolished and under saturating conditions (5 mM) wALADin1 caused a stimulation of enzymatic activity. At lower pH (7.0) an inhibitory effect was clearly evident even at 1 mM 5-ALA, 100 mM KCl (**Fig. 3.27 b**). Taken together, it was found that the outcome of modulation of pALAD activity by wALADin1 varied substantially with the buffer conditions. High pH ($\geq$ 8.5), KCl and 5-ALA induced the predomi-

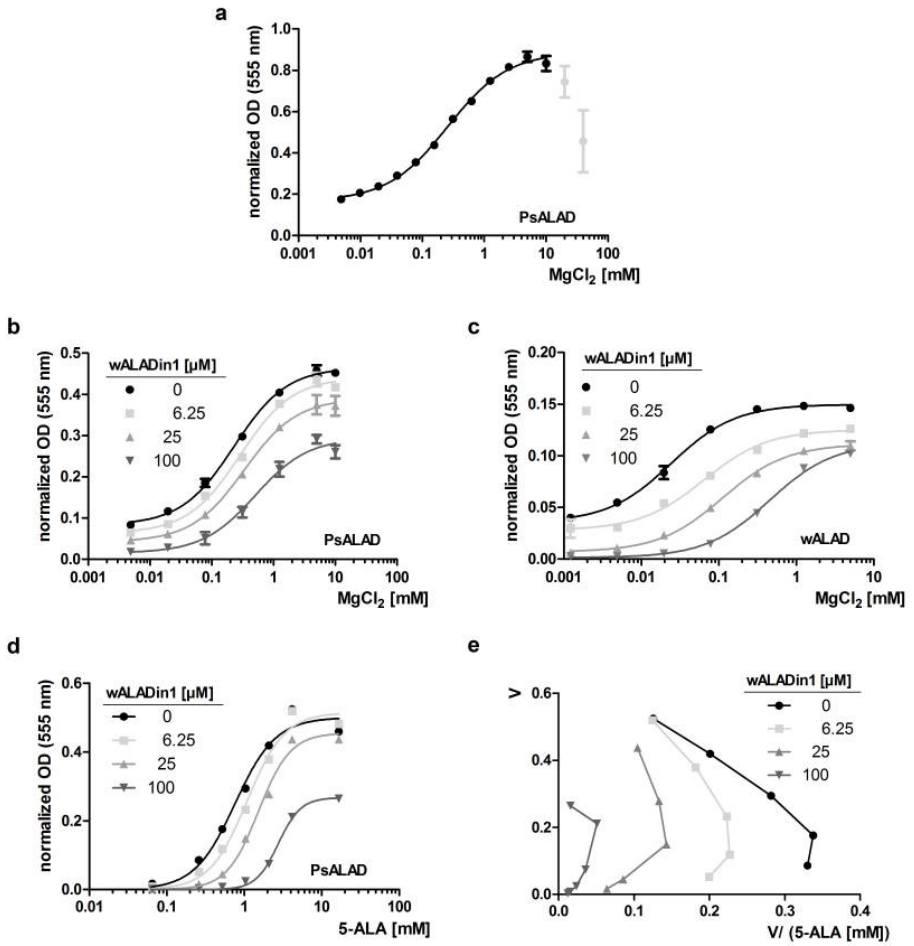

Figure 3.26: Inhibitory mechanism of wALADin1 on *P. sativum* ALAD
a) Mg^{2+}-response curve measured at 5-ALA saturation (EC_{50} ~257 μM) The gray data points at high inhibitory concentrations were excluded for non-linear regression. **b)** wALADin1 induced a weak rightward-shift of the dose-response curve but decreases V_{max}. **c)** At identical 5-ALA concentration (10 mM) wALADin1 induced a 10-fold more pronounced rightward shift of the wALAD (!) Mg^{2+}-response curve. **e)** Substrate concentration series of PsALAD at different concentrations of wALADin1 assuming an "*Allosteric sigmoidal*" fit indicating mixed competitive/non-competitive inhibition (increased Kprime, reduced V_{max}). **f)** The Eadie-Hofstee diagram had a non-linear progression preventing a clear interpretation. (For presentation of the Eadie-Hofstee diagram data for the highest and lowest values per data set were excluded). Graphs are representative of 2 experiments and show means ± SD of triplicates.

nant stimulatory phenotype, whereas lower pH ($\leq$ 7.5) and low 5-ALA favoured an inhibitory outcome.

Both stimulatory and inhibitory effects and the relevance of certain buffer components on the outcome of modulation by wALADin1 were characterized in more detail. Experiments measuring stimulation were performed at pH 8.0, 100 mM KCl, 1 mM $MgCl_2$ and a saturating 5-ALA concentration (5 mM) as standard conditions. The resulting KCl-response curve progressed more steeply with increasing concentrations of wALADin1 (**Fig. 3.28 a**) and higher percent stimulation values were obtained at high KCl concentrations (% stimulation at 200 μM wALADin1: No KCl - 92%; 1.2 mM KCl - 119%; 11 mM KCl - 129%; 100 mM KCl - 140%). The $MgCl_2$-response curve revealed an elevated plateau of the enzymatic velocity with increasing wALADin1 concentrations (**Fig. 3.28 b**). Mg^{2+}-EC_{50} and Hill slope values were not consistently changed in a concentration-dependent manner (assuming "*log(agonist) vs. response - variable slope*" non-linear regression). Finally, a substrate concentration-curve revealed that modulation by wALADin1 increased V_{max}, but had no consistent effect on K_M (**Fig. 3.28 c, d**).

The inhibitory effect of wALADin1 on pALAD was analyzed at pH 7.5 in the absence of KCl, at 1 mM $MgCl_2$ and a non-saturationg 5-ALA concentration (200 μM) as standard conditions. Under these conditions K^+ did not stimulate enzymatic activity of pALAD, however, it antagonized the inhibitory effect of wALADin1 (**Fig. 3.29 a**). The Mg^{2+}-response curve was shifted to the right by wALADin1 in a concentration-dependent manner indicating functional competition with allosteric activation by Mg^{2+}. It is important to note that allosteric Mg^{2+} is the only Mg^{2+}-ion reported for this ortholog. It may therefore be stated that the corresponding Mg^{2+}-induced allosteric activation of pALAD allows to overcome the inhibitory effects of wALADin1 at high Mg^{2+}-concentrations (**Fig. 3.29 b**). The substrate concentration row was measured at 0.5 mM $MgCl_2$ to increase the inhibitory detection window. However, description of the resulting effects is complex. At all wALADin1-concentrations tested (50 - 200 μM), a wALADin1-concentration dependent increase in the K_{Prime} (approximation for K_M assuming an "*Allosteric sigmoidal*" fit) was consistently observed (K_{Prime} values: At 6.7% DMSO - 0.10 mM; 50 μM wALADin1 - 0.19 mM; 100 μM wALADin1 - 0.22 mM; 200 μM wALADin1 - 0.74 mM) (**Fig. 3.29 c, d**). Thus, wALADin1 decreased the affinity of pALAD for 5-ALA. However, V_{max} of pALAD is reduced at 50 μM (V_{max} = 0.039; At 6.7% DMSO - V_{max} = 0.047), but started to increase again at higher concentrations of wALADin1 (100 μM wALADin1 - V_{max} = 0.041; 200 μM wALADin1 - V_{max} = 0.057). This pattern was reproducibly found and concurred with the results from the initial buffer scan experiments where at 5 mM 5-ALA wALADin1 stimulated pALAD activity while it inhibited pALAD at 0.2 mM 5-ALA (**Fig. 3.27 a, c**). This non-linear relationship between wALADin1 and 5-ALA might be explained by functionally different binding sites for 5-ALA and/or wALADin1 present in the oligomeric protein as discussed later in this thesis. Summarizing, wALADin1 may act agonistically or antagonistically on pALAD and the outcome of the small molecule - induced modulation is the result a subtle balance of different environmental factors like pH, monovalent cations, and substrate concentrations that govern the overall conformation of the protein.

In order to verify binding of wALADin1 to pALAD under stimulatory conditions, both in the presence and absence of 100 mM KCl (pH 8.0), thermal shift assays were performed. Despite its activating effect in the enzymatic assay, KCl had no influence on the progression of the melting curve and the melting temperature of pALAD (**Fig. 3.30 a, b**). ΔT_m-values induced by wALADin1 were equivalent for both conditions. This finding indicates that the thermodynamics of binding of wALADin1 to pALAD are similar under both conditions.

Besides *P. aruginosa* ALAD, a stimulatory effect was also observed for the

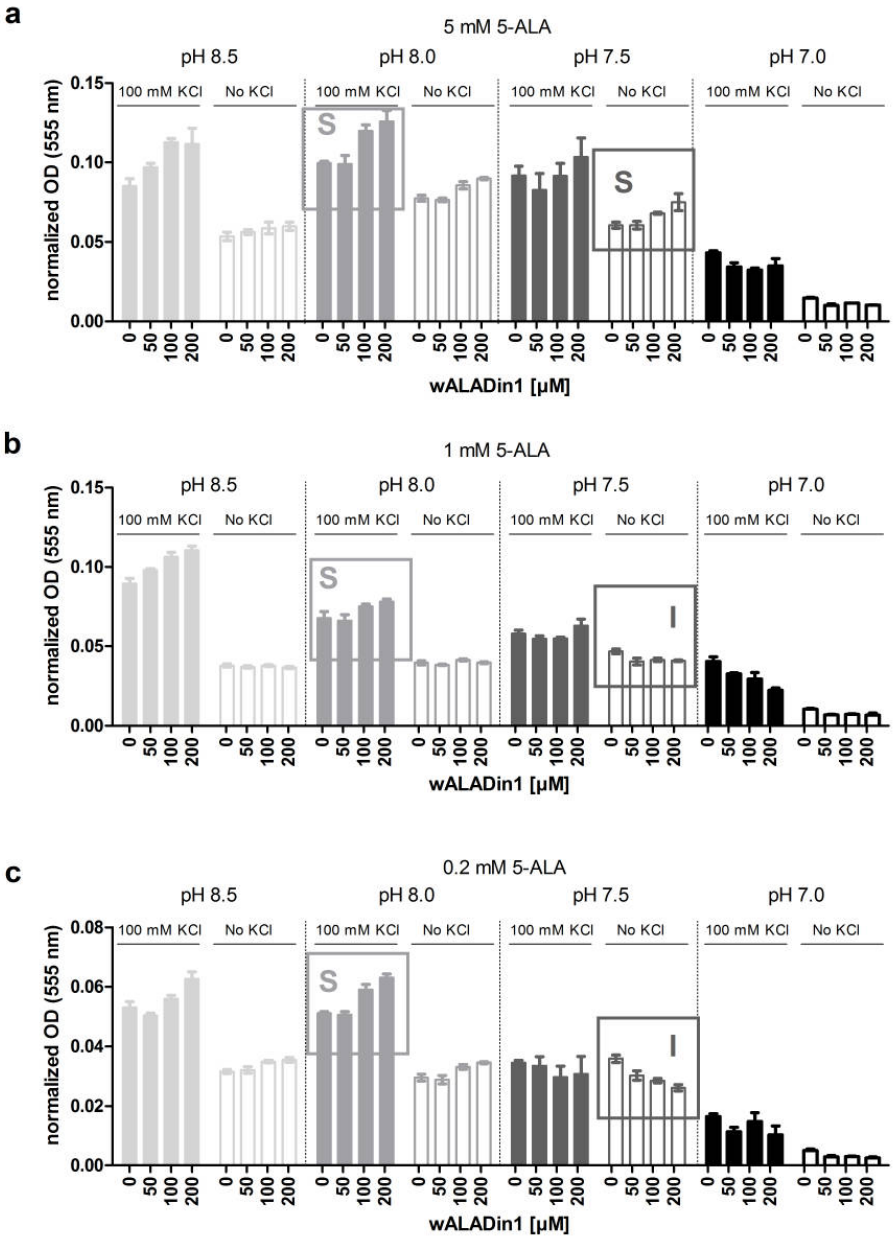

Figure 3.27: Effects of buffer components on the stimulatory effect of wALADin1 on pALAD

The effect of wALADin1 (0, 50 μM, 100 μM, 200 μM) on pALAD was scanned against pH (8.5, 8.0, 7.5, 7.0 - 100 mM Tris) and the presence/absence of 100 mM KCl at different concentration of 5-ALA: **a)** 5 mM 5-ALA, **b)** 1 mM 5-ALA and **c)** 0.2 mM 5-ALA. Light gray boxes indicate standard stimulatory conditions (pH 8.0, 100 mM KCl), dark gray boxes indicate conditions (pH 7.5, 0 mM KCl) under which inhibition occurred at low 5-ALA concentrations and stimulation occurred at high 5-ALA conditions. "S" marks stimulatory, "I" marks inhibitory influence of wALADin1 at the respective conditions. Graphs show means ± SD of triplicates.

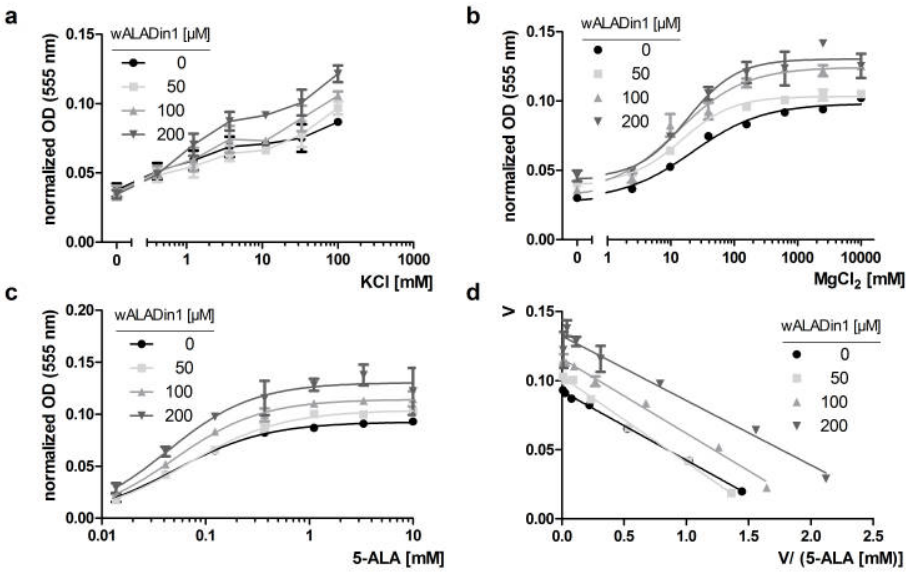

Figure 3.28: The stimulatory effect of wALADin1 on pALAD
Enzymatic assays conducted under standard conditions for stimulation: 100 mM Tris pH 8.0, 100 mM KCl, 1 mM $MgCl_2$, 5 mM 5-ALA (saturating), if not stated otherwise. **a)** KCl-response curve: Steeper progression in the presence of wALADin1. Graph shows means ± SD of two independent experiments. **b)** $MgCl_2$-response curve fit with "*log(agonist) vs. response - variable slope*" NLR algorithm (R^2: 0.9154 - 0.9807). Stimulatory activity of wALADin1 is evident in increased enzymatic velocity. **c)** 5-ALA concentration curve fit by "*Allosteric sigmoidal*" NLR (R^2: 0.9206 - 0.9936). wALADin1 reduces V_{max} but does not consistently alter K_{Prime}. **d)** Linearized Eadie-Hofstee representation of the data shown in **c**. **b - d** are representative of two experiments and show means ± SD of triplicates.

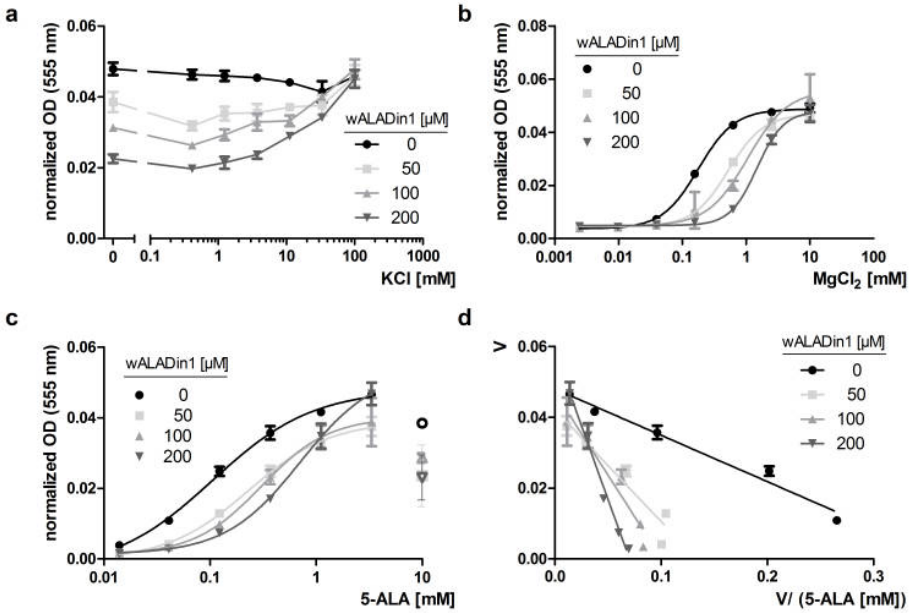

Figure 3.29: The inhibitory effect of wALADin1 on pALAD
Enzymatic assays were conducted under standard conditions for inhibition: 100 mM Tris pH 7.5, no KCl, 1 mM $MgCl_2$, 0.2 mM 5-ALA (non-saturating), if not stated otherwise. **a)** KCl-response curve fit with "*log(agonist) vs. response - variable slope*" NLR algorithm (R^2: 0.9628 - 0.9982). The inhibitory effect of wALADin1 was antagonized by K^+. **b)** $MgCl_2$-response curve fit with "*log(agonist) vs. response - variable slope*" NLR algorithm (R^2: 0.9628 - 0.9982)": Rightward-shift of the responce curve was induced by incrasing wALADin1. **c)** 5-ALA - concentration series fit by "*Allosteric sigmoidal*" NLR (R^2: 0.9676 - 0.9935) and **d)** linearized Eadie Hofstee representation. wALADin1 reduced the affinity (K_{Prime}) of pALAD to 5-ALA. At 50 μM wALADin1 V_{max} was decreased but it increased again at higher concentrations (despite increased K_{Prime}). Graphs are representative of two experiments and show means ± SD of triplicates.

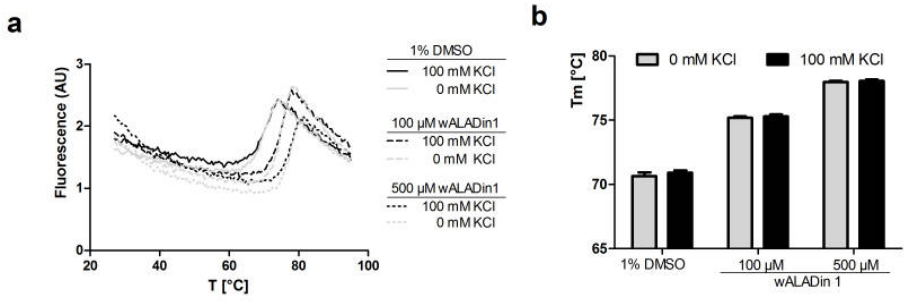

Figure 3.30: Thermal shift assay with pALAD and wALADin1
a) Incubation of 5 μM pALAD with 1% DMSO, 100 μM or 500 μM wALADin1 in the presence or absence of 100 mM KCl. Buffer conditions were 100 mM Tris (pH 8.0), 10 mM $MgCl_2$, 8X Sypro®Orange. **b)** pALAD melting temperatures T_M under the different conditions. The addition of 100 mM KCl does not alter the melting temperature. ΔTm for 100 μM or 500 μM wALADin1 is equivalent for both conditions.

orthologs from *V. cholerae*, *Y. enterocolitica* and *E. coli*. In order to determine whether a similar stimulatory/inhibitory dichotomy was also present for these orthologs, a buffer scan experiment was performed testing the stimulatory properties of different concentrations of wALADin1 (0, 50, 100, 200 μM) against different pH values of the Bis-tris propane buffer (7.0, 7.5, 8.0, 8.5) and KCl (0 vs. 100 mM) at non-saturating 5-ALA (200 μM) (**Fig. 3.31**). Thus, the conditions for which inhibition was most pronounced for pALAD were covered. In contrast to the *P. aeruginosa* enzyme, throughout all conditions wALADin1 acted in a stimulatory fashion on these orthologs. Although it may not be ruled out that wALADin1 (or some of its derivatives) may inhibit these proteins under conditions not-tested, apparently the stimulatory effect of wALADin1 on these orthologs is more robust and predominant than for pALAD.

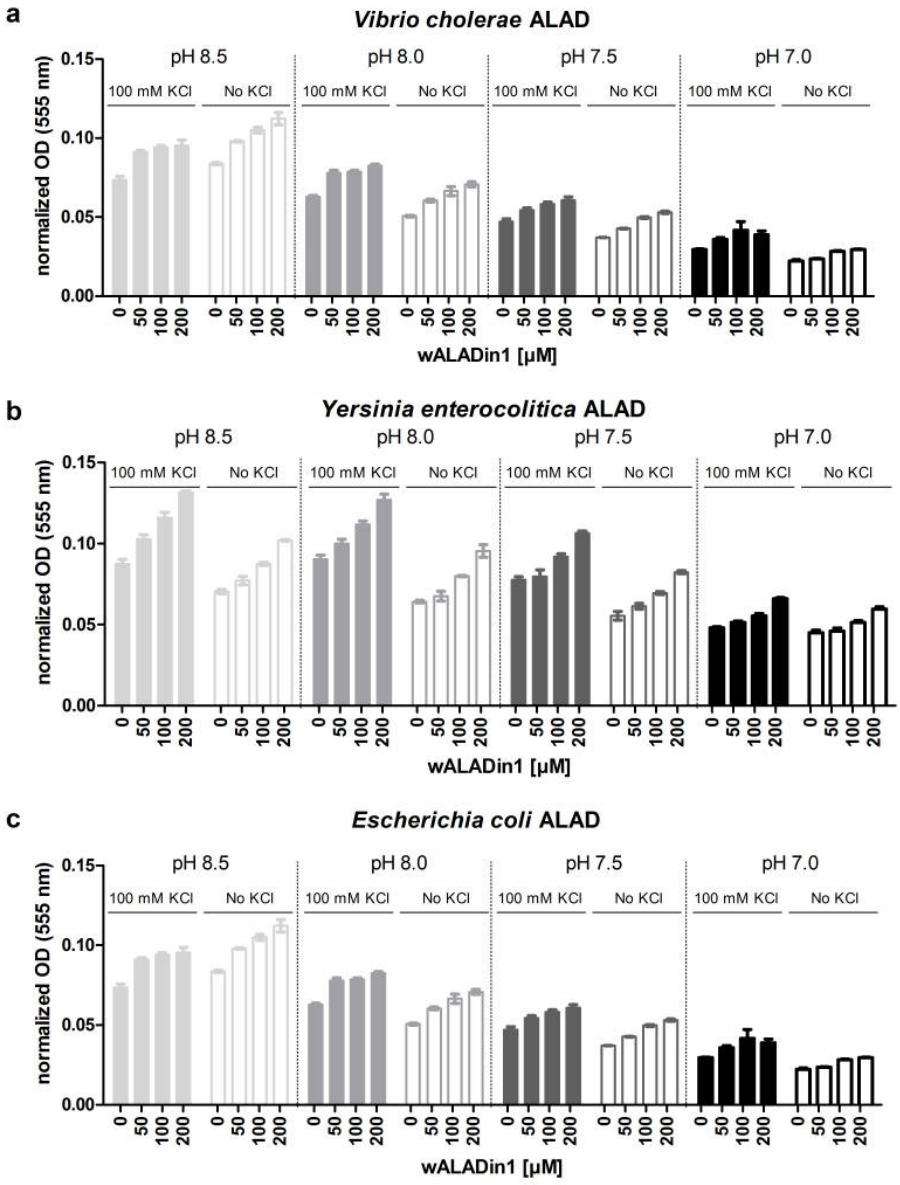

Figure 3.31: Buffer scan experiment of different ALAD orthologs against wALADin1

Effects of wALADin1 (0, 50 μM, 100 μM, 200 μM) scanned against pH (8.5, 8.0, 7.5, 7.0 - 100 mM BTP) and the presence/absence of 100 mM KCl at non-saturating 5-ALA concentrations (200 μM) for the following ALAD orthologs: **a)** *V. cholerae* ALAD; **b)** *Y. enterocolitica* ALAD; **c)** *E. coli* ALAD.

3.8 Antiprotozoal effects of wALADin1

On the background of the potent inhibitory activity of wALADin1 on both *Wolbachia* and pea chloroplast ALAD and its stimulatory/inhibitory dichotomy on pALAD and other bacterial ALAD enzymes, wALADins may have a broad effector spectrum on a variety of human pathogens. *Plasmodium falciparum* and *Toxoplasma gondii* are two apicomplexan parasites with apicoplast-targeted ALAD stimulated by Mg^{2+}. While the *T. gondii* ortholog shows minor Mg^{2+}-independent activity [227] the *P. falciparum* enzyme is essentially active without Mg^{2+}, but Mg^{2+} may stimulate an additional ∼20 - 30% of PfALAD activity [66]. In the absence of recombinantly expressed *P. falciparum* and *T. gondii* ALAD proteins for enzymatic inhibition studies, wALADin1 was tested in *P. falciparum* and *T. gondii* cell culture for any antiprotozoal effects.

3.8.1 wALADins in *P. falciparum* culture

The effect of wALADin1 and its derivatives was tested on *P. falciparum* 3D7 culture cultivated in RBC for 4 days. Parasitemia was determined on a daily basis with 3 days as the standard readout time. wALADin derivatives were initially tested at 62.5 μM. An antiplasmodial effect was visible for wALADin1, **6** and **9**. All other derivatives including the potent wALAD inhibitor **3** and wALADin2 did not inhibit replication of the malarial parasite *in vitro* (**Fig. 3.32 a**). The mentioned compounds were able to clear parasitemia completely, with **6** as the most potent antiplasmodial compound (IC_{50} 7.7 ± 1.7 μM), followed by **9** (IC_{50} 12.8 ± 0.02 μM) and wALADin1, which had ∼5-fold reduced activity (IC_{50} 39.3 ± 11.7 μM) compared to **6** (**Fig. 3.32 b, c**). While the dose-response curves for **9** had a comparatively shallow progression (Hill slope values: -1.3 to -1.5), the progression for wALADin1 (Hill slope values: -1.8 to -9.6) and **6** (Hill slope values: -3.1 to -6.7) was steeper with considerable interexperimental variation. Time-curves of parasitemia further revealed that this effect was consistent throughout the course of the experiment (**Fig. 3.32 d - f**).

Although it remains to be determined whether the antiplasmodial effect is due to the inhibition of endogenous heme biosynthesis in the apicoplast, the potent inhibitory activity with an IC_{50} as low as ∼ 8 μM for **6** demands further investigations on the antiplasomdial effect of wALADin benzimidazoles and their potential use as antimalarial drug candidates.

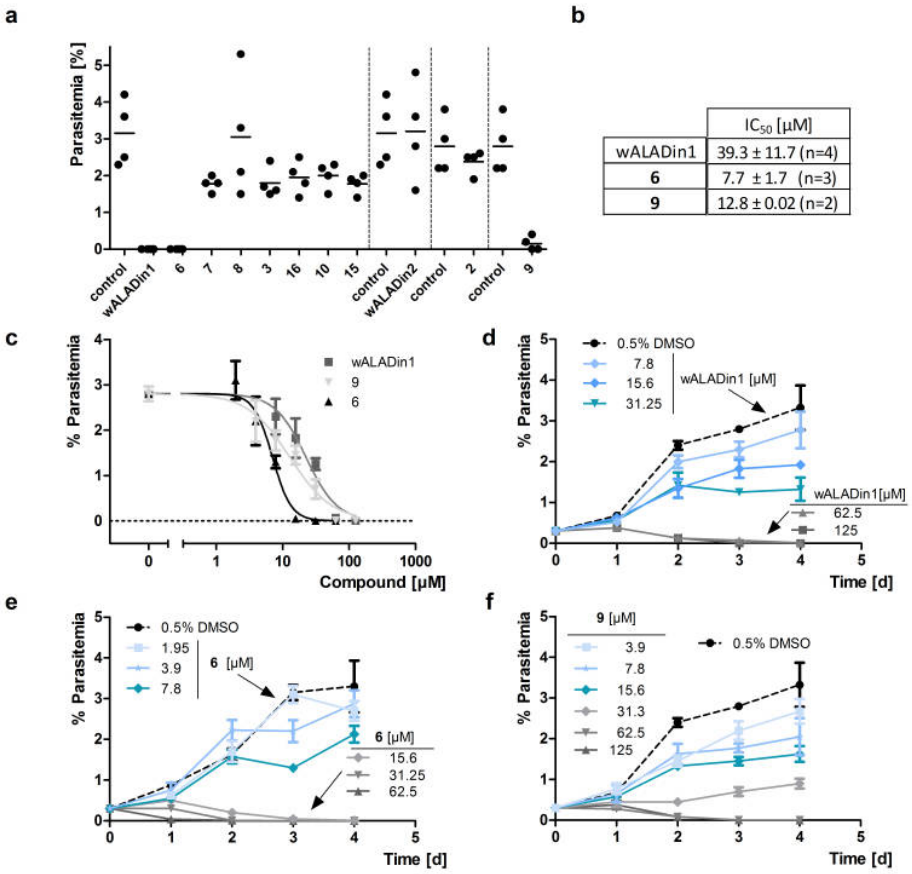

Figure 3.32: Activity of wALADin1, 6 and 9 in *P. falciparum* culture
a) Percent *P. falciparum* 3D7 parasitemia in RBC culture after 3 days of exposure to different wALADin derivatives assayed at 62.5 μM compound. Dashed vertical lines seperate different experiments. **b)** Mean IC_{50} values determined for wALADin1, **6** and **9** on the basis of 2 - 4 independent experiments (3 days of culture). **c)** Dose-response curves for wALADin1, **6** and **9** after 3 days of culture. Curves were fit using the the "*log(inhibitor) vs. normalized response - Variable slope*" non-linear regression algorithm of Prism 5.0 (bottom = 0; top = Shared by all data sets). **d) - f)** Time curve of the development of parasitemia for treatment with **d)** wALADin1 , **e) 6** and **f) 9**, respectively. Graphs **c - f** are representative of $\geq$ two experiments and show means $\pm$ SD of four replicates. d = days.

3.8.2 wALADins in *T. gondii* culture

In order to measure drug effects on the replication of *T. gondii* parasites a cell culture assay was established that uses infection of LLC-MK2 cells with *T. gondii* tachyzoites. After a cultivation period of ∼2 days cells were lysed and parasite and host cell numbers were quantified by Realtime PCR. While the standard anti-toxoplasma drug pyrimethamine showed potent inhibition of replication (IC_{50} ∼1 μM) wALADin1 and **6** were not active until the 3-digit μM range (IC_{50} = 340 μM and 825 μM, respectively; **Fig. 3.33**). These values were more than one order of magnitude higher than those observed in the *P. falciparum* culture assay. In this range also slight non-specific effects on the proliferation of LLC-MK2 cells became visible (compare **Fig. 3.9** and **Fig. 3.17**) and due to their rapid proliferation *T. gondii* tachyzoites may be slightly more susceptible to these non-specific effects than LLC-MK2 cells are. Thus, inactivity of wALADin1 and **6** in the *T. gondii* culture revealed that the antiprotozoal effect of thes compounds was *Plasmodium*-specific.

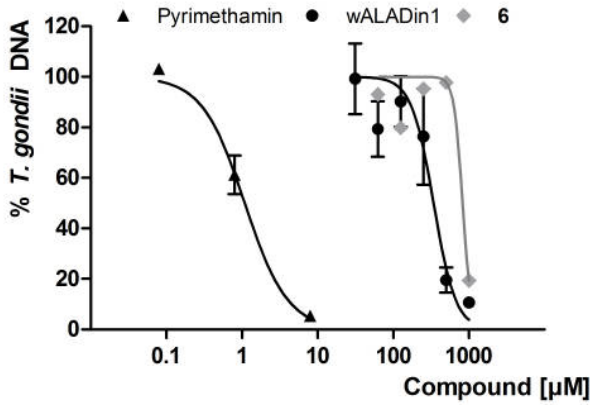

Figure 3.33: wALADin1 in *T. gondii* culture
Replication of *T. gondii* in LLC-MK2 exposed to different concentrations of pyrimethamine, wALADin1 and **6** for ∼44 h was measured as the levels of *T. gondii* DNA normalized to LLC-MK2 *β-actin*. While pyrimethamine and wALADin1 curves show means ± SEM pooled from 2-3 experiments, for compound **6** data from a single experiment is shown. Curves were fit using the the "*log(inhibitor) vs. normalized response - Variable slope*)" non-linear regression algorithm of GraphPad Prism 5.0. IC_{50} values were 1 ± 0.2 M μM for pyrimethamine, 340 ± 50 μM for wALADin1 and 825 ± 206 μM for **6**.

3.9 PPDK HT-Screening

3.9.1 Establishment of PPDK enzymatic screening assay

In order to establish a HTS-compatible enzymatic assay for PPDK (of *Wolbachia* of *B. malayi*), a DNPH-based assay system [181] was used to detect the reaction product pyruvate (**Fig. 3.34**). **Fig. 3.35 a** shows that the Pyruvate Detection Reagent (PDR) allows the specific detection of pyruvate at concentrations ≥ 10 μM. The PPDK-DNPH assay was downscaled to microplate format and assay conditions were adjusted to allow a robust, yet sensitive assay suitable for HTS for inhibitors in a semi-automated fashion involving a robotic work station. With this aim, the concentrations of cosubstrates were adjusted: Single substrate concentration curves were measured for each substrate (AMP, PEP, PP_i, **Fig. 3.35 b - d**) with the other two substrate concentrations kept constant. Screening assay concentrations were chosen such that the concentration of each substrate was at the upper end of the linear phase of the substrate concentration curve before reaching saturation. This allowed for sufficient sensitivity avoiding a bias for the detection of inhibitors with a certain mode of action. Final assay concentrations were 200 μM PEP, 200 μM AMP and 500 μM PP_i. A time curve experiment under assay conditions revealed that at 50 min of reaction at RT the reaction was in the linear steady state phase as required for a sensitive screening assay. The assay quality parameter Z'-factor [274] was determined by measurement of eight replicates each of positive and negative control values (**Fig. 3.35 e**). For the given assay Z' was 0.58 which indicated good and robust assay performance and allowed employment of this assay in HTS.

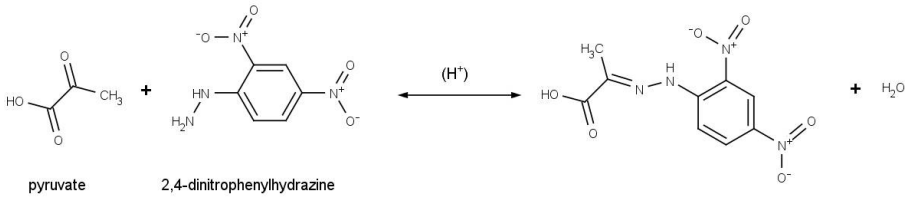

Figure 3.34: Reaction scheme of the detection of pyruvate with DNPH
2,4-dinitrophenylhydrazine (DNPH) reacts with pyruvate to a hydrazone which elicits increased absorption at 395 nm [180, 181] in an addition-elimination mechanism: Reaction starts with a nucleophilic attack of the primary amino group of the hydrazine to the carbonyl carbon atom of pyruvate followed by elimination of water.

3.9.2 PPDK screening

A library of ~18,000 drug-like small molecules was screened for inhibitors of the PPDK-DNPH Assay. An overview of the workflow of the screening assay, assay conditions, hit validation and the results is given in **Fig. 3.36**. The hit threshold was initially set at the mean of the DMSO control - 3 SD which was equivalent 60% of inhibition. Although the mean Z'-factor throughout the screening was satisfactory (0.5 ± 0.20), for some screening plates, the bulk of compounds showed some 10 - 30% background interference with the assay (compare **Fig. 3.37 a, b**) leading to a high number of primary hits (383 hits, hit rate: 2.1%). When the hit-threshold was set more restrictively to 80% inhibition, the number of hits was reduced to 35 (hit rate: 0.2%), a more feasible number for further validation. The top 20 of these hit structures plus two manually selected compounds from lower scoring hit clusters were rescreened in triplicate measurements under HTS-conditions. 9 out of

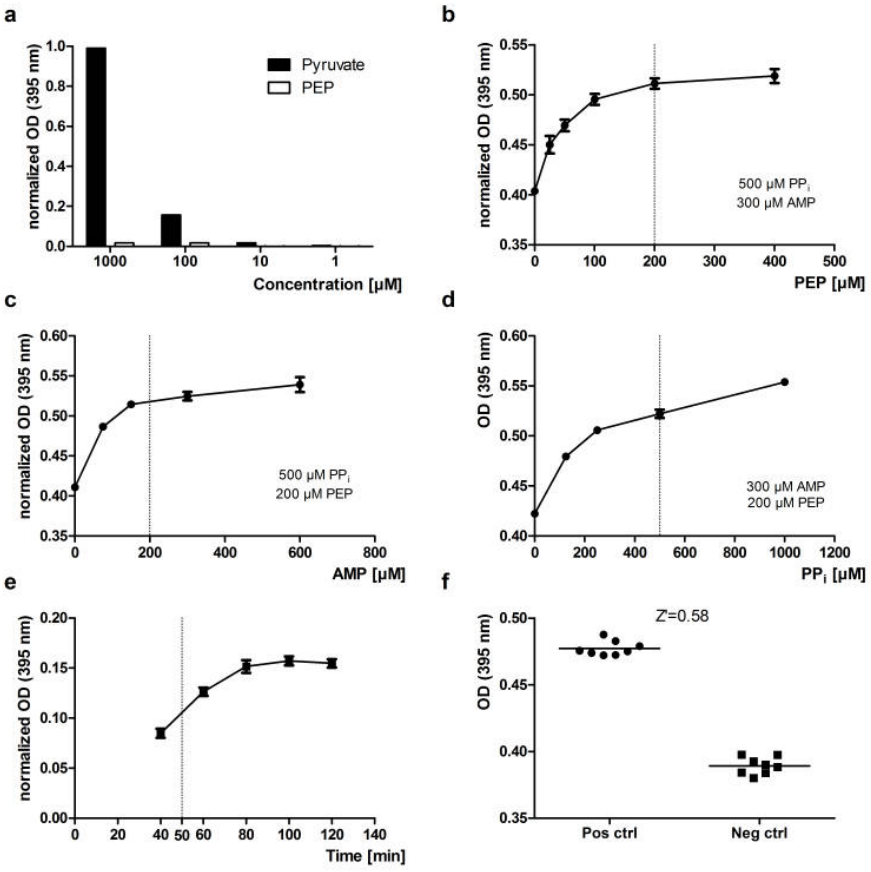

Figure 3.35: Establishment of PPDK-DNPH HT-Screening assay
a) Specific detection of pyruvate $\geq$ 10 μM by PDR. **b)** Substrate concentration curve for PEP, **c)** AMP and **d)** PP_i while the concentration of other substrates was kept constant as indicated. PPDK concentration was 100 nM. Final HTS assay conditions are indicated as dotted lines. **e)** Time curve of the PPDK-catalysed reaction. The standard reaction time chosen was 50 min, at which the reaction was still in its linear phase. **f)** Test Z'-factors under these conditions with eight replicates was 0.58 indicating robust assay quality.

22 compounds were confirmed to be inhibitory to PPDK by more than 50% at 37.5 μM (**Fig. 3.37 c, Table 3.5**). None of these compounds interfered non-specifically with the direct detection of pyruvate. An overview of all confirmed screening hit structures is shown in **Appendix A**.

Table 3.5: Confirmed PPDK Screening hits

Compound	% Inhibition Primary Screen	% Inhibition Rescreen	% Inhibition Pyruvate Detection	IC_{50} PPDK [μM]	IC_{50} Pyruvate Kinase [μM]
CG6 32F2	100	97.2	none	2.3	1.4
CG5 27H5	100	91.1	none	5.2	1.8
CG4 19G2	98.8	90.9	none	21	27
CG2 4E2	81.8	87.7	none	35	6.9
CG3 16H9	82.5	82.7	none	20	none
CG1 3E10	88.2	79.3	none	11	39
CG2 3E5	83.4	72.5	none	30	36
CG1 1H10	74.9	57.1	none	n.d.	n.d.
CG2 2B3	85.2	54.1	none	n.d.	n.d.
CG2 2A8	84.2	44.8	none	n.d.	n.d.
CG4 1G3	100	36.1	none	n.d.	n.d.
CG4 23G5	84.2	45.9	none	n.d.	n.d.
CG4 16F9	89.2	36.1	none	n.d.	n.d.
CG5 9B8	92.8	34.8	none	n.d.	n.d.

n.d: not determined

3.9.3 Hit validation

Confirmed hits were successively validated for specificity of inhibition. The top hits CG5 27H5 and CG6 32F2 shared a chemical scaffold and both inhibited PPDK activity by $> 90\%$ at 37.5 μM with IC_{50}-values of 5.2 and 2.3 μM, respectively (**Fig. 3.38 a**). When tested against rabbit Pyruvate Kinase (PK) in an analogous DNPH-based assay system, these compounds were shown to also be a potent inhibitors of PK with IC_{50}-values of 1.8 and 1.2 μM. Six of the residual 7 confirmed hits showed a similar non-specific inhibition pattern on both PPDK and PK (**Table 3.5**). As these compounds hold no promise in the development of specific inhibitors of PPDK that would specifically target *Wolbachia*, they were disregarded in the following validation procedure. One remaining hit structure, CG3 16H9, was a specific inhibitor of PPDK ($IC_{50} = 20$ μM) and was therfore termed **PPDK in**hibitor **1** (PPDKin1) (**Fig. 3.38 b**). The chemical structure of PPDKin1 is shown in **Fig. 3.38 c**. The inhibitory activity of PPDKin1 was further tested in a secondary PPDK assay setup, which was the standard PPDK assay coupled to LDH-activity monitoring the turnover of $NADH/H^+$ to NAD^+ as a decrease in OD_{340nm} in realtime (**Fig. 3.38 d, e**). Inhibitory activity of PPDKin1 was evident by decreased $NADH/H^+$ turnover rates (slopes) and resulting decreased percent activity values.

Solubility of PPDKin1

As extinction and solubility of PPDKin1 was low and no differential absorption spectrum compared to control samples containing 3.75% DMSO could be obtained, solubility was determined by visually rating the presence of a pellet of precipitated compound. Solutions were prepared in PPDK-PBS buffer or H_2O by adding equal

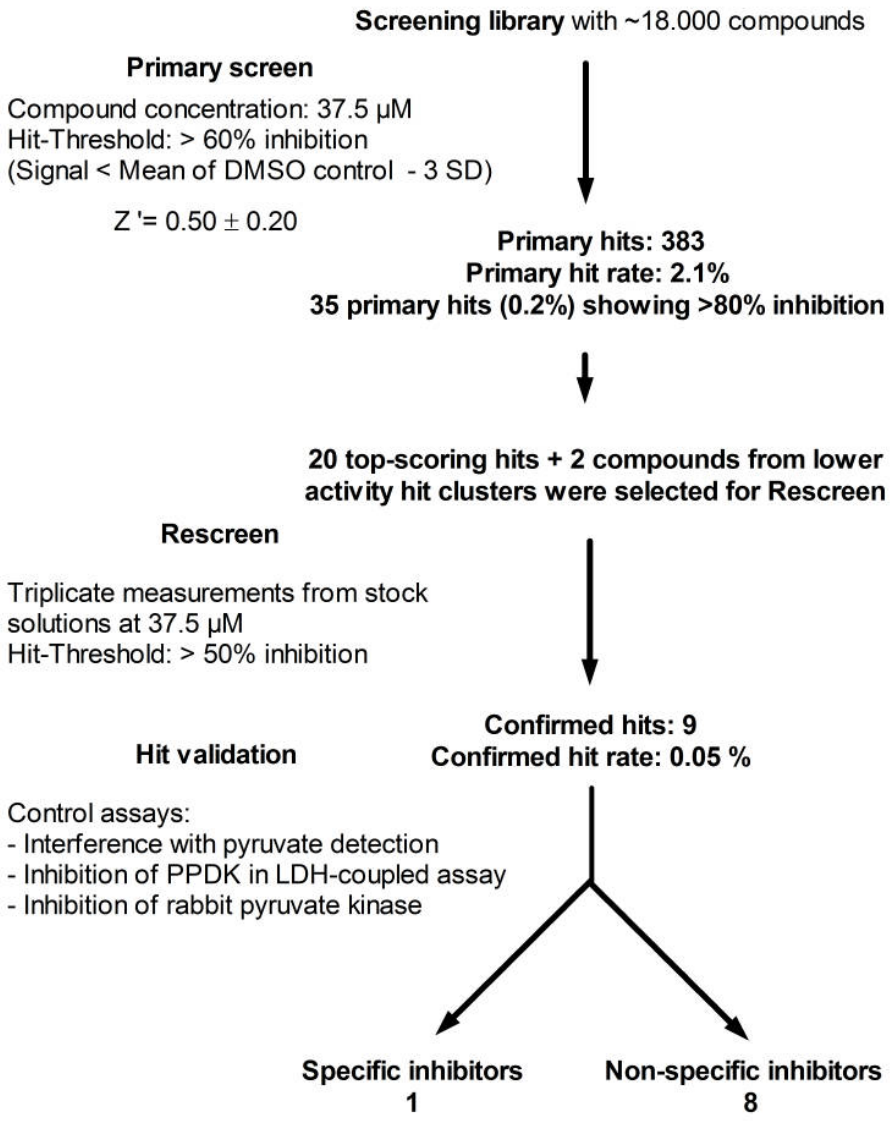

Figure 3.36: Workflow of PPDK HT-Screening and hit validation

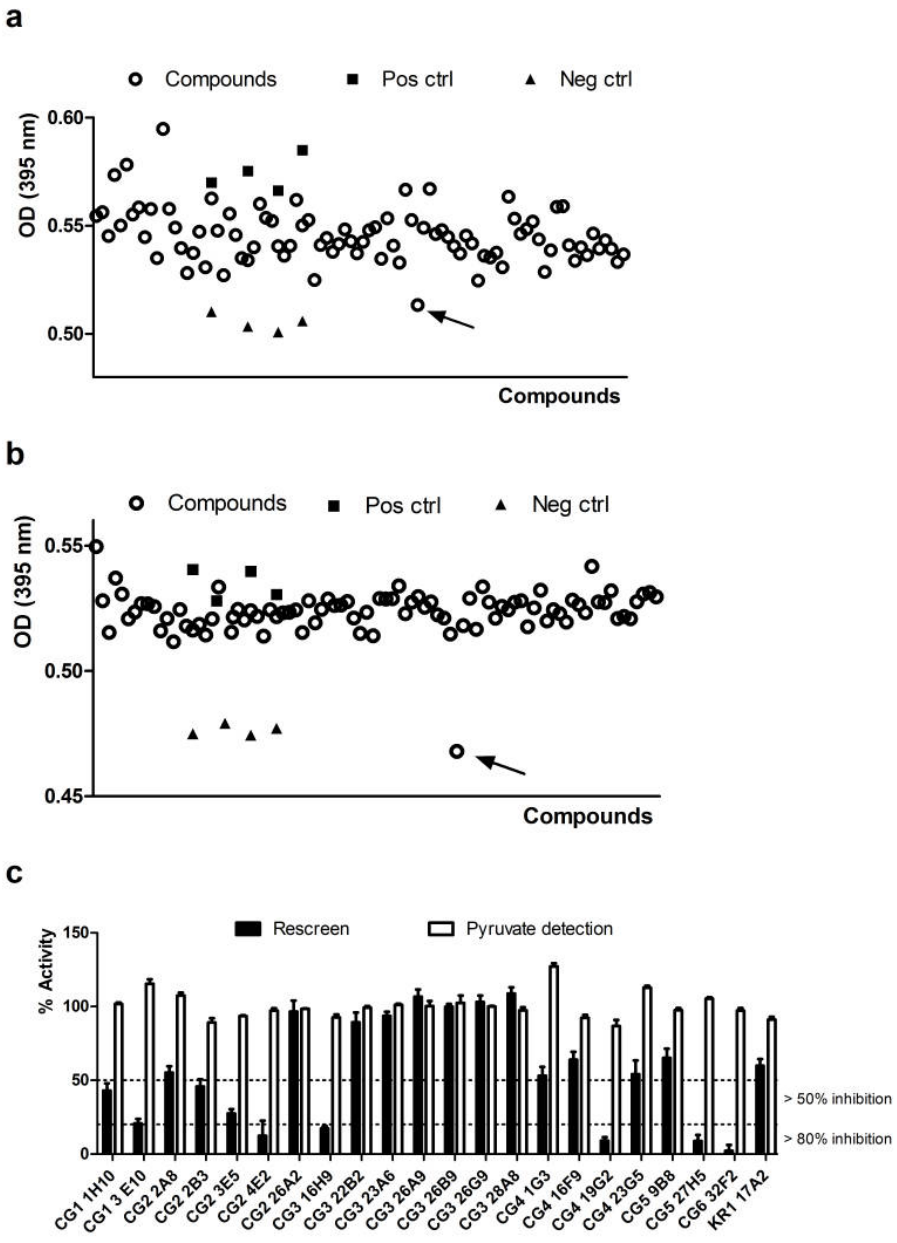

Figure 3.37: Results of PPDK screening and rescreen
a), **b)** Primary data from two exemplary screening plates. PPDK was very sensitive for background interference for certain classes of chemicals as those in **a**. Arrows point to two confirmed screening hits (CG1 3E10 in **a** and CG6 32F2 in **b**). **c)** Performance of the top 20 screening hits in the rescreen and pyruvate detection control assay.

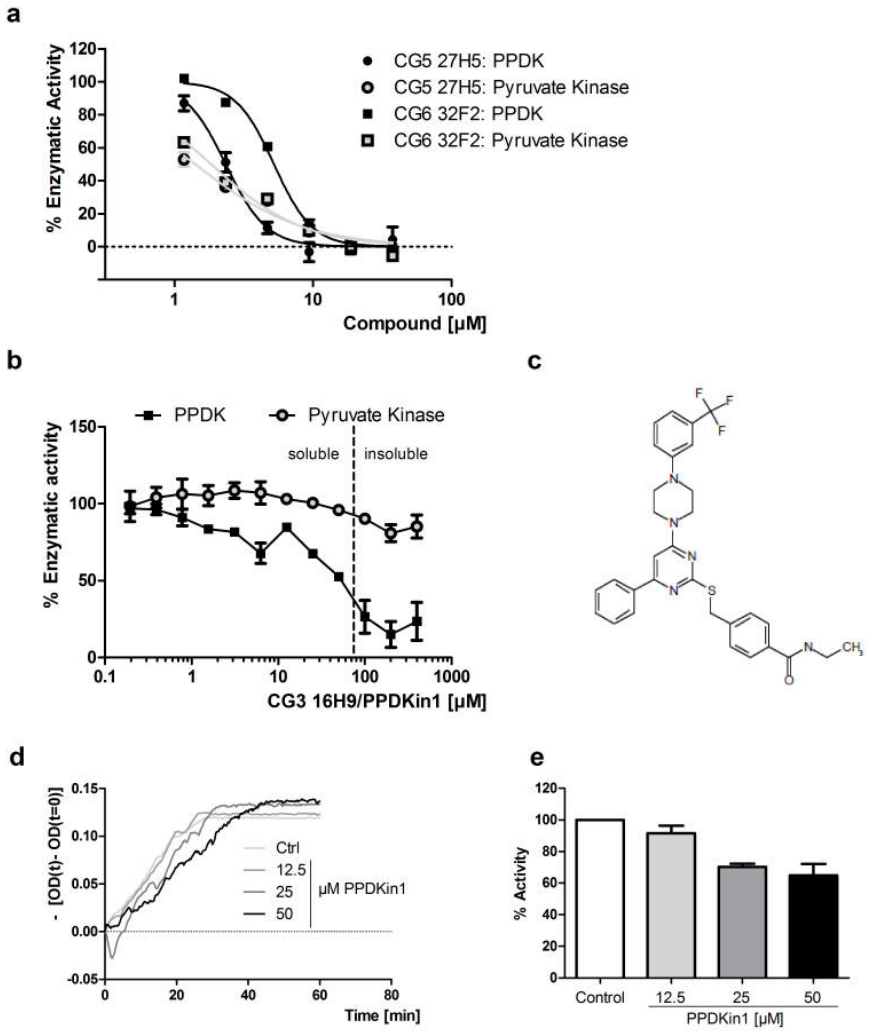

Figure 3.38: PPDK Screening hits

a) The chemically related potent PPDK inhibitors CG5 27H5 and CG6 32F2 are also potent inhibitors of rabbit pyruvate kinase. **b)** CG3 16H9 specifically inhibits PPDK of *Wolbachia* while it does not affect activity of pyruvate kinase and is therefore called PPDKin1. Solubility limit of PPDKin1 in PPDK-PBS Buffer was between 50 and 100 μM. Graphs are representative of two experiments. **c** Chemical structure of PPDKin1. **d)** PPDKin1 also inhibits activity of PPDK in the PPDK-LDH assay (mean normalized OD_{340nm} data indicative of NADH/H^+ turnover of a duplicate experiment and is representative of two experiments). **e**) Percent activity values were calculated as the slopes of PPDKin1-treated samples in the PPDK-LDH assay reaction normalized on the slopes of 3.75% DMSO-treated controls set to 100% activity. Slopes were calculated by linear regression of normalized OD data between 2 and 18 min and lines were forced to go through (X=0/Y=0). The graph depicts mean pooled percent activity data from two experiments performed in duplicates.

amounts of substance in a concentration series, where a two-fold increase in concentration involved a two-fold decrease of the volume. In PPDK-PBS buffer pellets of precipitated inhibitor were evident at concentrations $\geq$ 100 μM, in $H_2O \geq 50$ μM. This indicates that the limit of solubility of PPDKin is between 25 μM and 50 μM in H_2O and between 50 μM and 100 μM in PPDK-PBS buffer. The limit of solubility is displayed for PPDKin1-concentration curves in **Fig. 3.38 b**.

3.9.4 Determination of the type-of-inhibition

The mechanism underlying the inhibition of PPDK by PPDKin1 was analyzed by a set of substrate concentration series in the presence of different concentrations of inhibitor under saturating cosubstrate concentrations. For PEP and AMP, the inhibitory potential increases with substrate concentration (**Fig. 3.39 a - d**) and requires a threshold of $\sim$100 μM to be exceeded. This is in accordance with an uncompetitive mode-of-inhibition in which the inhibitor binds to the enzyme-substrate-complex. This conclusion is supported by non-linear regression analysis, where the assumption of an uncompetitive inhibition model algorithm gives superior fits [R^2(AMP) = 0.9419; R^2(PEP) = 0.9736] than non-competitive or competitive models and is equivalent to a "*Mixed Model Inhibition*" NLR where α was close to 0 (characteristic of uncompetitive inhibition). Due to the dimeric nature of PPDK, simple hyperbolic curve fits did not sufficiently represent the progression of the data and hence the "*Allosteric sigmoidal*" algorithm (Prism 5.0) accounting for possible cooperative effects was applied. In contrast to PEP and AMP, inhibitory potency was not influenced by the PP_i concentration, indicating noncompetitive inhibition [R^2(PEP) = 0.9890] with respect to this cosubstrate (**Fig. 3.39 e, f**). At 500 μM PEP/AMP and assuming noncompetitive inhibtion with respect to PP_i the dissociation constant K_I was predicted by NLR to be 52.6 $\pm$ 4.6 μM. Taken together, PPDKin1 is a novel specific inhibitor of PPDK which acts by a an AMP/PEP-uncompetitive mechanism.

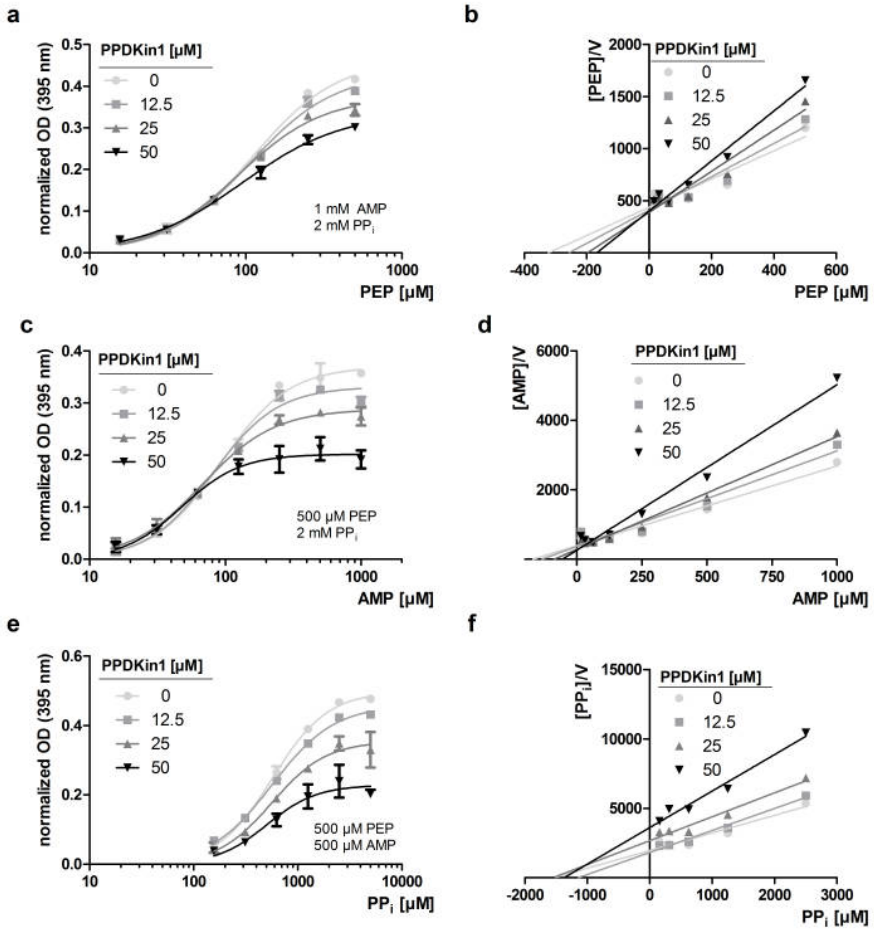

Figure 3.39: Inhibition studies with PPDKin1

Inhibitory properties of PPDKin1 in the presence of different concentrations of co-substrate was tested. The left panel (**a, c, e**) shows normalized OD_{395nm} values. Curves were fit using the "*Allosteric sigmoidal*" NLR algorithm of GraphPad Prism 5.0. The right panel (**b, d, f**) shows the corresponding data in the linearized Hanes-Woolf representation. Data points for $\geq$ 0.5 PP_i and $\geq$ 1 mM PEP were excluded from linear regression in the Hanes-Woolf plot due to beginning substrate inhibition. **a), b)** PPDKin1 acts in an uncompetitive fashion with respect to PEP and **c**), **d)** AMP (PPDKin1 reduces both V_{max} and K_M; the y-axis intercept K_M/V_{max} remains nearly constant) and **e), f)** is a non-competitive inhibitor with respect to PP_i (reduction in V_{max}, nearly constant K_M).

Chapter 4

Discussion

4.1 The rationale for HTS-based drug discovery of novel antifilarial compounds acting on *Wolbachia* targets

The rational design of antifilarial drugs acting on nematode targets is hindered due to the generally high sequence homology between worm and mammalian proteins leaving only a very limited number of suitable drug targets e.g. in nematode-specific processes such as molting [96] or synthesis of the disaccharide trehalose [154, 155]. In contrast, thanks to their different physiology and sequence divergence, prokaryotic *Wolbachia* endosymbionts provide ideal targets for the development of potent and specific antifilarial drugs. The annotation of the *B. malayi* and *Wolbachia* endosymbiont of *B. malayi* (*w*Bm) genomes [81, 93, 124] had a major impact on antifilarial and anti-*Wolbachia* drug discovery and enabled the identification of putative drug targets within essential biochemical pathways of the bacteria that may be exploited for target-based drug discovery [208, 232]. As the biological effects induced by *Wolbachia*-targeting drugs may be manifold, the following classification scheme shall be introduced that classifies endobacterial drug targets into two different categories: 1) Target proteins required for bacterial homeostasis, including the targets of classical antibiotics like protein translation (doxycycline) [118, 47], transcription [224] or cell-wall biosynthesis [109]. Inhibition of these processes will lead to a depletion of endobacteria from the filarial hosts with secondary effects on the filarial host as described (a block of embryogenesis and death). 2) Drugs directly targeting the putative pathways of symbiosis, i.e. biosynthetic pathways of metabolites that *Wolbachia* is considered to provide to its host. Such drugs, which have not been reported for *Wolbachia* so far, are likely to affect the worm directly, with the neat circumstance that the molecular target is prokaryotic.

The current study aimed at the target-based discovery of novel inhibitors of two putative enzymatic drug targets of *Wolbachia*: 1) Pyruvate phosphate dikinase, an enzyme without mammalian ortholog that fulfils an essential biochemical function in the energy metabolism and thus homeostasis of *Wolbachia* 2) δ-Aminolevulinic acid dehydratase, catalyzing the second step of biosynthesis of heme in *Wolbachia* that likely sustains filarial demands for porphyrins. For both target proteins enzymatic assays were established and subjected to High-Throughput Screening against a diversity-based compound library comprising ~18,000 drug-like small molecules. Although both assys met stability criteria required for HTS [274], performance of the wALAD screening assay was superior to that of PPDK producing lower primary hit rates and a higher number of validated hits. While for PPDK only one

specific inhibitor was identified, screening for wALAD inhibitors revealed a cluster of potent species-selective inhibitors along with several other hit structures with less pronounced or absent discriminatory power between certain ALAD orthologs. Compared to industrial-scale screening libraries comprising > 50,000 compounds in designated academic HTS-facilities [38] or up to 2 million compounds in pharmaceutical companies [87], the size ot the screened library in this study was modest. However, both assay systems established may be set up and running to screen further compound libraries. While the identification of a magic bullet within this restricted set of compounds would have been serendipitous, the provided hit structures, especially wALADin1 benzimidazoles, fulfil the aims of the screening campaign. They represent previously undescribed chemical entities with biological activity as inhibitors of putative enzymatic targets in antifilarial drug discovery. In the following, structural and mechanistic aspects of the biological effects of the hit compounds originating from both screening campaigns and their suitability as lead structures in antifilarial drug discovery and beyond will be discussed.

4.2 Targeting Pyruvate Phosphate Dikinase of *Wolbachia*: Interfering with endobacterial energy metabolism

4.2.1 The biochemistry of PPDK

PPDK is a ∼96 kDa homodimeric protein that contains three independently-folded domains [111, 54, 189, 163]. The crystal structures of *Clostridium symbiosum*, *Trypanosoma brucei* and maize PPDK revealed a C-terminal TIM-barrel domain involved in PEP/pyruvate-binding and an N-terminal ATP-grasp domain that contains the AMP/ATP-binding site. Both remote domains contain distinct active sites and are interconnected by a swivelling phosphohistidine carrier domain where His-455 (of *Clostridium symbiosum* PPDK) mediates the phosphoryl transfer.
The reaction catalyzed by PPDK is the reversible conversion of PEP, AMP and PP_i to pyruvate, ATP and P_i (see page 19 for overall **Equation 1.1**). It can be divided into the following three partial reactions [268, 257]:

$$PPDK - His + \overset{\beta}{P}EP \Longleftrightarrow PPDK - His - \overset{\beta}{P} + pyruvate \tag{4.1}$$

$$PPDK - His - \overset{\beta}{P} + \overset{\gamma}{P}\overset{\delta}{P}_i \Longleftrightarrow PPDK - His - \overset{\beta}{P}\overset{\gamma}{P} + \overset{\delta}{P}_i \tag{4.2}$$

$$PPDK - His - \overset{\beta}{P}\overset{\gamma}{P} + AMP \Longleftrightarrow PPDK - His + \overset{\beta\gamma}{A}TP \tag{4.3}$$

The increased energy balance of PPDK-dependent compared to PK-dependent glycolysis due to substrate-level phosphorylation is of major advantage for anaerobic organisms that do not produce energy by oxidative phosphorylation but depend on glyolysis and fermentation [231]. Consequently PPDK is present in a variety of anaerobic protists of clinical relevance: For *Giardia intestinalis* a role for PPDK in glucose metabolism has been demonstrated by knock-down of PPDK mRNA and PPDK of *G. lamblia* and *E. histolytica* are considered promising drug targets. Interestingly these parasites also have an ortholog of PK [75]. Other anaerobic protists like *Trichomonas vaginalis* do not have PPDK but a pyrophosphate dependent version of phosphofructokinase [178]. Furthermore PPDK orthologs have been found in trypanosomatids, a variety of plants [104, 184] and eubacterial phylae including proteobacteria (*Wolbachia, Rickettsia*), Firmicutes (*Streptococcus, Staphylococcus,*

Clostridium), Spirochaetes (*Treponema*) and others [231]. In *Trypanosoma cruzi* PPDK is present in specialized metabolic compartments termed glycosomes, where in the absence of pyrophosphatase the role of PPDK is suggested to consume PP_i in a highly exergonic reaction and thus thermodynamically drive other energetically less favourable reactions that depend on PP_i production and turnover [5]. In this case the PPDK reaction is regarded as irreversible due to the high ΔG of ∼-5.2 kcal/mol.

PPDK orthologs from different species have been attributed opposing roles. For PPDK from *Entamoeba histolytica* the enzyme has been suggested to function mainly to provide pyruvate [213, 257], for *Propionibacterium shermanii* [74] and plants [104] a gluconeogenetic role in the synthesis of pyruvate has been proposed. Whether in *Wolbachia* PPDK has its major physiological role in glycolysis or gluconeogenesis remains to be verified. For *Wolbachia*, and *Rickettsiales* in general, neither pyruvate kinase nor pyruvate carboxylase/PEP carboxykinase orthologs have been found [212]. Inorganic pyrophosphatase has been annotated in the *Wolbachia* of *B. malayi* genome (Uniprot ID: Q5GS53), although its expression levels, localization and functional importance will have to be verified. In the absence of alternative metabolic and biosynthetic routes, these findings suggest a possible dual role of PPDK in these organisms: 1) Catabolism of glucose, respectively downstream-metabolites acquired through the filarial host, in the energy metabolism. 2) Anabolism of C_4-carbohydrates and glucose from non-carbohydrates. As PPDK is not present in mammalian cells it is a prime target for antiinfective drug discovery for those species depending on its activity, including *Wolbachia* of *Brugia malayi* [212].

4.2.2 Previously described inhibitors of PPDK and screening assays

The first known inhibitor of PPDK was phosphonopyruvate, a substrate analog of PEP [112] which may also bind to other PEP-binding enzymes and the physicochemical properties are not drug-like (two negative charges, 6 oxygen atoms). Recently, a new class of flavone-based inhibitors has been identified combining *in vitro* enzymatic assay screening and virtual screening against the ATP-grasp domain of *Clostridium symbiosum* PPDK. These flavone structures represent the most promising class of PPDK inhibitors with K_I values between 1.6 and 25 μM and act as competitive inhibitors of AMP at the active site. Two other studies have also engaged computer-based drug-design approaches by *in silico* screening for ligands of the active site of the N-terminal nucleotide-binding domain of *Entamoeba histolytica* [236] and more recently of the *Wolbachia* of *B. malayi* ortholog [197]. Both dockings were done using homology models of the respective protein sequences against the crystal structure of *C. symbiosum* PPDK. However, for either of the proposed sets of top-scoring ligands experimental evidence for binding let alone inhibition is still lacking. Another biochemical screening approach has been taken to identify inhibitors of C_4 plant PPDK from organic extracts of marine macroscopic organisms [67] and marine fungal extract libraries [188]. The screening was done on the basis of a phosphoenolpyruvate-carboxylase and nicotinamide adenine dinucleotide–malate dehydrogenase coupled activity assay [67]. Screenings included 6679 and 2245 extracts and primary hit-rates of 4.9% and 13.2%, respectively, were obtained. The hits then required further validation as to which of the screening enzymes was the actual target. The simple one-step and screening-assay presented in the current work using detection of pyruvate by a DNPH-reagent is an easy-to-analyze alternative superior to coupled assays when only inhibitors of PPDK are of interest. By reducing the concentration of screening compounds and increasing Mg^{2+} and the substrate concentrations, assay robustness may be easily increased for future screening of compound libraries, although sensitivity against competitive inhbitors

may thus be reduced. Motti et al. presented unguinol as a specific-inhibitor of the C_4 plant PPDK with an IC_{50} value of 42 ± 0.8 μM that was noncompetitive with respect to PEP and AMP, but uncompetitive to PP_i [188]. However, unguinol was also shown to inhibit growth of three tested cancer cell lines with GI_{50} values of 28 - 51 μM and of Gram-positive *S. aureus* and *V. harveyi* (GI_{50}: 8.7 and 69.5 μM, respectively), but not of Gram-negative *E. coli* bacteria. Although unguinol may be considered as a lead structure for the development of novel herbicides as the authors suggest, it is not suited as an antibiotic lead-structure due to expected non-specific cytotoxic effects on human cells which do not possess PPDK. In conclusion, no generally applicable PPDK inhibitor had been described so far. The novel inhbitor of *Wolbachia* PPDK, PPDKin1, may be the cornerstone for the development of more potent and specific inhibitors of PPDK that may find their way to pharmaceutical applications.

4.2.3 PPDKin1, a novel inhibitor of *Wolbachia* PPDK

High-Throughput Screening for inhibitors of the *Wolbachia* PPDK enzymatic reaction initially provided a large number of primary hits (2.1%). Given the observed instability [212] and thermal denaturation of the protein at low temperatures (ΔTm ~43 °C), PPDK might be especially sensitive to non-specific effects caused by high concentrations of certain classes of molecules. For future screening approaches using other libraries of small molecules it is recommended to screen at lower compound concentrations, e.g. 10 μM, which is a standard concentration for small molecule screens [130, 191]. However, due to the previous success of the wALAD screen (at 67 μM compound), these effects of 37.5 μM compound were unforeseen. Notwithstanding, when the top 22 hit compounds were analyzed, 9 compounds were confirmed with more than 50% of inhibition while 5 others showed 30% - 50% of inhibition, which underlines the general validity of the primary screening results. 8 out of 9 confirmed hits, including the chemically related molecules CG5 27H5 and CG6 32F2 which inhibit PPDK potently with IC_{50}-values in the one-digit μM range, were also active against mammalian pyruvate kinase. In light of the absence of sequence homology between PPDK and PK this finding is very surprising. A possible explanation is that these compounds are promiscuous inhibitors that target general protein motifs or they specifically target single residues or 3D-structural arrangements shared by both proteins, e.g. for PEP-binding, which cannot be easily recognized by primary structure analysis.

The remaining inhibitor CG3 16H9 was found to specifically inhibit PPDK with a K_I-value of ~53 μM and was termed PPDKin1. It acts by a mechanism that is uncompetitive with respect to the substrates PEP and AMP and non-competitive with respect to PP_i. This mechanism is unprecedented and illustrates the specificity of the compound. However, in PPDK-PBS buffer, solubility of the compound is between 50 and 100 μM. Therefore PPDK activity may not be completely inhibited under the conditions tested, but a maximum inhibition of ~75% was reached. The inhibitory potency of wALADin1 is comparative to that of unguinol [188], but lower than the potency of the flavone inhibitors [271]. However, the unique PEP/AMP-uncompetitive mechanism of PPDKin1 may be superior in terms of specificity, as it does not target a conserved site such as the active site of a nucleotide-binding domain which is the target site of the flavone inhibitors [271]. The low solubility of PPDKin1 will be a major impediment for the use of this compound in *in vivo* studies. But as the physiological environment of PPDK function in *Wolbachia* and substrate concentrations are unknown, PPDK may be more active and more susceptible to uncompetitive inhibition by PPDKin1 *in vivo*.

The uncompetitive nature of PPDKin1 with respect to PEP and AMP indicates, that it binds to the enzyme-substrate complexes with bound PEP and/or

AMP. The central His-domain is connected to the N- and C-terminal domain, respectively, with linker arms LC and LH, that do not actively direct catalysis, but are able to restrict the conformational space of the His-domain and thus indirectly guide the swivelling motion [263]. However, independently expressed central and N-terminal domains that are unlinked are unable to form a complex able to catalyze the nucleotide-partial reaction [164]. So how can PPDK1 sense the presence of PEP and AMP which have remote and seemingly independent binding sites? Either there are, although unexpected [263], indeed conformational changes mediated across the different domains upon binding of the two substrates that would expose a previously hidden binding site for PPDKin1, e.g. in the linker regions or in the central His-domain. The differential crystal structures of maize PPDK with and without PEP showed that upon substrate binding an interaction between the C-terminal domain and the linker domain was freed, allowing a swiveling motion to occur [189]. Thus, at least neighboring linker regions may be conformationally influenced by the catalytic sites, although far-ranging cross-domain interactions remain to be demonstrated. Alternatively, the enzyme substrate PPDK-PEP complex (which is required to form first) may be contemplated *after* completion of the first partial reaction (**Equation 4.1**). Although formed pyruvate may be released, the β-phosphate of PEP is bound to the His-residue of the central domain and undergoes the swivelling motion from the PEP-domain towards the nucleotide-domain. When AMP is then bound to the nucleotide-domain the formed binary complex of phosphorylated PPDK and AMP [257] may present the binding-site of PPDKin1, e.g. in the interface of His-domain and nucleotide-domain. However, given the non-competitive inhibition with respect to PP_i, it should be extraneous to PPDKin1-binding, whether or not PP_i is bound to the nucleotide-binding domain. Future elucidation of the binding site of PPDKin1 will help unravel the precise molecular mode of action which is currently subject to mere speculation. As different kinetic mechanisms have been described for PPDK orthologs from different species [257], it will be fascinating to study the inhibitory properties of PPDKin1 on the different organisms. Knowledge of the molecular interactions involved in inhibition will allow the rational design of inhibitors with higher potency, improved solublity and general drug-like physico-chemical properties. Understanding the PPDKin1-mediated inhibition may further give important insight into the coordination of the swivelling reaction and catalysis, which is still an open question in PPDK biochemistry.

4.2.4 Summary PPDK

An HTS-compatible enzymatic assay for PPDK based on the colorimetric detection of pyruvate by DNPH was established. Small molecule library screening identified PPDKin1 as a specific inhibitor of PPDK of *Wolbachia*. This inhibitor has a unique molecular mode of action involving uncompetitive inhibition with respect to PEP and AMP and non-competitive inhibition with respect to PP_i and may be used to probe the biochemistry of PPDK enzymes. In the absence of broadly applicable, potent and specific inhibitors of PPDK, the identificaton of PPDKin1 is a major innovation which allows future synthesis of derivatives with improved potency and solubility. Given the broad range of target organisms depending on PPDK function PPDKin1-derived inhibitors may have a future as herbicidal, antiprotozoal and antibacterial compounds including their potential use as antifilarials by targeting *Wolbachia* endosymbionts.

4.3 Interfering with the heme biosynthesis of *Wolbachia* endobacteria

While tetrapyrrole biosynthesis belongs to biochemical pathways best conserved throughout all domains of life, the only eukaryotes reported to lack (i.e. have lost during evolution) the ability to synthesize heme *de novo* are either unicellular parasites like *Leishmania spp.* that likely salvage heme or precursors from their hosts [199] or nematodes [211, 93]. The free-living nematode *C. elegans* is considered to use heme-transporters to take up heme from its natural environment [211, 209], a strategy that may also be pursued by parasitic filarial nematodes like *Loa loa* and *A. viteae*. A different strategy to cover their heme demand was apparently adopted by parasitic filarial nematodes such as *Brugia malayi* (and all other causative agents of LF and Oncho) that harbor *Wolbachia* endosymbionts. The *B. malayi* genome only has a gene encoding ferrochelatase catalyzing the last enzymatic step of heme biosynthesis. In contrast, the endobacteria, which are considered to have lost all non-essential genes during co-evolution with their hosts, have conserved all genes for the entire heme biosynthetic pathway within their otherwise restricted 1.1 Mb genome [81]. The only gene not identified in the *Wolbachia* genome was an ortholog of the *hemY* or *hemG* gene. It has been observed that the oxidative function of protoporphyrinogen IX oxidase is replaced by other enzymes. Coproporphyrinogen III oxidase was demonstrated to exert this function in *hemG* independent *E. coli* mutants [190], but complementation assays in *E. coli* using the homologous *Wolbachia* gene did not restore catalytic activity. However, this work presents evidence that protoporphyrin IX oxidase function in *Wolbachia* is possibly exerted by a homolog of the translation product of the *slr1790* gene of *Synechocystis spp.* [146]. Genes with significant homology were identified by tblastn searches in the genome of *Wolbachia* of filarial nematodes.

As a consequence, it is expected that the endobacteria supply their filarial hosts with tetrapyrroles [93, 270, 232] although it may be possible that *Wolbachia* synthesize heme only for their own needs. It is expected that the *Wolbachia*-devoid filariae *L. loa* and *A. viteae* have had horizontal transfer of certain endobacterial genes to the nuclear genome of the filariae [175] and it may be speculated that the development of molecular transport systems allowing these worms to exploit exogenous heme sources was part of the evolutionary trigger that helped these filariae to become independent of *Wolbachia*. However, this scenario has not been verified experimentally. During a defined life-stage (as young adults) *L. sigmodontis* ingest host red blood cells, presumably for the take-up of nutrients due to temporarily high energy consumption at this life-stage [11]. Although it may not be completely ruled out that at certain life stages even *Wolbachia*-containing filariae may, indeed, take up tetrapyrroles from their human host, studies have collected compelling evidence for a vital role of endobacterial heme biosynthesis for survival of filarial nematodes: 1) Antifilarial activity of heme biosynthesis inhibitors in *B. malayi* females in an *ex vivo* culture system could not be rescued by the addition of exogenous heme [270]. 2) Depletion of *Wolbachia* from *L. sigmodontis* by tetracycline treatment in a natural infection model caused upregulated expression of genes encoding several mitochondrial heme-dependent respiratory-chain complex subunits [241]. This finding is interpreted as a regulatory response of the filariae to overcome lack of heme biosynthesis. Thus, inhibiting the enzymatic function of δ-aminolevulinic acid dehydratase of *Wolbachia* (ALAD) that catalyzes the second step of endobacterial heme biosynthesis (i.e. the condensation of 5-aminolevulinic acid to porphobilinogen) is considered a suitable strategy to block biosynthesis of tetrapyrroles in *Wolbachia* and to deprive the worms of their essential cofactor heme. Lack of heme would cause a malfunction of heme-dependent processes such as oxidative phophorylation

and may lead to oxidative stress due to a lack of catalase/peroxidase function and will eventually result in death of the worm.

However, targeting endobacterial porphobilinogen production could synergize with a second effector pathway. In principle, inhbition of wALAD should elicit a pathophysiological condition in the worms similar to the effects of lead intoxication in man, where Pb^{2+} displaces Zn_B^{2+} from the cysteine-rich binding site in the active center with a corresponding loss of human ALAD activity [132]. It has been suggested that the neuropathological symptoms of lead poisoning may be caused by increased levels of 5-ALA [262]: Due to its structural analogy, 5-ALA may act as an agonist on γ-amino butyric acid (GABA)-autoreceptors [39] and exert prooxidating effects [65, 59, 23]. In analogy, inhibition of ALAD in *Wolbachia* will inherently lead to the accumulation of 5-ALA in the endobacteria and, possibly, in the entire worm, where 5-ALA may induce oxidative stress. Furthermore, essential biological functions of nematodes such as locomotion and defecation were shown to be under the control of GABA-ergic signalling [142] and the anhelminthic piperazine is a low-potency agonist of GABA receptors as shown for the gastro-intestinal roundworm *A. suum* [168] and the filaria *A. viteae* [48]. Notably, the most efficient antifilarial drug, dieethylcarbamazine (DEC), is based on a piperazine ring, although DEC, itself, was shown not to interact with GABA receptors of *Ascaris suum* [168]. In this study, I demonstrated that exposure of adult *L. sigmodontis* worms to exogenously added 5-ALA in the *ex vivo* culture system revealed a macrofilaricidal effect at 5-ALA concentrations of 1 mM and 5 mM, but not 200 μM. Resulting concentrations in the worm are expected to be lower, as the cuticle represents a barrier to polar substances like GABA [48]. Given a K_M of $\sim$300 μM, it is easily conceivable that in the pathophysiological context of ALAD inhibition excess 5-ALA concentrations in the range of 1 mM may accumulate in the worm, although the physiological concentrations of 5-ALA in the filariae remain to be determined. As outlined in **Figure 4.1**, it must be considered that the antifilarial effects elicited by inhibition of ALAD are not merely a consequence of heme-depletion, but also involve toxicity of excess 5-ALA. Thus, inhibitory effects on a single target (ALAD) may trigger two independent, potentially filaricidal, biological effector pathways (heme-deprivation and 5-ALA-induced toxicity) underlining the excellence of wALAD as an antifilarial drug target candidate.

4.3.1 Currently known inhibitors, structure analogs

A variety of ALAD inhibitors is already known. The most prominent class comprises substrate analogs that mostly do not have a species-selective inhibitory profile. These analogs are similar to the substrate 5-aminolevulinic acid (5-amino-4-oxo pentanoic acid) and are usually keto acids, e.g. levulinic acid (4-oxo-pentanoic acid), succinyl acetone (SA, 4-6, dioxoheptanoic acid) or 4-keto-5-amino hexanoic acid, that undergo Schiff base formation with a conserved active site lysine residue (Lys263 of yeast ALAD) involved in binding of A-side ALA [69]. SA was initially identified as a naturally occurring metabolite in patients with hereditary tyrosinemia [165] and is most commonly used as a specific, though not species-selective, ALAD inhibitor in order to probe the biological effects of a blockade of heme biosynthesis [242, 270]. The longer diketo diacid inhibitor 4,7-dioxo-sebacic acid (4,7-DOSA) was demonstrated to cross-link the A-site and P-site by forming Schiff bases with lysine residues of both sites (Lys263 and Lys210, yeast ALAD) [68]. For 4,7-DOSA, a certain discrimination of ALAD orthologs was observed with a preference for Zn^{2+} utilizing enzymes like human ALAD [149], while 4-oxo-sebacic acid preferentially inhibits the Zn^{2+}-dependent *E.coli* enzyme, but not the human nor any Zn^{2+}-independent enzyme [136].

Another 5-ALA analog is 5-acetamido-4-oxo-5-hexenoic acid which was named

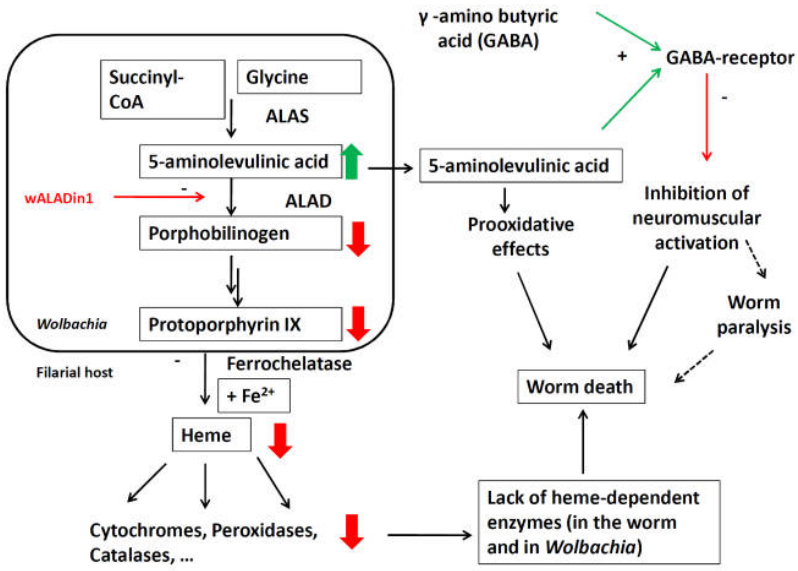

Figure 4.1: Scheme depicting the presumed biological effects of ALAD inhibition in *Wolbachia* endobacteria

The genes necessary for *de novo* biosynthesis of heme are conserved in the genome of *Wolbachia*, while the filarial host *B. malayi* only possesses the final enzyme ferrochelatase. Inhibition of δ-aminolevulinic acid dehydratase of *Wolbachia* (wALAD) by wALADin1 leads to reduced formation of porphobilinogen and the following heme precursors. Heme-deprivation will result in a deficiency of heme-dependent enzymes like cytochromes (energy transport chain) and catalases and peroxidases (detoxification of hydrogen peroxide), and is expected to lead to the death of the worm. Besides, as a consequence of ALAD inhibition 5-ALA will accumulate. This molecule may have prooxidative and thus toxic effects on the worm. Furthermore, it might activate GABA-receptors as an agonist resulting in reduced neuromuscular activation that may further lead to paralysis and death of the filaria.

Alaremycin ("**ALA**-**re**lated antibiotic produced by *Strepto**myc**es sp.*") according to its producing bacterial strain [13, 108]. Alaremycin binds to *P. aeruginosa* ALAD and leads to its inhbition by conventional Schiff base formation of its keto-group with P-site lysine.
A recently emerging strategy for the design of species-selective ALAD inhibitors exploits the allosteric nature of the morpheein ALAD and the intrinsically different catalytic activities of different quaternary structure assemblies. Crystal structures of *P. sativum* ALAD and other orthologs revealed a surface cavity and putative small molecule binding site unique to the low-activity hexameric assemblies [161]. *In silico* docking approaches were able to identify small molecules ligands of these sites (so-called "morphlocks") that perturb the oligomeric equilibrium of *P. sativum* ALAD by stabilizing inactive assemblies (here: hexamers) and thus inhibit enzymatic activity. As these allosteric cavities are phylogenetically very variable, this strategy allows the design of ortholog-selective inhibitors as was shown for morphlocks targeting *P. sativum* and human ALAD [161, 160]. A similar study revealed compounds targeting inactive dimeric assemblies of *P. aeruginosa* ALAD although the true inhibitory properties of these compounds were not reported [214].

4.4 wALADins as novel species-selective ALAD inhibitors: Structure and Function at the molecular level

4.4.1 A novel Mg-dependent type of inhibition

In the current study a novel class of ALAD inhibitors, tri-substituted benzimidazoles of the wALADin1 family, with a species-selective inhibitory profile was discovered. ***W**olbachia* **ALAD in**hibitor **1** (wALADin1), the most potent inhibitor (wALAD: IC_{50} ~11 μM) displayed pronounced species-discrimination with a marked preference for the endobacterial ortholog compared to the human enzyme (> 70-fold reduced potency).

wALADin1 is based on a benzimidazole scaffold with a 3-trifluoromethyl benzyl group at benzimidazole atom $N_1(R_1)$, a 2-[(2-thienylcarbonyl)amino]ethyl substituent at C_2 (R_2) and a carboxylic acid function at C_5 (R_3). Thus, the chemical structure of wALADin1 does not have any evident similarity with 5-ALA and lacks the keto acid motif of common substrate analogs required for Schiff base formation with a conserved active site lysine residue. Instead, the inhibitory mechanism was found to be a mixed competitive/non-competitive inhibition. It is further demonstrated that the compound functionally competes with the activation by a Mg^{2+} cofactor, although maximum enzymatic activity could not be restored completely by increasing Mg^{2+} concentration. Binding of allosteric Mg^{2+} is a major inducer of pro-octamer dimers and enzymatically active octameric assemblies in *P. sativum*, while removal of Mg^{2+} acts in favour of the inactive hexameric conformation [37, 135, 137]. However, the Mg^{2+} antagonizing effect of wALADin1 does not interfere with the oligomeric equilibrium as morphlock inhibitors do [161], rather this novel inhibitor targets the wALAD octamer as documented by the native PAGE experiments. Thus, the inhibitory mechanism of wALADin1 is novel and its Mg^{2+}-competitive character is the likely basis for the observed species-selective inhibitory profile.

4.4.2 Metal-cofactor requirements of ALAD orthologs

A general classification of ALAD orthologs into four classes according to the presence or absence of conserved metal binding sites was suggested by Eileen K. Jaffe [133]. One criterion is the presence or absence of the cysteine-rich Zn^{2+}-binding site in the active center (Zn_b or $Metal_b$-site). For Zn^{2+}-dependent orthologs, tetrahedral complexation of Zn_B to three conserved cysteine residues and A-side 5-ALA is an absolute requirement for catalytic activity. Binding of other less-well documented Zn^{2+}-binding sites (Zn_A) in the active center are considered dispensible for the catalytic process and may represent "reserve ions" [132, 134, 223]. The second classification criterion is the presence or absence of the allosteric Mg^{2+}-binding site (Mg_c-site) at the interface of the N-terminal arm with the α/β_8-barrel of the neighboring subunit that stabilizes the active site lid. This allosteric binding site forms an octahedron with Mg^{2+} coordinated to a conserved glutamic acid residue and five H_2O molecules.

According to this classification four groups exist, to which all orthologs that were used in this study can be assigned:

Group A: Zn^{2+}-dependent, without allosteric Mg^{2+} site
Mammalian or yeast enzymes including hALAD [132, 70]

Group B: Zn^{2+}-dependent, with allosteric Mg^{2+} site for further stimulation
Many bacterial orthologs like *E. coli* ALAD [71]

Group C: Zn^{2+}-independent, without allosteric Mg^{2+} site
Very few members like *Rhodobacter spp.* ALAD [27] that was not available for the current study

Group D: Zn^{2+}-independent, with allosteric Mg^{2+} site
Plant (*P. sativum*) and many bacterial orthologs including ALAD from *Wolbachia* [270], *P. aeruginosa* [83], *Y. enterocolitica* and *V. cholerae*

In addition to these categories Zn^{2+}-independent enzymes may further differ in the use of active site metal cofactors. The active-site Cys-residues of Zn^{2+}-dependent enzymes are mostly replaced by aspartic acid residues [26]. For several of these Zn^{2+}-independent enzymes baseline catalytic activity has been shown to be independent of the presence of divalent metal ions at the active site, e.g. for the *P. aeruginosa* and *P. falciparum* enzymes [84, 66]. For other orthologs, like that of the soy been root α-proteobacterial endosymbiont *Bradyrhizobium japonicum*, *Pisum sativum* or the apicomplexan parasite *Toxoplasma gondii* a role for active site Mg^{2+} has been proposed. Biphasic Mg^{2+}-response curves and determination of binding stoichiometries measured for *B. japonicum* ALAD in the presence and absence of 5-ALA suggest binding of Mg^{2+} to different sites of the protein with different affinities [205]. Tightly binding Mg^{2+} was 5-ALA dependent and was considered to correspond to metal-binding sites in the active center, whereas the looser binding Mg^{2+} should correspond to the allosteric metal binding site (Me_c-site). Magnetic-resonance studies using ^{13}C-labeled porphobilinogen at characteristic Mg^{2+} or Mn^{2+} concentratons futher supported this conclusion [204]. Site-directed mutagenesis studies replacing the active site alanine and aspartic acid residues by cysteines induced the loss of Mg^{2+}-dependency and the introduction of Zn^{2+}-dependency to the previously Zn^{2+}-independent *B. japonicum* enzyme although enzymatic activity of the mutant was very low [45, 85]. Similar observations were made in site-directed mutagenesis studies inducing Zn^{2+}-dependency into the *P. aeruginosa* enzyme [85]. For the chlorplast protein from pea and the apicoplast protein from *T. gondii* evidence for the presence of catalytic Mg^{2+} in addition to allosteric Mg^{2+} was mainly derived by biphasic Mg^{2+}-response curves interpreted

as binding to different sites with different Mg^{2+}-binding affinities [148, 227]. In addition, atomic absorption spectroscopy revealed binding of up to 3 Mg^{2+} per subunit of the pea protein [148]. Regardless of the binding stoichiometries, it might be considered that the two phases of the Mg^{2+} response curves represent binding to the same (allosteric) binding site in different subpopulations of the oligomeric equilibrium (characteristic for the morpheein) with distinct affinities rather than to two different binding sites. Finally, the presence of catalytic Mg^{2+}-ions at the active site of any Zn^{2+}-independent orthologs remain undocumented by crystal structures and thus without final experimental proof, whereas the allosteric Mg_C ion is documented by a number of crystal structures [83, 138].

Furthermore, monovalent ions like K^+ have been reported to activate certain ALAD orthologs and increase the protein's affinity for Mg^{2+}, as demonstrated for *B. japonicum* [205], *P. aeruginosa* [84], *V. cholerae* and *Y. enterocolitica* (Eileen K. Jaffe, personal communication). In the active site of the *P. aeruginosa* ortholog a monovalent cation (Na^+) has been identified in a crystal structure, indicating that monovalent cations, though being differentially coordinated, might fulfil the function of catalytic Zn^{2+} in Zn-$^{2+}$-dependent proteins [86].

4.4.3 Mg^{2+}-usage of wALAD

Which role does Mg^{2+} play in the activation of the *Wolbachia* protein? The answer is not trivial and remains evidence-based and thus equivocal in the absence of a crystal structure that might document the metal cofactor usage. The evidence we have is the following: All orthologs for which a catalytic Mg^{2+} is considered also possess the allosteric Mg_C site and show a biphasic Mg^{2+}-response curve. *Wolbachia* ALAD gives a monophasic response to Mg^{2+}. Although a second binding site may be hidden in the progression of a monophasic response curve, if the resolution is not sufficiently high, the uniform rightward shifts of the Mg^{2+}-response curve elicited by wALADin1 gave no evidence for a second binding site. However, it is unlikely that the inhibitor has a quantitatively equivalent competitive effect with respect to two different Mg^{2+} binding sites at the same time. It is therefore concluded that the activation of wALAD is only driven by binding of Mg^{2+} to one site.

In all ALAD orthologs that possess the allosteric Mg_c site, i.e. they possess the conserved glutamic acid residue (Glu_{245} of P. aeruginosa ALAD [83]), the allosteric stimulation may be monitored as an increase in enzymatic activity although the extent of this allosteric stimulation varies between species [84, 131, 66]. The corresponding glutamate residue is also conserved in the structure of *Wolbachia* ALAD. On the basis of this experimental evidence and the still ambiguous proof for the presence of catalytic Mg^{2+}, it is assumed that stimulation of wALAD by Mg^{2+} is due to the allosteric activation by binding to the conserved Mg_C site. A rather unusual effect for allosteric stimulation by Mg_C is the relatively high affinity (EC_{50} ~11 μM) observed in this study. For the pea protein dissociation constants of ~35 μM for the putative catalytic Mg^{2+} and 2.6 mM for the putative allosteric Mg_C were predicted [148]. Interestingly, in the present study a monophasic progression was observed even for the pea protein, with an EC_{50} of ~257 μM which is in-between dissociation constants reported in the literature, under the assay conditions used, presumably reflecting allosteric Mg^{2+}. Importantly, again the curve shift induced by wALADin1 was homogenous and did not reveal a biphasic nature. For the *T. gondii* protein two distinct Mg^{2+} ions have been proposed with a dramatically higher affinity to both ions with K_D values of ~0.7 μM and 84 μM, respectively, for the presumed catalytic and allosteric sites [227]. Although the oberved affinity of wALAD to Mg^{2+} is rather in the range of presumed catalytic ions, in light of the large variations in affinity for the allosteric ions in *P. sativum* and *T. gondii*, tight binding of allosteric Mg^{2+} in wALAD is conceivable. On this background, it may not be completely ruled out that

active site/catalytic Mg^{2+} may be involved, unless the metal cofactor usage of this protein has unambiguously been determined. However, for the *P. aeruginosa* ALAD under the conditions tested in this study (pH 7.5, no KCl, low 5-ALA) wALADin1 acts as an inhibitor and leads to reduced affinity for Mg^{2+}. As this enzyme is independent of catalytic divalent metal ions, but features the allosteric Mg^{2+} [84], it is evident that the inhibitory mechanism involves functional competition with the common Mg^{2+}-induced allosteric activation mechanism. Therefore, these data strongly suggest that the Mg^{2+}-interfering effect on wALAD and PsALAD are related to the allosteric Mg^{2+}.

4.4.4 The inhibitory mechanism of wALADin1 discussed at the structural level

With respect to the observed inhibitory mechanism of wALADin1 several possibilities exist. wALADin1 may antagonize binding of Mg^{2+} at an allosteric Mg_C-site or a catalytic Mg_B-site. Alternatively, it may bind to a different site in the protein and interfere with the allosteric activation process induced by Mg_C acting as a negative allosteric modulator itself. Thus, it may interrupt closure of the active site lid, a structural requirement for catalysis that is allosterically regulated by Mg_C in the *P. aeruginosa* enzyme [83].

wALADin1 is an inhibitor with a mixed substrate-competitive and non-competitive inhbitory mechanism. This means that, although 5-ALA is not able to overcome inhbition by wALADin1, 5-ALA binding reduces the affinity of the protein for the inhibitor. It is therfore unlikely that wALADin1 acts as a binding competitor of allosteric Mg_C as it is not evident how this effect might be influenced by binding of 5-ALA to the remote active site. Competition with a putative catalytic Mg_B at the active site itself is still conceivable. The allosteric scenario may also be united with the observed inhibitory mechanism, because the conformation of the active site lid is governed both by the allosteric Mg_C and by binding of A-side 5-ALA to the active site, which represents the final trigger for closure of the lid [134]. Thus, both Mg_C and A-side 5-ALA would be in favor the catalytically active conformation, while wALADin1 may induce an alternative catalytically inactive conformation.

4.4.5 Mechanistic aspects of the stimulatory/inhibitory dichotomy of wALADin1

While wALADin1 is a similarly potent inhibitor of both *Wolbachia* and *P. sativum* ALAD and nearly inactive against the Mg^{2+}-independent human ortholog, wALADin1 had a surprising effect on the enzymatic activity of ALAD from *P. aeruginosa*, *E. coli*, *V. cholereae* and *Y. enterocolitica*. For these orthologs that all feature the allosteric Mg_C-site but different requirements for catalytic metal ions, wALADin1 had a stimulatory effect, while for *P. aeruginosa* ALAD the stimulatory effect could be turned towards inhibition under certain conditions.

One mechanism that might account for the stimulatory properties of wALADin1 would be stabilization of the octameric assembly and thus a shift of the oligomeric equilibrium towards the active form resulting in increased enzymatic activity. However, effects on the oligomeric equilibrium are hysteretic processes that require longer preincubation times at elevated temperatures in order to promote dissociation of preformed assemblies [246, 135, 161]. Such conditions were not used for the conducted enzymatic assays with only 5 min preincubation at room temperature before the enzymatic reaction occurred for 10 min at 36 °C. Although a stimulatory effect of wALADin1 via the oligomeric equilibrium may not be ruled out, another mechanism that supports an allosteric effector model for wALADin1 is more likely.

Under the assumption that the binding site of wALADin1 is the same in these orthologs as for wALAD, these stimulatory effects are hard to reconcile with a model of wALADin1 binding to the active site. Instead, an allosteric model may well explain these results. wALADin1 may bind to structural features involved in the allosteric activation by Mg_C (a common feature for all orthologs at which wALADin1 shows considerable biological activity) such as the active site lid. As an allosteric modulator, in some orthologs wALADin1 may act agonistically with the allosteric activation process by Mg_C causing stimulation, while in others it may antagonize this effect, depending on different molecular architectures of the wALADin binding site and other structural features involved in the allosteric process.

Intriguingly, it was found that the inhibitory/stimulatory dichotomy may apply even for a single protein, as seen for the *P. aeruginosa* ortholog where the buffer conditions that influence enzymatic activity and determine the overall protein conformation (pH, monovalent cations, substrate concentration) drive modulation by wALADin1 towards stimulation or inhibition. Furthermore, monovalent cations, divalent cations and substrate concentration determine sensitivity of the protein for modulation by wALADin1. As such, depending on the physiological pH, cytosolic ion concentrations and other interaction partners of ALAD that might exist in the cell, wALADin1 may act both agonistically or antagonistically on *P. aeruginosa* ALAD in the bacterium *in vivo*. The complexity of the underlying events is especially evident for the interplay of substrate and wALADin1 under inhibitory conditions, where wALADin1 consistently reduced affinity (K_M) of pALAD for the substrate, while V_{max} is reduced at low concentrations of inhibitor but starts to increase at high concentrations of inhibitor where increased V_{max}-values may lead to overall stimulation although affinity to the substrate is decreased. This scenario may be explained by multiple and functionally different binding sites for 5-ALA and/or wALADin1. As binding of both A-side and P-side 5-ALA is required for catalytic activity, it is unlikely that these two sites account for this outcome. Instead, the observed effects may be correlated to the oligomeric nature of the protein and the phenomenon of half-sites reactivity: This term is used to describe that in the four asymmetric dimers that assemble into the octamer, the two monomers are functionally different (asymmetric) and only one of these contained 5-ALA bound to the active site and a closed active site lid in the *P. aeruginosa* ALAD crystal structure [83]. Thus, half of the active sites in the octamer are assumed to be in an "active" conformation while the complementary four subunits populate an "inactive" state. It is thus conceivable that, in addition to the primary effects occurring at the "active subunits" with high affinity, at high concentrations of wALADin1 and 5-ALA low-affinity binding sites present in the second type of subunit (putatively the inactive subunit) are filled with a contrasting functional outcome that may help explain the increase in V_{max} at high wALADin1 concentrations. Understanding the interplay of the different influence on protein structure, e.g. on the basis of a crystal structure, may help design tailored agonists or antagonists of *P. aeruginosa* ALAD and potentially other orthologs on the basis of the wALADin-modulators.

4.4.6 The inhibitory mechanism of wALADin2

Intriguingly, the tricyclic quinoline carboxylic acid derivative and potent wALAD inhibitor wALADin2 acts by a different mechanism. It is an entirely non-substrate-competitive inhibitor with an apparently more pronounced Mg^{2+}-competitive character. As this inhibitor was identified due to its structural similarity to wALADin1 and as it also involved functional competition with Mg^{2+}, it is assumed that these two inhibitors share a common binding site. However, the functional outcome of wALADin2 binding to the presumed binding site is different. These results suggest that the substrate-competitive component and the non-substrate competitive com-

ponent, which is presumably functional antagonization of activation by Mg^{2+}, may be separated on a structural basis. Interestingly, wALADin2 is even more specific for wALAD than wALADin1 is. The only other ortholog which it inhibits is the chloroplast protein from *P. sativum*, although with an ∼10-fold reduced potency. In contrast, it neither led to stimulation of the enzymatic activity of those orthologs stimulated by wALADin1, nor did it induce any background inhibition of hALAD. The following considerations can be made with regard to the inhibitory mechansim. Although wALADin2 only inhibited the *Wolbachia* protein where Mg^{2+} usage is unclear and the pea ortholog, for which a role for catalytic Mg^{2+} has been suggested [148], it appears rather unlikely that this inhibitor targets the active site and competes with catalytic Mg^{2+}. If present, catalytic Mg^{2+} is considered to be required for the recruitment of A-side 5-ALA to the active site, replacing the function of Cys-coordinated Zn_B of Zn^{2+}-dependent orthologs. As any catalytic Mg^{2+} and A-side 5-ALA would need to be functionally and spatially tightly linked, it appears very unlikely that an inhibitor like wALADin2 targets the active site, undergoing a competition with catalytic Mg^{2+}, and is *not* influenced by 5-ALA at the same time. Thus, interference with allosteric activation by Mg_C seems likely.

4.4.7 SAR of benzimidazole derivatives

Activity testing of a variety of benzimidazole-based wALADin1 derivatives revealed several important features in the interplay of structure and function. An absolute requirement for inhibitory activity was the carboxylate function at the R_3 position. This residue may be involved in salt-bridge formation at the molecular binding site, e.g. with a lysine or arginine residue.

Changes in the chemical structure of the R_1 group, which conveys optimal potency as the 3-trifluoromethyl benzyl in wALADin1, leads also to pronounced reductions in inhibitory potency (**Fig. 3.15**). The benzyl ring appears indispensible even for weak inhibitory activity of the *Wolbachia* ortholog, while the R_1-H derivative **2** still has considerable inhibitory potency for the pea protein. In both cases, position and identity of further substituents at the R_1 benzyl moiety are major determinants of inhibitory potency. The introduction of fluorines from -CH_3 to -CF_3 involves a major gain in potency (∼10-fold) that may result from increased lipophilicity, increased size or altered electronic effects [102, 183] to name a few possible effects.

The R_2-2-[(2-thienylcarbonyl)amino]ethyl substitutent of wALADin1 was apparently dispensible for inhibition of wALAD as its exchange to -H (in **3**) had nearly no effect on inhibitory potency. However, on the basis of a different parent molecule, the same subsitutent was responsible for the $>$ 2-fold increased potency of **9** over **10**. Of note, for the *P.sativum* ALAD wALADin1 had greater inhibitory potency than **3**, while **9** and **10** had similar activities. This indicates that R_2 should not be simply neglected, but that substituents at this position may contribute additional potency to the parent molecule. It is conceivable that substituents other than 2-[(2-thienylcarbonyl)amino]ethyl may confer additional potency even to the wALADin1-scaffold. Another important aspect of R_2 is its role as a mediator of species-selectivity. For the human ortholog the bulky 2-[(2-thienylcarbonyl)amino]ethyl substitutent represents a major impediment for inhibitory activity, e.g. by imposing a steric hindrance, while most smaller R_2-H compounds (including **3**) show weak to intermediate inhibitory activity and some molecules even display an inhibitory preference for the human enzyme over the *Wolbachia* enzyme. Intriguingly, for those orthologs at which wALADin1 acts stimulatory, the R_2 2-[(2-thienylcarbonyl)amino]ethyl is an absolute requirement. This structural feature is common to all stimulatory active derivatives (wALADin1, **6**, **7**, **9**) and its absence leads to a loss of activity (**3**, **10**). The fact that the only

bioactive compounds are all constitutional isomers varying in the position of the -COOH or -CF_3 position indicates a rather strict molecular binding corset.

Summarizing the role of the R_2-2-[(2-thienylcarbonyl)amino]ethyl for biological activity can be described as follows. It prevents inhibition of hALAD and is structurally required for activity at orthologs stimulated by wALADin1 while it is of minor importance for *Wolbachia*/pea ALAD. This substituent represents a key determinant of biological activity and specificity across different members of the ALAD family.

4.4.8 ALAD-inhibitors based on a different molecular scaffold

The benzimidazole scaffold of wALADin1 (**Fig. 3.15**) is not the only chemical scaffold which allows the building of ALAD inhibitors with wALADin-like properties. Such inhibitors had been detected by functional screening in the wALAD assay, after molecules with chemical similarity to wALADin1 had been selected. Besides providing a broader chemical foundation for the design of improved inhibitors in the future, these molecules may also contribute to the identification of structural features of functional importance. The other scaffolds identified included substituted 1,3-dihydro-2H-benzimidazol-2-one, phenylthiophene carboxylic acid and tricyclic quinoline derivatives (**Fig. 3.21**). For the 1,3-dihydro-2H-benzimidazol-2-one compounds, presence of an ionizable group was a selection criterion. However, all inhibitory compounds of these classes feature a carboxylic acid group while the only quinoline derivative without was inactive. This finding highlights again the functional importance of this moiety as discussed above for the benzimidazole derivatives.

The 1,3-dihydro-2H-benzimidazol-2-one derivatives do not incorporate an R_2 substituent at the C_2 atom of the benzimidazole ring that carries the carbonyl moiety, but they feature another substituent at the N_3 atom (in the following termed R_4) with a spatially similar orientation as the R_2 of wALADin1. As R_2 was demonstrated to be a major determinant of specificity it is intriguing that varying R_4 substituents determine the specificity profile of the 1,3-dihydro-2H-benzimidazol-2-one compounds although these compounds all had at best intermediate potency. Yet, it must be considered that the loss or aromaticity in one of the core rings of these compounds introduces a lack of planarity, which will also have an impact on spatial projections of the substituents.

The small R_2-H compounds are the only inhibitors well tolerated by the human ortholog. It is therfore a remarkable coincidence that the small phenylthiophene structures are the most potent inhibitors of hALAD identified in these studies with IC_{50} values between 80 and 100 μM. These compounds also inhibited wALAD but with somewhat lower potency. Finally, the class of tricyclic quinoline derivatives has to be mentioned again, of which the already discussed inhibitor wALADin2 was the only active member, indicating a very steep structure-activity profile for this exciting chemotype.

4.4.9 Summarizing the functional characterization of wALADin inhibitors at the molecular level

The current study has identified a novel class of benzimidazole-based inhibitors of ALAD of *Wolbachia* with a species-selective inhibitory profile. It is suggested that wALADin1, the most potent benzimidazole inhibitor, acts as an allosteric modulator that may cause inhibition or stimulation of ALAD activity in different species depending on the molecular context. Inhibition consists of a substrate-competitive component and a non-competitive component which is considered to be equivalent

with a functional competition with (a putatively allosteric) Mg^{2+} ion. wALADin1 (as well as **3**) involves both inhibitory components, while the tricyclic quinoline derivative wALADin2 only acts exclusively by functional competition with Mg^{2+} and shows improved specificity. The potency of wALADin2 is independent of the substrate concentration, whereas the potency of wALADin1 is high at low 5-ALA concentrations, but decreases upon accumulation of 5-ALA or at high initial 5-ALA concentrations. Thus, biological activity of these two inhibitors in the physiological environment is expected to be different and both compounds may complement one another. Further structural components have been identified as determinants of inhibitory potency and specificity. Finally wALADin-like inhibitors based on other chemotypes have been discovered.

These novel inhibitors mark a significant advancement in the search for species-selective ALAD inhibitors of potential therapeutic utility. The profound characterization of structural and functional aspects of benzimimdazoles and other chemotypes along with their inhibitory mechanisms provides the foundation for the design of improved inhibitors with desired nanomolar inhibitory potency and tailored biological activity.

4.5 The antifilarial effect of wALADins

Beyond being an efficient inhibitor of the *Wolbachia* ALAD *in vitro*, this study demonstrates that wALADin1 also has pronounced antifilarial activity in an *ex vivo* survival assay employing the *Wolbachia*-harboring rodent filarial nematode *Litomosoides sigmodontis*. *L. sigmodontis* worms exposed to wALADin1 at concentrations from 125 - 500 μM displayed continuously reduced motility and temporarily a specific ball-like low-motility phenotype. Viability measurements revealed an EC_{50} concentration of $\sim$100 μM and demonstrate that wALADin1 kills *L. sigmodontis*, i.e. has macrofilaricidal activity. The specificity of this effect was confirmed by parallel tests on *Wolbachia*-free filaria *Acanthocheilonema viteae*, on which wALADin1 had only slight effects. Exposure to wALADin1 had evidently no effect on viability of *A. viteae* in the MTT assay which is the most reliable readout for the documentation of antifilarial effects. However, at the highest concentration tested, motility of *A. viteae* was immediately reduced by 1 motility score unit within 2 h of exposure, but motility did not decline further for the following 10 days. These studies revealed that the filaricidal effect of wALADin1 on *L. sigmodontis* is dependent on *Wolbachia* and is presumably due to an inhibition of ALAD within the endobacteria, followed by deprivation of heme and/or 5-ALA toxicity. Nevertheless, a secondary non-specific effector component was dissected causing the non-specific decline of *A. viteae* motility at 500 μM. This activity likely acts in addition or in synergy to the specific *Wolbachia*-dependent activity on *L. sigmodontis*. This non-specific activity may be correlated to the observed cytotoxic effects of wALADin1 in eukaryotic cell culture at concentrations $\geq$ 500 μM.

wALADin derivative **6** is a significantly less potent inhibitor of wALAD that showed no cytotoxicity below 1 mM. This compound (at 500 μM) still showed considerable though less pronounced antifilarial effects with a rapid onset comparable to the non-specific effect wALADin1 had on *A. viteae*. Although viability was affected, the characteristic ball-like phenotye was not observed. It is therefore likely that the biological activity of this compound is mostly derived from activity on a secondary target. Compound **3**, an equally potent inhibitor of wALAD as wALADin1 which had no cytotoxic activity at these concentrations, although it showed reduced species-selectivity of $\sim$15-fold, revealed contrasting biological activity. Onset of the antifilarial effect was delayed compared to wALADin1, but it became evident in reduced motility values for all concentrations tested reaching motility scores of 3-4

at the end of treatment that were similar those achieved by wALADin1. Importantly *L. sigmodontis* worms exposed to **3** also featured the ball-like appearance characteristic for wALADin1-treated worms. Viability was significantly reduced by 64% only for the highest concentrations although the trend was sustained also for the lower concentrations. Although the antifilarial effect of **3** was quantitatively weaker than that of wALADin1, it displayed a very similar phenotype. In **3**, the entire R_2 substituent of wALADin1, which comprises about one third of the entire molecule, is missing. Despite this chemical modification, **3** has obviously retained the wALAD-inhibitory potency, but it may easily have lost activity on putative secondary targets with unique strucure-activity profiles of their own. Hence **3** might display a more ALAD-specific biological profile. It may be expected that it takes a while until the inhibition of ALAD (especially when not complete) translates into heme-deficiency, depending on the turnover rates of preformed heme in the worm, and becomes evident in reduced fitness of the worm. Also accumulation of toxic 5-ALA levels may not occur immediately. Therefore, the antifilarial effect elicited by **3** may be a more specific result of interference with endobacterial heme biosynthesis than the stronger and more rapid effect of wALADin1, that at least at 500 μM likely represents an overlap of activity at ALAD and at a secondary target.

Taken together, the pronounced antifilarial acitivity of wALADin1 and **3**, the most potent benzimidazole inhibitors of wALAD, and the *Wolbachia*-dependent activity of wALADin1 reveal that the specific heme-biosynthesis inhibitors of the wALADin benzimidazole family are a promising novel class of antifilarial agents.

4.5.1 Potential secondary target effects

Potential secondary targets of wALADin1 in *Wolbachia* or the nematode may be deduced from known targets of chemically related molecules. The most closely related class of bioactive benzimidaziole structures has been reported to target the human kinesin spindle protein (KSP or *Hs* Eg5) [157, 228]. As inhibition of this protein leads to a misassembly of the mitotic spindle and cell cycle arrest followed by the death of cancer cells, it is an attractive target for the development of anticancer drugs. The recently reported class of hKSP-inhibitors were 2-aminobenzimidazoles with further substituents at the amino group and at benzimidazole atoms N_1 and C_5, equivalent to the R_1 and R_3 substituents of wALADin1-benzimidazoles (**Fig. 4.2**). Although these inhibitors have tolerated a carboxyl group at the R_1 position (as required by wALADins for inhibitory activity), they had a preference for a primary amide at R_1. The R_2 residue of most KSP inhibitors is a 2-trifluoromethyl benzyl and is thus similar to the 3-trifluoromethyl benzyl of wALADin1. The largest structural difference is in the R_2 postion, where KSP inhibitors require an amino-linked aromatic substituent in order to be characterized as active in an *in vitro* assay system (IC_{50} values below 20 μM). Nevertheless, at the high concentrations used in the filarial co-culture assay wALADins may have an effect on filarial orthologs of this mitosis-releted protein.

The benzimidazole core of wALADins represents a structural link to classical benzimidazole anthelmintics like albendazole. These anhelmintics target the filarial β-tubulin and cause a destabilization of microtubules [156]. While the lack of a carboxylic acid function will prevent inhibitory activity of benzimidazole anhelmintics on wALAD (for albendazole this was even experimentally verified, although the data is not shown), nematode microtubules may be a secondary target of wALADin inhibitors. Most benzimidazoles like albendazole, flubendazole and mebendazole feature a carbamate moiety at the R_2 position and differ in their R_3 moieties although the active metabolites are often biotransformed molecules [89]. In case of albendazole, both albendazole and its *in vivo* metabolite albendazole sulfoxide target worm β-tubulin. Its other major metabolite albendazole sulfone has recently

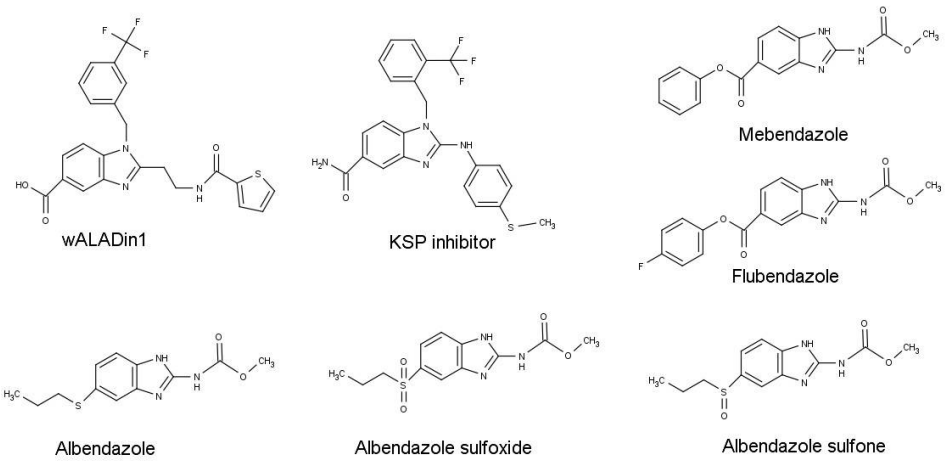

Figure 4.2: Chemical structures of selected benzimidazole compounds
The chemical structures of wALADin1, the KSP inhbitor with highest potency [228] and of selected benzimidazole anthelminthics including, mebendazole, flubendazole, albendazole and its metabolites albendazole sulfoxide and albendazole sulfone are shown.

been shown to have a bacteriostatic effect on *Wolbachia* proliferation in *B. malayi* and to disrupt binary fission [226]. It may not be ruled out that the *Wolbachia*-dependent activity of wALADin1 is based, at least in part, on this yet unidentified endobacterial benzimidazole target, although this scenario is highly speculative.

Besides testing of wALADin1 and derivatives in enzymatic assays for secondary target candidates, if available, comparative analysis of the filarial and *Wolbachia* phenotypes under exposure to wALADin1 and other chemical probes such as albendazole sulfone may help unravel secondary targets and effector pathways of wALADin1.

4.5.2 *In vivo* activity of wALADin1

The proof-of-principle experiments demonstrating the macrofilaricidal effects of wALADin1 and derivatives in the *ex vivo* co-culture system revealed that the *in vitro* ALAD-inhibitory activity of wALADin1 can be translated into an antifilarial effect in the living worms. However, providing the required high concentrations of > 100 μM in an *in vivo* infecion model of *L. sigmodontis* in BALB/c mice is not a trivial task. Despite continued administration of wALADin1 of up to 4 mg/mouse for up to four weeks, the use of different formulations and administration routes (intraperitoneal injections and intrathoracic injections to the site of infection) no antifilarial effect of wALADin1 treatment was observed. Treatmtent was tolerated well without evident signs of toxicity. Although it may not be ruled out that the filariae have access to host-derived heme sources in their physiologic environment [11] and thus be naturally resistant to inhibition of endobacterial heme biosynthesis, it is likely that the concentration of wALADin1 in the biophase is simply too low to reach a biological effect. Possible pharmacokinetic reasons are manifold, but determination of the pharmakokinetic profile and ADME parameters (adsorption, distribution, metabolization and excretion) of wALADin1 in the mouse were beyond the scope of the current study and represent a project of its own. In the mouse, wALADin1 may be rapidly metabolized and excreted or sequestered by promiscuous non-specifically binding proteins of the host such as serum albumin. For the benzimidazole anthelminthic albendazole the major pharmakokinetic handicap is poor absorption from the intestinal tract after oral administration [89]. This obstacle was

circumvented in the present study as wALADin1 was administered intraperitoneally or intrathoracically. However, in the human intestinal mucosa and the liver, albendazole is rapidly metabolized to albendazole sulfoxide, albendazole sulfone and several further metabolites [182]. Rapid hepatic and mucosal biotransformation has also been reported for other benzimidazole drugs, i.e. flubendazole in sheep [169]. Similar though non-analogous biotransformation of wALADin1 may occur in the mouse liver and yield non-inhibitory metabolites devoid of antifilarial activity. Pharmacokinetic shortcomings that prevent biologically active concentrations of a compound are, of course, structure bound. ADME properties are determined by defined chemical features and structural elements of a xenobiotic that e.g. represent contact points for biotransformation enzymes. In order to develop drug-like *Wolbachia* ALAD inhibitors with a potent antifilarial activity *in vivo* two considerations are imperative. First, inhibitory potency must be increased such that lower doses are sufficient to yield bioactive concentrations *in vivo*. Second, the pharmacokinetic profile must be enhanced, which may be achieved by the identification of inhibitors based on other chemical scaffolds that retain the biological activity. A first step towards the identification of such improved inhibitors has been undertaken and has led to the identification of the non-benzimidazole based inhibitor wALADin2, which has a slightly increased inhibitory potency and an improved specificity profile in the *in vitro* assay.

4.6 Applications of wALADin 1 beyond filarial nematodes

4.6.1 Inhibitory spectrum of wALADin and derivatives

Although the principal aim of this study was to develop specific inhbitors *Wolbachia* ALAD as antifilarial drug or lead candidates, the inactivity on the human Zn^{2+}-dependent ortholog and the Mg^{2+}-dependent inhibitory mechanism led to the consideration that wALADins might be universally applicable inhibitors specific for Mg^{2+}-dependent, respectively Mg^{2+}-stimulated orthologs. As most previously known inhibitors have no species-selective profile or exhibit higher activities on the mammalian enzymes [270, 227], it has not been possible to specifically target heme biosynthesis of any human pathogen without affecting the mammalian host. However, exploitation of microbial heme biosynthesis pathways as drug targets may now be possible by wALADin-like inhibitors. By determining the spectrum of ALAD orthologs from different species on which wALADin1 and derivatives act inhibitory or not, it was concluded for which species these wALADin-like inhibitors might represent potential therapeutics. Generally, ALAD enzymes were assigned into three groups according to whether they were X) insensitive to wALADin1, Y) inhibited by wALADin1, or Z) stimulated by wALADin1 (Naming the groups X,Y,Z shall prevent confusion with the classification of A-D introduced above). Each group had characteristic structural requirements of the benzimidazole compounds for the respective bioactivity.

As a prerequisite for any therapeutic use of wALADins, the human enzyme, representative of group X, is insensitive to inhibition by wALADin1. According to phylogenetic similarity, this may also apply for other metazoa and yeast. Thus, potential use of wALADin-like inhibitors is given in veterinary medicine, but they are not expected to be efficient antifungal agents.

For group Y ALAD enzymes, wALADins represent potent inhibitors and are of potential therapeutic use. This class comprised the *Wolbachia* and the chloroplast *P. sativum* protein. Potent inhibition of plant ALAD, a phylogenetically rather homogenous group [133], reveals that wALADins are potential herbicides in addition

to their prospective utility in antifilarial drug discovery. The *Wolbachia* ortholog was the only α-proteobacterial ortholog tested, however, in light of the close relationship of other intracellular human pathogens like *Rickettsia spp.*, *Bartonella spp.* and *Brucella spp.* [36]. Plant chloroplasts originate from primary symbiosis with a cyanobacterium [8]. Thus, susceptibility to wALADin1 of the chloroplast and α-proteobacterial ortholog may be an evolutionary coincidence or a feature conserved throughout evolution that dates back to a common ancestor.

ALAD orthologs that cluster in group Z are from diverse human pathogenic or opportunistic bacteria including *E. coli*, *P. aeruginosa*, *Y. enterocolitica* and *V. cholerae*. Although metal cofactor usage of these enzymes is highly variable (see above, **Section 4.4.2**), the allosteric Mg_C-site is found in all structures. Furthermore the parent species of these proteins are all γ-proteobacteria. Under the described experimental conditions wALADin1 led to a distinct stimulation of enzymatic activity. Although dysregulation of heme biosynthesis that involve increased porphobilinogen and porphyrin production may have a slight toxic effect, a drug-like use of wALADin stimulators does not appear as promising as for an inhibitory compound. However, as demonstrated for *P. aeruginosa* ALAD environmental factors may drive the wALADin-elicited modulation towards inhibition, maybe even in the physiological context. Future investigations will have to dissect the adequacy of modulating ALAD activity of these species as a potential antibiotic mechanism of action.

Although the current data are consistent with a classification based on taxonomy of the parent organisms (chloroplasts, cyanobacteria and α-proteobacteria vs. γ-proteobacteria) such a model would need to be corroborated by testing of further members of the different classes. However, as no obvious structural elements can be identified that are phylogenetically conserved in the different groups, the taxonomic model appears to be the best approximation for classification. Susceptibility may be best predicted by determining the phylogenetic distance to members of either group on a case-to-case basis and for those species with ALAD orthologs most closely related to either the chloroplast or *Wolbachia* proteins, wALADin-like inhibitors may be suitable herbicide and antibiotic candidates.

4.6.2 An introduction to malaria

Malaria tropica is a life-threatening infectious disease caused by the unicellular apicomplexan parasite *Plasmodium falciparum* that is transmitted by anopheles mosquitoes. Several other less severe forms of human malaria exist that are caused by other plasmodial species. While roughly half of the world's population is at risk of contracting malaria, for 2010, 216 million malaria episodes, predominantly in Africa and South-East Asia, and 655 000 malaria deaths (mostly in African children under the age of 5) have been estimated [266, 267].

Plasmodium sporozoites, the infectious stage transmitted through the mosquito salivary glands during the blood meal, infect human hepatocytes where the parasite multiplies extensively within a parasitophorous vacuole (liver schizont stage) and rupture of the infected hepatocytes finally leads to the release of thousands of merozoites. These extracellular forms of the parasite then invade erythrocytes where they are referred to as trophozoites. The following, repetitively occuring blood stage cycle involves intraerythrocytic division rounds and rupture of blood stage schizonts releasing more erythrocyte-infecting merozoites as well as male and female gametocytes required for sexual reproduction in the mosquito vector [100].

Sequestration of *P. falciparum* infected red blood cells to the endothelium of the brain microvasculature may trigger neural pathogenesis culminating in potentially fatal cerebral malaria [179]. Further symptoms of severe malaria are hyperthermia, severe anemia, respiratory-distress and multi-organ failure [100]. In the absence of

an efficient malaria vaccine, malaria prevention programs mostly rely on exposition and vector control [266, 267]. A variety of antimalarial drugs exists for chemoprophylaxis and chemotherapy, however the rapid development of resistance of the most virulent malarial parasite *P. falciparum* to curent drugs requires a continuous expansion of the antimalarial drug portfolio [64]. Drugs targeting the liver stage parasites and gametocytes are sparse.

4.6.3 ALAD and heme biosynthesis as a potential drug target in apicomplexan parasites

Apicoplast-derived ALAD has been suggested as a potential drug target for two human pathogenic unicellular parasitic protists, *P. falciparum* [66] and *T. gondii* [227] that cause malaria and toxoplasmosis, respectively. The apicoplast is a non-photosynthetic relict plastid that has been acquired by an ancestor of the apicomplexan parasite via secondary endosymbiosis of a red alga [171]. Thus, the apicoplast stands in evolutionary relationship with the primary plastids (chloroplasts) of plants and algae, with the photosynthetic red alga *Chromera velia* as the living missing link [185, 139]. The biological function of the apicoplast is uncertain. It was shown that *T. gondii* parasites do not die immediately upon depletion of the apicoplast, but upon invasion of new cells [105] highlighting the general importance of the apicoplast for the parasite. Apicoplast-derived isopentenyl pyrophosphate, a product of isoprenoid biosynthesis and precursor of vital biomolecules such as heme and dolichols, is required for survival of blood stage *P. falciparum* [140]. However, at this life stage and under experimental conditions, the apicoplast was shown to be dispensible when exogenous isopentenyl pyrophosphate was provided [272]. Yet, the apicoplast may have further biological functions in other life stages of the parasite and drug-induced clearance or functional deficiency of the apicoplast may affect blood stage plasmodia by preventing isoprenoid biosynthesis in the apicoplast. Due to its essential and unique biological function and prokaryotic origin the apicoplast is considered a promising antimalarial drug target [78, 210, 33].

In 1992, Surolia and Padmanaban discovered that *P. falciparum* is able to synthesize heme *de novo* although the parasite is flooded with host-hemoglobin-derived heme that the parasite has to detoxify by polymerization to hemozoin [242]. The authors further revealed that inhbition of parasite heme biosynthesis by succinyl acetone leads to reduced viability of the parasites thereby validating plasmodial heme biosynthesis as a target pathway for antimalarial drug discovery. Although it was then reported that blood stage *P. falciparum* can import host-ALAD from the parasitized red blood cell [28], further studies revealed an active plasmodial ALAD ortholog is encoded in the *P. falciparum* genome [222]. Finally, it was unravelled that the plasmodial ALAD is targeted to the apicoplast and that apicoplast-derived heme-biosynthesis constitutes only ∼10% of total ALAD acitivity in the parasite [66]. Hence, it is speculated that heme-biosynthesis in the apicoplast may provide porphyrins exclusively for the plastid. Dhanasekaran et al. recombinantly expressed ALAD from the malarial parasite that showed low activity and was independent of any metal ions, but allosteric activation through Mg^{2+} could confer additional ∼20 - 30% of catalytic activity [66]. An active ALAD ortholog has also been expressed from *T. gondii* which is presumed to require both catalytic and allosteric Mg^{2+} for optimal activity and inhibition of *T.gondii ALAD* by succinyl acetone induced death of the parasites [227, 138]. Thus, species-specific inhibition of apicomplexan ALAD enzymes in the apicoplast could be a promising strategy in the design of novel drugs to cure the diseases caused by these parasites.

4.6.4 Potent Antiplasmodial activity *in vitro*

In the absence of the recombinant enzymes for enzymatic inhibition tests, potential inhibitory effects of wALADins were tested in cell culture systems that measured the proliferation of blood stage *P. falciparum* in erythrocytes and *T. gondii* in LLC-MK2 cells. Three wALADin benzimidazoles (wALADin1, **6** and **9**) showed antiplasmodial activity in the blood stage culture system with IC_{50} values in the low μM range between 7 and 40 μM. From a structural perspective, antiplasmodial activity required the presence of the R_2-2-[(2-thienylcarbonyl)amino]ethyl side chain and tolerated minor changes in the positioning of the R_3-COOH and the CF_3 at the R_1-benzyl substituent. All further modifications abrogated activity against blood stage *P. falciparum*, a finding that indicates a clear structure-activity profile underlying these antiplasmodial effects. Of note, the R_3-COOH consitutional isomer **6** killed the malarial parasites with the greatest potency (IC_{50} $\sim$7.7 μM) and also had the steepest progression of the dose-response curve, which is likely due to an additive or synergistic effect of activities on different targets in the parasites.

For wALADin1 and **6** no such inhibitory effect was observed on replication of *T. gondii* tachyzoites, revealing that the antiprotozoal activity of the mentioned wALADins was specific for the malarial parasites.

Parallel to the present study, recombinant expression of the *T. gondii* and *P. falciparum* ALAD orthologs and characterization of the inhibitory properties of wALADins was carried out by Silke Strassel in her diploma thesis at our institute [240]. That study revealed that the *T. gondii* enzyme is weakly stimulated by wALADin1, while the *P. falciparum* enzym is inhibited at concentrations equivalent to those required for weak inhibition of the insensitive human enzyme. These concentrations are 1-2 magnitudes higher than IC_{50} concentrations measured in the trophozoite culture system [240]. Thus the antimalarial acitivity of wALADin1, **6** and **9** may not be explained by inhibition of heme biosynthesis in the apicoplast, but are expected to be derived from activity at other targets instead. These targets might be homologs of β-tubulin/microtubules and kinesin spindle protein as discussed as potential secondary targets for the filariae. Biological activity has been demonstrated for benzimidazoles targeting β-tubulin for other protozoan parasites like *Trichomonas vaginalis* and *Giardia lamblia* [145].

Although activity of wALADins on *P. falciparum* are apparently not a result of inhibition of heme biosynthesis, the potent antimalarial activity puts these compounds in line for the development of urgently needed novel drugs against malaria. Elucidation of the molecular targets of wALADins in *P. falciparum* is an important goal of future research as it may unravel new attractive options for antimalarial chemotherapy and help optimize antimalarial activity of wALADins. Finally, it will help to elucidate the global biological profile of the novel class of wALADin benzimidazoles.

4.7 wALADin inhibitors in light of current trends in drug development

The 20^{th} century experienced a pharmaceutical and clinical success story in the advent of antiinfective drugs from antibiotics over antimalarials to anthelminthics and many prematurely declared victory in the combat against infectious diseases. Although being true also for other antiinfectives such as anthelminthics [141], two important trends are menacing the achievements of this golden age that are most evident for antibiotics: 1) There is rapid emergence of multi-drug resistant pathogens (like meticillin- and vancomycin resistant *Staphylococcus aureus* and multi-drug resistant gram negative bugs) causing increasing numbers of fatalities. 2) In contrast,

numbers of novel antibiotics introduced to the market have been constantly decreasing over the last 30 years involving very few true innovations, i.e. novel mechanisms of action [79, 34]. It was recently shown that antibiotic resistance mechanisms including those conferring resistance to β-lactamases, tetracyclines or vancomycin are ancient and date back more than 30,000 years [58]. It is therefore considered that the upcoming clinical use of natural product-derived antibiotics rapidly selected for the presence and transfer of preformed resistance genes [269]. As most "new" drugs represent enhancements of existing drugs with existing resistance mechanisms, resistance development is inherent and only a matter of time. However, even for entirely synthetic drugs like oxazolidinones (linezolid, besides the lipopeptides and mutilins the only new classes of marketed antibiotic since 1962!) resistance has developed [97]. Genomics-based broad-spectrum antibiotic discovery strategies pursued by the pharmaceutical industry focussed mostly on single-target-based screenings of synthetic combinatorial chemistry libraries and were abandoned as fruitless. Most compounds, although being highly potent inhibitors of their target enzymes *in vitro*, did not enter the bacteria, were shuttled out or targets proved to be functionally redundant [200]. Also for malaria, drug and resistance developement represent an arms race [220] and there is a pressing need to identify and to further characterize known bioactive compounds [87] and feed them into the drug development pipeline. Within the field of anthelmintic drug discovery, since the introduction of macrocyclic lactones (ivermectin) to the market in 1981 [44] and, of less importance, cyclooctadepsipeptides in the 1990's [103], the most important innovation has been the repurposing of tetracycline antibiotics for depletion of *Wolbachia* endosymbionts from filarial worms [118]. However, no truly novel drugs were registered as anthelmintics in the last 20 years, although single, recently discovered candidate drugs currently hold promise such as amino-acetonitrile derivatives (monepantel) [143].

All subdisciplines of infectious disease research share the need for major innovations in order to enable discovery of mechanistically novel or chemically improved drugs that are able to circumvent conventional resistance mechanisms, e.g. directly targeting mediators of resistance like efflux pumps [196] or using drug combinations and drug adjuvants [234, 250]. The use of synergistic drug combinations may affect different functional nodes in biological systems (such as microbes) with tremendous downstream biological (i.e. antimicrobial) effects although single targets are not necessarily completely inhibited [273, 216]. While highly specific single-target inhibitors were long believed to be the ideal drugs, a paradigm-shift is ongoing advocating the benefits of "dirty drugs" that affect multiple targets to target complex diseases and pathogenic organisms [57, 187, 126]. Besides increased efficiency a major advantage of promiscuous drugs (or drug combinations) is that resistance development is impeded, as single amino acid mutations in one target are no longer sufficient to confer resistance. Therefore the understanding of drug interaction networks and drug polypharmacology may contribute essentially to the design of efficient future drugs [126]. Concurring with this paradigm certain promiscuity is also evident for registered antifiarial agents. Although the above mentioned primary molecular targets had been defined for antifilarial drugs like ivermectin and albendazole, for ivermectin several lower potency targets are known [123] and for albendazole an important secondary effect on *Wolbachia in vitro* has recently been reported [226].

The current study may bring inovation into the field of antiinfective drug discovery based on its target pathway and the inhibitory chemotype. Pathogen-specific targeting of heme biosynthesis by wALADin inhibitors represents an unprecedented approach in antiinfectective drug discovery. Since the ALAD-targeting antibiotic Alaremycin is produced by *Streptomyces spp.* [13, 108], ALAD has apparently evolved as a suitable antimicrobial drug target in nature which indicates that targeting the heme biosynthesis pathway is a promising antimicrobial strategy.

The biological effects of wALADin1, *Wolbachia*-dependency of the antifilarial effect of wALADin1 and its antiplasmodial activity, indicate succesful cellular uptake of the drug by the endobacteria and *P. falciparum*. The effect on *P. falciparum* is apparently not ALAD-dependent and secondary targets are discussed above for filarial nematodes (**Section 4.5.1**). By the use of activity-based chemical probes derived from the wALADin1-scaffold these targets may be pulled down using bioorthogonal chemistry and identified by mass-spectrometric analysis [24, 106]. Alternatively, chemical similarity approaches may be applied to predict secondary targets [147]. An understanding of the different biological effector pathways as well as identification of secondary molecular targets and the corresponding strucure-activity relationships may enable the design of efficient multi-target drugs. Given the obvious chemical similarity to benzimidazole anthelminthics a tempting approach would be the design of an antifilarial "wALADinazole" drug that combines ALAD-dependent activity of wALADin1 and the β-tubulin-dependent activity of albendazole.

Notwithstanding potential secondary target effects, improvement of the inhibitory potency on wALAD is a prerequisite for any potential wALADin-like drug lead candidate. Determination of a co-crystal structure of wALAD and wALADin1 and identification of the binding site would greatly facilitate this enterprise. However, crystallization of both wALAD and pea ALAD are difficult, as no crystal structure of either ortholog has been published. Although the presence of wALADin1 during co-crystallization of wALAD or pea ALAD may be beneficial, a shortcut may be taken by using X-ray crystallography to determine the binding mode of wALADin1 on a group Z ALAD ortholog which is stimulated by wALADin1. For several group Z ALAD orthologs, e.g. *P. aeruginosa* [83] or *E. coli* [71], crystallization has already been done successfully and should also be feasible in combination with wALADin1. Subsequent homology modelling may then yield the desired approximation for the endobacterial ortholog. In conjunction with the wealth of SAR-data presented in this study, knowledge of the molecular binding site will provide a powerful framework for the design of tailored drug-like inhibitors with improved potency and pharmakokinetic properties.

Chapter 5

Summary

Filarial nematodes are the causative agents of vector-borne diseases known as lymphatic filariasis and onchocerciasis. More than 150 million inhabitants of endemic tropical and subtropical countries are infected and may develop severe and chronic pathologies such as lymphedema, hydrocele or river blindness. While prolonged mass drug administration programs with annual treatment rounds are underway to block the transmission of larval stages, adult worms persist in the mammalian host for years. Thus, resistance development against the mainstay of antifilarial chemotherapy, i.e. ivermectin and diethylcarbamazine, poses a serious threat to the desired containment of filarial diseases which calls for the discovery of novel, preferentially adulticidal, drugs to cure and eradicate these diseases.

A prominent target for the development of antifilarial drugs are *Wolbachia* endobacteria, as depletion of the endosymbiont by antibiotic treatment leads to sterilisation and death of adult worms. However, the regimens of currently available antibiotic therapies are not compatible with mass drug administration programs. Annotation of the genome of *B. malayi*, a causative agent of lymphatic filariasis, and its endosymbiont, have revealed a variety of essential endobacterial biochemical pathways that may be exploited as antifilarial drug targets. The current study pursued a target-based drug discovery strategy aimed at the discovery of novel inhibitors of two enzymatic targets of *Wolbachia*: One is the glycolytic/gluconeogenetic enzyme pyruvate phosphate dikinase (PPDK) that catalyzes the reversible conversion of phosphoenol pyruvate to pyruvate. The other is δ-aminolevulinic acid dehydratase (ALAD) which converts 5-aminolevulinic acid to porphobilinogen as the first common step of heme biosynthesis. PPDK is only found in bacteria, protozoa and plants and is thus also a potential target for more broadly-applicable antibiotics. For ALAD, a human ortholog exists (hALAD) that is, however, phylogenetically different from the endobacterial enzyme (wALAD) and depends on Zn^{2+} for catalytic activity, while wALAD requires Mg^{2+}. Exploitation of these distinct metal-dependent catalytic and allosteric mechanisms must be adressed in order to develop species-selective inhibitors of potential therapeutic use.

High-throughput compatible screening assays were established for both recombinantly expressed proteins and screened against a diversity-based compound library comprising ~18,000 drug-like small molecules for the identification of novel inhibitors and potential drug lead candidates. For PPDK a single specific inhibitor (PPDKin1) of moderate potency (K_I ~53 μM) was discovered that was uncompetitive with respect to cosubstrates AMP and PEP.

For wALAD, a cluster of novel tri-substituted benzimidazole-5-carboxylic acid structures was discovered and shown to specifically bind to and inhibit the Mg^{2+}-responsive *Wolbachia* and pea orthologs with little effect on the human enzyme. For the most potent compound, termed wALADin1 (IC_{50} = 11 μM), a novel and specific

inhibitory mechanism was revealed that is partially substrate-competitive and partially non-competitive. It further involves competition with enzymatic activation by a Mg^{2+} ion on a functional level. Based on experimental evidence and analogy to other orthologous enzymes, activation of wALAD by Mg^{2+} is assumed to be allosterically driven and it is suggested that the corresponding conformational change is antagonized by binding of wALADin1. It was further revealed that wALADin1 is able to stimulate enzymatic activity of several Mg^{2+}-stimulated γ-proteobacterial orthologs suggesting that wALADins may, in general, be described as (putatively allosteric) modulators of ALAD.

Antifilarial activity of wALADin1 was successfully demonstrated in a proof-of-principle experiment using the rodent filarial nematode *L. sigmodontis* in an *ex vivo* setup, in which wALADin1 and derived inhibitors elicited a characteristic phenotype in treated worms and affected both motility and viability of these worms (EC_{50} for wALADin1 $\sim$100 μM). Control studies on the *Wolbachia*-free filaria *A. viteae* revealed that the macrofilaricidal effect of wALADin1 was dependent on the presence of *Wolbachia* and thus likely a result of inhibition of heme biosynthesis in the endosymbionts. However, no antifilarial effect could be detected for wALADin1 in the course of *L. sigmodontis* infection in mice *in vivo* which is presumably explained by pharmakokinetic shortcomings.

In a first approach to identify improved inhibitors several derivatives of the benzimidazole wALADin1 and chemically similar non-benzimidazole compounds were tested for their wALAD inhibitory properties. These studies allowed the delineation of essential chemical features required for inhibitory potency, such as the carboxylate group, and for species-selectivity of wALADin-benzimidazoles. Further bioactive chemotypes were identified including a tricyclic quinoline derivative (wALADin2) with improved potency and specificity that acted by a related but not identical inhibitory mechanism.

Finally, it was shown that wALADin1 and, even more strongly, two of its derivatives have pronounced activity against blood stage *Plasmodium falciparum*, the causative agent of malaria tropica, the most devastating parasitic disease of man, *in vitro* with IC_{50} values in the low μM range. This potent and specific, though putatively not ALAD-dependent, activity on *P. falciparum* indicates wALADin benzimidazoles may be useful in antimalarial drug discovery.

Taken together, with the identification of a novel class of specific wALAD inhibitors with their unique inhibitory mechanism, proof-of-principle demonstration of their related antifilarial biological activity and detailed investigations on the structural-functional foundations, this study provides the framework for the development of more potent wALADin-like inhibitors targeting *Wolbachia* and related pathogens as potential lead structures in the development of novel antifilarial drugs and narrow-spectrum antibiotics.

Bibliography

[1] Onchocerciasis: elimination is feasible. *Wkly Epidemiol Rec*, 84(37):382–383, Sep 2009.

[2] African Programme for Onchocerciasis Control: meeting of national task forces, September 2011. *Wkly Epidemiol Rec*, 86(48):541–549, Nov 2011.

[3] Global Programme to eliminate lymphatic filariasis: progress report on mass drug administration, 2010. *Wkly Epidemiol Rec*, 86(35):377–388, Aug 2011.

[4] Progress towards eliminating onchocerciasis in the WHO Region of the Americas in 2011: interruption of transmission in Guatemala and Mexico. *Wkly Epidemiol Rec*, 87(33):309–314, Aug 2012.

[5] Héctor Acosta, Michel Dubourdieu, Wilfredo Quiñones, Ana Cáceres, Frederic Bringaud, and Juan Luis Concepción. Pyruvate phosphate dikinase and pyrophosphate metabolism in the glycosome of *Trypanosoma cruzi* epimastigotes. *Comp Biochem Physiol B Biochem Mol Biol*, 138(4):347–356, Aug 2004.

[6] Robert S. Alexander and Anthony R. Butler. Electrophilic Substitution in Pyrroles. Part 1. Reaction with 4-Dimethylaminobenzaldehyde (Ehrlich's Reagent) in Acid Solution. *J. Chem. Soc., Perkin Trans. 2*, 6:696–701, 1976.

[7] Judith E. Allen, Ohene Adjei, Odile Bain, Achim Hoerauf, Wolfgang H. Hoffmann, Benjamin L. Makepeace, Hartwig Schulz-Key, Vincent N. Tanya, Alexander J. Trees, Samuel Wanji, and David W. Taylor. Of mice, cattle, and humans: the immunology and treatment of river blindness. *PLoS Negl Trop Dis*, 2(4):e217, 2008.

[8] John M. Archibald and Patrick J. Keeling. Recycled plastids: a 'green movement' in eukaryotic evolution. *Trends Genet*, 18(11):577–584, Nov 2002.

[9] Sridhar Arumugam, Kenneth M. Pfarr, and Achim Hoerauf. Infection of the intermediate mite host with *Wolbachia*-depleted *Litomosoides sigmodontis* microfilariae: impaired L1 to L3 development and subsequent sex-ratio distortion in adult worms. *Int J Parasitol*, 38(8-9):981–987, Jul 2008.

[10] L. R. Ash and J. M. Riley. Development of subperiodic *Brugia malayi* in the jird, *Meriones unguiculatus*, with notes on infections in other rodents. *J Parasitol*, 56(5):969–973, Oct 1970.

[11] T. Attout, S. Babayan, A. Hoerauf, D. W. Taylor, W. J. Kozek, C. Martin, and O. Bain. Blood-feeding in the young adult filarial worms *Litomosoides sigmodontis*. *Parasitology*, 130(Pt 4):421–428, Apr 2005.

[12] Tarik Attout, Coralie Martin, Simon A. Babayan, Wieslaw J. Kozek, Chiara Bazzocchi, François Oudet, Iain J. Gallagher, Sabine Specht, and Odile Bain. Pleural cellular reaction to the filarial infection *Litomosoides sigmodontis* is determined by the moulting process, the worm alteration, and the host strain. *Parasitol Int*, 57(2):201–211, Jun 2008.

[13] Yuuki Awa, Noritaka Iwai, Tomohiko Ueda, Kenji Suzuki, Shoji Asano, Junichi Yamagishi, Kazuo Nagai, and Masaaki Wachi. Isolation of a new antibiotic, alaremycin, structurally related to 5-aminolevulinic acid from *Streptomyces sp.* A012304. *Biosci Biotechnol Biochem*, 69(9):1721–1725, Sep 2005.

[14] K. Awadzi, E. T. Addy, N. O. Opoku, A. Plenge-Bönig, and D. W. Büttner. The chemotherapy of onchocerciasis XX: ivermectin in combination with albendazole. *Trop Med Parasitol*, 46(4):213–220, Dec 1995.

[15] Simon Babayan, Marie-Noëlle Ungeheuer, Coralie Martin, Tarik Attout, Elodie Belnoue, Georges Snounou, Laurent Rénia, Masataka Korenaga, and Odile Bain. Resistance and susceptibility to filarial infection with *Litomosoides sigmodontis* are associated with early differences in parasite development and in localized immune reactions. *Infect Immun*, 71(12):6820–6829, Dec 2003.

[16] Simon A. Babayan, Andrew F. Read, Rachel A. Lawrence, Odile Bain, and Judith E. Allen. Filarial parasites develop faster and reproduce earlier in response to host immune effectors that determine filarial life expectancy. *PLoS Biol*, 8(10):e1000525, 2010.

[17] O. Bain, G. Petit, and M. Diagne. [*Litomosoides*, parasites of rodents; taxonomic consequences]. *Ann Parasitol Hum Comp*, 64(4):268–289, 1989.

[18] Laura Baldo, Lorenzo Prendini, Angelique Corthals, and John H. Werren. *Wolbachia* are present in southern african scorpions and cluster with supergroup F. *Curr Microbiol*, 55(5):367–373, Nov 2007.

[19] Laura Baldo and John H. Werren. Revisiting *Wolbachia* supergroup typing based on WSP: spurious lineages and discordance with MLST. *Curr Microbiol*, 55(1):81–87, Jul 2007.

[20] C. Bandi, T. J. Anderson, C. Genchi, and M. L. Blaxter. Phylogeny of *Wolbachia* in filarial nematodes. *Proc Biol Sci*, 265(1413):2407–2413, Dec 1998.

[21] C. Bandi, A. M. Dunn, G. D. Hurst, and T. Rigaud. Inherited microorganisms, sex-specific virulence and reproductive parasitism. *Trends Parasitol*, 17(2):88–94, Feb 2001.

[22] C. Bandi, J. W. McCall, C. Genchi, S. Corona, L. Venco, and L. Sacchi. Effects of tetracycline on the filarial worms *Brugia pahangi* and *Dirofilaria immitis* and their bacterial endosymbionts *Wolbachia*. *Int J Parasitol*, 29(2):357–364, Feb 1999.

[23] Etelvino J H. Bechara, Fernando Dutra, Vanessa E S. Cardoso, Adriano Sartori, Kelly P K. Olympio, Carlos A A. Penatti, Avishek Adhikari, and Nilson A. Assunção. The dual face of endogenous alpha-aminoketones: prooxidizing metabolic weapons. *Comp Biochem Physiol C Toxicol Pharmacol*, 146(1-2):88–110, 2007.

[24] Michael D. Best. Click chemistry and bioorthogonal reactions: unprecedented selectivity in the labeling of biological molecules. *Biochemistry*, 48(28):6571–6584, Jul 2009.

[25] Moses J. Bockarie and Rinki M. Deb. Elimination of lymphatic filariasis: do we have the drugs to complete the job? *Curr Opin Infect Dis*, 23(6):617–620, Dec 2010.

[26] Q. F. Boese, A. J. Spano, J. M. Li, and M. P. Timko. Aminolevulinic acid dehydratase in pea (*Pisum sativum L.*). identification of an unusual metal-binding domain in the plant enzyme. *J Biol Chem*, 266(26):17060–17066, Sep 1991.

[27] David W. Bollivar, Cheryl Clauson, Rachel Lighthall, Siiri Forbes, Bashkim Kokona, Robert Fairman, Lenka Kundrat, and Eileen K. Jaffe. *Rhodobacter capsulatus* porphobilinogen synthase, a high activity metal ion independent hexamer. *BMC Biochem*, 5:17, Nov 2004.

[28] Z. Q. Bonday, S. Taketani, P. D. Gupta, and G. Padmanaban. Heme biosynthesis by the malarial parasite. import of delta-aminolevulinate dehydrase from the host red cell. *J Biol Chem*, 272(35):21839–21846, Aug 1997.

[29] S. R. Bordenstein, F. P. O'Hara, and J. H. Werren. *Wolbachia*-induced incompatibility precedes other hybrid incompatibilities in *Nasonia*. *Nature*, 409(6821):707–710, Feb 2001.

[30] Seth Bordenstein and Rebeca B. Rosengaus. Discovery of a novel *Wolbachia* super group in Isoptera. *Curr Microbiol*, 51(6):393–398, Dec 2005.

[31] Seth R. Bordenstein, David H A. Fitch, and John H. Werren. Absence of *Wolbachia* in nonfilariid nematodes. *J Nematol*, 35(3):266–270, Sep 2003.

[32] Seth R. Bordenstein, Charalampos Paraskevopoulos, Julie C. Dunning Hotopp, Panagiotis Sapountzis, Nathan Lo, Claudio Bandi, Hervé Tettelin, John H. Werren, and Kostas Bourtzis. Parasitism and mutualism in *Wolbachia*: what the phylogenomic trees can and cannot say. *Mol Biol Evol*, 26(1):231–241, Jan 2009.

[33] Cyrille Y. Botté, Faustine Dubar, Geoffrey I. McFadden, Eric Maréchal, and Christophe Biot. *Plasmodium falciparum* apicoplast drugs: targets or off-targets? *Chem Rev*, 112(3):1269–1283, Mar 2012.

[34] Helen W. Boucher, George H. Talbot, John S. Bradley, John E. Edwards, David Gilbert, Louis B. Rice, Michael Scheld, Brad Spellberg, and John Bartlett. Bad bugs, no drugs: no ESKAPE! An update from the Infectious Diseases Society of America. *Clin Infect Dis*, 48(1):1–12, Jan 2009.

[35] Catherine Bourguinat, Kathy Keller, Aron Bhan, Andrew Peregrine, Timothy Geary, and Roger Prichard. Macrocyclic lactone resistance in *Dirofilaria immitis*. *Vet Parasitol*, 181(2-4):388–392, Sep 2011.

[36] Dwight D. Bowman. Introduction to the alpha-proteobacteria: *Wolbachia* and *Bartonella*, *Rickettsia*, *Brucella*, *Ehrlichia*, and *Anaplasma*. *Top Companion Anim Med*, 26(4):173–177, Nov 2011.

[37] Sabine Breinig, Jukka Kervinen, Linda Stith, Andrew S. Wasson, Robert Fairman, Alexander Wlodawer, Alexander Zdanov, and Eileen K. Jaffe. Control of tetrapyrrole biosynthesis by alternate quaternary forms of porphobilinogen synthase. *Nat Struct Biol*, 10(9):757–763, Sep 2003.

[38] Ruth Brenk, Alessandro Schipani, Daniel James, Agata Krasowski, Ian Hugh Gilbert, Julie Frearson, and Paul Graham Wyatt. Lessons learnt from assembling screening libraries for drug discovery for neglected diseases. *ChemMedChem*, 3(3):435–444, Mar 2008.

[39] M. J. Brennan and R. C. Cantrill. Delta-aminolaevulinic acid is a potent agonist for GABA autoreceptors. *Nature*, 280(5722):514–515, Aug 1979.

[40] Dietrich W. Büttner, Samuel Wanji, Chiara Bazzocchi, Odile Bain, and Peter Fischer. Obligatory symbiotic *Wolbachia* endobacteria are absent from *Loa loa*. *Filaria J*, 2(1):10, May 2003.

[41] M. Casiraghi, G. Favia, G. Cancrini, A. Bartoloni, and C. Bandi. Molecular identification of *Wolbachia* from the filarial nematode *Mansonella ozzardi*. *Parasitol Res*, 87(5):417–420, May 2001.

[42] M. Casiraghi, J. W. McCall, L. Simoncini, L. H. Kramer, L. Sacchi, C. Genchi, J. H. Werren, and C. Bandi. Tetracycline treatment and sex-ratio distortion: a role for *Wolbachia* in the moulting of filarial nematodes? *Int J Parasitol*, 32(12):1457–1468, Nov 2002.

[43] Maurizio Casiraghi, Odile Bain, Ricardo Guerrero, Coralie Martin, Vanessa Pocacqua, Scott L. Gardner, Alberto Franceschi, and Claudio Bandi. Mapping the presence of *Wolbachia pipientis* on the phylogeny of filarial nematodes: evidence for symbiont loss during evolution. *Int J Parasitol*, 34(2):191–203, Feb 2004.

[44] J. C. Chabala, H. Mrozik, R. L. Tolman, P. Eskola, A. Lusi, L. H. Peterson, M. F. Woods, M. H. Fisher, W. C. Campbell, J. R. Egerton, and D. A. Ostlind. Ivermectin, a new broad-spectrum antiparasitic agent. *J Med Chem*, 23(10):1134–1136, Oct 1980.

[45] S. Chauhan and M. R. O'Brian. A mutant *Bradyrhizobium japonicum* delta-aminolevulinic acid dehydratase with an altered metal requirement functions in situ for tetrapyrrole synthesis in soybean root nodules. *J Biol Chem*, 270(34):19823–19827, Aug 1995.

[46] J. P. Chippaux, M. Boussinesq, J. Gardon, N. Gardon-Wendel, and J. C. Ernould. Severe adverse reaction risks during mass treatment with ivermectin in loiasis-endemic areas. *Parasitol Today*, 12(11):448–450, Nov 1996.

[47] I. Chopra and M. Roberts. Tetracycline antibiotics: mode of action, applications, molecular biology, and epidemiology of bacterial resistance. *Microbiol Mol Biol Rev*, 65(2):232–60; second page, table of contents, Jun 2001.

[48] D. Christ, M. Goebel, and H. J. Saz. Actions of acetylcholine and GABA on spontaneous contractions of the filariid, *Dipetalonema viteae*. *Br J Pharmacol*, 101(4):971–977, Dec 1990.

[49] Thomas S. Churcher, Sébastien D S. Pion, Mike Y. Osei-Atweneboana, Roger K. Prichard, Kwablah Awadzi, Michel Boussinesq, Richard C. Collins, James A. Whitworth, and María-Gloria Basáñez. Identifying sub-optimal responses to ivermectin in the treatment of River Blindness. *Proc Natl Acad Sci U S A*, 106(39):16716–16721, Sep 2009.

[50] T. Spencer Cobbold. Haematozoa: Fresh discoveries by Dr. Lewis. *Lancet*, 105:216–217, 1875.

[51] T. Spencer Cobbold. On *Filaria bancrofti*. *Lancet*, 110:495–496, 1877.

[52] Johanna E. Cornah, Matthew J. Terry, and Alison G. Smith. Green or red: what stops the traffic in the tetrapyrrole pathway? *Trends Plant Sci*, 8(5):224–230, May 2003.

[53] Maria Almira Correia, Peter R. Sinclair, and Francesco De Matteis. Cytochrome P450 regulation: the interplay between its heme and apoprotein moieties in synthesis, assembly, repair, and disposal. *Drug Metab Rev*, 43(1):1–26, Feb 2011.

[54] Lawrence W. Cosenza, Frederic Bringaud, Theo Baltz, and Frederic M D. Vellieux. The 3.0 A resolution crystal structure of glycosomal pyruvate phosphate dikinase from *Trypanosoma brucei*. *J Mol Biol*, 318(5):1417–1432, May 2002.

[55] Catherine Covacin and Stephen C. Barker. Supergroup F *Wolbachia* bacteria parasitise lice (Insecta: Phthiraptera). *Parasitol Res*, 100(3):479–485, Feb 2007.

[56] H. F. Cross, M. Haarbrink, G. Egerton, M. Yazdanbakhsh, and M. J. Taylor. Severe reactions to filarial chemotherapy and release of *Wolbachia* endosymbionts into blood. *Lancet*, 358(9296):1873–1875, Dec 2001.

[57] Péter Csermely, Vilmos Agoston, and Sándor Pongor. The efficiency of multitarget drugs: the network approach might help drug design. *Trends Pharmacol Sci*, 26(4):178–182, Apr 2005.

[58] Vanessa M. D'Costa, Christine E. King, Lindsay Kalan, Mariya Morar, Wilson W L. Sung, Carsten Schwarz, Duane Froese, Grant Zazula, Fabrice Calmels, Regis Debruyne, G Brian Golding, Hendrik N. Poinar, and Gerard D. Wright. Antibiotic resistance is ancient. *Nature*, 477(7365):457–461, Sep 2011.

[59] Adriana De Siervi, Elba S. Vazquez, Carolina Rezaval, María V. Rossetti, and Alcira M. del Batlle. Delta-aminolevulinic acid cytotoxic effects on human hepatocarcinoma cell lines. *BMC Cancer*, 2:6, Mar 2002.

[60] Alexander Yaw Debrah, Sabine Mand, Yeboah Marfo-Debrekyei, Linda Batsa, Anna Albers, Sabine Specht, Ute Klarmann, Kenneth Pfarr, Ohene Adjei, and Achim Hoerauf. Macrofilaricidal Activity in *Wuchereria bancrofti* after 2 Weeks Treatment with a Combination of Rifampicin plus Doxycycline. *J Parasitol Res*, 2011:201617, 2011.

[61] Alexander Yaw Debrah, Sabine Mand, Yeboah Marfo-Debrekyei, Linda Batsa, Kenneth Pfarr, Marcelle Buttner, Ohene Adjei, Dietrich Büttner, and Achim Hoerauf. Macrofilaricidal effect of 4 weeks of treatment with doxycycline on *Wuchereria bancrofti*. *Trop Med Int Health*, 12(12):1433–1441, Dec 2007.

[62] Alexander Yaw Debrah, Sabine Mand, Sabine Specht, Yeboah Marfo-Debrekyei, Linda Batsa, Kenneth Pfarr, John Larbi, Bernard Lawson, Mark Taylor, Ohene Adjei, and Achim Hoerauf. Doxycycline reduces plasma VEGF-C/sVEGFR-3 and improves pathology in lymphatic filariasis. *PLoS Pathog*, 2(9):e92, Sep 2006.

[63] F. Dedeine, F. Vavre, F. Fleury, B. Loppin, M. E. Hochberg, and M. Boulétreau. Removing symbiotic *Wolbachia* bacteria specifically inhibits oogenesis in a parasitic wasp. *Proc Natl Acad Sci U S A*, 98(11):6247–6252, May 2001.

[64] Michael Delves, David Plouffe, Christian Scheurer, Stephan Meister, Sergio Wittlin, Elizabeth A. Winzeler, Robert E. Sinden, and Didier Leroy. The activities of current antimalarial drugs on the life cycle stages of *Plasmodium*: a comparative study with human and rodent parasites. *PLoS Med*, 9(2):e1001169, Feb 2012.

[65] M. Demasi, C. A. Penatti, R. DeLucia, and E. J. Bechara. The prooxidant effect of 5-aminolevulinic acid in the brain tissue of rats: implications in neuropsychiatric manifestations in porphyrias. *Free Radic Biol Med*, 20(3):291–299, 1996.

[66] Shanmugham Dhanasekaran, Nagasuma R. Chandra, B. K. Chandrasekhar Sagar, Pundi N. Rangarajan, and Govindarajan Padmanaban. Delta-aminolevulinic acid dehydratase from *Plasmodium falciparum*: indigenous versus imported. *J Biol Chem*, 279(8):6934–6942, Feb 2004.

[67] Jason R. Doyle, James N. Burnell, Dianne S. Haines, Lyndon E. Llewellyn, Cherie A. Motti, and Dianne M. Tapiolas. A rapid screening method to detect specific inhibitors of pyruvate orthophosphate dikinase as leads for C4 plant-selective herbicides. *J Biomol Screen*, 10(1):67–75, Feb 2005.

[68] P. T. Erskine, L. Coates, R. Newbold, A. A. Brindley, F. Stauffer, S. P. Wood, M. J. Warren, J. B. Cooper, P. M. Shoolingin-Jordan, and R. Neier. The X-ray structure of yeast 5-aminolaevulinic acid dehydratase complexed with two diacid inhibitors. *FEBS Lett*, 503(2-3):196–200, Aug 2001.

[69] P. T. Erskine, R. Newbold, A. A. Brindley, S. P. Wood, P. M. Shoolingin-Jordan, M. J. Warren, and J. B. Cooper. The x-ray structure of yeast 5-aminolaevulinic acid dehydratase complexed with substrate and three inhibitors. *J Mol Biol*, 312(1):133–141, Sep 2001.

[70] P. T. Erskine, R. Newbold, J. Roper, A. Coker, M. J. Warren, P. M. Shoolingin-Jordan, S. P. Wood, and J. B. Cooper. The Schiff base complex of yeast 5-aminolaevulinic acid dehydratase with laevulinic acid. *Protein Sci*, 8(6):1250–1256, Jun 1999.

[71] P. T. Erskine, E. Norton, J. B. Cooper, R. Lambert, A. Coker, G. Lewis, P. Spencer, M. Sarwar, S. P. Wood, M. J. Warren, and P. M. Shoolingin-Jordan. X-ray structure of 5-aminolevulinic acid dehydratase from *Escherichia coli* complexed with the inhibitor levulinic acid at 2.0 A resolution. *Biochemistry*, 38(14):4266–4276, Apr 1999.

[72] P. T. Erskine, N. Senior, S. Awan, R. Lambert, G. Lewis, I. J. Tickle, M. Sarwar, P. Spencer, P. Thomas, M. J. Warren, P. M. Shoolingin-Jordan, S. P. Wood, and J. B. Cooper. X-ray structure of 5-aminolaevulinate dehydratase, a hybrid aldolase. *Nat Struct Biol*, 4(12):1025–1031, Dec 1997.

[73] P. Esterre, C. Plichart, Y. Sechan, and N. L. Nguyen. The impact of 34 years of massive DEC chemotherapy on *Wuchereria bancrofti* infection and transmission: the Maupiti cohort. *Trop Med Int Health*, 6(3):190–195, Mar 2001.

[74] H. J. Evans and H. G. Wood. The mechanism of the pyruvate, phosphate dikinase reaction. *Proc Natl Acad Sci U S A*, 61(4):1448–1453, Dec 1968.

[75] Xian-Min Feng, Li-Jing Cao, Rodney D. Adam, Xi-Chen Zhang, and Si-Qi Lu. The catalyzing role of PPDK in *Giardia lamblia*. *Biochem Biophys Res Commun*, 367(2):394–398, Mar 2008.

[76] Katelyn Fenn and Mark Blaxter. *Wolbachia* genomes: revealing the biology of parasitism and mutualism. *Trends Parasitol*, 22(2):60–65, Feb 2006.

[77] Emanuele Ferri, Odile Bain, Michela Barbuto, Coralie Martin, Nathan Lo, Shigehiko Uni, Frederic Landmann, Sara G. Baccei, Ricardo Guerrero, Sueli de Souza Lima, Claudio Bandi, Samuel Wanji, Moustapha Diagne, and Maurizio Casiraghi. New insights into the evolution of *Wolbachia* infections in filarial nematodes inferred from a large range of screened species. *PLoS One*, 6(6):e20843, 2011.

[78] M. E. Fichera and D. S. Roos. A plastid organelle as a drug target in apicomplexan parasites. *Nature*, 390(6658):407–409, Nov 1997.

[79] Michael A. Fischbach and Christopher T. Walsh. Antibiotics for emerging pathogens. *Science*, 325(5944):1089–1093, Aug 2009.

[80] Kerstin Fischer, Wandy L. Beatty, Daojun Jiang, Gary J. Weil, and Peter U. Fischer. Tissue and stage-specific distribution of *Wolbachia* in *Brugia malayi*. *PLoS Negl Trop Dis*, 5(5):e1174, May 2011.

[81] Jeremy Foster, Mehul Ganatra, Ibrahim Kamal, Jennifer Ware, Kira Makarova, Natalia Ivanova, Anamitra Bhattacharyya, Vinayak Kapatral, Sanjay Kumar, Janos Posfai, Tamas Vincze, Jessica Ingram, Laurie Moran, Alla Lapidus, Marina Omelchenko, Nikos Kyrpides, Elodie Ghedin, Shiliang Wang, Eugene Goltsman, Victor Joukov, Olga Ostrovskaya, Kiryl Tsukerman, Mikhail Mazur, Donald Comb, Eugene Koonin, and Barton Slatko. The *Wolbachia* genome of *Brugia malayi*: endosymbiont evolution within a human pathogenic nematode. *PLoS Biol*, 3(4):e121, Apr 2005.

[82] H. Francis, K. Awadzi, and E. A. Ottesen. The Mazzotti reaction following treatment of onchocerciasis with diethylcarbamazine: clinical severity as a function of infection intensity. *Am J Trop Med Hyg*, 34(3):529–536, May 1985.

[83] N. Frankenberg, P. T. Erskine, J. B. Cooper, P. M. Shoolingin-Jordan, D. Jahn, and D. W. Heinz. High resolution crystal structure of a Mg2+-dependent porphobilinogen synthase. *J Mol Biol*, 289(3):591–602, Jun 1999.

[84] N. Frankenberg, D. Jahn, and E. K. Jaffe. *Pseudomonas aeruginosa* contains a novel type V porphobilinogen synthase with no required catalytic metal ions. *Biochemistry*, 38(42):13976–13982, Oct 1999.

[85] Frederic Frère, Heike Reents, Wolf-Dieter Schubert, Dirk W. Heinz, and Dieter Jahn. Tracking the evolution of porphobilinogen synthase metal dependence in vitro. *J Mol Biol*, 345(5):1059–1070, Feb 2005.

[86] Frederic Frère, Wolf-Dieter Schubert, Frédéric Stauffer, Nicole Frankenberg, Reinhard Neier, Dieter Jahn, and Dirk W. Heinz. Structure of porphobilinogen synthase from *Pseudomonas aeruginosa* in complex with 5-fluorolevulinic acid suggests a double Schiff base mechanism. *J Mol Biol*, 320(2):237–247, Jul 2002.

[87] Francisco-Javier Gamo, Laura M. Sanz, Jaume Vidal, Cristina de Cozar, Emilio Alvarez, Jose-Luis Lavandera, Dana E. Vanderwall, Darren V S. Green, Vinod Kumar, Samiul Hasan, James R. Brown, Catherine E. Peishoff, Lon R. Cardon, and Jose F. Garcia-Bustos. Thousands of chemical starting points for antimalarial lead identification. *Nature*, 465(7296):305–310, May 2010.

[88] J. Gardon, N. Gardon-Wendel, Demanga-Ngangue, J. Kamgno, J. P. Chippaux, and M. Boussinesq. Serious reactions after mass treatment of onchocerciasis with ivermectin in an area endemic for *Loa loa* infection. *Lancet*, 350(9070):18–22, Jul 1997.

[89] R. L. Gaur, S. Dixit, M. K. Sahoo, M. Khanna, S. Singh, and P. K. Murthy. Anti-filarial activity of novel formulations of albendazole against experimental brugian filariasis. *Parasitology*, 134(Pt 4):537–544, Apr 2007.

[90] Timothy G. Geary, Catherine Bourguinat, and Roger K. Prichard. Evidence for macrocyclic lactone anthelmintic resistance in *Dirofilaria immitis*. *Top Companion Anim Med*, 26(4):186–192, Nov 2011.

[91] Timothy G. Geary and Charles D. Mackenzie. Progress and challenges in the discovery of macrofilaricidal drugs. *Expert Rev Anti Infect Ther*, 9(8):681–695, Aug 2011.

[92] Timothy G. Geary, Katherine Woo, James S. McCarthy, Charles D. Mackenzie, John Horton, Roger K. Prichard, Nilanthi R. de Silva, Piero L. Olliaro, Janis K. Lazdins-Helds, Dirk A. Engels, and Donald A. Bundy. Unresolved issues in anthelmintic pharmacology for helminthiases of humans. *Int J Parasitol*, 40(1):1–13, Jan 2010.

[93] Elodie Ghedin, Shiliang Wang, David Spiro, Elisabet Caler, Qi Zhao, Jonathan Crabtree, Jonathan E. Allen, Arthur L. Delcher, David B. Guiliano, Diego Miranda-Saavedra, Samuel V. Angiuoli, Todd Creasy, Paolo Amedeo, Brian Haas, Najib M. El-Sayed, Jennifer R. Wortman, Tamara Feldblyum, Luke Tallon, Michael Schatz, Martin Shumway, Hean Koo, Steven L. Salzberg, Seth Schobel, Mihaela Pertea, Mihai Pop, Owen White, Geoffrey J. Barton, Clotilde K S. Carlow, Michael J. Crawford, Jennifer Daub, Matthew W. Dimmic, Chris F. Estes, Jeremy M. Foster, Mehul Ganatra, William F. Gregory, Nicholas M. Johnson, Jinming Jin, Richard Komuniecki, Ian Korf, Sanjay Kumar, Sandra Laney, Ben-Wen Li, Wen Li, Tim H. Lindblom, Sara Lustigman, Dong Ma, Claude V. Maina, David M A. Martin, James P. McCarter, Larry McReynolds, Makedonka Mitreva, Thomas B. Nutman, John Parkinson, José M. Peregrín-Alvarez, Catherine Poole, Qinghu Ren, Lori Saunders, Ann E. Sluder, Katherine Smith, Mario Stanke, Thomas R. Unnasch, Jenna Ware, Aguan D. Wei, Gary Weil, Deryck J. Williams, Yinhua Zhang, Steven A. Williams, Claire Fraser-Liggett, Barton Slatko, Mark L. Blaxter, and Alan L. Scott. Draft genome of the filarial nematode parasite *Brugia malayi*. *Science*, 317(5845):1756–1760, Sep 2007.

[94] Illona Gillette-Ferguson, Katrin Daehnel, Amy G. Hise, Yan Sun, Eric Carlson, Eugenia Diaconu, Helen F. McGarry, Mark J. Taylor, and Eric Pearlman. Toll-like receptor 2 regulates CXC chemokine production and neutrophil recruitment to the cornea in *Onchocerca volvulus*/ *Wolbachia*-induced keratitis. *Infect Immun*, 75(12):5908–5915, Dec 2007.

[95] Susan K. Glendinning, Steven D. Buckingham, David B. Sattelle, Susan Wonnacott, and Adrian J. Wolstenholme. Glutamate-gated chloride channels of *Haemonchus contortus* restore drug sensitivity to ivermectin resistant *Caenorhabditis elegans*. *PLoS One*, 6(7):e22390, 2011.

[96] Christian Gloeckner, Amanda L. Garner, Fana Mersha, Yelena Oksov, Nancy Tricoche, Lisa M. Eubanks, Sara Lustigman, Gunnar F. Kaufmann, and

Kim D. Janda. Repositioning of an existing drug for the neglected tropical disease Onchocerciasis. *Proc Natl Acad Sci U S A*, 107(8):3424–3429, Feb 2010.

[97] R. D. Gonzales, P. C. Schreckenberger, M. B. Graham, S. Kelkar, K. DenBesten, and J. P. Quinn. Infections due to vancomycin-resistant *Enterococcus faecium* resistant to linezolid. *Lancet*, 357(9263):1179, Apr 2001.

[98] Sarah Gould and Robert C. Scott. 2-Hydroxypropyl-beta-cyclodextrin (HP-beta-CD): a toxicology review. *Food Chem Toxicol*, 43(10):1451–1459, Oct 2005.

[99] Lloyd D. Graham, Andrew C. Kotze, Ross T. Fernley, and Ronald J. Hill. An ortholog of the ecdysone receptor protein (EcR) from the parasitic nematode *Haemonchus contortus*. *Mol Biochem Parasitol*, 171(2):104–107, Jun 2010.

[100] Brian M. Greenwood, David A. Fidock, Dennis E. Kyle, Stefan H I. Kappe, Pedro L. Alonso, Frank H. Collins, and Patrick E. Duffy. Malaria: progress, perils, and prospects for eradication. *J Clin Invest*, 118(4):1266–1276, Apr 2008.

[101] Annelies Haegeman, Bartel Vanholme, Joachim Jacob, Tom T M. Vandekerckhove, Myriam Claeys, Gaetan Borgonie, and Godelieve Gheysen. An endosymbiotic bacterium in a plant-parasitic nematode: member of a new *Wolbachia* supergroup. *Int J Parasitol*, 39(9):1045–1054, Jul 2009.

[102] William K. Hagmann. The many roles for fluorine in medicinal chemistry. *J Med Chem*, 51(15):4359–4369, Aug 2008.

[103] Achim Harder and Georg von Samson-Himmelstjerna. Cyclooctadepsipeptides–a new class of anthelmintically active compounds. *Parasitol Res*, 88(6):481–488, Jun 2002.

[104] M. D. Hatch and C. R. Slack. A new enzyme for the interconversion of pyruvate and phosphopyruvate and its role in the C4 dicarboxylic acid pathway of photosynthesis. *Biochem J*, 106(1):141–146, Jan 1968.

[105] C. Y. He, M. K. Shaw, C. H. Pletcher, B. Striepen, L. G. Tilney, and D. S. Roos. A plastid segregation defect in the protozoan parasite *Toxoplasma gondii*. *EMBO J*, 20(3):330–339, Feb 2001.

[106] William P. Heal, T H Tam Dang, and Edward W. Tate. Activity-based probes: discovering new biology and new drug targets. *Chem Soc Rev*, 40(1):246–257, Jan 2011.

[107] Ilka U. Heinemann, Martina Jahn, and Dieter Jahn. The biochemistry of heme biosynthesis. *Arch Biochem Biophys*, 474(2):238–251, Jun 2008.

[108] Ilka U. Heinemann, Claudia Schulz, Wolf-Dieter Schubert, Dirk W. Heinz, Yang-G. Wang, Yuichi Kobayashi, Yuuki Awa, Masaaki Wachi, Dieter Jahn, and Martina Jahn. Structure of the heme biosynthetic *Pseudomonas aeruginosa* porphobilinogen synthase in complex with the antibiotic alaremycin. *Antimicrob Agents Chemother*, 54(1):267–272, Jan 2010.

[109] Beate Henrichfreise, Andrea Schiefer, Tanja Schneider, Edith Nzukou, Christina Poellinger, Theo-Julian Hoffmann, Kelly L. Johnston, Katja Moelleken, Imke Wiedemann, Kenneth Pfarr, Achim Hoerauf, and Hans Georg Sahl. Functional conservation of the lipid II biosynthesis pathway in the cell wall-less bacteria *Chlamydia* and *Wolbachia*: why is lipid II needed? *Mol Microbiol*, 73(5):913–923, Sep 2009.

[110] M. Hertig and S. B. Wolbach. Studies on *Rickettsia*-Like Micro-Organisms in Insects. *J Med Res*, 44(3):329–374.7, Mar 1924.

[111] O. Herzberg, C. C. Chen, G. Kapadia, M. McGuire, L. J. Carroll, S. J. Noh, and D. Dunaway-Mariano. Swiveling-domain mechanism for enzymatic phosphotransfer between remote reaction sites. *Proc Natl Acad Sci U S A*, 93(7):2652–2657, Apr 1996.

[112] Osnat Herzberg, Celia C H. Chen, Sijiu Liu, Aleksandra Tempczyk, Andrew Howard, Min Wei, Dongmei Ye, and Debra Dunaway-Mariano. Pyruvate site of pyruvate phosphate dikinase: crystal structure of the enzyme-phosphonopyruvate complex, and mutant analysis. *Biochemistry*, 41(3):780–787, Jan 2002.

[113] Kirsten Hilgenboecker, Peter Hammerstein, Peter Schlattmann, Arndt Telschow, and John H. Werren. How many species are infected with *Wolbachia*?–a statistical analysis of current data. *FEMS Microbiol Lett*, 281(2):215–220, Apr 2008.

[114] Amy G. Hise, Katrin Daehnel, Illona Gillette-Ferguson, Eun Cho, Helen F. McGarry, Mark J. Taylor, Douglas T. Golenbock, Katherine A. Fitzgerald, James W. Kazura, and Eric Pearlman. Innate immune responses to endosymbiotic *Wolbachia* bacteria in *Brugia malayi* and *Onchocerca volvulus* are dependent on TLR2, TLR6, MyD88, and Mal, but not TLR4, TRIF, or TRAM. *J Immunol*, 178(2):1068–1076, Jan 2007.

[115] A. Hoerauf, S. Mand, O. Adjei, B. Fleischer, and D. W. Büttner. Depletion of *Wolbachia* endobacteria in *Onchocerca volvulus* by doxycycline and microfilaridermia after ivermectin treatment. *Lancet*, 357(9266):1415–1416, May 2001.

[116] A. Hoerauf, K. Nissen-Pähle, C. Schmetz, K. Henkle-Dührsen, M. L. Blaxter, D. W. Büttner, M. Y. Gallin, K. M. Al-Qaoud, R. Lucius, and B. Fleischer. Tetracycline therapy targets intracellular bacteria in the filarial nematode *Litomosoides sigmodontis* and results in filarial infertility. *J Clin Invest*, 103(1):11–18, Jan 1999.

[117] A. Hoerauf, L. Volkmann, C. Hamelmann, O. Adjei, I. B. Autenrieth, B. Fleischer, and D. W. Büttner. Endosymbiotic bacteria in worms as targets for a novel chemotherapy in filariasis. *Lancet*, 355(9211):1242–1243, Apr 2000.

[118] A. Hoerauf, L. Volkmann, K. Nissen-Paehle, C. Schmetz, I. Autenrieth, D. W. Büttner, and B. Fleischer. Targeting of *Wolbachia* endobacteria in *Litomosoides sigmodontis*: comparison of tetracyclines with chloramphenicol, macrolides and ciprofloxacin. *Trop Med Int Health*, 5(4):275–279, Apr 2000.

[119] Achim Hoerauf. *Mansonella perstans*–the importance of an endosymbiont. *N Engl J Med*, 361(15):1502–1504, Oct 2009.

[120] Achim Hoerauf, Sabine Specht, Marcelle Büttner, Kenneth Pfarr, Sabine Mand, Rolf Fimmers, Yeboah Marfo-Debrekyei, Peter Konadu, Alexander Yaw Debrah, Claudio Bandi, Norbert Brattig, Anna Albers, John Larbi, Linda Batsa, Mark J. Taylor, Ohene Adjei, and Dietrich W. Büttner. *Wolbachia* endobacteria depletion by doxycycline as antifilarial therapy has macrofilaricidal activity in onchocerciasis: a randomized placebo-controlled study. *Med Microbiol Immunol*, 197(3):295–311, Sep 2008.

[121] Achim Hoerauf, Sabine Specht, Yeboah Marfo-Debrekyei, Marcelle Büttner, Alexander Yaw Debrah, Sabine Mand, Linda Batsa, Norbert Brattig, Peter Konadu, Claudio Bandi, Rolf Fimmers, Ohene Adjei, and Dietrich W. Büttner. Efficacy of 5-week doxycycline treatment on adult *Onchocerca volvulus*. *Parasitol Res*, 104(2):437–447, Jan 2009.

[122] W. Hoffmann, G. Petit, H. Schulz-Key, D. Taylor, O. Bain, and L. Le Goff. *Litomosoides sigmodontis* in mice: reappraisal of an old model for filarial research. *Parasitol Today*, 16(9):387–389, Sep 2000.

[123] Lindy Holden-Dye and Robert J. Walker. Anthelmintic drugs. *WormBook*, pages 1–13, 2007.

[124] Alexander G. Holman, Paul J. Davis, Jeremy M. Foster, Clotilde K S. Carlow, and Sanjay Kumar. Computational prediction of essential genes in an unculturable endosymbiotic bacterium, *Wolbachia* of *Brugia malayi*. *BMC Microbiol*, 9:243, 2009.

[125] A. D. Hopkins. Ivermectin and onchocerciasis: is it all solved? *Eye (Lond)*, 19(10):1057–1066, Oct 2005.

[126] Andrew L. Hopkins. Network pharmacology: the next paradigm in drug discovery. *Nat Chem Biol*, 4(11):682–690, Nov 2008.

[127] M. E. Huigens, R. F. Luck, R. H. Klaassen, M. F. Maas, M. J. Timmermans, and R. Stouthamer. Infectious parthenogenesis. *Nature*, 405(6783):178–179, May 2000.

[128] G. D. Hurst, F. M. Jiggins, and S. J. Robinson. What causes inefficient transmission of male-killing *Wolbachia* in *Drosophila*? *Heredity (Edinb)*, 87(Pt 2):220–226, Aug 2001.

[129] Masatoshi Iga and Hiroshi Kataoka. Recent studies on insect hormone metabolic pathways mediated by cytochrome P450 enzymes. *Biol Pharm Bull*, 35(6):838–843, 2012.

[130] James Inglese, Ronald L. Johnson, Anton Simeonov, Menghang Xia, Wei Zheng, Christopher P. Austin, and Douglas S. Auld. High-throughput screening assays for the identification of chemical probes. *Nat Chem Biol*, 3(8):466–479, Aug 2007.

[131] E. K. Jaffe, S. Ali, L. W. Mitchell, K. M. Taylor, M. Volin, and G. D. Markham. Characterization of the role of the stimulatory magnesium of *Escherichia coli* porphobilinogen synthase. *Biochemistry*, 34(1):244–251, Jan 1995.

[132] E. K. Jaffe, J. Martins, J. Li, J. Kervinen, and RL Dunbrack, Jr. The molecular mechanism of lead inhibition of human porphobilinogen synthase. *J Biol Chem*, 276(2):1531–1537, Jan 2001.

[133] Eileen K. Jaffe. An unusual phylogenetic variation in the metal ion binding sites of porphobilinogen synthase. *Chem Biol*, 10(1):25–34, Jan 2003.

[134] Eileen K. Jaffe. The porphobilinogen synthase catalyzed reaction mechanism. *Bioorg Chem*, 32(5):316–325, Oct 2004.

[135] Eileen K. Jaffe. Morpheeins–a new structural paradigm for allosteric regulation. *Trends Biochem Sci*, 30(9):490–497, Sep 2005.

[136] Eileen K. Jaffe, Jukka Kervinen, Jacob Martins, Frederic Stauffer, Reinhard Neier, Alexander Wlodawer, and Alexander Zdanov. Species-specific inhibition of porphobilinogen synthase by 4-oxosebacic acid. *J Biol Chem*, 277(22):19792–19799, May 2002.

[137] Eileen K. Jaffe and Sarah H. Lawrence. Allostery and the dynamic oligomerization of porphobilinogen synthase. *Arch Biochem Biophys*, 519(2):144–153, Mar 2012.

[138] Eileen K. Jaffe, Dhanasekaran Shanmugam, Anna Gardberg, Shellie Dieterich, Banumathi Sankaran, Lance J. Stewart, Peter J. Myler, and David S. Roos. Crystal structure of *Toxoplasma gondii* porphobilinogen synthase: insights on octameric structure and porphobilinogen formation. *J Biol Chem*, 286(17):15298–15307, Apr 2011.

[139] Jan Janouskovec, Ales Horák, Miroslav Oborník, Julius Lukes, and Patrick J. Keeling. A common red algal origin of the apicomplexan, dinoflagellate, and heterokont plastids. *Proc Natl Acad Sci U S A*, 107(24):10949–10954, Jun 2010.

[140] H. Jomaa, J. Wiesner, S. Sanderbrand, B. Altincicek, C. Weidemeyer, M. Hintz, I. Türbachova, M. Eberl, J. Zeidler, H. K. Lichtenthaler, D. Soldati, and E. Beck. Inhibitors of the nonmevalonate pathway of isoprenoid biosynthesis as antimalarial drugs. *Science*, 285(5433):1573–1576, Sep 1999.

[141] Kate E. Jones, Nikkita G. Patel, Marc A. Levy, Adam Storeygard, Deborah Balk, John L. Gittleman, and Peter Daszak. Global trends in emerging infectious diseases. *Nature*, 451(7181):990–993, Feb 2008.

[142] Erik M. Jorgensen. GABA. *WormBook*, pages 1–13, 2005.

[143] R. Kaminsky, N. Gauvry, S. Schorderet Weber, T. Skripsky, J. Bouvier, A. Wenger, F. Schroeder, Y. Desaules, R. Hotz, T. Goebel, B. C. Hosking, F. Pautrat, S. Wieland-Berghausen, and P. Ducray. Identification of the amino-acetonitrile derivative monepantel (AAD 1566) as a new anthelmintic drug development candidate. *Parasitol Res*, 103(4):931–939, Sep 2008.

[144] I. S. Kass, C. C. Wang, J. P. Walrond, and A. O. Stretton. Avermectin B1a, a paralyzing anthelmintic that affects interneurons and inhibitory motoneurons in *Ascaris*. *Proc Natl Acad Sci U S A*, 77(10):6211–6215, Oct 1980.

[145] S. K. Katiyar, V. R. Gordon, G. L. McLaughlin, and T. D. Edlind. Antiprotozoal activities of benzimidazoles and correlations with beta-tubulin sequence. *Antimicrob Agents Chemother*, 38(9):2086–2090, Sep 1994.

[146] Kazushige Kato, Ryouichi Tanaka, Shinsuke Sano, Ayumi Tanaka, and Hideo Hosaka. Identification of a gene essential for protoporphyrinogen IX oxidase activity in the cyanobacterium *Synechocystis sp.* PCC6803. *Proc Natl Acad Sci U S A*, 107(38):16649–16654, Sep 2010.

[147] Michael J. Keiser, Vincent Setola, John J. Irwin, Christian Laggner, Atheir I. Abbas, Sandra J. Hufeisen, Niels H. Jensen, Michael B. Kuijer, Roberto C. Matos, Thuy B. Tran, Ryan Whaley, Richard A. Glennon, Jérôme Hert, Kelan L H. Thomas, Douglas D. Edwards, Brian K. Shoichet, and Bryan L. Roth. Predicting new molecular targets for known drugs. *Nature*, 462(7270):175–181, Nov 2009.

[148] J. Kervinen, RL Dunbrack, Jr, S. Litwin, J. Martins, R. C. Scarrow, M. Volin, A. T. Yeung, E. Yoon, and E. K. Jaffe. Porphobilinogen synthase from pea: expression from an artificial gene, kinetic characterization, and novel implications for subunit interactions. *Biochemistry*, 39(30):9018–9029, Aug 2000.

[149] J. Kervinen, E. K. Jaffe, F. Stauffer, R. Neier, A. Wlodawer, and A. Zdanov. Mechanistic basis for suicide inactivation of porphobilinogen synthase by 4,7-dioxosebacic acid, an inhibitor that shows dramatic species selectivity. *Biochemistry*, 40(28):8227–8236, Jul 2001.

[150] Hyung J. Kim, Oleh Khalimonchuk, Pamela M. Smith, and Dennis R. Winge. Structure, function, and assembly of heme centers in mitochondrial respiratory complexes. *Biochim Biophys Acta*, 1823(9):1604–1616, Sep 2012.

[151] W. J. Kozek. Transovarially-transmitted intracellular microorganisms in adult and larval stages of *Brugia malayi*. *J Parasitol*, 63(6):992–1000, Dec 1977.

[152] W. J. Kozek and H. F. Marroquin. Intracytoplasmic bacteria in *Onchocerca volvulus*. *Am J Trop Med Hyg*, 26(4):663–678, Jul 1977.

[153] Sergey V. Kurkov and Thorsteinn Loftsson. Cyclodextrins. *Int J Pharm*, [Epub ahead of print], Jul 2012.

[154] Susheela Kushwaha, Prashant K. Singh, Ajay K. Rana, and Shailja Misra-Bhattacharya. Cloning, expression, purification and kinetics of trehalose-6-phosphate phosphatase of filarial parasite *Brugia malayi*. *Acta Trop*, 119(2-3):151–159, Aug 2011.

[155] Susheela Kushwaha, Prashant Kumar Singh, Mohd Shahab, Manisha Pathak, and Shailja Misra Bhattacharya. In vitro silencing of *Brugia malayi* trehalose-6-phosphate phosphatase impairs embryogenesis and in vivo development of infective larvae in jirds. *PLoS Negl Trop Dis*, 6(8):e1770, Aug 2012.

[156] E. Lacey. Mode of action of benzimidazoles. *Parasitol Today*, 6(4):112–115, Apr 1990.

[157] Brian R. Lahue, Yao Ma, Gerald W Shipps, Jr, Wolfgang Seghezzi, and Ronald Herbst. Substituted benzimidazoles: A novel chemotype for small molecule hKSP inhibitors. *Bioorg Med Chem Lett*, 19(13):3405–3409, Jul 2009.

[158] Frédéric Landmann, Jeremy M. Foster, Barton Slatko, and William Sullivan. Asymmetric *Wolbachia* segregation during early *Brugia malayi* embryogenesis determines its distribution in adult host tissues. *PLoS Negl Trop Dis*, 4(7):e758, 2010.

[159] N. G. Langworthy, A. Renz, U. Mackenstedt, K. Henkle-Dührsen, M. B. de Bronsvoort, V. N. Tanya, M. J. Donnelly, and A. J. Trees. Macrofilaricidal activity of tetracycline against the filarial nematode *Onchocerca ochengi*: elimination of *Wolbachia* precedes worm death and suggests a dependent relationship. *Proc Biol Sci*, 267(1448):1063–1069, Jun 2000.

[160] Sarah H. Lawrence, Ursula D. Ramirez, Trevor Selwood, Linda Stith, and Eileen K. Jaffe. Allosteric inhibition of human porphobilinogen synthase. *J Biol Chem*, 284(51):35807–35817, Dec 2009.

[161] Sarah H. Lawrence, Ursula D. Ramirez, Lei Tang, Farit Fazliyez, Lenka Kundrat, George D. Markham, and Eileen K. Jaffe. Shape shifting leads to small-molecule allosteric drug discovery. *Chem Biol*, 15(6):586–596, Jun 2008.

[162] Emilie Lefoulon, Laurent Gavotte, Kerstin Junker, Michela Barbuto, Shigehiko Uni, Frederic Landmann, Sauli Laaksonen, Susanna Saari, Sven Nikander, Sueli de Souza Lima, Maurizio Casiraghi, Odile Bain, and Coralie Martin. A new type F *Wolbachia* from Splendidofilariinae (Onchocercidae) supports the recent emergence of this supergroup. *Int J Parasitol*, 42:1025–36, Oct 2012.

[163] Kap Lim, Randy J. Read, Celia C H. Chen, Aleksandra Tempczyk, Min Wei, Dongmei Ye, Chun Wu, Debra Dunaway-Mariano, and Osnat Herzberg. Swiveling domain mechanism in pyruvate phosphate dikinase. *Biochemistry*, 46(51):14845–14853, Dec 2007.

[164] Ying Lin, Jacqueline D. Lusin, Dongmei Ye, Debra Dunaway-Mariano, and James B. Ames. Examination of the structure, stability, and catalytic potential in the engineered phosphoryl carrier domain of pyruvate phosphate dikinase. *Biochemistry*, 45(6):1702–1711, Feb 2006.

[165] B. Lindblad and G. Steen. Identification of 4,6-dioxoheptanoic acid (succinylacetone), 3,5-dioxooctanedioic acid (succinylacetoacetate) and 4-Oxo-6-hydroxyheptanoic acid in the urine from patients with hereditary tyrosinemia. *Biomed Mass Spectrom*, 9(10):419–424, Oct 1982.

[166] Cesare Mancuso, Marzia Perluigi, Chiara Cini, Carlo De Marco, Anna Maria Giuffrida Stella, and Vittorio Calabrese. Heme oxygenase and cyclooxygenase in the central nervous system: a functional interplay. *J Neurosci Res*, 84(7):1385–1391, Nov 2006.

[167] Sabine Mand, Kenneth Pfarr, Prakash K. Sahoo, Ashok K. Satapathy, Sabine Specht, Ute Klarmann, Alexander Y. Debrah, Balachandran Ravindran, and Achim Hoerauf. Macrofilaricidal activity and amelioration of lymphatic pathology in bancroftian filariasis after 3 weeks of doxycycline followed by single-dose diethylcarbamazine. *Am J Trop Med Hyg*, 81(4):702–711, Oct 2009.

[168] R. J. Martin. gamma-Aminobutyric acid- and piperazine-activated single-channel currents from *Ascaris suum* body muscle. *Br J Pharmacol*, 84(2):445–461, Feb 1985.

[169] Laura Maté, Guillermo Virkel, Adrián Lifschitz, Mariana Ballent, and Carlos Lanusse. Hepatic and extra-hepatic metabolic pathways involved in flubendazole biotransformation in sheep. *Biochem Pharmacol*, 76(6):773–783, Sep 2008.

[170] S. McCavera, T. K. Walsh, and A. J. Wolstenholme. Nematode ligand-gated chloride channels: an appraisal of their involvement in macrocyclic lactone resistance and prospects for developing molecular markers. *Parasitology*, 134(Pt 8):1111–1121, 2007.

[171] Geoffrey Ian McFadden. The apicoplast. *Protoplasma*, 248(4):641–650, Oct 2011.

[172] Helen F. McGarry, Ken Pfarr, Gill Egerton, Achim Hoerauf, Jean-Paul Akue, Peter Enyong, Samuel Wanji, Sabine L. Kläger, Albert E. Bianco, Nick J. Beeching, and Mark J. Taylor. Evidence against *Wolbachia* symbiosis in *Loa loa*. *Filaria J*, 2(1):9, May 2003.

[173] Helen F. McGarry, Leigh D. Plant, and Mark J. Taylor. Diethylcarbamazine activity against *Brugia malayi* microfilariae is dependent on inducible nitric-oxide synthase and the cyclooxygenase pathway. *Filaria J*, 4:4, Jun 2005.

[174] D. J. McLaren, M. J. Worms, B. R. Laurence, and M. G. Simpson. Micro-organisms in filarial larvae (Nematoda). *Trans R Soc Trop Med Hyg*, 69(5-6):509–514, 1975.

[175] Samantha N. McNulty, Jeremy M. Foster, Makedonka Mitreva, Julie C. Dunning Hotopp, John Martin, Kerstin Fischer, Bo Wu, Paul J. Davis, Sanjay Kumar, Norbert W. Brattig, Barton E. Slatko, Gary J. Weil, and Peter U. Fischer. Endosymbiont DNA in endobacteria-free filarial nematodes indicates ancient horizontal genetic transfer. *PLoS One*, 5(6):e11029, 2010.

[176] Samantha N. McNulty, Andrew S. Mullin, Jefferson A. Vaughan, Vasyl V. Tkach, Gary J. Weil, and Peter U. Fischer. Comparing the mitochondrial genomes of *Wolbachia*-dependent and independent filarial nematode species. *BMC Genomics*, 13:145, 2012.

[177] E. Mertens. ATP versus pyrophosphate: glycolysis revisited in parasitic protists. *Parasitol Today*, 9(4):122–126, Apr 1993.

[178] E. Mertens, E. Van Schaftingen, and M. Müller. Pyruvate kinase from *Trichomonas vaginalis*, an allosteric enzyme stimulated by ribose 5-phosphate and glycerate 3-phosphate. *Mol Biochem Parasitol*, 54(1):13–20, Aug 1992.

[179] Danny A Milner, Jr. Rethinking cerebral malaria pathology. *Curr Opin Infect Dis*, 23(5):456–463, Oct 2010.

[180] Y. Milner and H. G. Wood. Isolation of a pyrophosphoryl form of pyruvate, phosphate dikinase from *Propionibacteria*. *Proc Natl Acad Sci U S A*, 69(9):2463–2468, Sep 1972.

[181] Y. Milner and H. G. Wood. Steady state and exchange kinetics of pyruvate, phosphate dikinase from *Propionibacterium shermanii*. *J Biol Chem*, 251(24):7920–7928, Dec 1976.

[182] A. Mirfazaelian, S. Dadashzadeh, and M. R. Rouini. A high performance liquid chromatography method for simultaneous determination of albendazole metabolites in human serum. *J Pharm Biomed Anal*, 30(4):1249–1254, Nov 2002.

[183] Klaus Müller, Christoph Faeh, and François Diederich. Fluorine in pharmaceuticals: looking beyond intuition. *Science*, 317(5846):1881–1886, Sep 2007.

[184] A. Moons, R. Valcke, and M. Van Montagu. Low-oxygen stress and water deficit induce cytosolic pyruvate orthophosphate dikinase (PPDK) expression in roots of rice, a C3 plant. *Plant J*, 15(1):89–98, Jul 1998.

[185] Robert B. Moore, Miroslav Oborník, Jan Janouskovec, Tomás Chrudimský, Marie Vancová, David H. Green, Simon W. Wright, Noel W. Davies, Christopher J S. Bolch, Kirsten Heimann, Jan Slapeta, Ove Hoegh-Guldberg, John M. Logsdon, and Dee A. Carter. A photosynthetic alveolate closely related to apicomplexan parasites. *Nature*, 451(7181):959–963, Feb 2008.

[186] Yovany Moreno, Joseph F. Nabhan, Jonathan Solomon, Charles D. Mackenzie, and Timothy G. Geary. Ivermectin disrupts the function of the excretory-secretory apparatus in microfilariae of *Brugia malayi*. *Proc Natl Acad Sci U S A*, 107(46):20120–20125, Nov 2010.

[187] Richard Morphy, Corinne Kay, and Zoran Rankovic. From magic bullets to designed multiple ligands. *Drug Discov Today*, 9(15):641–651, Aug 2004.

[188] Cherie A. Motti, David G. Bourne, James N. Burnell, Jason R. Doyle, Dianne S. Haines, Catherine H. Liptrot, Lyndon E. Llewellyn, Shilo Ludke, Andrew Muirhead, and Dianne M. Tapiolas. Screening marine fungi for inhibitors of the C4 plant enzyme pyruvate phosphate dikinase: unguinol as a potential novel herbicide candidate. *Appl Environ Microbiol*, 73(6):1921–1927, Mar 2007.

[189] Tsugumi Nakanishi, Toru Nakatsu, Makoto Matsuoka, Kanzo Sakata, and Hiroaki Kato. Crystal structures of pyruvate phosphate dikinase from maize revealed an alternative conformation in the swiveling-domain motion. *Biochemistry*, 44(4):1136–1144, Feb 2005.

[190] S. Narita, S. Taketani, and H. Inokuchi. Oxidation of protoporphyrinogen IX in *Escherichia coli* is mediated by the aerobic coproporphyrinogen oxidase. *Mol Gen Genet*, 261(6):1012–1020, Jul 1999.

[191] Björn Niebel, Christian Lentz, Monika Pofahl, Günter Mayer, Achim Hoerauf, Kenneth M. Pfarr, and Michael Famulok. ADLOC: an aptamer-displacement assay based on luminescent oxygen channeling. *Chemistry*, 16(36):11100–11107, Sep 2010.

[192] Mike Y. Osei-Atweneboana, Kwablah Awadzi, Simon K. Attah, Daniel A. Boakye, John O. Gyapong, and Roger K. Prichard. Phenotypic evidence of emerging ivermectin resistance in *Onchocerca volvulus*. *PLoS Negl Trop Dis*, 5(3):e998, 2011.

[193] E. A. Ottesen. Efficacy of diethylcarbamazine in eradicating infection with lymphatic-dwelling filariae in humans. *Rev Infect Dis*, 7(3):341–356, 1985.

[194] E. A. Ottesen, M. M. Ismail, and J. Horton. The role of albendazole in programmes to eliminate lymphatic filariasis. *Parasitol Today*, 15(9):382–386, Sep 1999.

[195] Jeannie J. Padgett and Kathryn H. Jacobsen. Loiasis: African eye worm. *Trans R Soc Trop Med Hyg*, 102(10):983–989, Oct 2008.

[196] Jean-Marie Pagès and Leonard Amaral. Mechanisms of drug efflux and strategies to combat them: challenging the efflux pump of Gram-negative bacteria. *Biochim Biophys Acta*, 1794(5):826–833, May 2009.

[197] Malathy Palayam, Karthik Lakshminarayanan, Manohar Radhakrishnan, and Gunasekaran Krishnaswamy. Preliminary analysis to target pyruvate phosphate dikinase from *Wolbachia* endosymbiont of *Brugia malayi* for designing anti-filarial agents. *Interdiscip Sci*, 4(1):74–82, Mar 2012.

[198] M. W. Pantoliano, E. C. Petrella, J. D. Kwasnoski, V. S. Lobanov, J. Myslik, E. Graf, T. Carver, E. Asel, B. A. Springer, P. Lane, and F. R. Salemme. High-density miniaturized thermal shift assays as a general strategy for drug discovery. *J Biomol Screen*, 6(6):429–440, Dec 2001.

[199] Nitin Patel, Sudha B. Singh, Sandip K. Basu, and Amitabha Mukhopadhyay. *Leishmania* requires Rab7-mediated degradation of endocytosed hemoglobin for their growth. *Proc Natl Acad Sci U S A*, 105(10):3980–3985, Mar 2008.

[200] David J. Payne, Michael N. Gwynn, David J. Holmes, and David L. Pompliano. Drugs for bad bugs: confronting the challenges of antibacterial discovery. *Nat Rev Drug Discov*, 6(1):29–40, Jan 2007.

[201] C. A. Peixoto, A. Rocha, A. Aguiar-Santos, and M. S. Florêncio. The effects of diethylcarbamazine on the ultrastructure of microfilariae of *Wuchereria bancrofti* in vivo and in vitro. *Parasitol Res*, 92(6):513–517, Apr 2004.

[202] D. J. Pemberton, C. J. Franks, R. J. Walker, and L. Holden-Dye. Characterization of glutamate-gated chloride channels in the pharynx of wild-type and mutant *Caenorhabditis elegans* delineates the role of the subunit GluCl-alpha2 in the function of the native receptor. *Mol Pharmacol*, 59(5):1037–1043, May 2001.

[203] G. Petit, M. Diagne, P. Maréchal, D. Owen, D. Taylor, and O. Bain. Maturation of the filaria *Litomosoides sigmodontis* in BALB/c mice; comparative susceptibility of nine other inbred strains. *Ann Parasitol Hum Comp*, 67(5):144–150, 1992.

[204] R. M. Petrovich and E. K. Jaffe. Magnetic resonance studies on the active site and metal centers of *Bradyrhizobium japonicum* porphobilinogen synthase. *Biochemistry*, 36(43):13421–13427, Oct 1997.

[205] R. M. Petrovich, S. Litwin, and E. K. Jaffe. *Bradyrhizobium japonicum* porphobilinogen synthase uses two Mg(II) and monovalent cations. *J Biol Chem*, 271(15):8692–8699, Apr 1996.

[206] K. M. Pfarr, A. Y. Debrah, S. Specht, and A. Hoerauf. Filariasis and lymphoedema. *Parasite Immunol*, 31(11):664–672, Nov 2009.

[207] K. M. Pfarr, U. Heider, C. Schmetz, D. W. Büttner, and A. Hoerauf. The mitochondrial heat shock protein 60 (HSP60) is up-regulated in *Onchocerca volvulus* after the depletion of *Wolbachia*. *Parasitology*, 135(4):529–538, Apr 2008.

[208] Kenneth Pfarr and Achim Hoerauf. The annotated genome of *Wolbachia* from the filarial nematode *Brugia malayi*: what it means for progress in antifilarial medicine. *PLoS Med*, 2(4):e110, Apr 2005.

[209] Abbhirami Rajagopal, Anita U. Rao, Julio Amigo, Meng Tian, Sanjeev K. Upadhyay, Caitlin Hall, Suji Uhm, M. K. Mathew, Mark D. Fleming, Barry H. Paw, Michael Krause, and Iqbal Hamza. Haem homeostasis is regulated by the conserved and concerted functions of HRG-1 proteins. *Nature*, 453(7198):1127–1131, Jun 2008.

[210] S. A. Ralph, M. C. D'Ombrain, and G. I. McFadden. The apicoplast as an antimalarial drug target. *Drug Resist Updat*, 4(3):145–151, Jun 2001.

[211] Anita U. Rao, Lynn K. Carta, Emmanuel Lesuisse, and Iqbal Hamza. Lack of heme synthesis in a free-living eukaryote. *Proc Natl Acad Sci U S A*, 102(12):4270–4275, Mar 2005.

[212] Sylvine Raverdy, Jeremy M. Foster, Erica Roopenian, and Clotilde K S. Carlow. The *Wolbachia* endosymbiont of *Brugia malayi* has an active pyruvate phosphate dikinase. *Mol Biochem Parasitol*, 160(2):163–166, Aug 2008.

[213] R. E. Reeves, R. A. Menzies, and D. S. Hsu. The pyruvate-phosphate dikinase reaction. The fate of phosphate and the equilibrium. *J Biol Chem*, 243(20):5486–5491, Oct 1968.

[214] Allen B. Reitz, Ursula D. Ramirez, Linda Stith, Yanming Du, Garry R. Smith, and Eileen K. Jaffe. *Pseudomonas aeruginosa* porphobilinogen synthase assembly state regulators: hit discovery and initial SAR studies. *ARKIVOC*, 2010:175–188, Jun 2010.

[215] C.V. Riley. Elephantiasis, or filarial disease. *Science*, ns-1:419–421, 1883.

[216] Terry Roemer, Julian Davies, Guri Giaever, and Corey Nislow. Bugs, drugs and chemical genomics. *Nat Chem Biol*, 8(1):46–56, Jan 2012.

[217] J. R. Roth, J. G. Lawrence, and T. A. Bobik. Cobalamin (coenzyme B12): synthesis and biological significance. *Annu Rev Microbiol*, 50:137–181, 1996.

[218] F. Rousset, D. Bouchon, B. Pintureau, P. Juchault, and M. Solignac. *Wolbachia* endosymbionts responsible for various alterations of sexuality in arthropods. *Proc Biol Sci*, 250(1328):91–98, Nov 1992.

[219] Simone M. Rowley, Robert J. Raven, and Elizabeth A. McGraw. *Wolbachia pipientis* in Australian spiders. *Curr Microbiol*, 49(3):208–214, Sep 2004.

[220] Juliana M. Sá, Jason L. Chong, and Thomas E. Wellems. Malaria drug resistance: new observations and developments. *Essays Biochem*, 51:137–160, 2011.

[221] Amélie v Saint André, Nathan M. Blackwell, Laurie R. Hall, Achim Hoerauf, Norbert W. Brattig, Lars Volkmann, Mark J. Taylor, Louise Ford, Amy G. Hise, Jonathan H. Lass, Eugenia Diaconu, and Eric Pearlman. The role of endosymbiotic *Wolbachia* bacteria in the pathogenesis of river blindness. *Science*, 295(5561):1892–1895, Mar 2002.

[222] Shigeharu Sato and R J M. Wilson. The genome of *Plasmodium falciparum* encodes an active delta-aminolevulinic acid dehydratase. *Curr Genet*, 40(6):391–398, Mar 2002.

[223] Nori Sawada, Noriyuki Nagahara, Tadashi Sakai, Yoshiaki Nakajima, Masayasu Minami, and Tomoyuki Kawada. The activation mechanism of human porphobilinogen synthase by 2-mercaptoethanol: intrasubunit transfer of a reserve zinc ion and coordination with three cysteines in the active center. *J Biol Inorg Chem*, 10(2):199–207, Mar 2005.

[224] Andrea Schiefer, Alexander Schmitz, Till F. Schäberle, Sabine Specht, Christine Lämmer, Kelly L. Johnston, Dmitry G. Vassylyev, Gabriele M. König, Achim Hoerauf, and Kenneth Pfarr. Corallopyronin A specifically targets and depletes essential obligate *Wolbachia* endobacteria from filarial nematodes in vivo. *J Infect Dis*, 206(2):249–257, Jul 2012.

[225] Guillermo Senisterra, Irene Chau, and Masoud Vedadi. Thermal denaturation assays in chemical biology. *Assay Drug Dev Technol*, 10(2):128–136, Apr 2012.

[226] Laura R. Serbus, Frederic Landmann, Walter M. Bray, Pamela M. White, Jordan Ruybal, R Scott Lokey, Alain Debec, and William Sullivan. A Cell-Based Screen Reveals that the Albendazole Metabolite, Albendazole Sulfone, Targets *Wolbachia*. *PLoS Pathog*, 8(9):e1002922, Sep 2012.

[227] Dhanasekaran Shanmugam, Bo Wu, Ursula Ramirez, Eileen K. Jaffe, and David S. Roos. Plastid-associated porphobilinogen synthase from *Toxoplasma gondii*: kinetic and structural properties validate therapeutic potential. *J Biol Chem*, 285(29):22122–22131, Jul 2010.

[228] Payal R. Sheth, Gerald W Shipps, Jr, Wolfgang Seghezzi, Catherine K. Smith, Cheng-Chi Chuang, David Sanden, Andrea D. Basso, Lev Vilenchik, Kimberly Gray, D Allen Annis, Elliott Nickbarg, Yao Ma, Brian Lahue, Ronald Herbst, and Hung V. Le. Novel benzimidazole inhibitors bind to a unique site in the kinesin spindle protein motor domain. *Biochemistry*, 49(38):8350–8358, Sep 2010.

[229] P. M. Shoolingin-Jordan, P. Spencer, M. Sarwar, P. E. Erskine, K-M. Cheung, J. B. Cooper, and E. B. Norton. 5-Aminolaevulinic acid dehydratase: metals, mutants and mechanism. *Biochem Soc Trans*, 30(4):584–590, Aug 2002.

[230] A. Shukla-Dave, M. Degaonkar, R. Roy, P. K. Murthy, P. S. Murthy, P. Raghunathan, and R. K. Chatterjee. Metabolite mapping of human filarial parasite, *Brugia malayi* with nuclear magnetic resonance. *Magn Reson Imaging*, 17(10):1503–1509, Dec 1999.

[231] Claudio H. Slamovits and Patrick J. Keeling. Pyruvate-phosphate dikinase of oxymonads and parabasalia and the evolution of pyrophosphate-dependent glycolysis in anaerobic eukaryotes. *Eukaryot Cell*, 5(1):148–154, Jan 2006.

[232] Barton E. Slatko, Mark J. Taylor, and Jeremy M. Foster. The *Wolbachia* endosymbiont as an anti-filarial nematode target. *Symbiosis*, 51(1):55–65, Jul 2010.

[233] Sabine Specht, Sabine Mand, Yeboah Marfo-Debrekyei, Alexander Yaw Debrah, Peter Konadu, Ohene Adjei, Dietrich W. Büttner, and Achim Hoerauf. Efficacy of 2- and 4-week rifampicin treatment on the *Wolbachia* of *Onchocerca volvulus*. *Parasitol Res*, 103(6):1303–1309, Nov 2008.

[234] Michaela Spitzer, Emma Griffiths, Kim M. Blakely, Jan Wildenhain, Linda Ejim, Laura Rossi, Gianfranco De Pascale, Jasna Curak, Eric Brown, Mike Tyers, and Gerard D. Wright. Cross-species discovery of syncretic drug combinations that potentiate the antifungal fluconazole. *Mol Syst Biol*, 7:499, 2011.

[235] V. J. Stella and R. A. Rajewski. Cyclodextrins: their future in drug formulation and delivery. *Pharm Res*, 14(5):556–567, May 1997.

[236] Preyesh Stephen, Ramachandran Vijayan, Audesh Bhat, N. Subbarao, and R N K. Bamezai. Molecular modeling on pyruvate phosphate dikinase of *Entamoeba histolytica* and in silico virtual screening for novel inhibitors. *J Comput Aided Mol Des*, 22(9):647–660, Sep 2008.

[237] Alejandro A. Schaffer Jinghui Zhang Zheng Zhang Webb Miller Stephen F. Altschul, Thomas L. Madden and David J. Lipman. Gapped BLAST and PSI-BLAST: a new generation of protein database search programs. *Nucleic Acids Res*, 25:3389–3402, 1997.

[238] Wilma A. Stolk, Gerrit J. Van Oortmarssen, S. P. Pani, Sake J. De Vlas, S. Subramanian, P. K. Das, and J Dik F. Habbema. Effects of ivermectin and diethylcarbamazine on microfilariae and overall microfilaria production in bancroftian filariasis. *Am J Trop Med Hyg*, 73(5):881–887, Nov 2005.

[239] R. Stouthamer, J. A. Breeuwert, R. F. Luck, and J. H. Werren. Molecular identification of microorganisms associated with parthenogenesis. *Nature*, 361(6407):66–68, Jan 1993.

[240] Silke Strassel. Biochemische und enzymkinetische Analyse der delta-Aminolävulinsäure-Dehydratase aus *Toxoplasma gondi*i und *Plasmodium falciparum*. Diplomarbeit; Institut für Medizinische Mikrobiologie, Immunologie und Parasitologie, Universitätsklinikum Bonn, 2012.

[241] Uta Strübing, Richard Lucius, Achim Hoerauf, and Kenneth M. Pfarr. Mitochondrial genes for heme-dependent respiratory chain complexes are up-regulated after depletion of *Wolbachia* from filarial nematodes. *Int J Parasitol*, 40(10):1193–1202, Aug 2010.

[242] N. Surolia and G. Padmanaban. De novo biosynthesis of heme offers a new chemotherapeutic target in the human malarial parasite. *Biochem Biophys Res Commun*, 187(2):744–750, Sep 1992.

[243] Babila Tachu, Smitha Pillai, Richard Lucius, and Thomas Pogonka. Essential role of chitinase in the development of the filarial nematode *Acanthocheilonema viteae*. *Infect Immun*, 76(1):221–228, Jan 2008.

[244] Francesca Tamarozzi, Nicholas Tendongfor, Peter A. Enyong, Mathias Esum, Brian Faragher, Samuel Wanji, and Mark J. Taylor. Long term impact of large scale community-directed delivery of doxycycline for the treatment of onchocerciasis. *Parasit Vectors*, 5:53, 2012.

[245] Ayumi Tanaka and Ryouichi Tanaka. Chlorophyll metabolism. *Curr Opin Plant Biol*, 9(3):248–255, Jun 2006.

[246] Lei Tang, Sabine Breinig, Linda Stith, Adele Mischel, Justin Tannir, Bashkim Kokona, Robert Fairman, and Eileen K. Jaffe. Single amino acid mutations alter the distribution of human porphobilinogen synthase quaternary structure isoforms (morpheeins). *J Biol Chem*, 281(10):6682–6690, Mar 2006.

[247] M. J. Taylor and A. Hoerauf. A new approach to the treatment of filariasis. *Curr Opin Infect Dis*, 14(6):727–731, Dec 2001.

[248] Mark J. Taylor, Claudio Bandi, and Achim Hoerauf. *Wolbachia* bacterial endosymbionts of filarial nematodes. *Adv Parasitol*, 60:245–284, 2005.

[249] Mark J. Taylor, Achim Hoerauf, and Moses Bockarie. Lymphatic filariasis and onchocerciasis. *Lancet*, 376(9747):1175–1185, Oct 2010.

[250] Patricia L. Taylor, Laura Rossi, Gianfranco De Pascale, and Gerard D. Wright. A Forward Chemical Screen Identifies Antibiotic Adjuvants in *Escherichia coli*. *ACS Chem Biol*, 7(9):1547–1555, Sep 2012.

[251] Simon Townson, Senyo Tagboto, Helen F. McGarry, Gillian L. Egerton, and Mark J. Taylor. *Onchocerca* parasites and *Wolbachia* endosymbionts: evaluation of a spectrum of antibiotic types for activity against *Onchocerca gutturosa* in vitro. *Filaria J*, 5:4, 2006.

[252] George Tzertzinis, Ana L. Egaña, Subba Reddy Palli, Marc Robinson-Rechavi, Chris R. Gissendanner, Canhui Liu, Thomas R. Unnasch, and Claude V. Maina. Molecular evidence for a functional ecdysone signaling system in *Brugia malayi*. *PLoS Negl Trop Dis*, 4(3):e625, 2010.

[253] S. Uni, O. Bain, H. Takaoka, M. Miyashita, and Y. Suzuki. *Onchocerca dewittei japonica* n. subsp., a common parasite from wild boar in Kyushu Island, Japan. *Parasite*, 8(3):215–222, Sep 2001.

[254] Shigehiko Uni, Odile Bain, Kazuo Suzuki, Takeshi Agatsuma, Masashi Harada, Masaharu Motokawa, Coralie Martin, Emilie Lefoulon, Masako Fukuda, and Hiroyuki Takaoka. *Acanthocheilonema delicata* n. sp. (Nematoda: Filarioidea) from Japanese badgers (*Meles anakuma*): Description, molecular identification, and *Wolbachia* screening. *Parasitol Int*, 62(1):14–23, Aug 2012.

[255] Giel G. van Dooren, Alexander T. Kennedy, and Geoffrey I. McFadden. The use and abuse of heme in apicomplexan parasites. *Antioxid Redox Signal*, 17(4):634–656, Aug 2012.

[256] T. T. Vandekerckhove, S. Watteyne, A. Willems, J. G. Swings, J. Mertens, and M. Gillis. Phylogenetic analysis of the 16S rDNA of the cytoplasmic bacterium *Wolbachia* from the novel host *Folsomia candida* (Hexapoda, Collembola) and its implications for wolbachial taxonomy. *FEMS Microbiol Lett*, 180(2):279–286, Nov 1999.

[257] Marcela Varela-Gómez, Rafael Moreno-Sánchez, Juan Pablo Pardo, and Ruy Perez-Montfort. Kinetic mechanism and metabolic role of pyruvate phosphate dikinase from *Entamoeba histolytica*. *J Biol Chem*, 279(52):54124–54130, Dec 2004.

[258] Lars Volkmann, Kerstin Fischer, Mark Taylor, and Achim Hoerauf. Antibiotic therapy in murine filariasis (*Litomosoides sigmodontis*): comparative effects of doxycycline and rifampicin on *Wolbachia* and filarial viability. *Trop Med Int Health*, 8(5):392–401, May 2003.

[259] Denis Voronin, Darren A N. Cook, Andrew Steven, and Mark J. Taylor. Autophagy regulates *Wolbachia populations* across diverse symbiotic associations. *Proc Natl Acad Sci U S A*, 109(25):E1638–E1646, Jun 2012.

[260] Henri Wajcman, Laurent Kiger, and Michael C. Marden. Structure and function evolution in the superfamily of globins. *C R Biol*, 332(2-3):273–282, 2009.

[261] Samuel Wanji, Nicholas Tendongfor, Theolbald Nji, Mathias Esum, Julious N. Che, Armand Nkwescheu, Fifen Alassa, Geremy Kamnang, Peter A. Enyong, Mark J. Taylor, Achim Hoerauf, and David W. Taylor. Community-directed delivery of doxycycline for the treatment of onchocerciasis in areas of coendemicity with loiasis in Cameroon. *Parasit Vectors*, 2(1):39, 2009.

[262] M. J. Warren, J. B. Cooper, S. P. Wood, and P. M. Shoolingin-Jordan. Lead poisoning, haem synthesis and 5-aminolaevulinic acid dehydratase. *Trends Biochem Sci*, 23(6):217–221, Jun 1998.

[263] M. Wei, D. Ye, and D. Dunaway-Mariano. Investigation of the role of the domain linkers in separate site catalysis by *Clostridium symbiosum* pyruvate phosphate dikinase. *Biochemistry*, 40(45):13466–13473, Nov 2001.

[264] J. H. Werren, W. Zhang, and L. R. Guo. Evolution and phylogeny of *Wolbachia*: reproductive parasites of arthropods. *Proc Biol Sci*, 261(1360):55–63, Jul 1995.

[265] Claire Whitton, Jennifer Daub, Mike Quail, Neil Hall, Jeremy Foster, Jennifer Ware, Mehul Ganatra, Barton Slatko, Bart Barrell, and Mark Blaxter. A genome sequence survey of the filarial nematode *Brugia malayi*: repeats, gene discovery, and comparative genomics. *Mol Biochem Parasitol*, 137(2):215–227, Oct 2004.

[266] WHO. World malaria report, 2011.

[267] WHO. Malaria fact sheet n°94, 2012.

[268] H. G. Wood, W. E. O'brien, and G. Micheales. Properties of carboxytransphosphorylase; pyruvate, phosphate dikinase; pyrophosphate-phosphofructikinase and pyrophosphate-acetate kinase and their roles in the metabolism of inorganic pyrophosphate. *Adv Enzymol Relat Areas Mol Biol*, 45:85–155, 1977.

[269] Gerard D. Wright and Hendrik Poinar. Antibiotic resistance is ancient: implications for drug discovery. *Trends Microbiol*, 20(4):157–159, Apr 2012.

[270] Bo Wu, Jacopo Novelli, Jeremy Foster, Romualdas Vaisvila, Leslie Conway, Jessica Ingram, Mehul Ganatra, Anita U. Rao, Iqbal Hamza, and Barton Slatko. The heme biosynthetic pathway of the obligate *Wolbachia* endosymbiont of *Brugia malayi* as a potential anti-filarial drug target. *PLoS Negl Trop Dis*, 3(7):e475, 2009.

[271] Chun Wu, Debra Dunaway-Mariano, and Patrick S. Mariano. Design, Synthesis, and Evaluation of Inhibitors of Pyruvate Phosphate Dikinase. *J Org Chem*, [Epub ahead of print], Nov 2012.

[272] Ellen Yeh and Joseph L. DeRisi. Chemical rescue of malaria parasites lacking an apicoplast defines organelle function in blood-stage *Plasmodium falciparum*. *PLoS Biol*, 9(8):e1001138, Aug 2011.

[273] Pamela Yeh, Ariane I. Tschumi, and Roy Kishony. Functional classification of drugs by properties of their pairwise interactions. *Nat Genet*, 38(4):489–494, Apr 2006.

[274] Zhang, Chung, and Oldenburg. A Simple Statistical Parameter for Use in Evaluation and Validation of High Throughput Screening Assays. *J Biomol Screen*, 4(2):67–73, 1999.

[275] Rumin Zhang and Frederick Monsma. Fluorescence-based thermal shift assays. *Curr Opin Drug Discov Devel*, 13(4):389–402, Jul 2010.

[276] Marcel Zámocký, Paul G. Furtmüller, and Christian Obinger. Evolution of catalases from bacteria to humans. *Antioxid Redox Signal*, 10(9):1527–1548, Sep 2008.

[277] Marcel Zámocký, Paul G. Furtmüller, and Christian Obinger. Evolution of structure and function of Class I peroxidases. *Arch Biochem Biophys*, 500(1):45–57, Aug 2010.

List of Figures

List of Tables

Appendix A

Chemical structure appendix

A.1 wALAD High-Throughput Screening hits

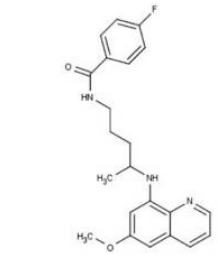

CG1 23H9

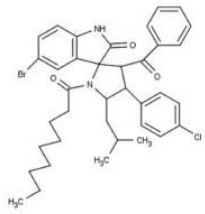

CG2 17G2

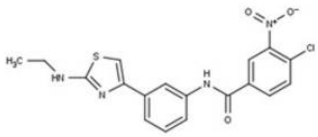

CG2 27D2

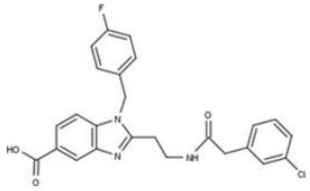

CG3 5B9

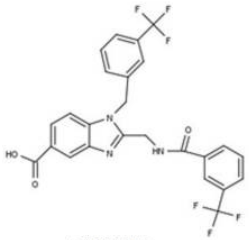

CG3 7H5

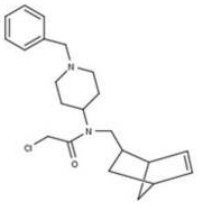

CG5 12B7

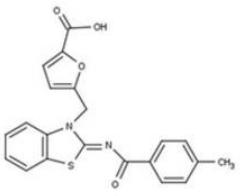

CG6 23G7

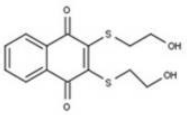

KR1 3F10

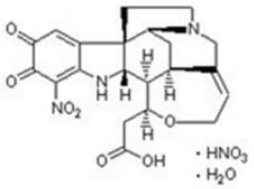

KR1 4G3
Cacotheline

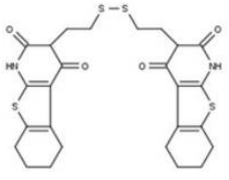

KR1 7D9

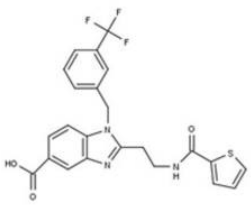

wALADin 1

A.2 wALADin1 derivatives

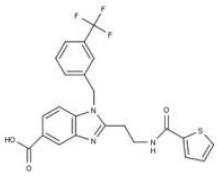

wALADin1

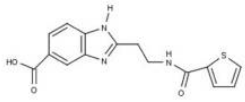

2

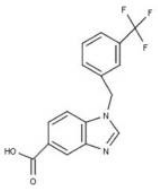

3

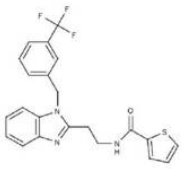

4

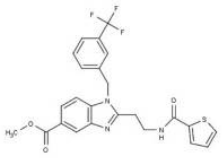

5

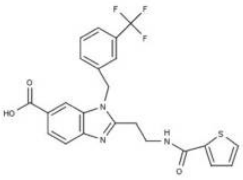

6

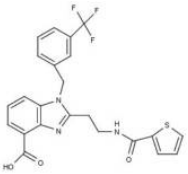

7

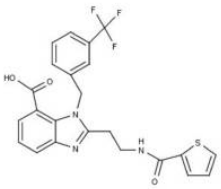

8

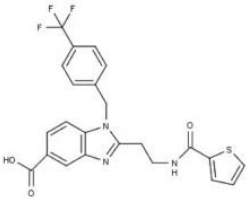

9

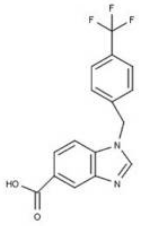

10

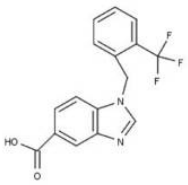

11

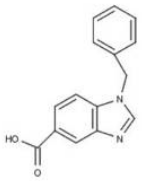

12

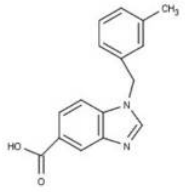

13

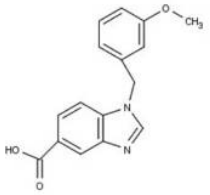

14

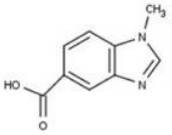

15

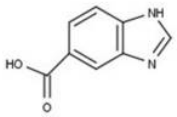

16

A.3 Virtual screening hits

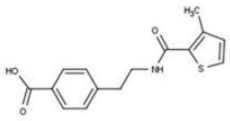

VS1

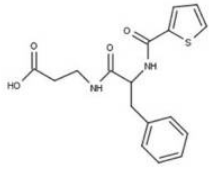

VS2

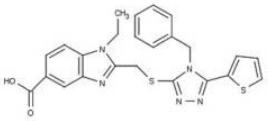

VS3

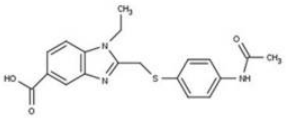

VS4

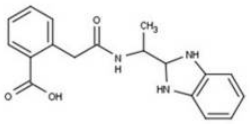

VS5

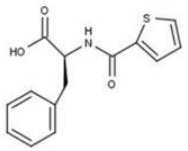

VS6

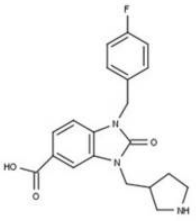

VS7

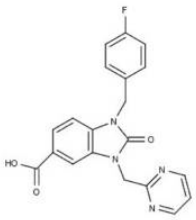

VS8

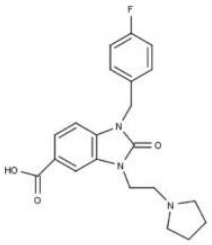

VS9

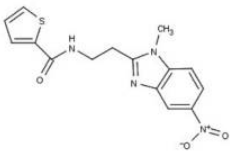

VS10

A.4 Selected compounds from the Peakdale set

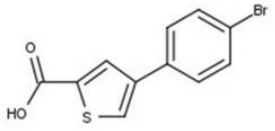

PD 481

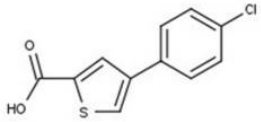

PD 593

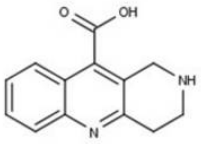

PD 636

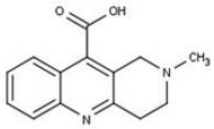

PD 637

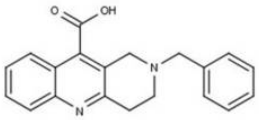

PD 638

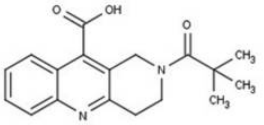

PD 639

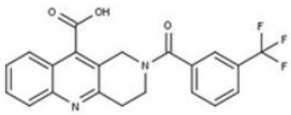

PD 640

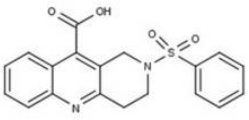

PD 641

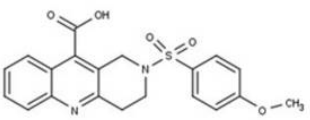

PD 642

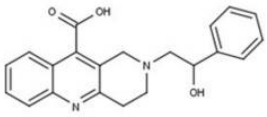

PD 643

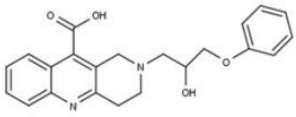

PD 644

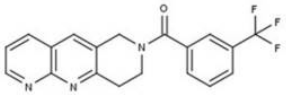

PD 2O

A.5 Validated PPDK High-Throughput Screening hits

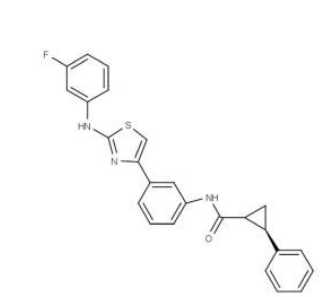

CG1 1H10

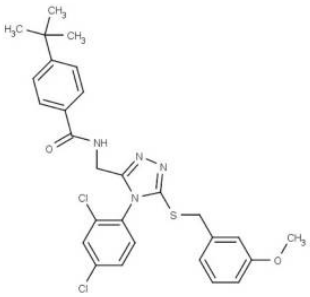

CG2 2A8

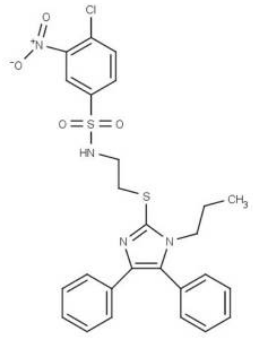

CG2 2B3

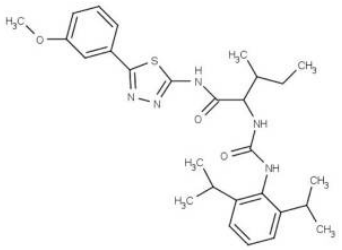

CG2 3E5

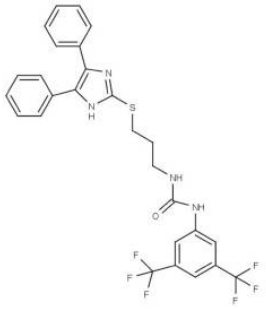

CG2 4E2

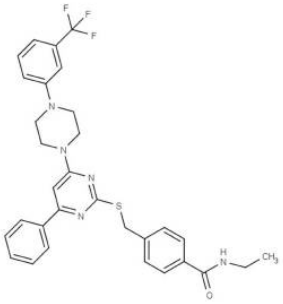

CG3 16H9

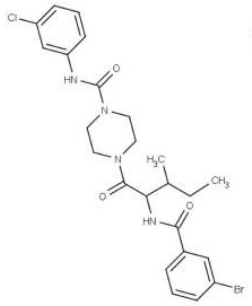

CG4 1G3

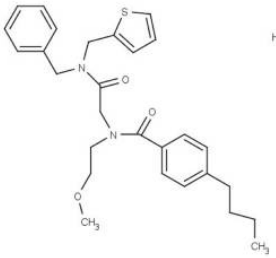

CG4 16F9

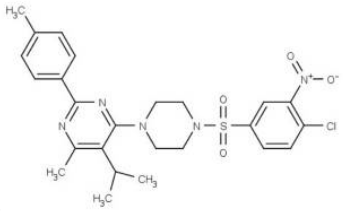

CG4 19G2

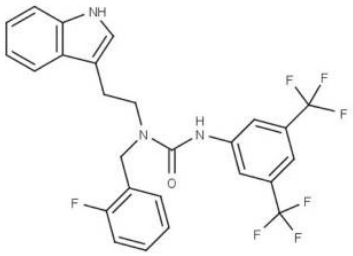

CG4 23G5

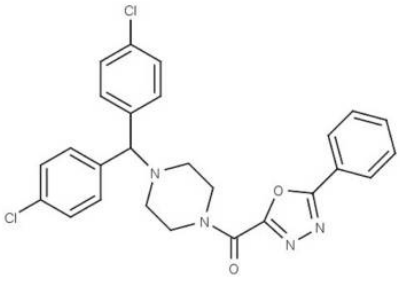

CG5 9B8

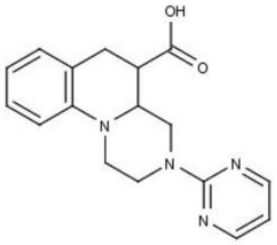

CG5 27H5

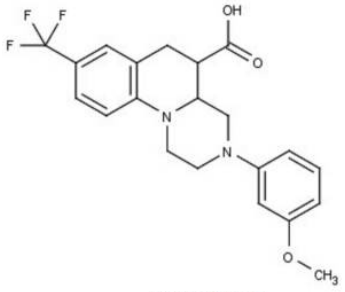

CG6 32F2

Appendix B

Supplementary videos

Supplementary videos 1 - 5 are contained on the multimedia CD enclosed with this work illustrating the phenotype of *L. sigmodontis* (*Ls*) and *A. viteae* (*Av*) worms in the *ex vivo* experiments, i.e. under exposure to different concentrations of wALADin1 or derivatives for 14 - 17 days. In the following overview the video contents are listed and the time point, the filarial species and the identity and concentration of the tested compounds are indicated. Median motility scores corresponding to the worms shown in the video samples at the selected time points (6 worms per group on 1 plate) are indicated in brackets.

Video 1: Day 0 - *L. sigmodontis* and *A. viteae* before start of treatment: *Ls* 1% DMSO group (5); *Ls* 500 μM wALADin1 group (5); *Av* 1% DMSO group (5); 500 μM wALADin1 group (5).

Video 2: Day 5 - *L. sigmodontis*: 1% DMSO (5) ; 125 μM wALADin1 (5); 250 μM wALADin1 (4); 500 μM wALADin1 (3); 125 μM compound **3** (5); 250 μM compound **3** (5); 500 μM compound 3 (4); 500 μM compound **6** (4)

Video 3: Day 17 - *L. sigmodontis*: 1% DMSO (5) ; 125 μM wALADin1 (4); 250 μM wALADin1 (3); 500 μM wALADin1 (0); 125 μM compound **3** (4); 250 μM compound **3** (3.5); 500 μM compound **3** (3); 500 μM compound **6** (1).

Video 4: Day 5 - *A. viteae*: 1% DMSO (5); 250 μM wALADin1 (5); 500 μM wALADin1 (4)

Video 5: Day 14 - *A. viteae*: 1% DMSO (5); 250 μM wALADin1 (5); 500 μM wALADin1 (2)